



The
University
Of
Sheffield.

Innovative Sustainable Strengthening Systems for Unreinforced Masonry using Natural Fibre Textiles embedded in Inorganic Matrices

By:

Niki Trochoutsou

A thesis submitted in partial fulfilment of the requirements for the degree of Doctor of Philosophy

The University of Sheffield
Faculty of Engineering
Department of Civil and Structural Engineering

Sheffield, December 2020

[This page is intentionally left blank]

DECLARATION OF STATEMENT

I, the author, confirm that the Thesis is my own work. I am aware of the University's Guidance on the Use of Unfair Means (www.sheffield.ac.uk/ssid/unfair-means). This work has not been previously presented for an award at this, or any other, university.

The publications arising from the thesis are the following:

Publications in peer-reviewed journal papers:

3. **N. Trochoutsou**, M. Di Benedetti, K. Pilakoutas, M. Guadagnini, In-plane Performance of Flax-TRM retrofitted masonry walls, *Mater. Struct.* (*to be submitted*)
2. **N. Trochoutsou**, M. Di Benedetti, K. Pilakoutas, M. Guadagnini, Bond of Flax Textile-Reinforced Mortars to Masonry, *Constr. Build. Mater.* 284 (2021) 122849.
doi: 10.1016/j.conbuildmat.2021.122849.
1. **N. Trochoutsou**, M. Di Benedetti, K. Pilakoutas, M. Guadagnini, (2020) Mechanical Characterisation of Flax and Jute Textile-Reinforced Mortars, *Constr. Build. Mater.* 271 (2021) 121564. doi: 10.1016/j.conbuildmat.2020.121564

Publications in international conferences:

2. **N. Trochoutsou**, M. Di Benedetti, K. Pilakoutas, M. Guadagnini, Tensile performance of lime-based natural-fibre composites as strengthening systems for masonry, in: Proceedings of "3rd international Conference on Bio-Based Building Materials", June 2019, Belfast, UK.
1. **N. Trochoutsou**, M. Di Benedetti, K. Pilakoutas, M. Guadagnini, Tensile behaviour of natural fibre textile-reinforced mortar, in: Proceedings of "International Conference on Sustainable Materials, Systems and Structures, March 2019, Rovinj, Croatia.

The nature and extent of the author of the thesis and the co-authors involved in each of the publications presented is summarised in the following CRediT authorship contribution statement:

Niki Trochoutsou: Conceptualization, Methodology, Formal analysis, Investigation, Writing - original draft, Visualization, Writing - review & editing. **Matteo Di Benedetti**: Formal analysis, Visualization, Writing - review & editing. **Kypros Pilakoutas**: Conceptualization, Methodology, Writing - review & editing, Supervision. **Maurizio Guadagnini**: Conceptualization, Methodology, Writing - review & editing, Supervision.

[This page is intentionally left blank]

To my Mom and Dad,
for always being my shelter, my best friends, my home.

[This page is intentionally left blank]

ABSTRACT

The unacceptable number of casualties and substantial economic losses caused by past earthquakes highlights the high seismic vulnerability of unreinforced masonry structures and the urgent need for resilient and cost-effective retrofitting solutions. In parallel, pressing sustainability requirements foster the need for alternative materials with minimum environmental impact. This study aims at developing an innovative composite retrofitting solution comprising natural fibre textiles embedded in a lime-based mortar (NTRM). Natural fibres have good mechanical properties and excellent environmental credentials, while lime mortars can ensure physical and mechanical compatibility with masonry. Both fibres and mortars are cost-effective and widely available, thus making NTRM systems easily applicable in both developed and developing countries. However, their implementation is hindered by the lack of a comprehensive understanding of their composite behaviour and the very limited experience in structural applications.

A systematic and holistic multi-scale experimental programme was undertaken to investigate the performance of NTRM and identify key performance parameters to enable the development of design guidelines. The proposed system was examined at composite level through detailed tensile and bond characterisation, and its effectiveness as in-plane seismic retrofitting solution was assessed through structural tests on medium scale unreinforced masonry walls. The parameters under investigation included: fibre type, textile architecture, mortar overlay thickness, number of NTRM layers, bonded area (length and width), and retrofitting configuration.

The results of this study confirm the potential of Flax-TRM as a seismic strengthening solution for unreinforced masonry structures and highlight the importance of yarn and textile architecture on the overall composite performance. Smaller diameter low linear density yarns with a higher level of twist develop a better composite action with the mortar and result in composites with good mechanical properties and high utilisation of the textile tensile strength. The use of mechanical reinforcement ratios greater than 3% were found to spread the cracking well and result in highly ductile behaviour. Flax-TRM was shown to provide significant in-plane strength and ultimate drift enhancement and promote the development of energy dissipation mechanisms, while ensuring structural integrity and delaying the development of brittle failure modes. Based on the experimental evidence and a detailed analysis of shear resisting mechanisms, it is recommended that the shear contribution mechanisms are further investigated, as they were found not to be additive. A simplified design model that accounts for the contribution of the mortar and adopts a more rational effective strain limit that can be developed in the textile is proposed.

Finally, design recommendations are provided to inform the selection of suitable reinforcing materials and the design of optimal NTRM strengthening systems.

[This page is intentionally left blank]

ACKNOWLEDGEMENTS

The present doctoral study was undertaken in the Department of Civil and Structural Engineering, at The University of Sheffield, as part requirement to obtain the degree of Doctor of Philosophy (PhD), between November 2016 and December 2020. The PhD programme was supervised by Senior Lecturer Dr Maurizio Guadagnini and Professor Kypros Pilakoutas, and was financially supported by the Doctoral Academy of the Faculty of Engineering (Doctoral Academy Award).

First of all, I would like to thank from the bottom of my heart my supervisor, Dr Maurizio Guadagnini, to whom I will be eternally grateful for his support, scientific guidance and excitement, encouragement and enormous patience. Over these four years, his help was proven invaluable and his belief in me held me sane the many times I wanted to give up. His involvement in all parts of the experimental campaign and his advice were a catalyst for this programme. I highly appreciate his knowledge and expertise in the field, but also his personality and character beyond the role of his academic identity. Without him, I wouldn't be here today.

A big heartfelt thank you to my co-supervisor, Professor Kypros Pilakoutas, for always being available and offering the most crucial advice in the most needed time. His experience and knowledge reflected in his apt observations and suggestions motivated me to dig deeper into research. But, above all, I cordially thank him for his directness, encouragement and trust during these four years. I will always consider him my “scientific” father.

I would also like to massively thank Dr Matteo Di Benedetti, for his practical help with the DIC analyses and his constructive feedback. He gave me responsibilities that shaped me into the researcher I am now. His door was always open for me, no matter the time or the nature of the problem.

Special thanks to Dr Panos Papastergiou, for helping me during my first experimental steps and being one of the most helpful and supportive people I have ever known.

Huge thanks to the technical staff at the Heavy Structures Laboratory: Kieran Nash, Don Jenkins, Robin Markwell, Shaun E. Waters, Paul Blackburn, Alex Cargill. I am truly lucky I met them and worked with them. My warmest thanks also to Giorgia Martinelli, Lisa Barilli and Stefano Basso for their great assistance and collaboration in the experimental programme.

Finally, I would like to thank my parents, for always being there for me and supporting me, making sure I always feel their love. Without them, I couldn't have done it.

Niki Trochoutsou
December 2020, Sheffield

[This page is intentionally left blank]

TABLE OF CONTENTS

ABSTRACT	vii
ACKNOWLEDGEMENTS	ix
TABLE OF CONTENTS	xi
List of Tables	xv
List of Figures	xvii
List of Acronyms	xxi
1. INTRODUCTION	1
1.1. Problem Statement	1
1.2. Research Significance	4
1.2.1. Innovations of the Proposed Research	4
1.2.2. Broader Impact	5
1.3. Aims and Objectives	5
1.4. Thesis Layout	6
2. LITERATURE REVIEW	8
2.1. Failure Mechanisms of URM	8
2.2. Existing Strengthening Techniques for URM	9
2.2.1. Traditional Techniques	9
2.2.2. Modern Techniques	10
2.3. Potential of Natural Fibre TRM	12
2.3.1. Need for Sustainability in Structures	12
2.3.2. Natural Fibre Properties and Behaviour	12
2.3.3. Challenges	16
2.3.4. Natural Fibre Composites for in Structural Applications	17
2.4. Performance of TRM/NTRM - Masonry Systems	18
2.4.1. Tensile Behaviour	18
2.4.2. Bond Behaviour	21
2.4.3. In-plane Shear Performance of URM Retrofitted with TRM/NTRM Systems	22
2.5. Concluding Remarks	24
3. RESEARCH METHODOLOGY	25
3.1. Overview	25
3.2. Brief Description of Experimental Programme	25
3.2.1. Phase 1	25

3.2.2.	Phase 2	26
3.2.3.	Phase 3	28
3.2.4.	Material Mechanical Characterisation	28
3.2.5.	Instrumentation	29
3.2.6.	Selection of Key Examined Parameters	29
4.	MECHANICAL CHARACTERISATION OF FLAX AND JUTE TEXTILE-REINFORCED MORTARS	31
4.1.	Introduction	32
4.2.	Materials and Methods	34
4.2.1.	Materials	34
4.2.2.	Tests on fibres	35
4.2.3.	Tests on yarns	36
4.2.4.	Tests on bare textiles	36
4.2.5.	Tests on NTRM composites	37
4.2.6.	Digital Image Correlation (DIC)	39
4.3.	Results and Discussion	39
4.3.1.	Tensile behaviour of fibres	39
4.3.2.	Tensile behaviour of yarns	40
4.3.3.	Tensile behaviour of textiles	41
4.3.4.	Tensile behaviour of NTRM composites	42
4.4.	General Discussion and Recommendations	54
4.4.1.	Interrelationship between natural fibres, yarns, textiles	54
4.4.2.	Critical parameters and recommendations for the design of NTRM composites	55
4.5.	Conclusions	56
5.	BOND OF FLAX TEXTILE-REINFORCED MORTARS TO MASONRY	57
5.1.	Introduction	58
5.2.	Experimental Programme	60
5.2.1.	Masonry	60
5.2.2.	FTRM	61
5.2.3.	Bond Specimen Preparation	61
5.2.4.	Experimental Set-up	63
5.2.5.	Instrumentation	63
5.3.	Results and Discussion	65

5.3.1.	Introductory Remarks	65
5.3.2.	Bond-slip Behaviour of Single-Layer FTRM and Effect of Bond Length	72
5.3.3.	Effect of Multiple FTRM Layers	76
5.3.4.	Effect of Bond Width	78
5.3.5.	Crack Initiation and Development	80
5.3.6.	Stress-Strain Distribution	81
5.3.7.	Load-slip Response of Individual Yarns	84
5.4.	General Discussion and Recommendations	85
5.4.1.	Experimental Procedures and Measurements	85
5.4.2.	Recommendations for Testing and Design	87
5.5.	Conclusions	88
6.	IN-PLANE SEISMIC PERFORMANCE OF MASONRY WALLS RETROFITTED WITH FLAX-TRM	90
6.1.	Introduction	91
6.2.	Experimental Programme	93
6.2.1.	Material Characterisation	93
6.2.2.	Specimen Preparation	95
6.2.3.	Experimental Setup	97
6.3.	Results and Discussion	101
6.3.1.	Hysteresis Response and Failure Modes	101
6.3.2.	Stiffness Degradation	108
6.3.3.	Bilinear Idealization of the Experimental Envelopes	109
6.3.4.	Energy Dissipation	113
6.3.5.	Assessment of the FTRM Retrofitting Technique	114
6.4.	Predictive Models	115
6.4.1.	Shear Contribution of Masonry, V_m	115
6.4.2.	Shear Contribution of FTRM, V_{TRM}	116
6.4.3.	Assessment of Predictive Models for V_{TRM}	120
6.4.4.	Proposed Model	123
6.5.	Conclusions	125
7.	CONCLUSIONS	127
7.1.	Synopsis	127
7.2.	Conclusions	127

7.2.1.	On the Mechanical Performance of NTRM	127
7.2.2.	On the Bond Performance of NTRM/Masonry	128
7.2.3.	On the In-plane Seismic Performance of URM Walls Retrofitted with NTRM	129
7.3.	Recommendations for Testing and Design of NTRM systems	130
7.4.	Recommendations for Future Research	130
	Reference List	133
	APPENDIX A -Mechanical Characterisation of Flax and Jute Textile-Reinforced Mortars	146
	APPENDIX B - Bond Performance of FLAX-TRM to Masonry	171
	APPENDIX C - In-Plane Seismic Performance of Masonry Walls Retrofitted with FLAX-TRM	180

LIST OF TABLES

Table 2.1	Natural fibre production countries and annual fibre production.	15
Table 2.2	Mechanical properties of natural and E-glass fibres.	17
Table 2.3	Summary of research studies on the mechanical characterisation of NTRM systems.	22
Table 2.4	Summary of research studies on the bond performance of NTRM/masonry systems.	25
Table 2.5	Summary of research studies on the in-plane shear performance of NTRM/masonry systems.	25
Table 4.1	Natural fibre textile characteristics as supplied by the manufacturer unless otherwise stated.	44
Table 4.2	Mechanical properties of flax and jute fibres (CoV in parentheses).	49
Table 4.3	Mechanical properties of flax and jute yarns (CoV in parentheses).	50
Table 4.4	Mechanical properties of flax and jute textiles (CoV in parentheses).	50
Table 4.5	Mechanical Properties of F1-TRM composites (CoV in parentheses)	53
Table 4.6	Mechanical Properties of F2-TRM composites (CoV in parentheses).	54
Table 4.7	Mechanical Properties of J-TRM composites (CoV in parentheses).	55
Table 5.1	Mechanical properties of masonry prisms and their constituents. CoV in parentheses.	75
Table 5.2	Tensile properties of FTRM constituents and coupons [5] (CoV in parentheses).	75
Table 5.3	Experimental results for single F1-TRM of 100 mm bond width (CoV in parentheses).	80
Table 5.4	Experimental results for single F2-TRM of 100 mm bond width (CoV in parentheses).	81
Table 5.5	Experimental results for multi-layer FTRM with 260 mm bond length and 100 mm bond width (CoV in parentheses).	81
Table 5.6	Experimental results for F2-TRM with 260 mm bond length and 50 mm bond width (CoV in parentheses).	82
Table 6.1	Masonry properties. CoV values are given in parentheses.	112
Table 6.2	Physical and mechanical properties of textile and composites. CoV values are given in parentheses.	113
Table 6.3	Specimens' configuration.	114
Table 6.4	Experimental results of in-plane cyclic tests.	119
Table 6.5	Maximum crack widths and average and maximum strains, as measured by DIC.	125
Table 6.6	Experimental and theoretical values of initial, elastic and effective stiffness for the tested specimens (kN/mm).	129
Table 6.7	Bilinear idealised response parameters, ductility and behaviour factors based on Kel.	131

Table 6.8	Analytical predictions - Shear resistance of URM (V_m).	134
Table 6.9	Theoretical in-plane resistance of specimen BW associated with possible failure modes (in kN).	134
Table 6.10	Comparison between different design approaches to estimate the shear contribution of TRM.	135
Table 6.11	Predicted in-plane shear capacity of retrofitted specimens (in kN).	138

LIST OF FIGURES

Fig. 1.1	URM failures during earthquake events: (a) L'Aquila, Italy, 2016 – Mw 6.3, (b) Kathmandu, Nepal, 2015 – Mw 7.8, (c) Rasht, Iran, 1990 – Mw 7.4 and (d) Long Beach, California, 1993 – Mw 6.3.	1
Fig. 1.2	Overview of the proposed externally bonded NTRM strengthening system.	6
Fig. 2.1	Characteristic failure modes of URM during seismic actions (adapted from [2]).	10
Fig. 2.2	Typical failure modes of URM walls under in-plane loading (adapted from [4]).	11
Fig. 2.3	Typical examples of textiles used in TRM systems: (a) Bi-directional carbon fibre grid, (b) Unidirectional steel wires (SRG), (c) Bi-directional Paraphenylene-Benzobisoxazole (PBO) fibre grid and (d) four-directional Glass fibre grid.	13
Fig. 2.4	Cost per weight of natural and E-Glass fibres (left); cost per unit length required to resist 100 kN tensile load (right).	16
Fig. 2.5	Chemical composition of natural fibre (after [54]).	17
Fig. 2.6	Moisture absorption effects in inorganic composites (adapted from [58]).	19
Fig. 2.7	Natural fibre degradation in highly alkaline environments (adapted from [59]).	19
Fig. 2.8	Stress-strain response of TRM systems under uniaxial tension [28]	21
Fig. 2.9	(a) Fibre rovings of a textile embedded in the inorganic matrix (adapted from [70]); (b) Telescopic failure mechanism [69].	21
Fig. 2.10	Failure modes observed in TRM/SRG systems (adapted from [9])	24
Fig. 3.1	Overview of experimental programme.	33
Fig. 3.2	Natural fibre textiles investigated in Study 1: (a) F1; (b) F2; (c) J. Scale in mm.	34
Fig. 3.3	Overview of experimental programme - Phase 1.	35
Fig. 3.4	Overview of experimental programme - Phase 2.	35
Fig. 3.5	Experimental test setup - Phase 2.	36
Fig. 3.6	Overview of experimental programme - Phase 3.	36
Fig. 3.7	Overview of material characterisation tests.	37
Fig. 4.1	(a) tensile test setup for fibres; (b) tensile test setup for yarns and capstan clamps details.	45
Fig. 4.2	Tensile test setup for bare textiles (F1t), gauge length of virtual extensometers and DIC analysis parameters.	46
Fig. 4.3	NTRM manufacturing process: (a) application of first mortar layer; (b) embedment of the textile; (c) application of top mortar layer; (d) use of gauge scraper to ensure constant mortar thickness	47
Fig. 4.4	(a) Geometry of NTRM coupons (all dimensions in mm); (b) clevis-type grips and DIC analysis parameters.	48

Fig. 4.5	Envelope curves for the stress-strain response of natural fibre yarns and representative specimens: (a) F1 (b) F2 and (c) J.	49
Fig. 4.6	Tensile stress-strain response of natural fibre bare textiles: (a1) F1 (b1) F2 and (c1) J (dashed lines represent the ultimate average mechanical properties of the corresponding single yarns); stress-strain distribution across the yarns for representative (a2) F1, (b2) F2 and (c2) J specimens. Note: L = left yarn, M =middle yarn and R = right yarn.	52
Fig. 4.7	Tensile stress-strain response of representative single-layer NTRM coupons, typical failure modes, crack stages and associated stiffness for: (a) F1-, (b) F2- and (c) J-TRM.	53
Fig. 4.8	Effect of number of NTRM layers on the tensile stress-strain response of representative specimens: a) F1-TRM, b) F2-TRM, and c) J-TRM (dashed lines represent the average tensile response of the corresponding bare textiles up to failure).	58
Fig. 4.9	Failure modes of representative NTRM specimens for each series and corresponding classification according to RILEM TC 250-CSM.	59
Fig. 4.10	Effect of number of reinforcing layers on: (a) maximum strength; and (b) strain at peak load. (c) normalised load bearing capacity as a function of the mechanical reinforcement ratio (dashed line represents the threshold defining the matrix-controlled fracture).	60
Fig. 4.11	Effect of mortar overlay thickness on the tensile response of (a) F1-TRM and (b) F2-TRM specimens.	62
Fig. 4.12	Crack development for a representative F2-TRM specimen: (a) strain field at subsequent crack formation stages with corresponding load and crack location; (b) calculation of the crack width (image at 100% of $f_{NTRM,max}$); and (c) development of average and maximum crack width.	63
Fig. 5.1	Flax textile reinforcements adopted in the present study: (a) Flax1 (F1) and (b) Flax2 (F2). Scale in mm.	74
Fig. 5.2	FTRM strengthening configuration (all dimensions in mm).	76
Fig. 5.3	Experimental test setup and instrumentation.	77
Fig. 5.4	(a) Instrumentation layout and typical speckle pattern for non-contact measurements; (b) location of optical targets; (c) virtual extensometers alongside the potentiometers and (d) virtual extensometers for slip measurements of individual yarns.	79
Fig. 5.5	Comparison between physical (POT) and virtual (POT _v) potentiometers on the basis of load-slip response: (a) for a typical specimen, (b1) for a specimen with unreliable potentiometer data and (b2) initiation displacement measurements for different instrumentation positions for the specimen shown in b1.	84
Fig. 5.6	Average tensile stress-strain relationship used in the analyses for (a) F1 and F2 textiles; (b) F2 yarns.	84
Fig. 5.7	(a) Typical crack development and (b) failure modes in single-lap shear bond tests (adapted from RILEM TC-250 CSM).	85

Fig. 5.8	Load-slip response curves of F1-TRM specimens for all bond lengths investigated.	86
Fig. 5.9	Load-slip response curves of F2-TRM specimens for all bond lengths investigated.	86
Fig. 5.10	Effect of bond length on (a) the ultimate load/strength and (b) slip at the textile/masonry developed by single-layer F1- and F2-TRM.	89
Fig. 5.11	Ductility of FTRM systems with respect to: (a,c) the bond length and (b,d) the number of TRM layers, for F1 and F2-TRM specimens respectively.	90
Fig. 5.12	Load-slip behaviour of specimens with multiple (a) F1- and (b) F2-TRM layers.	91
Fig. 5.13	Effect of number of FTRM layers on (a) normalised load capacity and (b) exploitation ratio.	92
Fig. 5.14	(a) Load-slip response curves of single and multi-layer F2-TRM systems of 50 mm bond width; (b) axial strength capacity normalised over bond width as a function of the number of F2-TRM layers.	94
Fig. 5.15	(a) Calculation of crack width for a typical specimen (F2L1-210-100-3); (b) displacement and strain profile along the centreline; (c) development of maximum crack width with the bond length and (d) the addition of multiple F2-TRM layers.	95
Fig. 5.16	F2-TRM systems. Strain profile across the width of the unbonded textile at different loading stages for a typical specimen with: (a) insufficient bond length (F2L1-65-100-1); (b) sufficient bond length (F2L1-210-100-2); (c) three TRM layers of 100 mm bond width (F2L3-260-100-2); (d) two TRM layers of 50 mm bond width (F2L2-260-50-1). Note: the dashed and the dotted line correspond to the textile and yarn strain at failure, respectively.	97
Fig. 5.17	Ratio of average strain at maximum load between top and bottom textile layer in multi-layer F2-TRM systems.	97
Fig. 5.18	(a,c) Global and local load development with time per individual yarn; (b,d) Global (Pb-gt) and local (Pj-gj) load-slip response of individual yarns.	99
Fig. 6.1	Flax textile used for TRM retrofitting. Scale in mm.	113
Fig. 6.2	i) Laying of first course in the steel channel; ii) application of rapid-hardening high strength grout; iii) positioning of capping system and use of injection guns for grout filling; iv) application of first mortar layer; v) embedment of flax textile; vi) application of top mortar layer and finishing.	115
Fig. 6.3	Test setup.	116
Fig. 6.4	(a) Displacement history for retrofitted specimens (LW, FL1W, FL2W); (b) Adopted loading regime for all wall specimens.	117
Fig. 6.5	Instrumentation layout: (a) front view; (b) side view; (c) mounting details	118
Fig. 6.6	Specimen preparation for DIC analyses: (a) wall fitted with laser cut stencils; (b) application of a matt black paint; (c) detail of speckle pattern after removal of stencils.	118

Fig. 6.7	a-e) Load-drift hysteresis responses of the wall specimens; (f) Experimental envelopes.	121
Fig. 6.8	Crack patterns and failure mode details at maximum drift for: (a) BW; (b) LW; (c) FL1W-2; (d) FL2W-1; and (e) FL2W-2. Note: Percentages correspond to the ratio of cracked/uncracked portion of wall.	122
Fig. 6.9	Development of maximum crack width with: (a) load and (b) drift; (c) Load versus damage evolution until Near Collapse.	126
Fig. 6.10	Stiffness degradation versus drift for bare and retrofitted specimens.	127
Fig. 6.11	Geometry and boundary conditions adopted in the FE model to estimate the elastic stiffness of (a) the bare wall and (b) the retrofitted walls	129
Fig. 6.12	Bilinear idealised response of bare and retrofitted wall specimens.	130
Fig. 6.13	Method of evaluation of (a) dissipated and (b) absorbed energy capacity.	131
Fig. 6.14	(a) Energy dissipation and (b) equivalent damping ratio versus drift for bare and retrofitted specimens.	131
Fig. 6.15	Comparison of experimental and analytical predictions of the shear contribution provided by 1 (1L) and 2 (2L) layers of FTRM.	137
Fig. 6.16	Estimated contribution of masonry, mortar layers and textile to total shear resistance for (a) FL1W-2; (b) FL2W-1; and (c) FL2W2 specimens.	141

LIST OF ACRONYMS

ACI	American Concrete Institute
EC	Eurocode
CoV	Coefficient of Variation
DIC	Digital Image Correlation
FEMA	Federal Emergency Management Agency
fib	Fédération internationale du béton
FRP	Fibre Reinforced Polymers
LVDT	Linear Variable Displacement Transducer
NTRM	Natural fibre Textile-Reinforced Mortars
TMS	The Masonry Society
TRM	Textile-Reinforced Mortars
URM	Unreinforced Masonry
NC	Near Collapse limit state
NTC	Norme Technique per le costruzioni (Italian Building Code - in Italian)
CNR	National Research Council - Advisory Committee On Technical Recommendations For Construction

1. INTRODUCTION

1.1. PROBLEM STATEMENT

Failures and collapses of unreinforced masonry (URM) elements during past earthquake events (e.g. Japan, 1978; Turkey, 1999; Haiti and Chili, 2010; Nepal, 2015; Italy, 2016; Mexico, 2017) resulted in high death tolls and catastrophic damage to buildings and civil infrastructure and highlighted the seismic vulnerability of these structures even to moderate intensity earthquakes (examples of URM failures after severe ground motions are shown in **Fig. 1.1**).



Fig. 1.1 URM failures during earthquake events: (a) L’Aquila, Italy, 2016 – Mw 6.3, (b) Kathmandu, Nepal, 2015 – Mw 7.8, (c) Rasht, Iran, 1990 – Mw 7.4 and (d) Long Beach, California, 1993 – Mw 6.3.

In the last 20 years alone, it is estimated that more than 75% of the number of fatalities due to earthquakes (more than 1 M) are caused by the collapse of buildings, with the greatest proportion (more than 80%) from the collapse of masonry buildings [1]. As stated by organisations like The Masonry Society (TMS) and the Federal Emergency Management Agency (FEMA) “failures of URM walls will result in more material damage and loss of human life than any other structural

material” [2]. A causal breakdown revealed that earthquake events resulted in \$300 Billion/year projected economic loss [3], while in Europe only, maintenance and rehabilitation of housing costs have been reported to exceed €340 Billion/year [1]. Inadequate construction practices, material deterioration, lax or non-efficient enforcement of seismic codes and/or non-compliance of old buildings with current seismic requirements are some of the major reasons for the seismic inadequacy of much of the existing masonry building stock [4]. Hence, the implementation of reliable assessment strategies and retrofitting methods is critical to preserving existing structures. This is in fact one of the “high” priorities in the forthcoming revision of the Eurocodes [5].

The selection and design of the most suitable strengthening solution is a complex issue. While strength increase is typically required in structural upgrade applications, ductility and energy dissipation characteristics are of major concern in seismic strengthening applications [6]. In both cases, the following aspects need to be considered:

- target of structural intervention (e.g. at element or structural level, increase of strength or ductility, change of structure’s functionality).
- availability of raw materials.
- selection of the most appropriate materials to achieve the target of the strengthening application (concrete, steel, composites) and the associated quantities.

In addition, key attributes include:

- reversibility.
- strength and stiffness compatibility between the strengthening system and the substrate.
- cost-effectiveness and time limits.
- non-violation of aesthetic requirements.
- minimal disruption to the structure’s geometry and occupancy.
- additional preservation criteria related to the restoration of cultural, architectural and historical heritage buildings.

More recently, a new requirement for construction/rehabilitation products was added in the current EU Regulation: sustainability [7]. The pressing need for sustainable development is now fuelling research into the development and use of new materials and techniques less harmful to the environment, promoting recyclability, reduction of carbon dioxide emissions and protection of resources [8].

It is evident that a plethora of strengthening materials and retrofit systems have been developed with the aim to address and satisfy partially or fully the aforementioned aspects. Advanced composite materials comprising high strength Fibre-Reinforced Polymers (FRP), in the form of externally bonded, in-situ impregnated jackets and strips, or as near surface mounted reinforcement (NSM), have been well established in the field of strengthening applications, owing to their high strength and stiffness at low weight, excellent corrosion resistance, formability, and ease and speed of installation with minimal change to the structure’s geometry [9]. These characteristics make FRP often preferable to more common traditional techniques (such as reinforced concrete jacketing), which can

significantly increase the lateral strength of the structure, but at the expense of deformability [10]. However, the organic matrices used to bind and impregnate the fibres in FRP composites (typically epoxy resins) suffer from important limitations [11], including high cost, poor behaviour at high temperatures, non-applicability on wet surfaces, chemical/mechanical incompatibility with masonry substrates resulting in premature debonding, lack of reversibility and recyclability.

Textile-Reinforced Mortar (TRM) systems have emerged as a solution to the problems arising from the use of epoxies, as an inorganic matrix is used for the impregnation of the reinforcement arranged in a grid-based form, the properties of which can be controlled independently in one or more directions. Advanced textiles consisting of glass, carbon, basalt, aramid, PBO fibres, steel cords and also hybrid combinations, such as glass-polypropylene [12] grids have been combined with cementitious, lime-based and, more recently, geopolymer mortars [13], often enriched with short fibres to control shrinkage and improve post-cracking behaviour, thus providing suitable TRM systems according to the required strengthening application. Furthermore, TRM can be combined with thermal insulation boards and provide an excellent integrated structural/energy retrofitting solution [14,15]. TRM have been applied successfully for the retrofitting of URM elements against both in-plane [11,17] and out-of-plane loading actions [18], in the strengthening of vaults, arches, pillars and lintels [19,20] and of masonry-infilled reinforced concrete frames [21,22], as well as in confinement of masonry columns [23,24]. Their potential was documented through several case studies [25], highlighting the significant increase offered by TRM in load-carrying capacity, but mainly deformation capacity as well as ductility. Few studies have compared the performance of FRP and TRM systems [18,26] and have highlighted the excellent potential of TRM in providing enhanced energy dissipation and in-plane shear deformability, as well as strength and deformation capacity in out-of-plane bending.

The superior mechanical properties of the advanced textiles currently used in TRM systems can rarely be fully utilized when applied to masonry substrates due to the vastly different strength and stiffness characteristics and incompatibility issues. As a result, the performance of such systems is often governed by premature debonding [27]. In addition, the high cost required for the manufacture of artificial fibres that are typically used in advanced TRM composites discourages their use, particularly in less favoured economies, and can cause significant environmental and disposal problems [28]. On the other hand, cement-rich mortars, that are typically dominating the field of inorganic matrix composites, result in further environmental pollution, with higher carbon dioxide emissions released into the atmosphere [29].

Given the advantages and limitations of advanced TRM as structural and seismic retrofitting solution for URM structures, this study aims at developing an innovative composite system comprising natural fibre textile reinforcement embedded into a lime-based mortar matrix (NTRM). The proposed system can potentially satisfy performance requirements and foster sustainable development. The rationale of using natural fibre textiles with lime mortars is based on the hypothesis that the resulting composite will combine the advantageous characteristics of: 1) natural fibres, which

are widely available and abundant, are characterised by excellent environmental credentials, and possess good mechanical properties [30]; and 2) lime mortar, which ensures vapour permeability, reversibility, excellent compatibility with masonry substrates [31] and provides, in parallel, a more sustainable solution to cement-rich mortars. Both constituents are cost-effective, hence the proposed composite system could be easily adopted by both developed and developing countries.

For such a new system to be developed, however, a series of scientific and technological challenges need to be addressed, ranging from the characterisation of the mechanical properties of the natural fibres, which are inherently very variable [32], to the assessment of the structural performance of the system, and the identification of simple design rules for its implementation. Despite the large amount of research on advanced TRM systems and their wide implementation in practical applications, there is still a lack of comprehensive understanding on the shear stress transfer mechanism between fibres, mortar and parent material. Textile properties and architecture, mortar matrix composition and properties, strengthening configuration (e.g. single or multi-layer TRM systems, full coverage or strengthening in strips) are key design parameters for TRM systems and their effect needs to be assessed for the development of optimal solutions. The complexity of the aforementioned issues is further increased given the novelty of NTRM systems and the very limited literature on the topic.

Although guideline documents on the mechanical characterisation of TRM systems have been recently published, their suitability to account for the unique behaviour of TRM comprising natural fibre textiles is yet to be assessed. In addition, the underlying philosophy of current design provisions for elements strengthened with advanced TRM need to be further evaluated to enable the uptake of NTRM strengthening solutions.

1.2. RESEARCH SIGNIFICANCE

1.2.1. Innovations of the Proposed Research

Although natural fibres are beginning to receive the attention of standardisation committees [33], the existing literature on the effectiveness of natural fibre TRM as a structural and seismic strengthening solution for masonry is still in its infancy. Available research has focused mainly on basic mechanical characterisation of composites and their constituents. However, the effectiveness of an externally bonded strengthening system in structural applications is governed by the bond between the strengthening system and the masonry substrate [34]. To the author's best knowledge, no systematic approach has been provided to date for the characterisation of the bond performance between NTRM and masonry systems, either through small-scale testing or through testing at a structural scale. The present study aims to fill this major gap in knowledge and provide additional insights on the scientific issues mentioned in the previous section through the implementation of a systematic and holistic multi-scale programme. The main expected outcomes are summarised below.

- Multiscale characterization of natural fibre textile reinforcements: key parameters for the design of efficient TRM systems to be identified and guidelines on minimum reinforcement ratios to be proposed.
- In-depth analysis on bond between NTRM and masonry: key design parameters to be identified and guidelines for testing and design to be recommended.
- Assessment of NTRM strengthening solutions at the structural level: the effectiveness of NTRM as seismic retrofitting solution for masonry walls to be examined through in-plane shear-compression cyclic testing and the performance of available design formulations to be assessed.

1.2.2. Broader Impact

The present research study addresses critical societal needs, as well as scientific and technological challenges that are of interest to academia, industry and code makers. The development of a strengthening solution for URM structures using natural fibres will: 1) provide an earthquake-resilient strengthening technology; 2) reduce the rehabilitation costs; and 3) satisfy the need for sustainability and sustainable development.

The combination of affordable, easily available and eco-friendly materials with lime-based mortars can be easily implemented in developing countries, where advanced composite systems are prohibitive due to the high material and installation costs. In addition, natural fibres are readily available and abundant and their use in civil engineering applications will create new opportunities for local industries, boost the local economy and foster innovation.

1.3. AIMS AND OBJECTIVES

The aim of this research is to develop an efficient yet cost-effective and “greener” seismic retrofitting solution for URM structures, and to identify key performance parameters, which can be used to inform the selection of suitable reinforcing materials and the design of optimal strengthening systems. The innovative retrofitting technique proposed herein includes the application of externally bonded composites comprising natural fibre textiles embedded in lime-based mortars as illustrated in **Fig. 1.2**.

The aim of the project is achieved through the following primary objectives:

1. Develop a better understanding of the mechanical performance of NTRM composites, through detailed characterisation of their constituents at all relevant scales (i.e. fibres, yarns, textile and mortar).
2. Investigate the performance of NTRM bonded to masonry substrates to assess the effectiveness of the system as strengthening solution for masonry and develop a better understanding of the shear stress transfer mechanism between fibres, mortar and parent material.

3. Evaluate the influence of different parameters on the tensile and bond behaviour of NTRM as well as the resulting failure modes and identify key design parameters.
4. Investigate and assess the effectiveness of NTRM systems for in-plane seismic retrofitting of URM walls.
5. Interrelate the results obtained at all scales, from material to structural level.
6. Assess the suitability of current testing methods and propose recommendations to account for the properties of natural fibre textiles.
7. Develop recommendations in line with European standards for the design of NTRM systems for in-plane shear strengthening of URM walls.

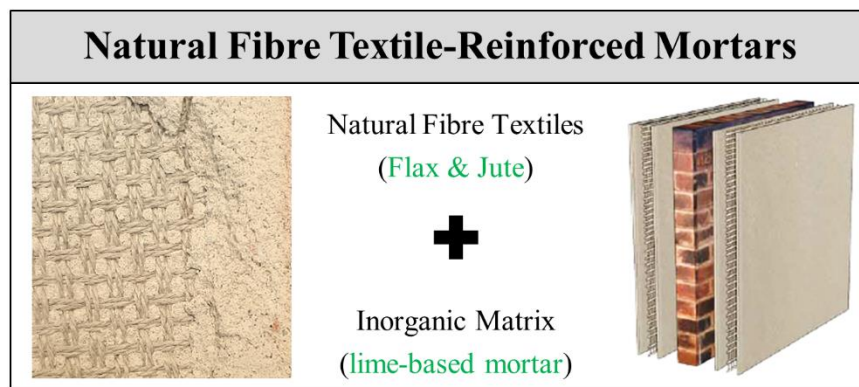


Fig. 1.2 Overview of the proposed externally bonded NTRM strengthening system.

1.4. THESIS LAYOUT

The present thesis is organised into seven Chapters. Chapters 1, 2, 3 and 7 are written in the traditional thesis format, while Chapters 4 - 6 consist of published (Chapter 4), submitted (Chapter 5 - under review) and planned for submission (Chapter 6) work in the form of stand-alone research journal papers. Complementary information as well as detailed results are given in the relevant appendices. A reference list is included at the end of each Chapter.

Chapter 2 discusses the state-of-the-art on TRM as a strengthening and seismic retrofitting solution for masonry. The tensile and bond behaviour of TRM to masonry are examined in detail to provide the required scientific background and form a basis of comparison with the behaviour exhibited by the NTRM systems examined in the subsequent chapters. Emphasis is given on the potential of using natural fibres as reinforcement in composites by presenting both advantages and current challenges and assessing the available research.

Chapter 3 presents the research methodology followed in this study and provides an overview of the experimental programme.

Chapter 4 (Trochoutsou et al. 2020) presents and discusses the first phase of the experimental programme. The mechanical characterisation of Flax- and Jute-TRM systems is presented in this chapter, along with a systematic analysis of the influence of key design parameters, such as textile architecture, number of TRM layers, and mortar overlay thickness. The results aim to highlight the

potential of Flax-TRM for strengthening applications. A discussion on critical mechanical reinforcement ratios for NTRM systems and recommendations for the design of NTRM composites are also included.

Chapter 5 (Trochoutsou et al. 2021) investigates the bond behaviour of Flax-TRM/masonry systems and examines the effect of critical parameters such as bond length, bond width, textile architecture and number of TRM layers. A detailed analysis on the strain distribution between multiple layers and across the width of the unbonded textile is also presented. The results, combined with the outcome of Phase 2, as presented in Chapter 4, aim to highlight the significant role of the textile architecture on the overall bond performance. Finally, recommendations for testing and design of NTRM systems are given in line with current existing procedures.

Chapter 6 investigates the effectiveness of Flax-TRM systems as a seismic retrofitting solution for masonry walls under in-plane shear loading. The performance of the adopted retrofitting solutions is analysed and discussed in terms of shear cracking, peak load, deformability and energy dissipation capacity, and an attempt is made at identifying the contribution of mortar and textile reinforcement. The predictions obtained from available design models are compared with the experimental results and commented upon, highlighting the need to credit the unique mechanical performance of NTRM.

Finally, *Chapter 7* summarises the main conclusions drawn from the three phases of this research study. Recommendations for design of NTRM systems for strengthening applications and future work are also provided.

2. LITERATURE REVIEW

2.1. FAILURE MECHANISMS OF URM

Masonry is an anisotropic material with distinct directional properties, mainly due to the presence of mortar joints, that act as planes of weaknesses [35]. This means that structural failures due to given loading conditions can rarely be attributed to a single cause. Hence, there is a need to develop a good understanding of the performance of URM elements under laterals so as to inform design and application of seismic retrofit solutions.

During seismic excitations, masonry walls are subjected to both in-plane shear and bending, as well as out-of-plane bending. Compressive axial load is normally transferred to walls from upper floors or from the roof. **Fig. 2.1** illustrates the most typical failure modes of masonry elements during seismic loading. For the dominant loading direction, the seismic action effects on unreinforced masonry include [36]:

- In-plane shear in shear walls.
- In-plane shear in beam-type elements (lintels).
- In-plane flexure in column- or beam- type elements (pillars and lintels).
- Out-of-plane flexure.

Failure modes are highly dependent on the geometry of the structure, the boundary conditions, the magnitude of the vertical loads, the characteristics of masonry units and mortar as well as of their interface [37]. While out-of-plane loading can be minimised by ensuring sufficient wall-diaphragm connections, the overall stability of the wall element is governed by its ability to effectively transfer the in-plane loads to the foundations.

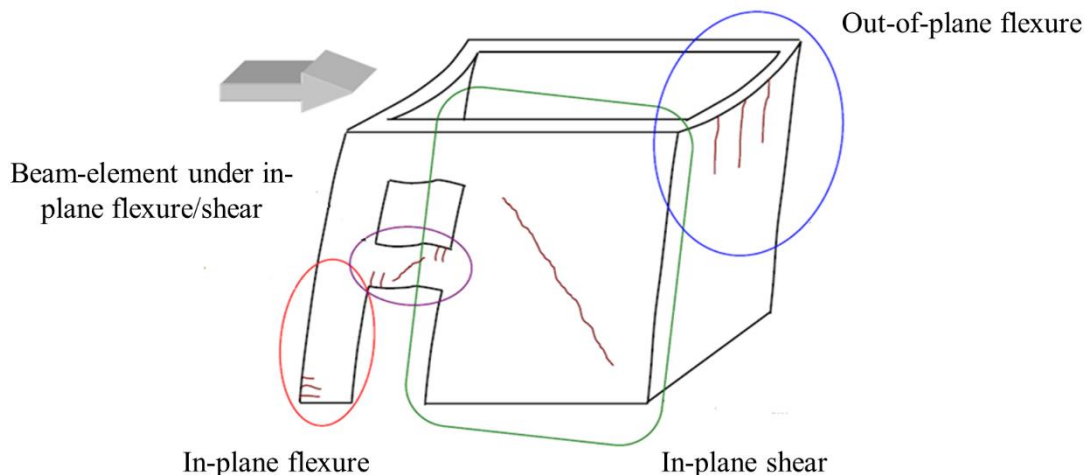


Fig. 2.1 Characteristic failure modes of URM during seismic actions (adapted from [2]).

Three main failure modes (**Fig. 2.2**) define the seismic behaviour of individual structural walls when subjected to in-plane loading include: 1) shear diagonal tension; 2) shear sliding; and 3) flexural failure (rocking, toe crushing) [6]. Diagonal tension occurs mostly in wall panels with high axial

load, low aspect ratio and low shear strength. It is characterised by the development of diagonal cracks following the mortar joints steps (when the masonry consists of high strength units and weak mortar) or involving both the joints and the masonry units (when masonry constituents are of relatively similar strength), with the latter resulting in a highly brittle failure. At low levels of axial load, and mainly when low quality mortars are used, shear sliding can occur and trigger the development of an horizontal crack along the bed joint, typically at the base of the wall. The third mode, rocking or flexural failure, takes place when bending moment to shear load ratio is high, in walls with high aspect ratio, and in cases in which masonry units have comparable strength to that of mortar, so that masonry behaves in a more homogenous manner. Flexural failure modes are characterised by crushing of the masonry and the development of rigid body rotation mechanisms at high displacements. Shear sliding and rocking can also develop simultaneously as the result of combined flexure and shear, which causes the URM elements to crack and concentrate the shear stresses in a smaller uncracked area [26].

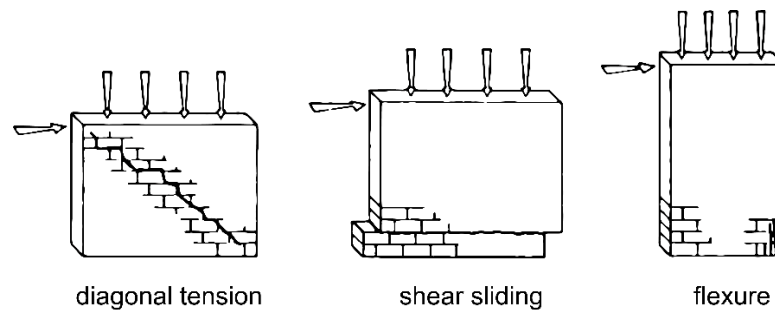


Fig. 2.2 Typical failure modes of URM walls under in-plane loading (adapted from [4]).

2.2. EXISTING STRENGTHENING TECHNIQUES FOR URM

A great number of strengthening and retrofitting solutions has been developed and experimentally tested by the research community. Depending on the materials used, the strengthening techniques currently in use for URM walls can be divided into two categories [11]: a) conventional techniques, which make use of traditional tools and materials and b) modern techniques, which mainly implement the use of advanced composite materials and application technologies.

2.2.1. Traditional Techniques

A detailed description of existing traditional techniques is beyond the scope of this thesis and extensive review documents can be found in the available literature [38-40]. The most commonly used techniques for masonry include surface treatment (mesh-reinforced shotcrete, ferrocement or reinforced plaster overlays), grout or epoxy injections to fill cracks and voids, reinforced concrete jacketing (with gunite or cast-in-situ concrete), crack stitching, external/internal post tensioning. Although these methods have been proven to increase shear and flexural strength and stiffness, as well as to provide monolithicity, they also have significant drawbacks [9,41], including:

- The mass of the structure is significantly increased due to the extra weight in case of RC jackets or shotcrete overlays, resulting in the modification of the dynamic response characteristics of the structure.
- Aesthetic requirements might be violated because of the increased thickness of the jackets and/or because of the reduction of the available free space.
- They require labour intensive and time-consuming procedures.
- They demand large quantities of raw materials (resulting in higher CO₂ emissions and energy consumption).

2.2.2. Modern Techniques

2.2.2.1. Fibre Reinforced Polymers (FRP)

During the last 30 years, the use of advanced composite materials has emerged as an alternative strengthening solution to address the aforementioned problems of conventional techniques. The use of externally bonded Fibre-Reinforced Polymers (FRP) represents the most popular modern strengthening solution and guidelines and recommendations for testing and design are already at an advanced stage of development [42,43, and the upcoming new versions of Model Code and EC2]. As briefly discussed in Chapter 1, the advantages offered by FRP include: a) high tensile strength in the direction of the fibres; b) low weight; c) excellent corrosion resistance; d) ease and speed of application; e) formability (sheets, laminates, strips); and f) minimal change to the structure's geometry. In strengthening applications, FRP have been shown to significantly improve the lateral strength and energy dissipation capacity, as well as the initial elastic stiffness of masonry elements [44].

However, FRP suffer from limitations related to the use of polymeric matrices, and to the overall performance when bonded to masonry substrates. The former mainly include [18,45]:

- High cost of resins and reinforcement fibres.
- Loss of strength when resins are exposed to high temperatures exceeding the glass transition temperature (70 – 80° C), thus possibly requiring expensive fire protection systems.
- Health and safety issues for the applications workers, since resins may cause irritation to eyes and skin and be harmful through inhalation.
- Non-applicability on wet surfaces or at low temperatures.
- Lack of vapour permeability/transpirability.
- Irreversibility. Reversibility is especially important in the rehabilitation of historic buildings, where the use of epoxy resins is not allowed.
- Non-recyclability.
- Difficulty to conduct post-earthquake assessment behind FRP jackets.

Additionally, the high incompatibility between the stiffness of the two materials is likely to result in brittle debonding failure modes in the FRP-strengthened system and limit the development of

adequate deformations and residual lateral capacity, thus compromising structural integrity against concurrent out-of-plane loading effects.

2.2.2.2. Textile-Reinforced Mortars (TRM)

To address the problems arising from the use of FRP materials, the polymeric matrix can be replaced with a fine-grained inorganic binder, such as a cementitious mortar. The granulometry of the mortar, however, impedes the full impregnation of the fabric and this leads to the development of a weak bond between the inorganic matrix (mortar) and the fibre sheet.

Textiles with an open mesh, grid-like configuration can improve bond conditions and ensure a good mechanical interlock within the inorganic mortar. Textile-Reinforced Mortar (TRM) composites combine the benefits of both conventional and modern techniques [11] and have emerged as an excellent alternative strengthening and retrofitting solution to FRP systems, especially for masonry applications [46]. In the literature, TRM are also referred to as Fibre-Reinforced Cementitious Mortar (FRCM), Textile-Reinforced Concrete (TRC - used mainly for precast elements with size of aggregates more than 2 mm), or Steel-Reinforced Grout (SRG) when steel meshes are used. RILEM TC 290-IMC has recently introduced the use of the term “Inorganic Matrix Composites” to encompass the different types of textile reinforced mortars. Advanced TRM composite systems, which have also been considered as an evolution of ferrocement [47], consist of:

- i) High strength structural fibre filaments assembled in yarns or rovings (woven, knitted or even unwoven) arranged in two or more directions, usually to form a two-dimensional textile (typical textiles are shown in **Fig. 2.3**);
- ii) Inorganic matrices (cement-based, lime-based or geopolymer mortars), which are responsible to protect the fibres and transfer stresses between the concrete or masonry substrate and the textile, and between the textile layers.

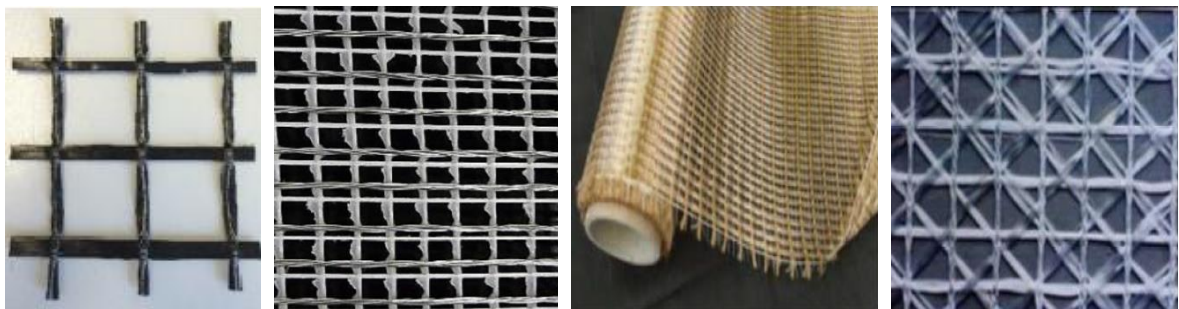


Fig. 2.3 Typical examples of textiles used in TRM systems: (a) Bi-directional carbon fibre grid, (b) Unidirectional steel wires (SRG), (c) Bi-directional Paraphenylene-Benzobisoxazole (PBO) fibre grid and (d) four-directional Glass fibre grid.

As stated in Chapter 1, TRM have been used successfully in a range of strengthening applications. A detailed literature review on their effectiveness as strengthening solutions, and on their potential, can be found in [48] for concrete structures, in [49] for masonry structures and in [50] for masonry-infilled RC frames. Selected case studies are also presented in [25].

The rapid uptake of TRM has been enabled by the significant effort of different national and international committees, which has led to the development of key testing protocols and design documents [51-55]. Standardised procedures for the uniaxial tensile characterisation of TRM systems have been proposed by the International Code Council-Evaluation Service [51] and RILEM Technical Committee TC 232-TDT [52], while test methods to assess bond between TRM/masonry systems have been recently published by RILEM TC 250-CSM [54]. The concerted effort of ACI committee 549 and RILEM TC 250-CSM has also resulted in the development of a unified document for the repair and strengthening of masonry structures using externally bonded TRM/SRG [56].

2.3. POTENTIAL OF NATURAL FIBRE TRM

2.3.1. Need for Sustainability in Structures

The construction industry has a significant impact on the environment [57] and most technological and production processes are associated with high embodied energy and material consumption and result in significant carbon dioxide emissions and waste generation. Ambitious targets have been set by regulatory bodies towards the reduction of energy consumption and carbon footprint and the European Union is committed to cut emissions by 80% by the end of 2050 [58]. Strengthening and rehabilitation of existing buildings with more sustainable materials would assist in achieving these goals by addressing the following areas:

- Energy Use: Buildings account for 40% of the total energy use, 90% of which is consumed during their lifetime and the remaining 10% is linked to materials, construction and demolition waste, both in developed and developing countries [59].
- CO₂ emissions due to cement production: The increase in total energy use results in higher carbon dioxide emissions released into the atmosphere, with the production of ordinary Portland Cement being highly energy intensive: for 1 ton of OPC produced, there is 1.25 tons of CO₂ released [29], while 4 billion tons of CO₂ are annually generated due to cement production [60].
- CO₂ emissions due to FRP production: Carbon footprint is increased by the production/processing and use of advanced fibres as well as the use of petroleum based matrix materials [61,62].
- Environmental problems due to disposal of advanced fibres: Advanced fibres are not recyclable, require hundreds of years to degrade and heavy metals and other additives are released into soil and groundwater during degradation [63], causing disposal and environmental problems [28].

2.3.2. Natural Fibre Properties and Behaviour

Natural fibres have attracted the interest of both academia and industry as they can satisfy performance and sustainability requirements, while contributing towards a “greener” and more sustainable development. Composites reinforced with natural fibres, known as “green”- or “bio”-composites, are stated to represent a “formidable adversary” of fossil fuel-based composites [8], with

sustainability credentials superior to glass fibre reinforced composites [64] and the potential to substitute advanced composites in applications that do not require significant load demands [65][66].

Natural fibres can offer several environmental benefits when compared with advanced synthetic fibres [32, 63,67-69]:

- ✓ Natural fibres are a renewable resource. They can be replenished with time naturally, without any human intervention and can regrow within a short period of time. Synthetic fibres, on the contrary, lead to depletion of natural resources.
- ✓ Natural fibres and their composites (if proper matrix is used) can be 100% biodegradable and recyclable at the end of their life cycle.
- ✓ Natural fibres are carbon neutral, i.e. they absorb the same amount of carbon they contain.
- ✓ The embodied production energy of natural fibres is 10 times less than that of synthetic fibres and natural fibre composites require 5 times less energy for production than synthetic composites [70].

In addition to their outstanding sustainability credentials, natural fibres have many advantages over synthetic fibres, especially glass fibres, making them potential candidates for structural applications:

- ✓ Lower cost: Flax, jute, sisal and hemp can compete with E-glass fibres in terms of cost per weight and per unit fibre length required to resist a given tensile load (**Fig. 2.4**). This is mainly due to the favourable combination of lower density and moderate tensile strength of natural fibres [8,28].
- ✓ Availability and abundance: Natural fibres are widely available in most countries [71], with developing countries producing a big part of the total world production. For instance, India produces annually 6 million tons of natural fibres, compared to 25 million tons of annual worldwide production [72]. The largest natural fibre production industries, along with annual production, are shown in **Table 2.1**.
- ✓ Light weight.
- ✓ Breathability and better thermal and acoustic insulation properties [73].

Table 2.1 Natural fibre producer countries and annual fibre production (data obtained from [74]).

Fibre Source	World's leading producer	World production (in 10 ³ tons)
Flax	Europe	841
Jute	India	2,000
Hemp	China	215

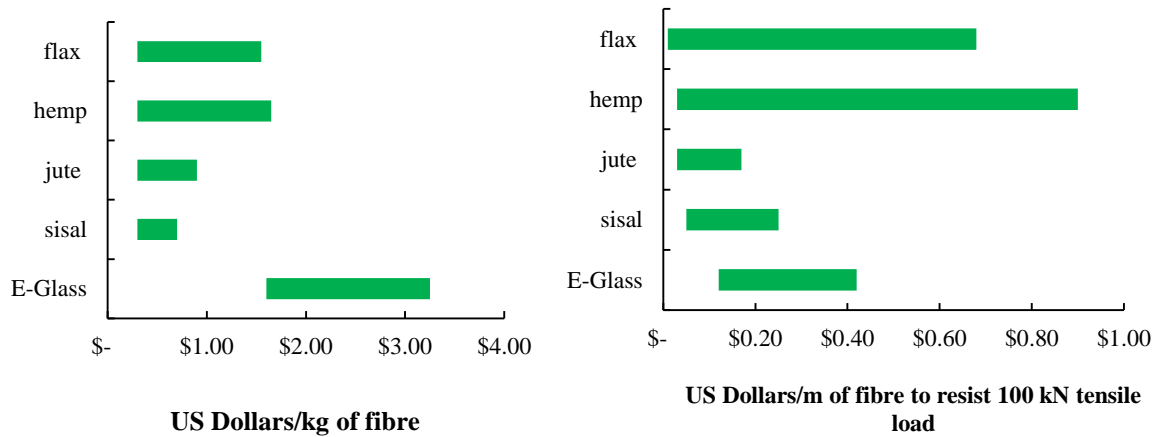


Fig. 2.4 Cost per weight of natural and E-Glass fibres (left); cost per unit length required to resist 100 kN tensile load (right).

Natural fibres are, by definition, fibres that are not synthetic or man-made, and according to their origin, can be divided into three general categories: animal, vegetable and mineral fibres [57]. Vegetable fibres (also referred to as plant or cellulosic fibres) are derived from different parts of plants and their main component is cellulose, whereas animal fibres are protein-based. Mineral fibres, mainly asbestos, are nowadays forbidden in many countries due to their carcinogenic effects, despite having been used extensively in the past [75].

Plant fibres are characterised by better mechanical properties (strength and stiffness), lower cost and are more readily available than most animal-based fibres [71,75], both as raw materials and products (textiles, ropes, composites). For these reasons, plant fibres (hereafter referred to as natural fibres) have attracted the interest of both academia and industry and have been considered as suitable alternative reinforcement for structural composites [70].

Natural fibre is a composite material itself, with a cellular structure, consisting of three basic chemical components: cellulose, hemicellulose and lignin [71]. Cellulose is the major component, representing roughly 60-80% of the natural fibre, while the content of hemicellulose and lignin falls between 15-20% and 5-10%, respectively. From a structural point of view, the cellulose provides the fibre with tensile strength, stiffness and stability, hence natural fibres rich in cellulose content (typically bast fibres such as flax, hemp and jute) have higher mechanical performance [76], while the lignin is the matrix in which the reinforcement (cellulose) is embedded, and the hemicellulose acts as bonding agent between cellulose and lignin (**Fig. 2.5**).

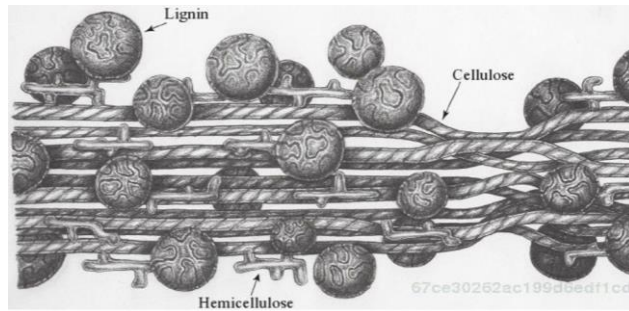


Fig. 2.5 Chemical composition of natural fibre (after [77]).

The chemical composition of each natural fibre and the concentration of each component are of crucial importance, since they affect the mechanical properties and the bond behaviour between the natural fibres and the surrounding matrix (when natural fibres are used in composite systems). In addition, the chemical composition may be affected by several other parameters, including moisture content, geographical location and climatic conditions, soil quality, harvesting duration, extraction and fibre processing [62,78]. All of these factors play a critical role in selecting the most suitable fibre type or system for a given application.

Table 2.2 shows typical mechanical properties of natural fibres, along with those E-glass fibres to enable meaningful comparisons. Despite the inherent high variability of natural fibres, it can be observed that:

- ✓ Bast fibres have higher strength and stiffness than leaf fibres (sisal fibres) due to the higher amount of cellulose content.
- ✓ Natural fibres have good strength and stiffness, with flax fibres exhibiting tensile strength and Young's modulus values very close to those of E-glass fibres.
- ✓ Natural fibres are characterised by low density, which when combined with the good tensile strength and stiffness, results in comparable specific mechanical properties (strength and stiffness divided by density) to those of E-glass fibres.
- ✓ Elongation at failure for natural fibres is comparable to that of E-glass fibres.

Table 2.2 Mechanical properties of natural and E-glass fibres (obtained from [71,75,79]).

Fibre Type	Tensile Strength (MPa)	Density (kg/m ³)	Young's modulus (GPa)	Elongation (%)	Specific Tensile Strength (MPa/g cm ⁻³)	Specific Young's modulus (GPa/g cm ⁻³)
Flax	345 - 2000	1380	75 - 90	1.2 - 3.2	475 - 1500	54 - 65
Jute	270 - 800	1230	35 - 60	1.5 - 3.1	220 - 650	28 - 49
Hemp	320 - 1110	1350	55 - 90	1.6 - 4.5	237 - 825	41 - 67
Sisal	300 - 855	1200	10 - 38	1.9 - 6	250 - 720	8 - 32
E-Glass	2000 - 3000	2500	70 - 76	1.8 - 4.8	800 - 1200	28 - 30

2.3.3. Challenges

The use of natural fibres in structural applications, although promising, is still limited due to the following open issues: 1) Variability of fibre properties, 2) Durability and 3) Standardisation and market acceptance.

2.3.3.1. Variability

As a result of the high variability in chemical composition, a high degree of variability in mechanical properties is expected among different types of fibres, as well as in different parts of the same fibre type. Although this issue could potentially be addressed by the implementation of advanced processing methods [32], these would inevitably add costs and affect their environmental credentials. Hence, the variability of natural fibres and their high anisotropy represent a limiting factor to the further development, implementation and commercialisation of natural fibre composites, as their mechanical properties are difficult to control and characterise.

2.3.3.2. Durability

Two major mechanisms can cause degradation of natural fibres in a TRM composite system: moisture absorption and exposure to a highly alkali environment.

The large amount of hydroxyl groups in the fibre cell wall attracts water molecules, rendering natural fibres highly hydrophilic. Natural fibres have a tendency to adjust to the surrounding environment and to keep a moisture equilibrium, by absorbing or losing moisture. During this process, fibres swell or shrink, thus altering fibre dimensions, permeability and stiffness [8]. Moreover, moisture uptake may have a detrimental effect on the composite integrity [80] as it compromises the bond that can be developed between the natural fibre and the matrix, either polymeric or inorganic. Polymers are hydrophobic and as a result a weak interfacial bond develops between a polymeric matrix and natural fibres [81]. When embedded in inorganic matrices, natural fibres absorb the inherent matrix moisture and swell, leading to cracking as the matrix is not strong enough during the first days of curing to prevent the expansion. Subsequently, the fibres adapt to the drier environment and shrink, leaving voids that affect the interfacial bond (**Fig. 2.6**).

The high alkalinity of cementitious matrices causes additional problems to the integrity of natural fibres as this environment can lead to dissolution of the lignin, hemicellulose and finally cellulose (**Fig. 2.7**), resulting in the complete degradation of the natural fibre [71]. In parallel, hydration products, mainly C-S-H and portlandite migrate to the fibre structure and cause fibre mineralization, which leads to fibre embrittlement and to significant loss of stress and strain capacity [67,71].

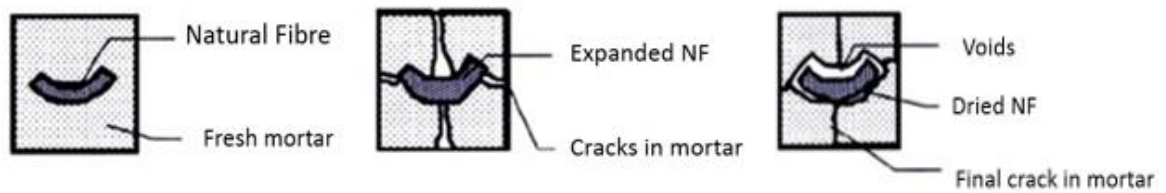


Fig. 2.6 Moisture absorption effects in inorganic composites (adapted from [82]).

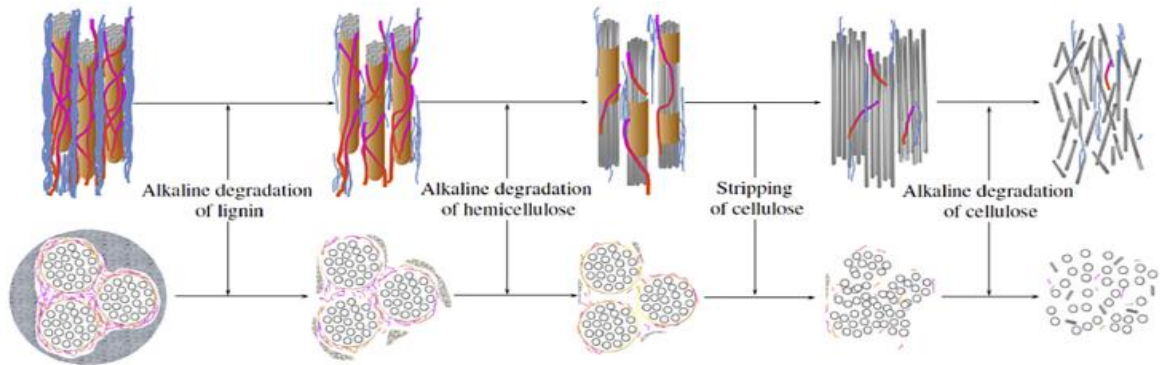


Fig. 2.7 Natural fibre degradation in highly alkaline environments (adapted from [83]).

2.3.3.3. Standardisation and Market Acceptance

To date, there are no universally accepted design codes or standards for the assessment and testing of natural fibre composites. As discussed in the following, research on the performance of these novel composites is still limited and more work is required to better understand their effectiveness in structural applications, as well as their long-term performance.

2.3.4. Natural Fibre Composites for in Structural Applications

The concept of using natural fibres in structural strengthening applications is not new. In ancient Egypt 3000 years ago, straw was used to reinforce sun-dried blocks made of mud, and horsehair was used to reinforce mortar for building purposes [84]. Modern natural fibre composites (“biocomposites” or “green composites”) comprise: i) Short dispersed natural fibres within cementitious materials or concrete (Natural Fibre Reinforced Cement or Concrete – NFRC [71]) or within geopolymers (Natural Fibre Reinforced Geopolymers or Geocomposites – NFRG [84]); ii) Fabrics combined with polymeric matrices (Natural Fibre Reinforced Polymers – NFRP [85]); and iii) Textiles combined with inorganic matrices (Natural fibre Textile-Reinforced Mortars – NTRM [86]). In addition, natural fibres have been used for the reinforcement of soil blocks [87] as well as the production of geo-textiles [88].

To date, NFRC composites have been investigated extensively for structural and non-structural members in building applications, with most studies focusing on durability issues [71]. NFRP composites have been recently examined as a flexural strengthening solution for masonry elements [89] as well as RC beams [72], providing encouraging evidence on their potential for structural applications.

Research on the use of NTRM systems is very limited and key scientific and technological needs must still be addressed (see Section 1.2.1). Available work on TRM and NTRM addressing the objectives of the present study is reviewed in the following section, while a more critical assessment of key design aspects is included in the relevant Chapters (Chapters 4-6).

2.4. PERFORMANCE OF TRM/NTRM - MASONRY SYSTEMS

2.4.1. Tensile Behaviour

The tensile behaviour of TRM systems depends on the physical and mechanical properties of the constituent materials (i.e. textile type/architecture and inorganic matrix) and the quality of the bond at the fibre/matrix interface. The test methodology adopted for its characterisation also plays a key role, as different testing configurations can promote different local failure mechanisms and lead to a different global response [90].

Under uniaxial tension, the behaviour of TRM is characterised by three stages as shown in **Fig. 2.8** and described below [90]:

i. Uncracked stage: The composite remains uncracked and the load is being carried by the inorganic matrix. The stiffness of the composite is governed by the stiffness of the matrix. This stage ends once the tensile strength of the mortar is reached and the first crack is formed.

ii. Crack development stage: New cracks in the mortar matrix appear at increasing tensile loads and a significantly reduced stiffness is observed. The textile fibres bridging the cracks are mobilised and work together with the mortar, which provides a tension stiffening effect. The stiffness of this second stage, as well as the level of strain that can be mobilised in the composite and the resulting crack pattern (crack spacing and width), depend on the bond between the textile and the surrounding mortar, the textile type/architecture, the reinforcement ratio and the mortar tensile strain as well as the presence of short dispersed fibres in the mortar. This stage ends when cracking is stabilised and no further cracks are formed.

iii. Post-cracking stage: the load is only sustained by the textile and the response is linear up to failure. During this stage, the existing cracks open and the stiffness of the composite is comparable to the textile's stiffness. If the textile is well anchored, failure occurs due to fibre rupture.

However, rupture of some of the filaments within the yarns may occur during the crack development stage, thus resulting in a reduced stiffness in the third stage. Moreover, depending on the adopted gripping method and on the quality of the bond between the TRM constituents, fibre slippage within the matrix may occur throughout stages 2 and 3, thus compromising the full exploitation of the textile strength [91]. The degree of mortar penetration within the yarn cross-section, which can be limited by the relative size of the lime or cement grains and the spacing between the individual filaments [92], is also an important factor as it can result in only the outer filaments being well anchored within the matrix and in the development of a “telescopic failure”, i.e. relative slip between the outer and inner filaments [93], as shown in **Fig. 2.9**.

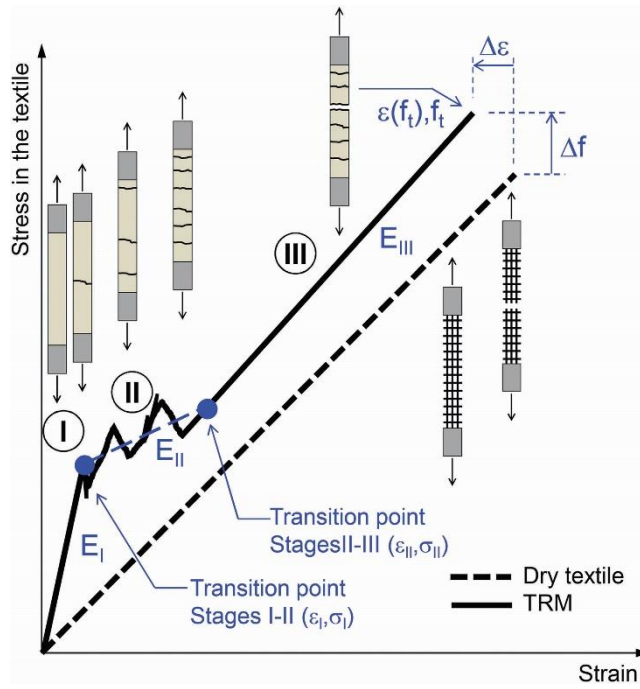


Fig. 2.8 Stress-strain response of TRM systems under uniaxial tension [56].

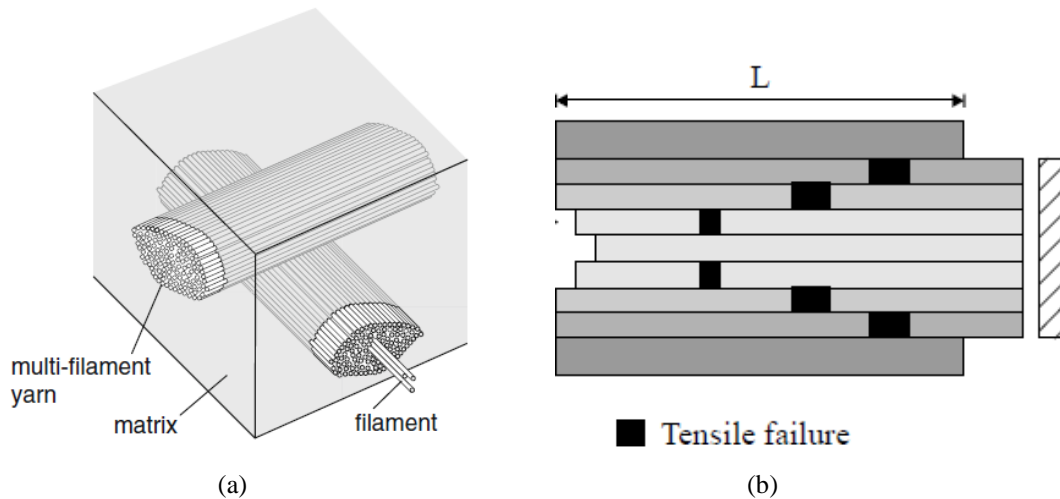


Fig. 2.9 (a) Fibre rovings of a textile embedded in the inorganic matrix (adapted from [94]); (b) Telescopic failure mechanism [93].

Coating or pre-impregnation of the textile with organic resins can be used to enhance the mechanical bond strength between fibres and mortar and minimise slippage between the filaments [95]. As a result, a better stress redistribution can be achieved and a more ductile behaviour attained [92]. However, the use of epoxies would have a negative impact on the sustainability credentials of natural fibres, and pre-impregnated textiles in advanced TRM have not shown to be as effective when bonded to curved masonry substrates [96].

Table 2.3 summarises the main findings from available literature on the mechanical characterisation of NTRM systems, along with details of the investigated NTRM systems and parameters.

Table 2.3 Summary of research studies on the mechanical characterisation of NTRM systems

Research Publication	Fibre Type	Inorganic Matrix	Examined Parameters	Main Remarks
Asprone et al. [97]	hemp	lime-based mortar	coating (latex, resin); number of NTRM layers (4 and 6); mesh size (10 and 20 mm)	Higher reinforcement ratio, either through denser meshes or addition of layers, improves flexural strength. Resin coating is more effective than latex, although composites with latex coated textiles exhibited significantly larger strains than with non-coated textiles.
Olivito et al. [98]	flax sisal	lime-based mortar; lime-based grout	composite thickness (5 and 8 mm).	Higher mechanical properties were achieved by Flax-TRM. Higher reinforcement ratio results in a more ductile behaviour and higher composite strength. Lime-based mortar is more suitable to be used as matrix, due to its lower alkalinity.
Cevallos and Olivito [99]	flax sisal glass	lime-based grout	number of NTRM layers (1-3)	Sisal-TRM showed poorer performance than Flax-TRM even at higher reinforcement ratios. High linear density yarns may hinder mortar penetrability. The reinforcement ratio significantly affects the crack pattern. Higher strength values were exhibited by glass-TRM, albeit at the expense of strain.
Codispoti et al. [69]	flax hemp sisal jute coir	cement-free mortar	fibre type	The best mechanical properties were exhibited by Flax-TRM, followed by jute and hemp, and lastly by sisal-TRM. Coir textiles did not develop values of strength or stiffness suitable for further development of TRM systems.
Mercedes et al. [100]	flax hemp sisal cotton	lime-based mortar	coating (epoxy or polyester)	The highest mechanical strength was achieved by flax and hemp TRM. Cotton-TRM had the largest elongation capacity. Epoxy coating significantly improves the exploitation of the textile's tensile strength, resulting in composites with mechanical properties comparable to those of advanced TRM.
Ferrara et al. [101]	flax	lime-based mortar	number of NTRM layers (1 and 2)	Higher reinforcement ratio does not significantly affect the mechanical performance or the bond at the fibre/mortar interface.
de Carvalho Bello et al. [102]	sisal	lime-based	impregnation of yarns	Sisal-TRM composites were characterised by moderate strength and exhibited ductile behaviour. Clamping of the bare textile instead of the composite should be implemented to prevent slippage.

The most studied natural fibres include flax, jute, sisal and hemp, while all studies used a lime-based mortar, due to its reduced alkalinity and expected less pronounced degradation of the natural fibre properties. Although a similar tensile behaviour to that of TRM systems has been observed for NTRM systems, two distinct differences have been documented in the studies presented herein: a) the mortar can significantly contribute to stress redistribution through crack formation, resulting in a highly ductile behaviour and the development of large deformations during the crack development stage, which is not always distinguishable from the 3rd stage; and b) a fourth “softer” stage can be identified as a result of the progressive rupture of the yarns. No slippage phenomena were developed in any of the tested composite systems, apart from cases where excessive compression was applied in the grips [102]. All studies provide encouraging evidence on the potential of flax fibre lime-based composites, as they developed strength and stiffness values suitable for strengthening applications. In addition, reinforcement ratio and textile architecture were found to affect significantly the overall

mechanical performance of NTRM. Studies have also shown that the use of coating or impregnation methods can improve fibre-to-mortar adhesion and lead to a mechanical performance equal to or greater than that of advanced TRM systems [100].

2.4.2. Bond Behaviour

The bond behaviour of TRM systems to masonry substrates involves complex stress-transfer mechanisms that can be developed both at the textile/matrix and at the composite system/substrate interface. As a result, a variety of failure modes have been observed for different TRM systems, depending on their physical/mechanical properties, dimensions of the bonded area, reinforcement ratio and additional parameters related to the adopted test setup (e.g. single-lap or double-lap shear tests). The following classification has been proposed by RILEM TC 250 – CSM (**Fig. 2.10**) [54]:

- A.** Cohesive debonding within the masonry substrate. It usually occurs in TRM systems with a strong matrix bonded to weak masonry substrates. To date this failure mode has only been reported in the case of Steel Reinforced Grout (SRG) systems.
- B.** Debonding at the composite system/substrate interface. It takes place when smooth surfaces are strengthened, or due to improper installation.
- C.** Debonding at the textile/matrix interface. It usually occurs when a dense fabric mesh is used, thus hindering good penetration of the matrix within the textile mesh openings.
- D.** Slippage of the textile within the mortar matrix with or without being coupled with mortar cracking. It usually occurs due to the poor bond between the textile and the mortar.
- E.** Tensile rupture of the textile either outside (E1) or inside (E2) the bonded area, when sparse meshes or weak relatively textiles are used.

Failure modes A-C are typically characterised by a linear behaviour in their load-slip response up to the debonding load, followed by a decreased slope indicating progressive debonding up to complete loss in load-carrying capacity [103]. Failure mode D is characterised by a similar behaviour, but after the peak load is attained, a softer decrease in the load-slip response is observed, indicating the progressive loss of bond between fibres and mortar, followed by an additional stage of constant load due to friction. Failure mode E is characterised by drops in load upon the attainment of the maximum strength, indicating the progressive rupture of individual yarns.

Combined failure mechanisms have also been reported [103], and issues related to “telescopic” failure modes, as explained in the previous section, may further affect the overall bond performance. The complexity of the bond behaviour is further increased by the development of non-uniform strain distributions along the textile during testing, driven by misalignments due to manufacture errors or when positioning the specimen within the testing rig. As a result, even in systems failing due to textile rupture, a reduced exploitation of the textile’s strength is normally observed.

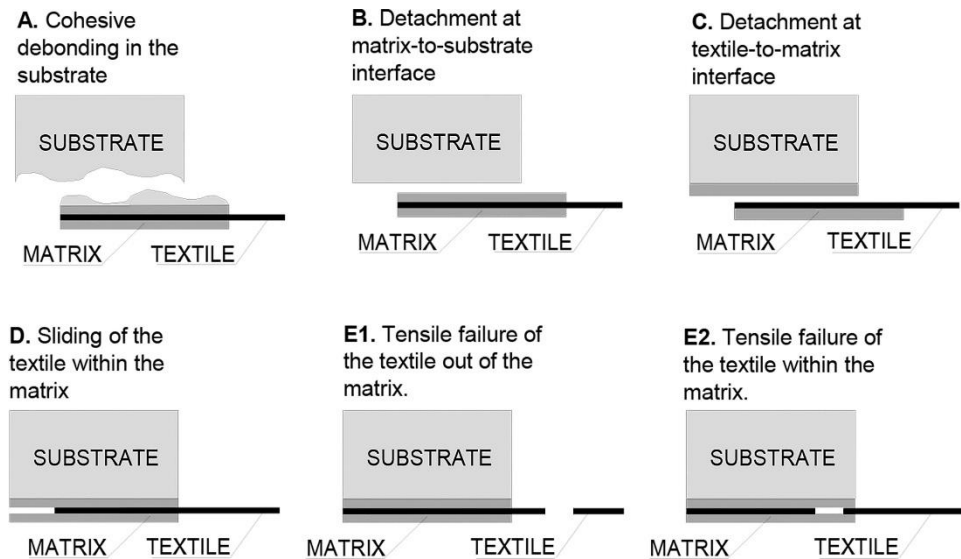


Fig. 2.10 Failure modes observed in TRM/SRG systems (adapted from [54]).

The main outcomes of available studies on the bond performance of NTRM/masonry systems are summarised in **Table 2.4**. With the exception of the study performed by Olivito et al. [104], bond tests were performed for basic characterisation and only the values of debonding load and failure mode were reported, with no further investigation or in-depth analysis of the shear stress transfer mechanism. However, all results provided encouraging evidence that when an effective bond length is employed, full exploitation of the natural fibre textile strength can be achieved and a good composite action between the composite system and the substrate can be developed. This is a superior advantage of NTRM/masonry systems against advanced TRM systems, as no premature debonding occurred to compromise their performance (also evidenced by a comparative analysis between bonded Flax- and PBO-TRM to masonry substrates [104]).

2.4.3. In-plane Shear Performance of URM Retrofitted with TRM/NTRM Systems

The in-plane shear performance of masonry walls retrofitted with TRM systems is highly dependent on the geometry of the specimen, the boundary conditions, the magnitude of the axial loads, the properties of the TRM and the textile architecture as well as the TRM strengthening configuration (single- or double-sided jackets applied in single or multiple layers, full coverage of surface or application in strips).

These aspects are difficult to reproduce in a laboratory environment and all the in-plane shear mechanisms involved can be captured only with in-plane shear-compression tests. Cyclic loading tests are also preferable when assessing the seismic performance of strengthening solutions [105]. Available literature on the in-plane behaviour of TRM strengthened walls, however, includes mainly monotonic diagonal compression tests, as they are easier to implement and can provide information on the shear strength/strain and the shear modulus [106]. Although TRM systems have been shown to provide significant strength enhancement (even up to 5-6 times of un-strengthened walls), their main advantage is the significant increase provided in terms of deformability (even up to 13 times),

ductility and energy dissipation capacity [17] and in the ability of the TRM system to promote distributed cracking and control the development of brittle failure modes, by ensuring the structural integrity of the wall [107]. Direct experimental analyses between TRM and FRP showed the better performance of the former with regards to deformation capacity [17].

The performance of NTRM systems as a retrofitting solution for URM elements has yet to be assessed. As it is shown in **Table 2.5**, encouraging evidence was provided by the two available studies on the topic. The results of these studies highlight the potential of NTRM systems in contributing to shear strength increase (up to 5 times) and promoting a pseudo-ductile behaviour of both tuff and clay masonry, accompanied by multiple cracking and rupture of yarns, without any visible sign of debonding. Reported values of strength and deformation capacity of NTRM-retrofitted elements are in line with those strengthened by advanced TRM systems.

A detailed review and assessment of design models for URM walls strengthened with TRM is included in Chapter 6.

Table 2.4 Summary of research studies on the bond performance of NTRM/masonry systems.

Research Publication	Fibre Type	Inorganic Matrix	Examined Parameters	Main Remarks
Olivito et al. [104]	Flax PBO	lime-based	Bond Length (50 and 100 mm)	The higher stiffness and lower strains of PBO fibres caused composite debonding from the masonry substrate leading to sudden failure. In contrast, Flax-TRM failed due to mortar cracking and tensile rupture of the yarns, with high exploitation of the textile strength. Both bond lengths examined ensured a good adhesion of the Flax-TRM and the substrate as no debonding occurred.
de Carvalho Bello et al. [102]	sisal	lime-based	impregnation of yarns	Failure occurred due to tensile rupture of the yarns and no debonding or sliding were observed. Yarn impregnation can result in a more uniform strain distribution. A bond length of 260 mm was used and proved adequate to ensure good adhesion of the sisal-TRM to masonry.
Ferrara et al. [108]	flax	lime-based	-	Failure occurred due to tensile fibre rupture and good adhesion at the composite/masonry interface was observed. A bond length of 260 mm was used and proved adequate to ensure good adhesion of the flax-TRM to masonry.

Table 2.5 Summary of research studies on the in-plane shear performance of NTRM/masonry systems.

Research Publication	Fibre Type	Inorganic Matrix	Examined Parameters	Main Remarks
Menna et al. [109]	hemp	pozzolanic-based mortar; lime-based mortar	anchor system; masonry substrate (tuff, clay brick)	An increase of maximum shear strength capacity by 2-3 and 5 times for tuff and clay masonry, respectively, was achieved. Failure mode was characterised by tensile rupture upon mortar crack formation. No premature debonding was observed. The use of the pozzolanic mortar resulted in a more ductile behaviour.
Ferrara et al. [108]	flax	lime-based	number of TRM layers (1-2)	Increase of the maximum shear strength by 1.3 times. Failure mode was characterised by tensile rupture upon mortar crack formation. No debonding was observed.

2.5. CONCLUDING REMARKS

Existing literature, albeit limited, has highlighted the potential of NTRM to be used in strengthening applications. NTRM exhibit adequate strength and deformability, as well as high ductility, a property that is particularly favourable for seismic strengthening applications. The combination of good relative strength and stiffness of the NTRM constituents and of the NTRM/masonry system has been shown to allow high exploitation of the textile strength before the occurrence of premature debonding. Having in mind their excellent environmental credentials, NTRM systems seem to offer a valid alternative to advanced TRM systems currently available in the market.

All studies, however, have focused on the investigation of the mechanical performance of NTRM systems and their durability, rather than on the bond and effectiveness of these systems as a seismic retrofitting solution for masonry applications. Fibre type, textile architecture and reinforcement ratio (through the addition of NTRM layers or through the use of thicker mortar overlays) were identified as key design parameters for the development of effective NTRM systems. Flax fibres were reported to be the most promising reinforcing solution for strengthening applications, followed by jute and hemp. Bi-directional textiles have been shown to have better bond behaviour due to the presence of transverse yarns as they provide additional mechanical anchorage. Denser meshes can result in lower bond properties, while high linear density yarns may suffer from limited penetrability and hence result in failure modes governed by detachment at the textile/mortar interface, especially when high reinforcement ratios are used. Moreover, while the reinforcement ratio significantly affects the crack pattern, the overall composite performance, the failure mode and the ductility, recommendations on critical reinforcement ratios are limited to geometrical ratios without taking into account the TRM constituent mechanical properties. Finally, the bond performance of any NTRM system, which is a function of the dimensions of the NTRM bonded area (length and width), is yet to be determined and assessed.

All of the aforementioned parameters need to be further investigated to develop a comprehensive understanding of the behaviour of natural fibres combined with inorganic matrices at composite and structural level. In addition, although testing protocols and design recommendations are available for advanced TRM, their suitability for NTRM needs to be assessed.

3. RESEARCH METHODOLOGY

3.1. OVERVIEW

The experimental programme conducted as part of this study consists of three interrelated phases as summarised in **Fig. 3.1** and detailed below.

Phase 1: Development and mechanical characterisation of natural-fibre TRM systems, through the implementation of a multi-scale approach.

Test methodology: direct tensile tests on single natural fibres, yarns, textiles and NTRM composites.

Key examined parameters: fibre type, textile architecture, number of TRM layers, mortar overlay thickness.

Phase 2: Investigation of the bond performance of the NTRM systems selected in Phase 1 as most suitable for the strengthening of masonry structures.

Test methodology: single-lap shear bond tests.

Key examined parameters: bond length, bond width, textile architecture, number of TRM layers.

Phase 3: Investigation of the structural performance of the NTRM systems selected in Phase 2 as a seismic retrofitting solution for unreinforced masonry against in-plane loading actions.

Test methodology: in-plane shear-compression tests under quasi-static cyclic loading.

Key examined parameters: strengthening configuration, number of TRM layers.

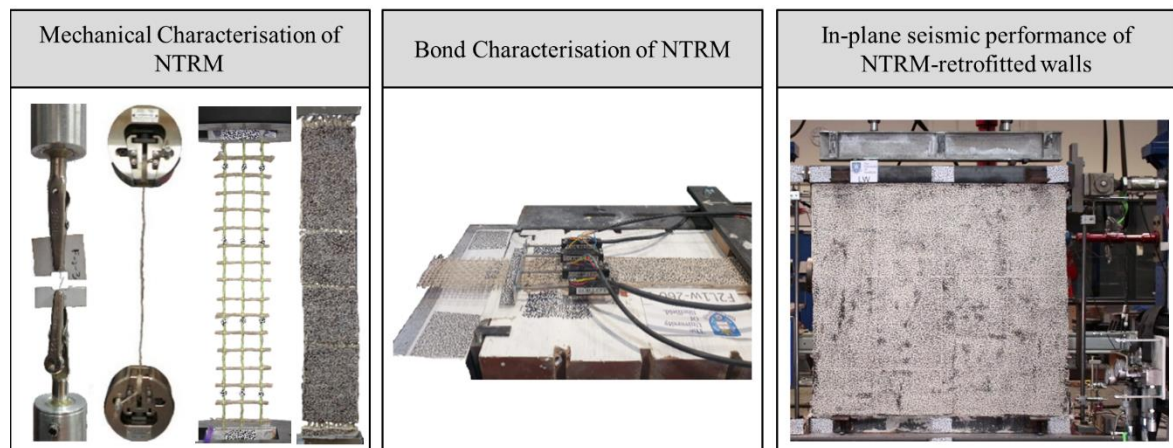


Fig. 3.1 Overview of experimental programme.

3.2. BRIEF DESCRIPTION OF EXPERIMENTAL PROGRAMME

3.2.1. Phase 1

The first phase of the experimental programme was designed to: a) characterise the mechanical properties of the NTRM systems at different scales; b) identify relationships across the different scales; and c) identify the key design parameters of NTRM systems and provide recommendations.

Two types of flax (F1 and F2) and one type of jute (J) textiles (**Fig. 3.2**) were examined as reinforcing materials, while the same lime-based mortar was used for all types of textiles. The flax textiles differed in their architecture and consisted of yarns with different linear density, twist level and weaving characteristics. In addition to the type of textile, the examined parameters included the number of TRM layers (varying from one to three) and the mortar overlay thickness (3 mm and 5 mm).

A summary of the experimental programme for Phase 1 is presented in **Fig. 3.3**. Clevis type grips were used for the uniaxial tensile characterisation of the TRM systems, as recommended by AC434 [51], to minimise bending and avoid local damage of the TRM specimens in the grip area. It should be noted that the lack of a lateral pressure in the region of the grips has been shown to lead to either textile rupture or slippage between the textile and the mortar (depending on the degree of bond between the textile and the matrix), and may result in the development of larger strains and lower tensile elastic modulus, thus to a “softer” stress-strain response [53]. Hence, it could be argued that this type of gripping methods represents more appropriately the actual boundary conditions in strengthening applications and reproduces better the behaviour of non-anchored TRM composites [110].

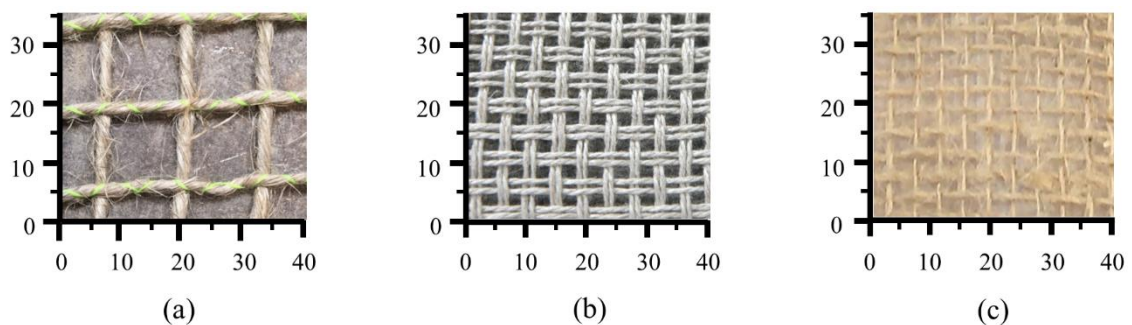


Fig. 3.2 Natural fibre textiles investigated in Study 1: (a) F1; (b) F2; (c) J. Scale in mm.

3.2.2. Phase 2

The two Flax-TRM systems examined in Phase 1 exhibited an overall better performance and were characterised by good composite action, along with tensile properties and a ductile behaviour suitable for strengthening applications. As a result, these the two Flax-TRM systems (F1-TRM and F2-TRM) were further examined in Phase 2 to assess their performance when bonded to a masonry substrate.

Three series of single-lap shear bond tests were carried out as summarised in **Fig. 3.4**. In addition to textile architecture (F1- versus F2-TRM), the key parameters examined in this phase of testing included the bond length (varying from 65 - 260), the number of TRM layers (varying from 1 to 3) and the bond width (50 and 100 mm).

The single-lap shear pull-push test setup recommended by RILEM TC 250-CSM [54] was implemented in this study as it eliminates issues related with the loss of symmetry that are inherent

to double-lap tests (**Fig. 3.5**). Masonry prisms were used as substrate to better represent real-life applications.

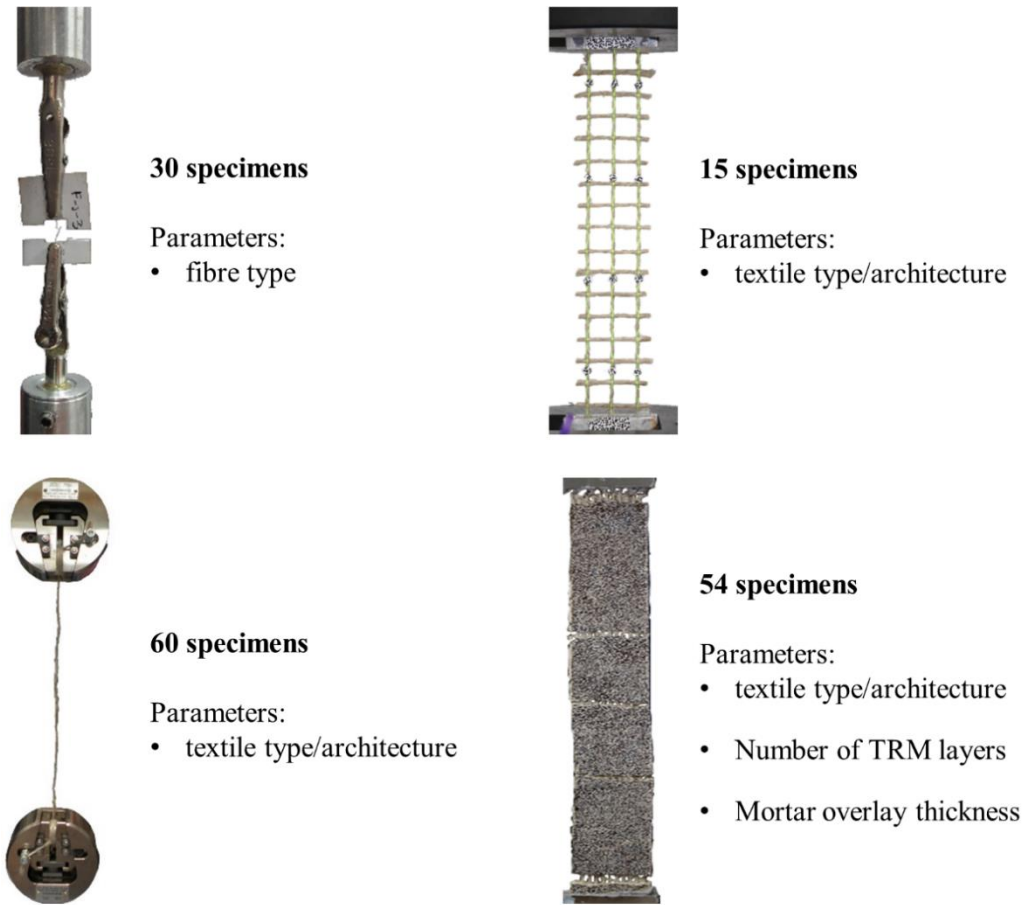


Fig. 3.3 Overview of experimental programme - Phase 1.

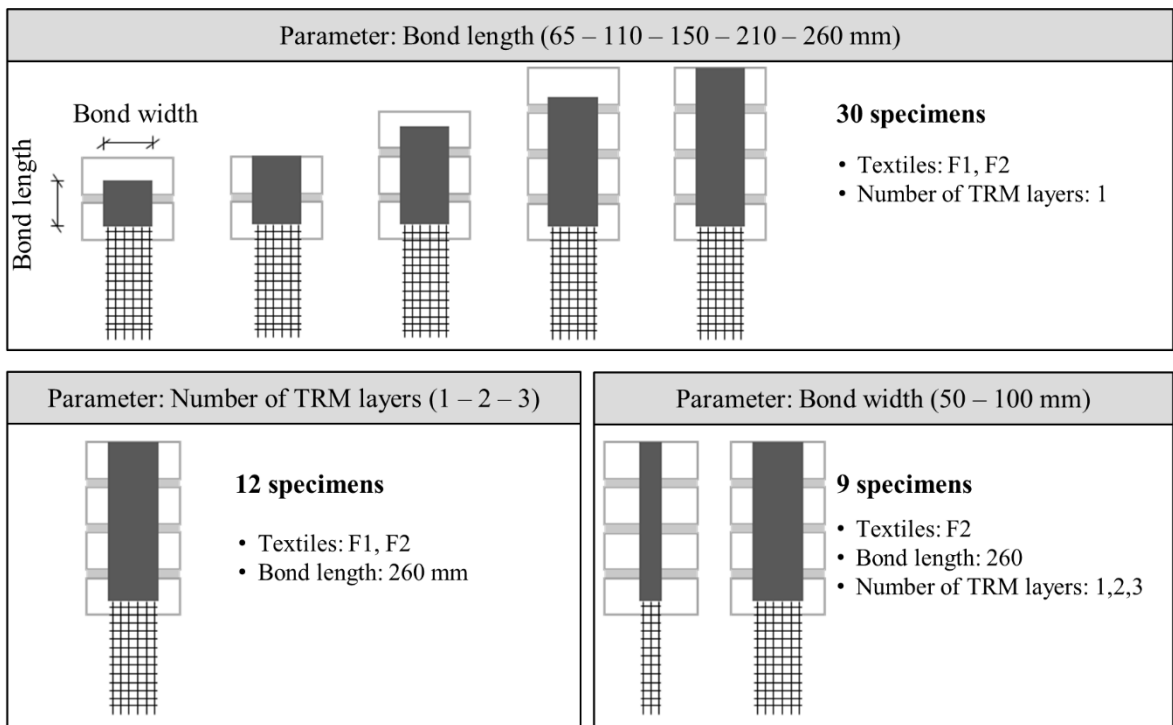


Fig. 3.4 Overview of experimental programme - Phase 2.

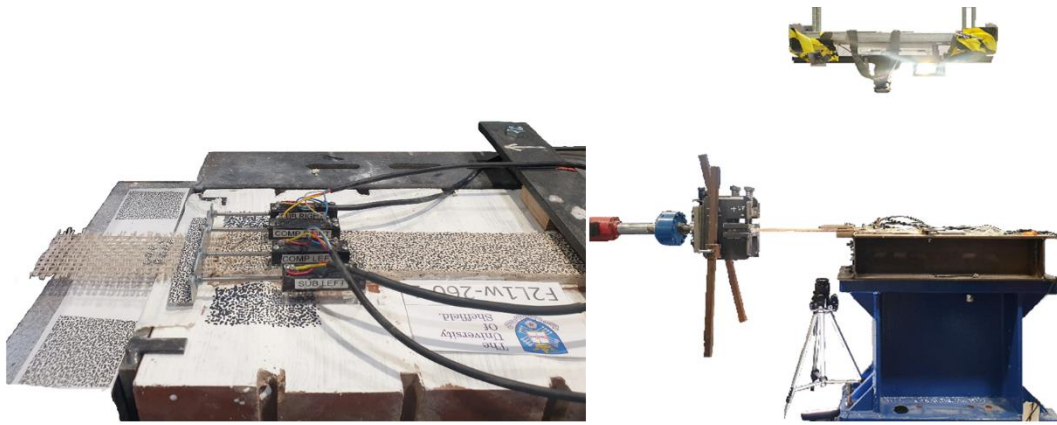


Fig. 3.5 Experimental test setup - Phase 2.

3.2.3. Phase 3

Phase 3 aimed to assess the performance of NTRM systems as a seismic retrofitting solution for unreinforced masonry walls. Based on the results of Phase 2, the Flax-TRM system comprising F2 textile was selected to be investigated in this phase of testing as it exhibited superior bond performance, along with high exploitation of the textile strength. In-plane shear tests were conducted on medium-scale walls, under quasi-static cyclic loading conditions. In-plane shear-compression tests were chosen over simpler diagonal compression tests as they would allow the development of all key shear resisting mechanisms and provide a more objective assessment of the strengthening system. The examined strengthening schemes and the experimental test setup are shown in **Fig. 3.6**.

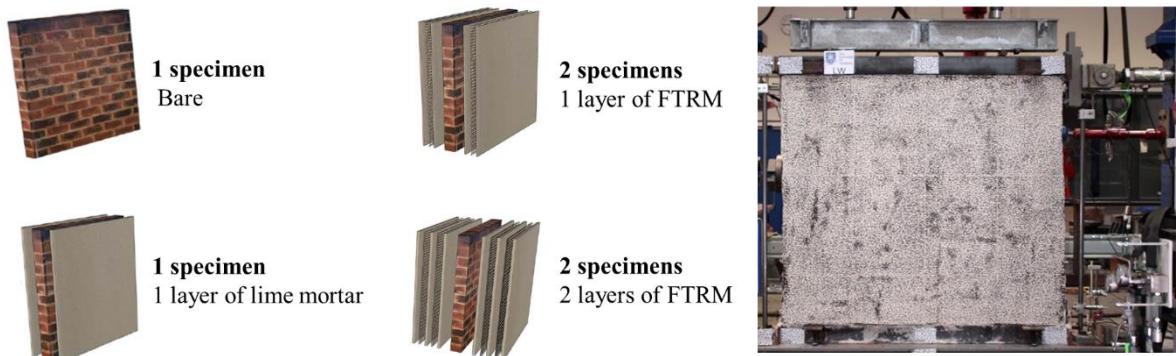


Fig. 3.6 Overview of experimental programme - Phase 3.

3.2.4. Material Mechanical Characterisation

The mechanical properties of the materials used in the three Phases of the experimental programme were assessed through standard material characterisation tests (**Fig. 3.7**). These included: flexural and compression tests on masonry and TRM mortar; compression tests on single bricks; compression tests on masonry prisms and wallettes; and shear tests on masonry triplets. Detailed information is reported in the relevant Chapters and Appendices.

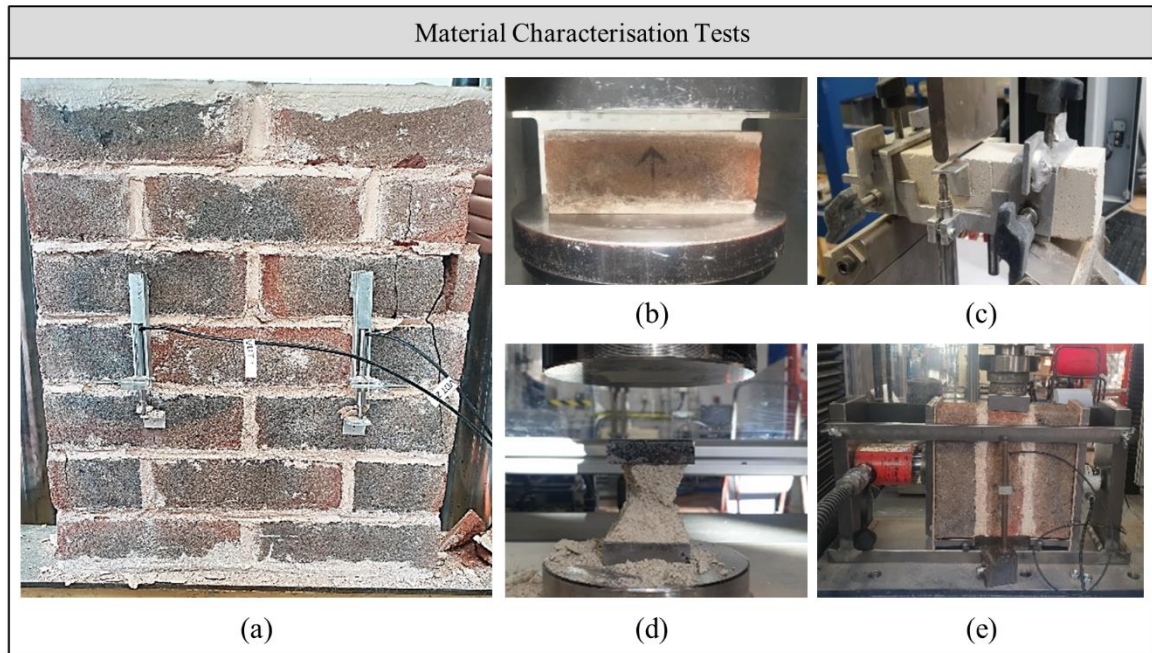


Fig. 3.7 Overview of material characterisation tests: (a) compression tests on masonry wallettes; (b) compression tests on brick units; (c) flexural tests on mortar prisms; (d) compression tests on mortar prism halves; (e) shear tests on masonry triplets.

3.2.5. Instrumentation

In all three experimental phases, tests were monitored using a comprehensive set of experimental measurements with a combination of contact and non-contact methods (2D-DIC).

3.2.6. Selection of Key Examined Parameters

The main motivation behind the selection of the key parameters examined in this programme is discussed in the following. Additional details are given in Chapters 4 – 6, along with the relevant literature review.

3.2.6.1. Fibre type

Flax and jute textiles were selected based on their promising mechanical properties, worldwide availability and cost of raw material [8], as well as on their effective performance when embedded in lime-based mortars, as discussed in Chapter 2.

3.2.6.2. Textile Architecture

The architecture of the textile affects the reinforcement ratio and the mechanical interlock between fibres and mortar [99,111,112]. The linear density of the yarns, the twist level, the mesh size and the weaving characteristics are critical parameters as they can promote or hinder the penetration of the mortar both within the mesh openings and within the yarn's cross-sectional area, thus affecting the overall performance of the TRM system.

3.2.6.3. Mortar overlay thickness

The geometry of the composite should be optimised to minimise the amount of material used and ensure adequate performance. While the thickness of the mortar overlay dictates the effective reinforcement ratio and can affect both tensile and bond characteristics, its effect on the performance of the resulting TRM still remains an open issue [69].

3.2.6.4. Number of TRM layers

The use of multiple TRM layers is often required to achieve a target increase in structural capacity. However, an increase in the number of TRM layers is not always accompanied by enhanced mechanical performance, as poor interfacial behaviour can compromise composite action [46,92], limit the exploitation of the mechanical properties of the textile reinforcement, and subsequently result in premature debonding from the substrate and decreased ductility [46,151,152]. In addition, although current guidelines estimate an increase in the in-plane shear capacity proportional to the number of TRM layers, this was not confirmed experimentally from diagonal compression tests performed on multi-layer NTRM-retrofitted masonry walls [108].

3.2.6.5. Bond Length

The bond length directly affects the performance of TRM strengthening systems as different bond lengths can trigger different failure modes [27,31]. Values varying from 50 to 450 mm have been examined for advanced TRM/masonry systems with the aim to determine the effective bond length, i.e. the minimum bond length required for the development of the maximum debonding load [150]. Although for advanced TRM/masonry systems a bond length of 260 mm was shown to ensure the development of an adequate stress transfer mechanism [54], the effective bond length of NTRM systems is yet to be determined. Only one study [104] examined Flax-TRM systems bonded to masonry over a length of 50 mm and 100 mm and provided evidence that both bond lengths ensured a good adhesion and resulted in the same stress level, without causing any debonding. However, no further investigation or in-depth analysis of the shear stress transfer mechanism has been reported.

3.2.6.6. Bond Width

Given the inherent variability across the length and width of the textile, the bond width of TRM with natural fibre textiles is believed to be of significant importance. Current studies on the effect of bond width on the bond performance of TRM systems provide contradictory evidence ([111,149] against [147]) and hence this parameter requires further investigation.

4. MECHANICAL CHARACTERISATION OF FLAX AND JUTE TEXTILE-REINFORCED MORTARS

N. Trochoutsou, M. Di Benedetti, K. Pilakoutas, M. Guadagnini, Mechanical Characterisation of Flax and Jute Textile-Reinforced Mortars, *Constr. Build. Mater.* 271 (2021), 121564. [doi: 10.1016/j.conbuildmat.2020.121564](https://doi.org/10.1016/j.conbuildmat.2020.121564)

Abstract

Natural fibre textiles embedded in inorganic matrices (NTRM) could offer a strengthening solution for unreinforced masonry structures that satisfies both performance and sustainability requirements. However, the limited understanding of their mechanical characteristics hinders their use. This paper investigates the mechanical performance of flax and jute lime-based composites under direct tension and assesses the mechanical contribution of the NTRM constituents through a multi-scale experimental study. Key design parameters for strengthening applications, such as textile geometry, number of TRM layers and TRM overlay thickness are examined in detail. The results show that textile geometry and reinforcement ratio significantly affect the composite performance. When mechanical reinforcement ratios greater than 3% are provided, flax textiles with smaller diameter and twisted yarns, arranged in denser meshes, ensure good composite action. Overall, flax-TRM composites resulted in a ductile behaviour and developed the highest strength (80–200 MPa) and elongation capacity (4–8%), making them a promising retrofitting solution for masonry, where the use of strengthening systems with moderate stiffness and compatibility with the substrate is of primary concern.

This chapter consists of a stand-alone journal paper and includes the associated reference list at the end of the chapter. Additional information and further test results are presented in Appendix A.

4.1. INTRODUCTION

The unacceptable number of casualties and substantial economic losses due to collapse of masonry elements in past earthquakes highlight the high seismic vulnerability of unreinforced masonry structures and the need to provide suitable strengthening solutions, especially for developing countries. In the last 20 years alone, the number of fatalities due to earthquakes exceeded 1 M, with \$300 Billion/year projected economic loss [3]. It is estimated that more than 75% of the fatalities attributed to earthquakes are caused by the collapse of buildings and the greatest proportion (more than 80%) is from the collapse of masonry buildings [1]. Among the numerous existing materials and retrofit systems, advanced composite materials dominate in developed countries due to their high specific mechanical properties and ease of application. These systems comprise high performance reinforcement (e.g. carbon, PBO, steel cords) embedded into organic (Fibre Reinforced Polymers - FRP) or inorganic matrices (Textile-Reinforced Mortars - TRM/ Fibre-Reinforced Cementitious Matrix - FRCM) and have been applied successfully for the strengthening and seismic retrofitting of structural masonry elements and masonry infilled reinforced concrete frames [9,21,49]. However, steel and synthetic fibres and resin-based composites have a high embodied energy and cannot be easily recycled, hence do not meet the global target for sustainable development [28]. Composites reinforced with natural fibres (green- or bio-composites) have recently attracted the interest of researchers as potential candidates for strengthening applications and are beginning to receive the attention of standardisation committees [33].

Natural fibres have excellent environmental credentials as they are renewable, biodegradable and recyclable [30]. Their specific mechanical properties are compatible with the masonry support, thus making them a valid alternative to high performance reinforcement, the properties of which cannot be fully exploited in masonry strengthening applications. Natural fibres are cost-effective and have been shown to be a competitive alternative to the cheapest commercially available E-glass fibres [64], and have a great potential to be used in hybrid composites [113]. Additionally, they are widely available and readily accessible by less favoured economies [71]. The use of a lime-based mortar as inorganic matrix is particularly suitable for masonry substrates, as it can offer better chemical and mechanical compatibility with the porous, uneven and rough masonry substrate than organic matrices, and can ensure vapour permeability and improved durability [114]. It also provides a more sustainable solution against cementitious matrices (predominantly used in TRM systems), can accommodate masonry movements during the hardening phase [115], and relies on materials readily available in most countries.

Despite the large body of work on the performance of cementitious composites reinforced with chopped natural fibres (NFRC) and on the performance of natural fibre polymer composites (NFRP) [71], limited attention has been paid on the effectiveness of natural fibre textile-reinforced mortars (NTRM) and their tensile behaviour. Available research on the topic includes experimental studies on the tensile behaviour of flax [98-101], sisal [98-100,102], hemp and cotton TRM [100], as well

as comparative studies between TRM comprising natural fibres (flax, jute or hemp) and their FRP counterparts [69]. The tensile behaviour of NTRM was found to be highly ductile [98,99,102], and differs from that of TRM systems with advanced textiles [90] in two main aspects: 1) the crack development stage is usually accompanied by large deformations [101] and 2) failure typically occurs due to the progressive rupture of the individual filaments/yarns, resulting in a softening part in the stress–strain response [99]. Flax-TRM are characterised by good mechanical properties [98,99,101] and flax fibres were reported as the most promising reinforcing solution for strengthening applications [69,100], followed by jute and hemp [69]. Sisal-TRM showed poorer tensile performance than flax-TRM even at relatively higher reinforcement ratios [99]. Some of the studies [98,116] explored the durability aspect of natural fibre textiles and concluded that natural fibres can be susceptible to moisture absorption and undergo severe degradation in alkaline environments, thus suggesting that cement-free matrices can lead to more durable NTRM systems [71]. However, the short-term mechanical performance of NTRM composites cannot be determined based on the properties of the constituent materials (as also observed for existing TRM solutions [117]). In addition, although some studies have examined promising solutions to improve the fibre-to-mortar adhesion [86], the stress transfer mechanism between matrix and fibres is still not well understood. Moreover, the effect of key design aspects on the tensile performance of TRM systems needs to be further examined, including the number of TRM layers, the geometry of the textile and the thickness of the mortar overlays. The number of applied TRM layers required to achieve the desired performance criteria in terms of strength, stiffness and deformability affects the tensile strength and ductility of the composite [118] as well as failure mode [46,92]. The geometry of the textile (i.e. mesh size, weaving characteristics) affects not only the reinforcement ratio, but also the mechanical interlock between fibres and mortar. Bi-directional textiles have been shown to have better bond behaviour due to the presence of transverse yarns as they provide additional mechanical anchorage [119], the effectiveness of which relies strongly on the weaving pattern. Yarns in woven textiles can typically benefit from the strong anchoring effect resulting from the crimped geometry [119]. The performance of woven textiles, however, can be limited by the development of stress concentrations at the intersection of warp and weft yarns, which can be avoided in stitched textiles comprising straight yarns [120]. Moreover, high linear density yarns may result in limited penetrability and promote detachment at the textile/mortar interface when high reinforcement ratios are used [99]. Finally, the influence of TRM overlay thickness remains an open issue [69], though the geometry of the composite should be optimised to minimise the amount of material used and ensure adequate performance. Despite the fact that the reinforcement ratio significantly affects the crack pattern and overall composite performance [99], very few studies provide recommendations on critical reinforcement ratios [99,119], and these are limited to geometrical ratios without taking into account the TRM constituent mechanical properties.

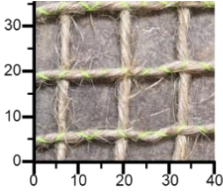
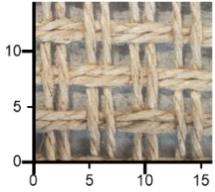
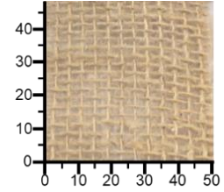
The present work aims to assess the effect of critical design parameters on the performance of NTRM and attempts to gain additional insights into the mechanical behaviour of NTRM by implementing a multi-scale experimental study. Flax and jute were selected for this study based on their mechanical properties, worldwide availability and cost of raw material [8]. Single and multi-layer TRM composites comprising a lime-based mortar reinforced with flax or jute textiles were tested in direct tension. The examined parameters include textile architecture, number of NTRM layers (from one to three) and mortar overlay thickness (3 and 5 mm). Testing of the NTRM constituents was also carried out to fully characterise the strengthening system, including tensile tests on single fibres, yarns and bare textiles. The present study is part of a larger research programme on the development of effective NTRM strengthening systems for masonry structures.

4.2. MATERIALS AND METHODS

4.2.1. Materials

Three types of natural fibre textile reinforcement were examined: two types of flax (F1 and F2) and jute (J). The flax textiles differ in their architecture (mesh size, yarn diameter), physical properties and weave characteristics: F1 grids are woven and comprise single “S” twist yarns held together at intersection points by a non-structural thread, while F2 grids comprise two-ply “S” twist yarns (i.e. two single yarns twisted together) arranged in pairs across the mesh. F2 and J textiles are plain woven, with the warp (longitudinal) and weft (transverse) yarns interlaced at right angles. All textiles are balanced bi-directional, with mesh openings being equal in the two orthogonal directions. The nominal characteristics of the selected textiles available from the manufacturers are summarised in **Table 4.1**. As the linear and bulk densities of the jute textiles were not provided, these were experimentally determined following EN ISO 1889:2009 [121] and ASTM D8171-18 [122], respectively. Five yarn samples were extracted from the textile and weighed in air and rapeseed oil after they were fully saturated in a vacuum desiccator. The determined values of linear and bulk densities were 241 Tex (coefficient of variation, CoV: 6%) and 1532.9 kg/m³ (CoV: 4%), respectively, which were found to be in line with previous literature studies [123].

Table 4.1 Natural fibre textile characteristics as supplied by the manufacturer unless otherwise stated.

Property			
	Flax1 (F1)	Flax2 (F2)	Jute (J)
Mesh size (mm)	14	4	4
Construction	0°/90°	0°/90°	0°/90°
Areal Weight (g/m ²)	215	300	183
Linear Density (TEX = g/km)	1500	324	241*
Bulk Density (g/cm ³)	1.35	1.50	1.53*

A widely available natural hydraulic lime -based mortar (NHL 2) [124], typically used in the field of restoration and repair of historic masonry structures, was used for the manufacture of the NTRM composites. The mortar contains siliceous and calcareous aggregates of maximum size smaller than 2 mm as well as short dispersed fibres to control shrinkage. A water/solid ratio of 0.23 was selected according to the supplier's instructions to obtain optimal workability and fluidity and ensure penetration through the mesh openings of the textiles. The mechanical properties of the mortar were experimentally determined according to EN 1015-11 [125]. Three-point bending tests were carried out on 30 prisms (160 x 40 x 40 mm), at a loading rate of 30 N/s, followed by compression tests on the resulting halves (60 specimens), at a loading rate of 400 N/s. The average values of flexural and compressive strength at 28 days were found to be 2.8 MPa (CoV:15%) and 7.7 MPa (CoV:15%), respectively, while the elastic modulus was found to be 3420 MPa (CoV:18%). A tensile strength of 1.2 MPa was determined based on Model Code 2010 [126] and adopted in the analyses.

4.2.2. Tests on fibres

Direct tension tests were performed on ten individual fibres extracted from yarns of each textile type. The fibres were fixed to cardboard frames using an ethyl 2-cyanoacrylate adhesive to facilitate mounting in the tensile testing machine and ensure a gauge length of 5 mm (**Fig. 4.1a**). The fibres were assumed to have a uniform and circular cross-section and their diameter was measured at five locations using a Nikon Eclipse TS100 optical microscope at 40x magnification coupled with an image analysis software (ImageJ). Although this assumption is known to overestimate the actual fibre area [127], it enables simple measurement of the fibre cross-sectional area and the determination of conservative average mechanical properties. The tests were performed in displacement control (1 mm/min) until rupture using a universal testing machine equipped (Zwick/Roell) with a 5 N load

cell. Specimens that failed in the proximity of the grips were discarded, resulting in six successful tests for J and F2 and four successful tests for F1.

4.2.3. Tests on yarns

Twenty yarns of each textile type were tested in direct tension according to ISO 2062:2009 [128], in a universal testing machine with a capacity of 10 kN. Capstan clamps were used to avoid premature failure of the yarns at the jaw faces (**Fig. 4.1b**). The overall gauge length was 560 mm for all specimens. The nominal area of the yarns was calculated as the linear density divided by the bulk density, as suggested by CNR-DT 200/2013 [43]. The tests were conducted in displacement control at a loading rate of 300 mm/min until rupture of the specimens, with an initial pre-load of 7.5 N for F1 and of 1.5 N for J and F2. The results from the specimens that failed due to breakage in the proximity to the clamping areas, slippage or fraying were discarded and not considered in the data processing. Load and displacement data were recorded by the integrated load-cell of the machine and the machine's cross-head displacement, respectively.

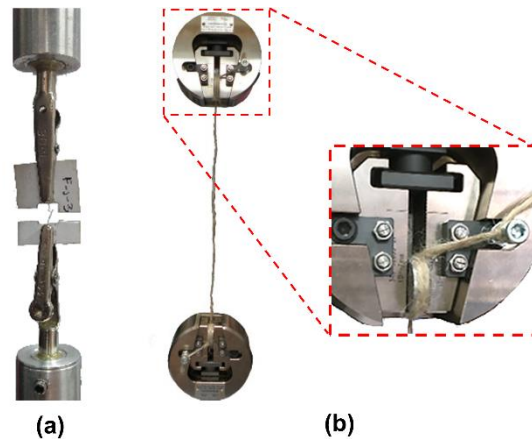


Fig. 4.1 (a) tensile test setup for fibres; (b) tensile test setup for yarns and capstan clamps details.

4.2.4. Tests on bare textiles

Five strips were cut from each textile type according to EN 13934-1:2013 [129]. Each strip measured 340 x 50 mm (length x width) and comprised several yarns, N_y , in the longitudinal direction to provide the same cross-sectional area of reinforcement used in the NTRM coupons (see also Section 4.2.5.1): three yarns of F1 (specimens F1_i), ten pairs of F2 yarns (F2_i) and ten yarns of J (J_i). Aluminium tabs were mounted at both ends of the textile specimens using a high-strength 2-part epoxy (shear strength > 60 MPa) to ensure adequate load transfer and prevent slippage within the gripping areas. The tabs measured 70 x 60 mm, leaving a gauge length of 200 mm. The tensile tests were carried out in displacement control at a rate of 2 mm/min using a universal testing machine equipped with a load cell of 300 kN capacity.

DIC was employed to measure the displacement of selected target areas and subsequently obtain strain values. The mean strain of the textile specimens was obtained by monitoring the displacement

of an optimized computer-generated speckle pattern glued to the gripping tabs and by applying a virtual extensometer connecting the top and bottom speckle-patterns over a gauge length l_a . Four additional rows of 4-mm diameter speckle-patterned markers were glued to three of the longitudinal yarns (left - L, middle - M, right - R) to monitor the strain distribution along the yarns and across the textile by means of virtual extensometers with gauge length l_c , (approximately 180 mm) and l_m (approximately 50 mm) (**Fig. 4.2**).

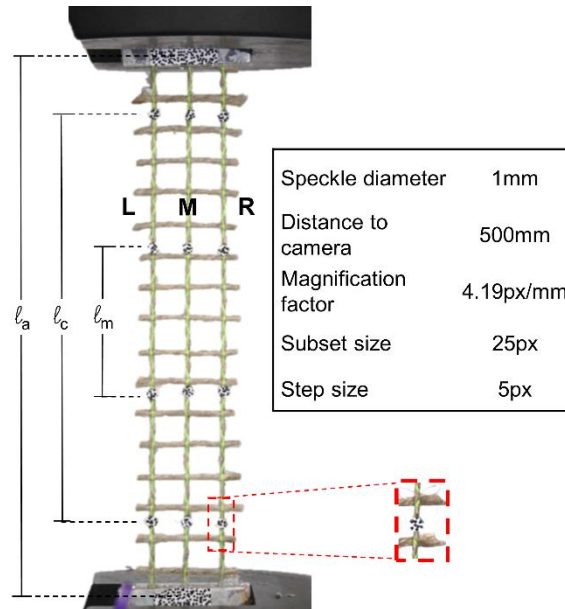


Fig. 4.2 Tensile test setup for bare textiles (F1t), gauge length of virtual extensometers and DIC analysis parameters.

4.2.5. Tests on NTRM composites

4.2.5.1. Specimen Preparation

Fifty-four prismatic specimens (6 replicates per NTRM configuration) measuring 600 x 50 mm were manufactured individually, according to the following steps, as shown in **Fig. 4.3**: a) a first mortar layer was trowelled in a plexiglass formwork; b) the textile reinforcement, which was previously cut to the required dimensions, was stretched between the two ends to ensure alignment of the longitudinal yarns and subsequently embedded in the mortar by pressing it slightly, until the mortar protruded through the mesh; c) a second mortar layer was applied and levelled by means of a scraper. A gauge scraper was used to ensure a constant thickness of all mortar layers (**Fig. 4.3d**). Steps b and c were repeated as needed to create the required number of layers. All textiles were placed dry into the fresh mortar. Whereas AC434 [51] do not specify the specimen thickness, a thickness of 3 mm was adopted for the mortar layers to comply with the minimum value recommended in RILEM TC 232-TDT [52], as well as to enable direct comparison with existing studies [98,99,101]. A width of 50 mm was selected for the composite specimens to comply with the minimum required number of 3 yarns per layer [51]. Six additional single-layer coupons were prepared using 5-mm thick mortar overlays (3 replicates for each flax-TRM system), to examine the

effect of mortar thickness on the tensile behaviour of the composites. This was made in an attempt to assess possible issues arising during on-site applications, where the thickness of the overlays cannot be easily controlled and typically more mortar is applied causing a reduction in the provided reinforcement ratio. The reinforcement ratios selected for this study varied between 0.67-1.67% for F1, 0.86-2.16% for F2 and 0.52-0.79% for J and were based on findings from the few studies available in the literature, according to which the critical volume content of fibres in cement composites is about 1-3% [99,119]. All NTRM coupons were cured in a mist room (approximately 20°C and 99% RH) for 28 days following the recommendations provided in [130], and then stored in standard laboratory conditions for at least 28 days before testing.

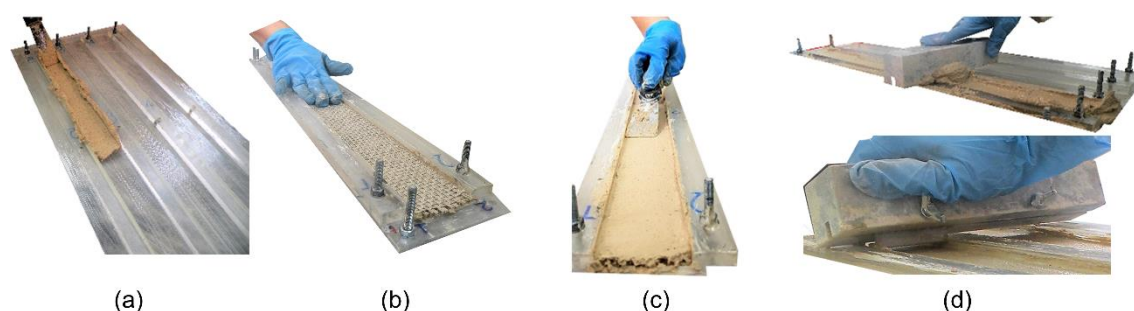


Fig. 4.3 NTRM manufacturing process: (a) application of first mortar layer; (b) embedment of the textile; (c) application of top mortar layer; (d) use of gauge scraper to ensure constant mortar thickness

4.2.5.2. Experimental Setup and Instrumentation

Prior to testing, aluminium tabs were epoxy-bonded to the ends of the composites for a length of 140 mm (**Fig. 4.4a**) to ensure effective load transfer and avoid local crushing of the NTRM system [92]. A pattern with 2 mm speckles was applied manually to the free length of the coupon (320 mm) on the side cast against the mould to ensure a flat surface for DIC analyses.

The direct tensile tests on the NTRM specimens were performed following the recommendations of AC434 [51]. The tests were carried out in displacement control in a universal testing machine of 10 kN capacity and the load was transferred through clevis-type grips (**Fig. 4.4b**). A displacement rate of 0.2 mm/min was used up to the occurrence of the first crack and 1 mm/min thereafter.

The specimen ID adopted uses the notation XY-Z-n, where X denotes the type of textile reinforcement (F1, F2 or J); Y is the number of TRM overlays (L1, L2 or L3); Z is the thickness of each mortar layer (3 or 5) and n is the replicate number (1 to 6). For instance, F1L2-3-4 stands for the fourth replicate comprising two textile layers of Flax1 sandwiched in 3-mm thick mortar layers.

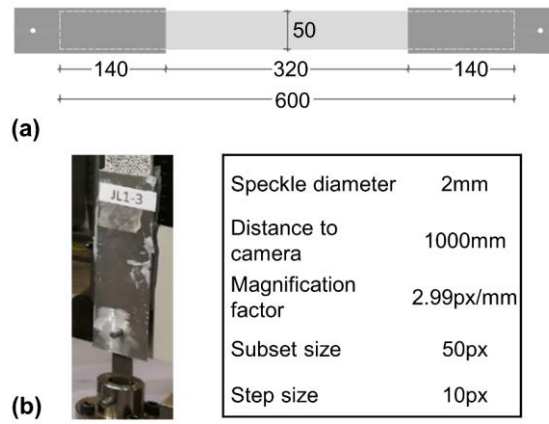


Fig. 4.4 (a) Geometry of NTRM coupons (all dimensions in mm); (b) clevis-type grips and DIC analysis parameters.

4.2.6. Digital Image Correlation (DIC)

A single camera digital image correlation setup (2D-DIC) was employed to obtain full-field displacement measurements for textiles and NTRM specimens. Although the implementation of a 2D system cannot capture out of plane movements, which could result in unreliable strain measurements, this contactless measuring technique [131] can be used successfully to examine the formation and evolution of the crack pattern [132], and to qualitatively assess the strain field over the monitored surface. Where presented, strain measurements were derived based on the tracking of optical targets.

Images were acquired with a CMOS digital camera having a 4272×2848 pixel resolution (Canon EOS 1100D) and were processed with GOM Correlate [133].

4.3. RESULTS AND DISCUSSION

4.3.1. Tensile behaviour of fibres

All fibres were characterised by a nearly linear stress-strain behaviour. The obtained average tensile properties are presented in **Table 4.2**, along with the corresponding average cross-sectional area. Flax fibres exhibited strength values between 680-865 MPa, with F2 fibres exhibiting the highest strength attained at a strain value (3.8%) almost double than that of F1 (2%). Jute fibres developed a strength of 560 MPa and an average ultimate strain of approximately 2%, resulting in stiffness values similar to those of F2 fibres. The mechanical properties of the tested fibres fall within the range reported in [71], which includes a large database comprising both physical and mechanical properties of various natural fibres. The large variability observed in the mechanical properties of the tested fibres (CoV up to about 40%) is consistent with data reported in the literature (CoV ranging from 20% to 65% [134,135]) and might be attributed to the inherent variability of the fibres, as well as the implementation of different methods to determine fibre geometry and test their tensile characteristics (e.g. different sample size, loading rate).

Table 4.2 Mechanical properties of flax and jute fibres (CoV in parentheses).

Fibre ID	A_f ($\text{mm}^2 \times 10^{-3}$)	$P_{f,\max}$ (N)	$f_{f,\max}$ (MPa)	$\varepsilon_{f,\max}$ (%)	E_f (GPa)
J_f	1.02 (35%)	0.53 (15%)	560.0 (26%)	2.1 (23%)	25.7 (28%)
$F1_f$	0.87 (42%)	0.49 (19%)	680.9 (41%)	2.0 (13%)	38.7 (28%)
$F2_f$	0.54 (31%)	0.43 (36%)	864.8 (37%)	3.8 (7%)	27.9 (43%)

4.3.2. Tensile behaviour of yarns

Fig. 4.5 shows the envelope of the tensile stress-strain responses obtained from all of the tested yarns along with the individual response of a representative sample (black curve). **Table 4.3** summarises the average values of maximum tensile strength $f_{y,\max}$, elongation at break ($\varepsilon_{y,\max}$), and elastic modulus (E_y) along with their CoV (given in brackets). The elastic modulus was estimated as the secant modulus between 60% and 90% of the maximum tensile strength, corresponding to the slope of the linear part in the stress-strain response curve (**Fig. 4.5**). The yarn cross-sectional area was assumed constant over its length during the tests.

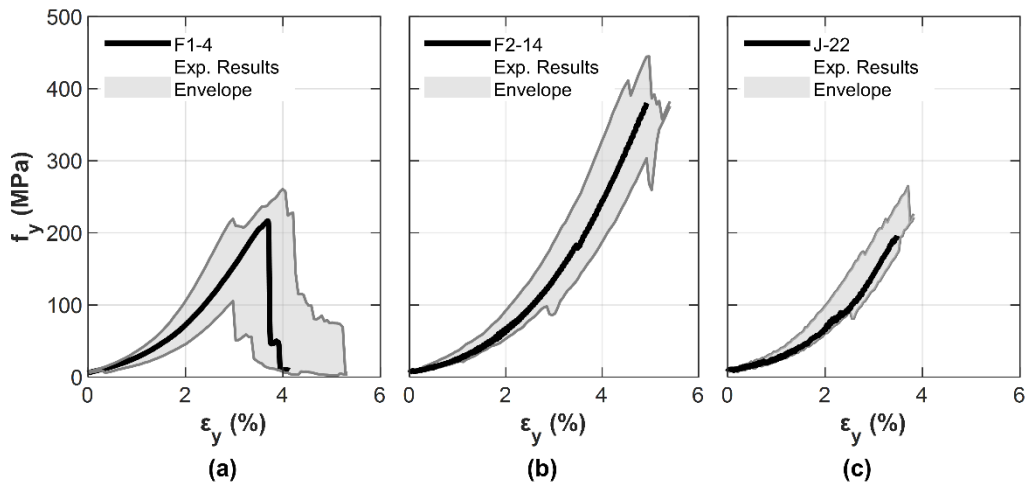


Fig. 4.5 Envelope curves for the stress-strain response of natural fibre yarns and representative specimens: (a) F1 (b) F2 and (c) J.

The mechanical properties of the tested yarns were found to be in line with those reported in previous studies [69,98] with values of failure strain ranging between 3-5%, strength varying between 200-380 MPa and stiffness between 10-14 GPa, thus highlighting their suitability for the manufacturing of technical textiles. Overall, Flax F2 achieved the best mechanical performance, exhibiting the highest strength and stiffness. The stress-strain response of all yarns was characterised by an initial inelastic branch, followed by an almost linear behaviour up to rupture. Rupture always occurred away from the clamps. The initial strain stiffening is due to the realignment of individual yarn filaments [136,140], a mechanism that contributes to the greater elongation of the yarns compared to that of the individual fibres. As a result of local damage/imperfections of the fibres or fibre/filament rearrangement within the yarn [137,138], a few specimens exhibited a small drop in the level of sustained stress at relatively low levels of imposed deformation (e.g. F2-14 in **Fig. 4.5**).

While F2 and J yarns failed in a very brittle manner, a more progressive failure was observed in the larger diameter F1 yarns, possibly due to a more pronounced shear lag effect (i.e. non-uniform stress transfer across the yarn cross-section) and the progressive rupture of the most stressed filaments.

Table 4.3 Mechanical properties of flax and jute yarns (CoV in parentheses).

Yarn ID	A_y (mm ²)	$P_{y,max}$ (N)	$f_{y,max}$ (MPa)	$\epsilon_{y,max}$ (%)	E_y (GPa)
Jy	0.157	31 (18%)	196.1 (17%)	3.3 (12%)	10.3 (10%)
F1y	1.111	236 (9%)	212.6 (9%)	3.6 (11%)	10.1 (12%)
F2y	0.216	82 (7%)	377.9 (7%)	4.9 (5%)	14.4 (12%)

4.3.3. Tensile behaviour of textiles

The average tensile properties of the tested textiles (determined from 5 specimens per fibre type) are summarised in **Table 4.4** in terms of maximum load ($P_{t,max}$), tensile strength ($f_{t,max}$), strain at peak load ($\epsilon_{t,max}$) and stiffness (E_t). The tensile strength was calculated by dividing the load by the corresponding textile area (A_t), which was in turn calculated as the product of the number of yarns across the width of the specimen (N_y - see Section 2.4) and the corresponding yarn average cross-sectional area (A_y - see **Table 4.3**), i.e. $A_t = N_y * A_y$. The strain development was derived from DIC analyses following the methodology described in Section 4.2.4. E_t was calculated as the secant modulus corresponding to the slope of the linear part in the stress-strain response curve. It should be noted that, although the protocol developed within RILEM TC 250-CSM [54] recommends calculation of the elastic modulus between 10% and 50% of the maximum tensile strength, this range was considered inappropriate for the natural fibre textiles examined in this study as it falls within their inelastic behaviour, thus not representing the maximum stiffness that can be developed.

Table 4.4 Mechanical properties of flax and jute textiles (CoV in parentheses).

Textile ID	A_t (mm ²)	$P_{t,max}$ (N)	$f_{t,max}$ (MPa)	$\epsilon_{t,max}$ (%)	E_t (GPa)
Jt	1.57	302 (12%)	190.0 (12%)	1.4 (9%)	20.9 (7%)
F1t	3.33	655 (11%)	196.4 (11%)	4.2 (10%)	7.1 (13%)
F2t	4.32	1156 (6%)	289.0 (6%)	3.8 (4%)	13.6 (7%)

Fig. 4.6 (a1,b1,c1) shows the tensile stress-strain behaviour of the tested textiles along with the maximum strength and strain values obtained from tests on the corresponding single yarns. The global response of the textiles was characterised by an initial inelastic branch followed by linear behaviour up to the peak stress and a softening stage resulting from the progressive failure of individual yarns. Flax textiles developed strength values ranging between 195-290 MPa, which are in good agreement with those reported in previous studies on similar flax textiles [98,116] albeit at a relatively higher stiffness. The jute textiles examined in this study developed similar strength to F1 textiles (190 MPa), although at a relatively lower strain of 1.4%. However, different mechanical

properties have also been reported in the literature for jute textiles [69], highlighting the variability in performance of different fibres, as well as the effect of different textile architectures.

F1 textiles developed a lower stiffness than the corresponding individual yarns (approximately 7 GPa) and exhibited an overall higher ultimate elongation. F2 textiles were characterised by a similar stiffness to that of individual F2 yarns (13.6 GPa), but achieved a lower strain at peak stress and lower maximum elongation. On the other hand, the stiffness developed by J textiles was higher than that of the corresponding individual yarns (20.9 GPa), though both the strain at peak stress and the maximum elongation were considerably smaller. The distinctively different behaviour of the textiles may be attributed to two main factors: the presence of the transverse yarns and the non-uniform strain distribution across the yarns. Although the transverse yarns do not carry any load, they provide an additional degree of restraint and can stiffen the longitudinal yarns, depending on the weave pattern [98]. However, the development of additional friction and transversal forces at the intersections between warp and weft yarns may induce stress concentrations, resulting in a strength reduction. During the tensile test, not all yarns are strained equally and progressive failure is usually observed, initiated by the rupture of the most highly stressed filaments [110]. This is illustrated in **Fig. 4.6** (a2,b2,c2), which shows the stress-strain behaviour up to the peak load of three longitudinal yarns (left, middle and right) of representative specimens of each textile type. The behaviour of the corresponding specimen (determined over a gauge length l_a - see **Fig. 4.2**) is also shown for comparison. As it can be seen, for a given level of average applied stress, a different strain level is developed in the three yarns. In addition, a different response can be obtained for different gauge lengths, as shorter lengths can capture the development of localised failures (e.g. **Fig. 4.6b2** - Ml_m versus Ml_c). In case of F1 textiles, the response of the textile specimen (black line) differs from that of the individual yarns (see **Fig. 4.6a2**). Owing to the F1 yarn's high linear density and diameter, not all yarn filaments within the epoxy-bonded gripping tabs were effectively impregnated, and thus engaged. This triggered the initiation of slip between the yarns' filaments and resulted in the specimen's softening behaviour and higher total elongation, which could not be captured when monitoring the elongation of the yarns over gauge lengths l_c and l_m . This highlights the complexity in characterising high linear density textiles, as well as the inability of the employed gripping system to effectively anchor the textile and allow the development of the full elongation capacity of the yarns.

4.3.4. Tensile behaviour of NTRM composites

The results obtained from the tensile tests on NTRM coupons are summarised in Tables 4.5-4.7, in terms of geometric reinforcement ratio (ρ_f), cracking load (P_{cr}), maximum load ($P_{NTRM,max}$), tensile strength ($f_{NTRM,max}$), ultimate strain ($\varepsilon_{NTRM,max}$), stiffness during the uncracked (E_I), crack development (E_{II}) and cracked (E_{III}) stage, average maximum crack width (w_{avg}), number of cracks (n_w) and

spacing (s). The geometric reinforcement ratio was estimated as the area of reinforcement divided by the area of the composite (A_f/A_c). The properties associated with crack development were derived from DIC analyses, while stiffness values were calculated as illustrated in **Fig. 4.7**. The corresponding CoV values are given in parentheses. The following sections include a detailed analysis of the performance of the tested NTRM specimens and discuss the effect of each of the examined parameters.

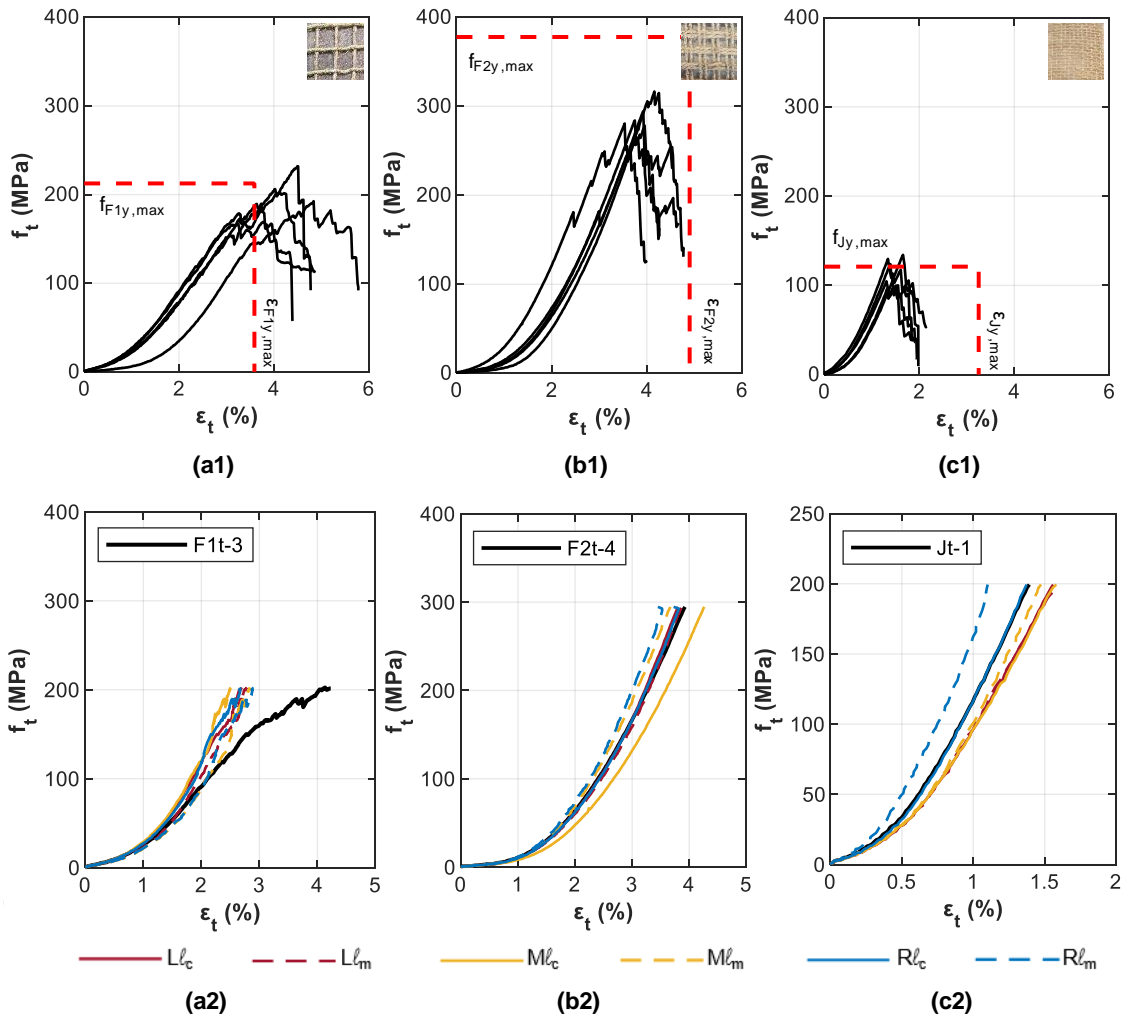


Fig. 4.6 Tensile stress-strain response of natural fibre bare textiles: (a1) F1 (b1) F2 and (c1) J (dashed lines represent the ultimate average mechanical properties of the corresponding single yarns); stress-strain distribution across the yarns for representative (a2) F1, (b2) F2 and (c2) J specimens. Note: L = left yarn, M = middle yarn and R = right yarn.

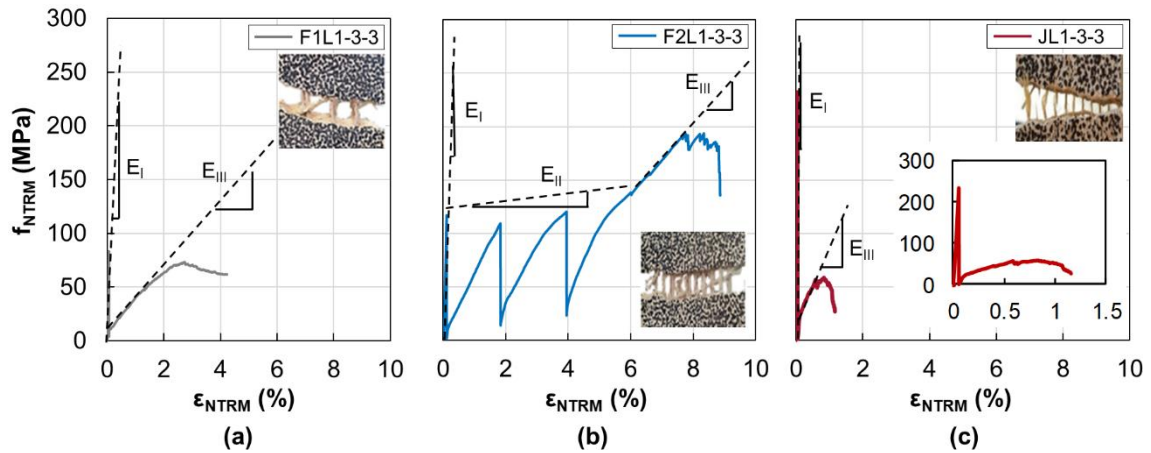


Fig. 4.7 Tensile stress-strain response of representative single-layer NTRM coupons, typical failure modes, crack stages and associated stiffness for: (a) F1-, (b) F2- and (c) J-TRM.

Table 4.5 Mechanical Properties of F1-TRM composites (CoV in parentheses).

NTRM ID	ρ_f (%)	P_{cr} (N)	$P_{NTRM,max}$ (N)	$f_{NTRM,max}$ (MPa)	$\epsilon_{NTRM,max}$ (%)	E_I (GPa)	E_{II} (GPa)	E_{III} (GPa)	w_{avg} (mm)	n_w	s (mm)
FIL1-3-1	-	-	287	86.2	3.5	-	-	2.31	10.7	1	-
FIL1-3-2	-	277	243	73.1	2.7	155.16	-	2.22	8.5	1	-
FIL1-3-3	1.11	-	294	88.4	5.6	-	-	1.87	5.9	3	108 (16%)
FIL1-3-4	-	-	214	64.1	3.9	-	-	1.62	6.1	2	144
FIL1-3-5	-	-	265	79.5	4.2	-	-	1.67	6.2	2	48
FIL1-3-6	-	-	340	102.0	4.4	-	-	2.41	7.2	1	-
AVG (CoV)	-	-	274 (15%)	82.2 (15%)	4.1 (22%)	-	-	2.02 (15%)	7.4 (23%)	-	100 (40%)
FIL1-5-1	-	197	171	51.5	2.5	84.71	-	1.68	9.8	1	-
FIL1-5-2	0.67	286	201	60.4	4.5	181.09	-	1.91	13.4	1	-
FIL1-5-3	-	338	203	60.9	3.3	162.43	-	2.13	10.6	1	-
AVG (CoV)	-	274 (21%)	192 (8%)	57.6 (8%)	3.4 (23%)	142.74 (29%)	-	1.91 (10%)	11.3 (14%)	-	-
FIL2-3-1	-	185	556	83.4	4.1	22.63	0.85	2.00	2.5	5	72 (24%)
FIL2-3-2	-	111	522	78.4	4.4	25.43	*	2.27	6.5	2	164
FIL2-3-3	1.48	101	559	83.9	5.0	24.28	0.71	1.79	5.2	3	112 (12%)
FIL2-3-4	-	108	625	93.9	5.2	43.72	0.66	2.01	5.4	3	104 (3%)
FIL2-3-5	-	-	446	66.9	3.9	-	1.53	-	3.8	2	73
FIL2-3-6	-	127	609	91.5	4.0	30.46	1.09	2.58	2.6	5	70 (52%)
AVG (CoV)	-	126 (24%)	553 (11%)	83.0 (11%)	4.4 (11%)	29.31 (26%)	0.82 (20%)	2.13 (13%)	4.3 (35%)	-	99 (34%)
FIL3-3-1	-	-	980	98.1	5.0	-	1.49	-	8.0	2	200
FIL3-3-2	-	-	923	92.4	4.9	-	1.60	0.81	6.4	2	186
FIL3-3-3	1.67	499	991	99.2	4.2	86.42	0.10	3.01	6.3	2	190
FIL3-3-4	-	-	626	62.7	4.0	-	0.08	1.57	6.2	2	219
FIL3-3-5	-	-	1017	101.8	5.5	-	0.16	2.65	8.7	2	247
FIL3-3-6	-	327	817	81.7	4.9	62.63	1.43	-	7.6	2	215
AVG (CoV)	-	413 (21%)	892 (15%)	89.3 (15%)	4.7 (10%)	-	0.81 (86%)	2.01 (43%)	7.2 (13%)	-	210 (10%)

*non-measurable

Table 4.6 Mechanical Properties of F2-TRM composites (CoV in parentheses).

NTRM ID	ρ_f (%)	P_{cr} (N)	$P_{NTRM,max}$ (N)	$f_{NTRM,max}$ (MPa)	$\varepsilon_{NTRM,max}$ (%)	E_I (GPa)	E_{II} (GPa)	E_{III} (GPa)	w_{avg} (mm)	n_w	s (mm)
F2L1-3-1		444	661	153.1	5.8	183.09	0.88	-	8.4	3	148 (5%)
F2L1-3-2		286	874	202.3	8.0	141.50	1.72	-	8.8	3	145 (35%)
F2L1-3-3	1.44	506	838	193.9	8.3	157.71	0.32	3.26	8.1	3	144 (39%)
F2L1-3-4		544	867	200.6	8.0	200.83	0.94	-	5.0	5	70 (41%)
F2L1-3-5		492	724	167.6	7.6	221.73	0.12	2.71	11.0	2	212
F2L1-3-6		412	644	149.2	5.8	178.07	0.94	-	5.9	3	103 (12%)
AVG (CoV)		448 (19%)	768 (12%)	177.8 (12%)	7.3 (14%)	180.49 (15%)	0.82 (63%)	2.98 (9%)	7.9 (25%)		137 (32%)
F2L1-5-1	0.86	-	929	215.1	9.8	-	1.46	-	6.1	5	75 (45%)
F2L1-5-2		-	976	225.9	7.7	-	1.01	-	7.8	3	134 (3%)
F2L1-5-3		-	991	229.3	7.5	-	2.19	4.92	5.8	4	89 (8%)
AVG (CoV)		-	965 (3%)	223.4 (3%)	8.3 (13%)	-	1.56 (31%)	-	6.6 (13%)		99 (25%)
F2L2-3-1		686	1826	211.4	7.7	99.39	0.57	3.46	4.8	5	80 (18%)
F2L2-3-2		534	1764	204.2	7.7	79.52	0.63	3.74	4.6	5	74 (20%)
F2L2-3-3	1.92	602	2052	237.5	8.5	100.89	0.90	3.59	5.3	5	79 (26%)
F2L2-3-4		695	1851	214.2	8.6	98.90	1.04	4.29	3.3	8	46 (31%)
F2L2-3-5		427	1769	204.7	6.7	92.97	0.56	4.44	3.5	6	58 (11%)
F2L2-3-6		675	1565	181.1	8.0	105.77	0.21	3.69	4.3	6	63 (20%)
AVG (CoV)		603 (16%)	1804 (8%)	208.9 (8%)	7.9 (8%)	96.24 (9%)	0.65 (41%)	3.87 (9%)	4.3 (17%)		66 (18%)
F2L3-3-1		807	2776	214.2	7.1	66.31	1.27	4.10	4.7	4	96 (50%)
F2L3-3-2		838	2847	219.6	7.5	79.19	0.94	4.01	6.3	4	94 (23%)
F2L3-3-3	2.16	516	2554	197.1	8.8	60.34	1.04	3.14	3.9	7	52 (31%)
F2L3-3-4		715	2631	203.0	7.3	58.57	1.39	4.39	3.6	6	59 (20%)
F2L3-3-5		805	2647	204.2	7.9	57.19	1.13	3.37	4.6	5	76 (13%)
F2L3-3-6		862	2488	191.9	6.6	82.19	0.86	3.80	2.9	7	51 (18%)
AVG (CoV)		757 (15%)	2657 (5%)	205.0 (5%)	7.5 (9%)	67.30 (15%)	1.11 (16%)	3.80 (11%)	4.3 (25%)		71 (26%)

Table 4.7 Mechanical Properties of J-TRM composites (CoV in parentheses).

NTRM ID	ρ_f (%)	P_{cr} (N)	$P_{NTRM,max}$ (N)	$f_{NTRM,max}$ (MPa)	$\epsilon_{NTRM,max}$ (%)	E_I (GPa)	E_{II} (GPa)	E_{III} (GPa)	w_{avg} (mm)	n_w	s (mm)
JL1-3-1		-	93	59.2	0.7	-	-	7.66	2.1	1	-
JL1-3-2		381	92	58.6	1.1	513.54	-	3.88	3.1	1	-
JL1-3-3	0.52	364	92	58.6	0.8	475.74	-	4.45	2.6	1	-
JL1-3-4		-	103	65.5	0.9	-	-	7.96	2.6	1	-
JL1-3-5		-	109	69.5	0.8	-	-	5.33	2.6	1	-
JL1-3-6		-	102	64.8	0.6	-	-	7.97	0.8	1	-
AVG (CoV)		373 (2%)	99 (7%)	62.7 (7%)	0.8 (19%)	494.64 (4%)	-	6.21 (28%)	2.3 (32%)	-	-
JL2-3-1		135	198	62.9	0.5	246.19	-	5.96	1.3	1	-
JL2-3-2		688	244	77.5	1.2	296.95	-	5.26	3.0	1	-
JL2-3-3	0.70	309	159	50.6	1.0	235.55	-	4.20	2.8	1	-
JL2-3-4		215	261	83.1	0.8	178.22	-	4.92	2.2	1	-
JL2-3-5		319	220	69.9	0.8	192.59	-	6.39	2.2	1	-
JL2-3-6		150	134	42.6	0.6	151.46	-	3.72	3.0	1	-
AVG (CoV)		303 (61%)	202 (22%)	64.6 (22%)	0.8 (29%)	216.83 (22%)	-	5.06 (18%)	2.4 (25%)	-	-
JL3-3-1		429	395	83.9	1.0	220.55	-	8.40	2.6	1	-
JL3-3-2		404	345	73.3	1.0	139.75	-	6.04	2.9	1	-
JL3-3-3	0.79	167	312	66.3	1.1	76.60	-	4.03	3.3	1	-
JL3-3-4		-	290	61.5	1.9	-	-	4.23	2.9	1	-
JL3-3-5		-	385	81.8	1.0	-	-	5.79	2.8	2	281
JL3-3-6		163	364	77.3	1.0	22.22	-	6.06	2.6	1	-
AVG (CoV)		291 (43%)	349 (11%)	74.0 (11%)	1.2 (29%)	114.78 (64%)	-	5.76 (25%)	2.8 (8%)	-	-

4.3.4.1. Tensile performance of singly reinforced NTRM specimens

Fig. 4.7 shows the tensile stress-strain response of representative TRM specimens reinforced with a single layer of F1, F2, and J textiles. All F2L1- and JL1-TRM composites failed due to the progressive rupture of the yarns, while F1L1-TRM specimens failed after developing large deformations at relatively low values of load. Failure of F1L1-TRM possibly occurred due to the non-homogenous penetration of the mortar matrix within the yarn cross-section that caused a “telescopic” failure mechanism resulting in the relative slip of the inner filaments [93,139].

The three typical stages of tensile response of TRM systems [90] are seen only in the case of F2L1 series. The F2L1 series are characterised by higher ductility (expressed as the ratio between strain at failure over strain at the first crack, accompanied by the formation of multiple cracks) and superior mechanical properties compared to their F1 and J counterparts. Overall, and in keeping with the performance of the corresponding yarns and textiles, flax-reinforced composites exhibited higher strength (80-200 MPa) and larger elongation values (4-8%) than jute-TRM (60 MPa and 0.8%, respectively). The jute-TRM tested in this study, however, exhibited better performance than that of other Jute-TRM systems reported in the literature [69], possibly due to the difference in the mechanical and physical properties of the jute textile at all scales examined (i.e. fibre, yarn, dry

textile). In some F2L1-TRM specimens, failure immediately followed the formation of the last crack, hence the third stage of stabilised cracking did not fully develop and the cracked stiffness could not be evaluated. As also observed in the tests on the corresponding textile specimens, the softening stage that followed the attainment of the peak load was triggered by the progressive failure of the filaments within individual yarns. Failure occurred when one or more yarns ruptured completely, causing a sudden drop in load. Although local debonding is expected to have developed in the proximity of the cracks, fracture of some of the yarns provides evidence that the textile was effectively anchored. It should be noted that the tests on the F1-TRM specimens were halted when the sustained load was approximately 80% of the maximum recorded load, at which point the specimens were deemed to have failed.

All JL1 and some of F1L1 specimens (e.g. F1L1-3-3) were characterised by the formation of one single crack at a level of load significantly higher than the maximum load attained during the cracked stage and no strain hardening was observed. This may be attributed to the low reinforcement ratio (0.52% and 1.1% for JL1 and F1L1 series, respectively) and to the fact that the stress released upon the first crack is high enough to damage some of the yarns within the reinforcement, thus decreasing the amount of reinforcement still able to carry the load. It should be noted that for these specimens, the maximum load of the corresponding TRM coupon was considered equal to the maximum load attained during the cracked stage, $P_{NTRM,max}$ (Tables 4.5 and 4.7). In the remaining F1L1 specimens, the crack development stage was observed, with few cracks being formed and widening significantly during the test. Although the formation of multiple cracks in F2L1 series throughout the entire load history underlines the contribution of the matrix to the overall composite performance, the development of relatively large discrete cracks accompanied by a large release of energy resulted in the limited contribution of the fibres to the overall strength. This suggests that the amount of F2 textile reinforcement provided (1.44%), although higher than the critical [119], was still relatively low (as also observed in [99]).

4.3.4.2. Effect of number of NTRM layers

The stress-strain response of representative specimens reinforced with multiple NTRM layers is shown in **Fig. 4.8**, along with the tensile behaviour of the corresponding reinforcing textile (dashed line). The increase in the reinforcement ratio, through the addition of NTRM layers, resulted in F1- and F2-TRM systems with better composite behaviour, as evidenced by the fact that all multi-layer F2-TRM and most of the F1-TRM specimens clearly exhibited all stages of crack initiation and development (i.e. uncracked, crack development, fully cracked and softening stage). An increase in the number of TRM layers promoted a more uniform stress distribution across the thickness of the F1 and F2 multi-layer TRM specimens due to the more uniform distribution of the yarns, and led to a post-cracking behaviour characterised by a higher number of cracks with a smaller width (see also Section 4.3.4.5). The reinforcement ratios of 1.48% for F1 and 1.92% for F2 were found to be

sufficient to develop composite action. This observation was also reported in previous experimental studies investigating the effect of the number of layers in similar flax-TRM composites [99,101]. Despite the increase in the number of layers, all J-TRM specimens developed only one single crack followed by a sudden drop in load, indicating that the maximum provided reinforcement ratio in these specimens (0.79% for the three-layer system) (**Table 4.7**) was still insufficient to enable stress redistribution, hence no composite action was achieved. None of the composite systems developed the full stress and stiffness of the associated bare textiles. This can be mainly attributed to two mechanisms: 1) the yarns of the bare textile specimens were embedded in resin, and not in mortar as for the coupons, which allowed for a better impregnation of the yarns, thus enabling a better distribution of stress within the yarns' cross-section; 2) the development of cracks across the coupons caused the yarns in correspondence of the wider part of the cracks to be highly stressed and rupture at an average value of stress lower than that observed for the textiles. The strength ratios ($f_{NTRM,max}/f_t$) varied between 0.30-0.45 for F1 and J and 0.62-0.77 for F2, while the stiffness of the NTRM was about 30% of that of the corresponding textile. Maximum average strain values similar to those of the bare textiles were developed by F1- and J-TRM, while F2-TRM specimens were characterised by a higher elongation than the bare textile due to the formation of multiple cracks and the progressive engagement of the individual yarns along the composite.

The increase in the number of NTRM layers did not change the failure mode of the composites and no delamination or slippage of the reinforcement in the gripping areas were observed in any of the tested specimens. The failure modes of representative specimens of each NTRM series are given in **Fig. 4.9**, along with their classification according to RILEM TC 250-CSM [54]: A) major crack in the gripping area; B) tensile failure and major crack in the middle of the specimen; and C) textile slippage in the gripping area. In addition, the telescopic mode of failure observed for some of the specimens is indicated as "T".

A combined tensile/flexural failure was observed for some of the specimens due to several factors, including: i) the lack of symmetry in the positioning of the reinforcement within the mortar layer (across both thickness and width); ii) non-uniform geometry of the mortar layers; and iii) non-uniform cross-section geometry along the specimen.

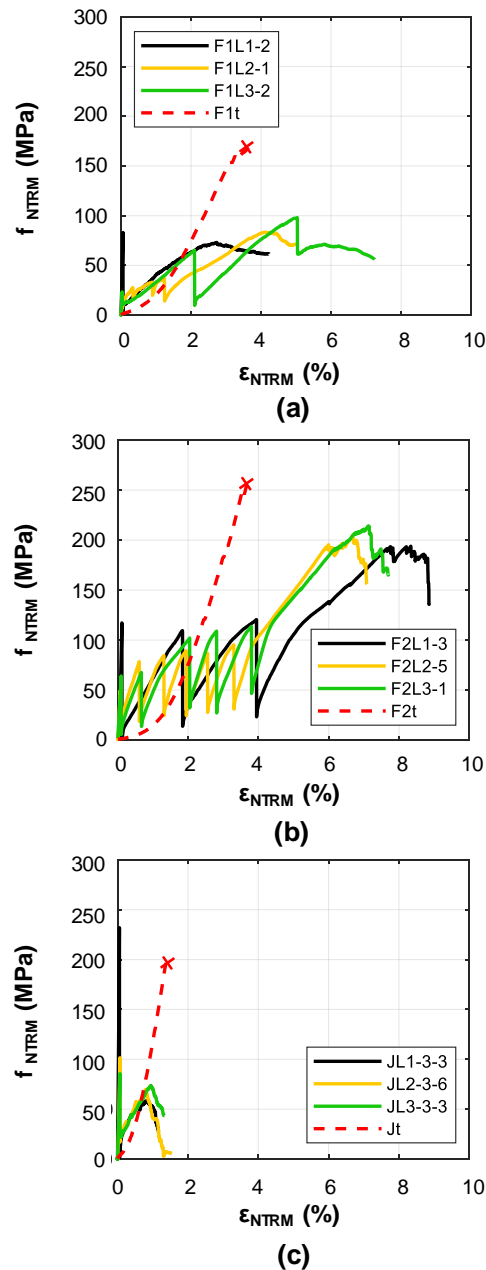


Fig. 4.8 Effect of number of NTRM layers on the tensile stress-strain response of representative specimens: a) F1-TRM, b) F2-TRM, and c) J-TRM (dashed lines represent the average tensile response of the corresponding bare textiles up to failure).

The effect of the number of NTRM layers on the mechanical properties of the composites is shown in **Fig. 4.10a-b**. An enhancement in the ultimate tensile strength ($f_{NTRM,max}$) and maximum elongation ($\epsilon_{NTRM,max}$) is seen in all cases. Normalising the ultimate mechanical properties to those of single-layer TRM specimens, F2 shows an increase of approximately 15% in both strength and elongation when using two and three layers. The maximum strain developed in F1-TRM increases proportionally with the number of layers (up to 20% for three layers), while the strength does not increase significantly. J-TRM specimens show the largest gain in terms of elongation with the

increase in the number of TRM layers, while only a moderate increase in strength was observed when increasing the number of layers from two to three (up to 20%), though the results display large variability (**Table 4.7**). With respect to the cracked stiffness, F2-TRM composites exhibit an increase of around 30% when two or three layers are used, while no considerable change is apparent for J-TRM and F1-TRM specimens. Variation in the stiffness values of the uncracked and crack development stages are not commented upon as the former depends on the matrix properties and the latter was absent in all specimens in the J-TRM series and in all F2L1-TRM and F1L1-TRM specimens.

The effect of increasing the mechanical reinforcement ratio ($\rho_f E_f / E_m$) on the normalised maximum load capacity of the tested composites (with respect to the theoretical resistance of the matrix - P_{mt}) is shown in **Fig. 4.10c**, along with the threshold defining the matrix-controlled fracture (horizontal dashed line). It can be seen that mechanical reinforcement ratios greater than 3% can successfully strengthen the matrix in Flax-TRM (critical reinforcement ratio). However, such an amount is not sufficient when using jute reinforcement due to poor fibre-mortar interaction (as evidenced by the absence of multiple cracks). As a result of the brittle nature of the matrix and the complexity of the bond behaviour at the fibre-mortar interface, the tensile response of natural fibre TRM composites cannot be predicted based solely on the amount of reinforcement, highlighting the need for more experimental data that can be used to develop reliable analytical models.

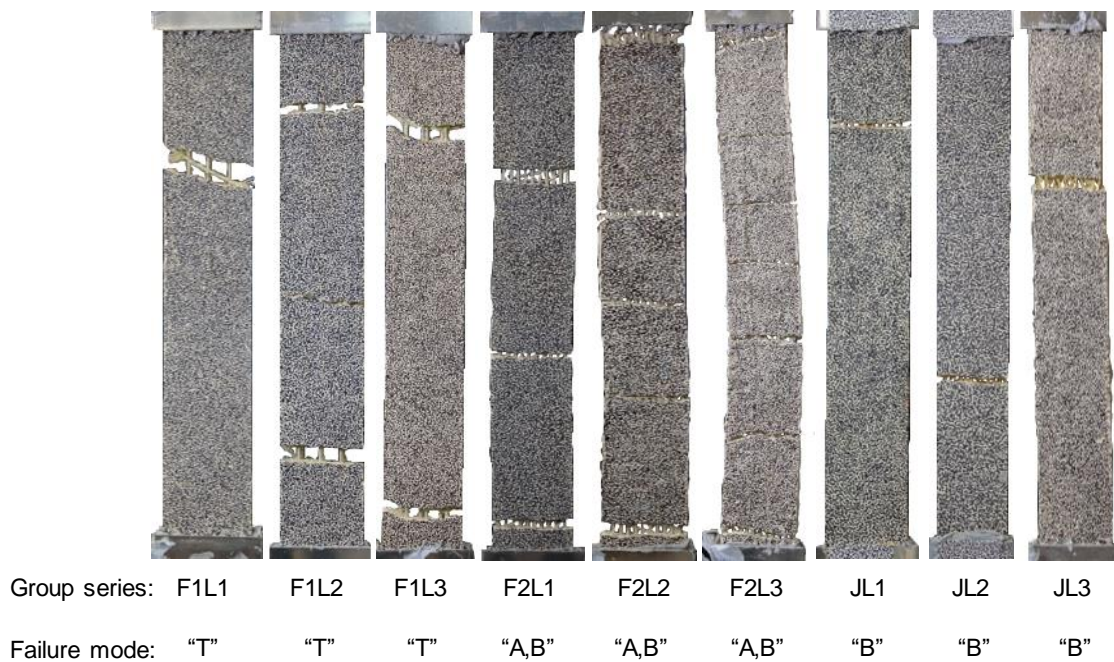


Fig. 4.9 Failure modes of representative NTRM specimens for each series and corresponding classification according to RILEM TC 250-CSM.

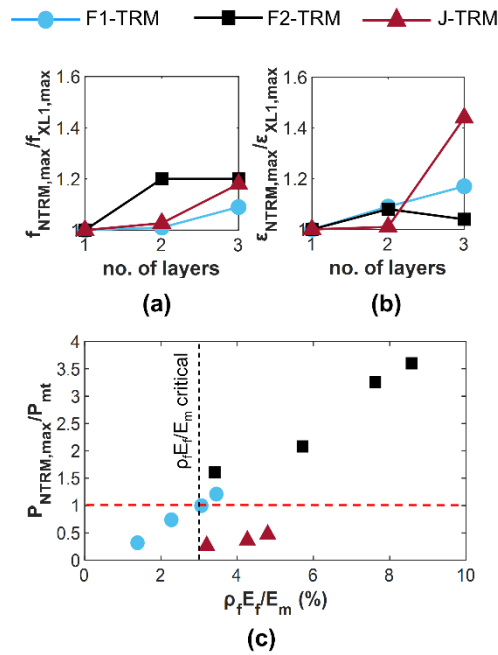


Fig. 4.10 Effect of number of reinforcing layers on: (a) maximum strength; and (b) strain at peak load. (c) normalised load bearing capacity as a function of the mechanical reinforcement ratio (dashed line represents the threshold defining the matrix-controlled fracture).

4.3.4.3. Effect of textile geometry

The effect of textile geometry on the crack pattern, composite performance and failure mode of the resulting composites was assessed for the flax-reinforced specimens. The specimens made with the F2 textile developed a relatively ductile response and a more pronounced tension stiffening effect, with more distributed cracking along the specimen at increasing reinforcement ratios. In addition to the inherent superiority of the mechanical properties of the F2 fibres (see **Table 4.2**), the better performance of the F2-TRM composites may be attributed to the better architecture of the F2 textiles, which comprise smaller, twisted yarns that can ensure a good mechanical interlock with the surrounding matrix and result in better bond performance. The relative dense mesh of the F2 textile does not seem to hinder the good penetration of the mortar through the mesh openings and no signs of interlaminar shear failure were observed. The tensile properties of the F2 textile-reinforced composites, along with their high ductility and cracking behaviour, are consistent with those of similar flax textile-reinforced lime-based composites investigated in previous studies [98,99,101].

On the contrary, the thicker, straight yarns used in the F1 textiles prevent adequate penetration of the matrix through the multiple filaments and promote telescopic failure. This has a direct influence on the interfacial bonding mechanism and impedes the exploitation of the full capacity of the F1 textile. In addition, despite the higher reinforcement ratio (1.11% for F1L1 and 0.86% for F2L1), the large mesh size of F1 textiles did not lead to effective control of cracking. The larger diameter of the F1 yarns may also have resulted in a higher moisture absorption, leading to premature cracking in the mortar and affecting the overall composite performance.

4.3.4.4. Effect of mortar thickness

The effect of thickness of the mortar overlays was examined for single-layer composites reinforced with flax textiles and the tensile stress-strain response is shown in **Fig. 4.11**. The increase in mortar thickness, and the consequent decrease in reinforcement ratio, has a negative impact on the tensile strength and strain developed by the composites reinforced with F1 textiles. On the contrary, a thicker overlay was beneficial in the case of F2-TRM specimens, resulting in higher tensile strength capacity and strain, albeit accompanied by larger energy release during the crack development stage. The amount of reinforcement, the textile characteristics and the textile bond performance play a key role in the performance of the resulting composites. F1-TRM specimens are characterised by insufficient reinforcement ratio, with inadequate bond between the fibres and the mortar (see also Section 4.3.4.3), and the higher load required to induce the mortar's failure in the thicker composites may have caused damage and premature failure to some of the yarns within the textile reinforcement. F2-TRM specimens are characterised by a low, yet sufficient amount of reinforcement (1.44% and 0.86% for 3 and 5 mm mortar overlays, respectively) with relative good bond, hence the higher amount of mortar in the thicker composites does not lead to a reduction in mechanical performance, despite the 40% reduction in the reinforcement ratio. Previous research has also shown that for a given reinforcement ratio, the use of thinner overlays could result in higher porosity and reduced mechanical properties [140]. Overall, the failure mode is not affected by the mortar thickness and is characterised by telescopic failure in F1-TRM specimens and progressive rupture of yarns in F2-TRM specimens.

4.3.4.5. Crack Development

The development of cracking along a representative specimen (F2L2-6) subjected to direct tension is illustrated in **Fig. 4.12a** at load values corresponding to the formation of each consecutive crack. Full-field DIC was used to analyse qualitatively the distribution of longitudinal strain along the specimen (y axis in **Fig. 4.12a**) and examine crack initiation (high strain concentration zones) and evolution, as well as exact crack location.

The width of individual cracks was computed as the average relative displacement of four pairs of points on opposite sides of each crack (see **Fig. 4.12b**), while the average crack width for a specimen being defined as the ratio between the sum of the widths of all the cracks prior to failure divided by the total number of cracks. The evolution of the average and maximum crack width for specimen F2L2-6 is plotted in **Fig. 4.12c**.

The maximum average crack width at peak load (w_{avg}), the number of cracks (n_w) and the saturation crack spacing (s) for all specimens are given in Tables 4.5-4.7. As mentioned previously, the F2-TRM specimens were characterised by a larger number of cracks evenly distributed along the length of the specimen, indicating a good stress-transfer mechanism at the fibre/matrix interface.

Maximum crack width values at peak load of about 8-11 mm were observed for specimens F1- and F2- TRM specimens with a single layer of textile, while the J-TRM counterparts exhibited a crack width of 2-3 mm.

In general, higher amounts of reinforcement lead to smaller average crack widths, and denser meshes result in smaller values of crack spacing. As discussed in Section 4.3.4.1, however, the use of different amounts of jute textiles does not affect the crack formation mechanisms, with only one crack developing in all of the tested specimens.

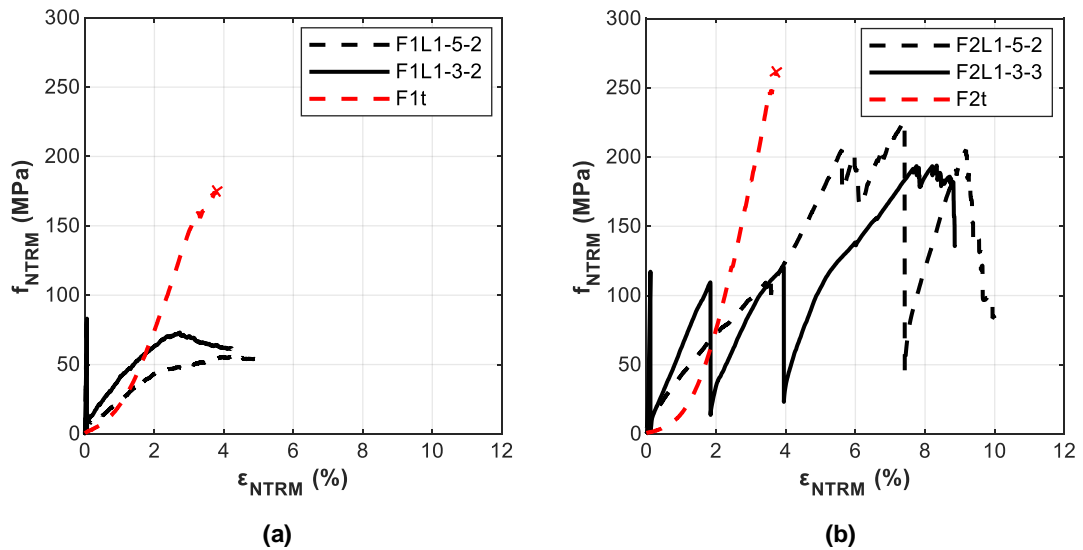


Fig. 4.11 Effect of mortar overlay thickness on the tensile response of (a) F1-TRM and (b) F2-TRM specimens.

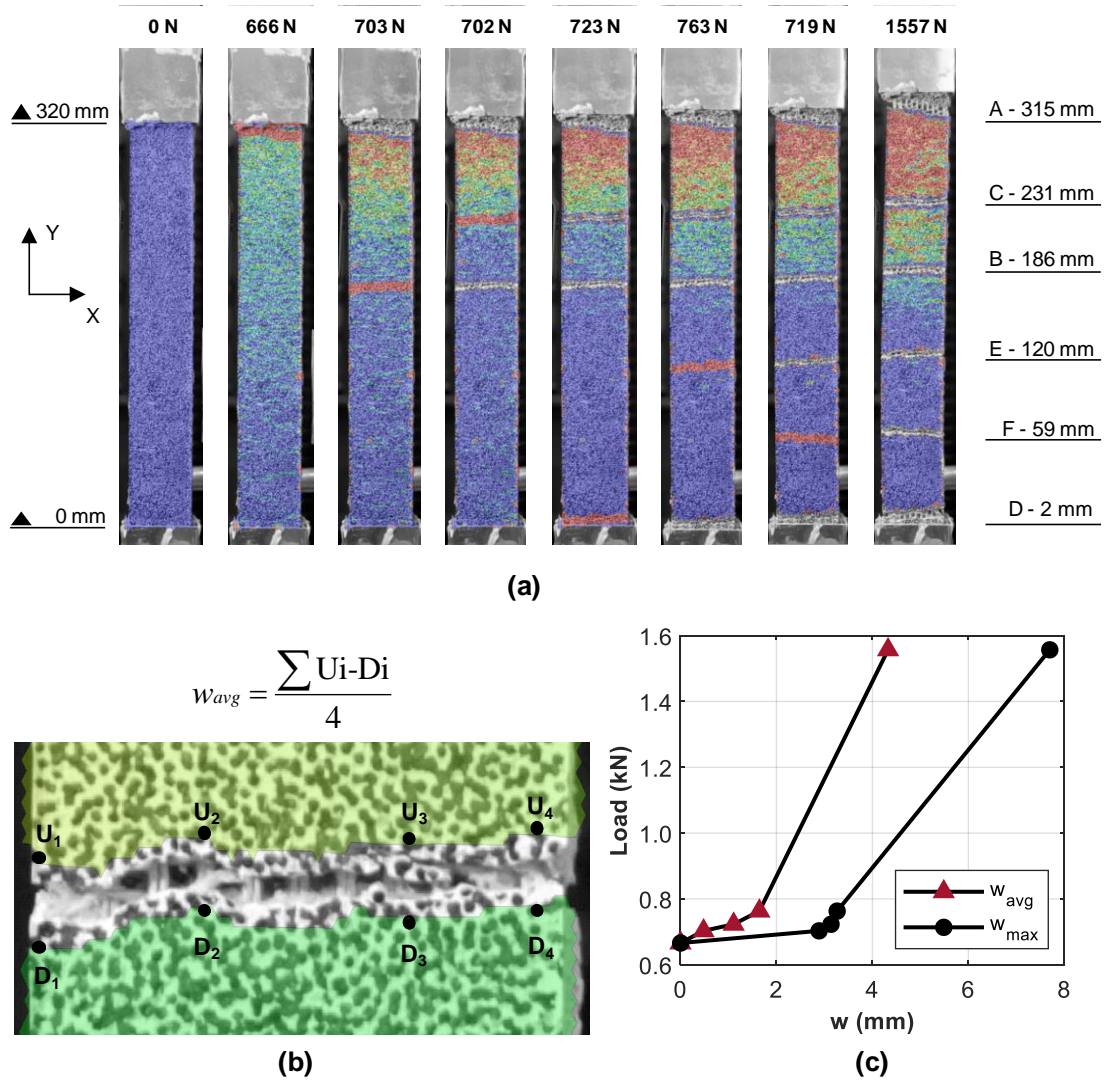


Fig. 4.12 Crack development for a representative F2-TRM specimen: (a) strain field at subsequent crack formation stages with corresponding load and crack location; (b) calculation of the crack width (image at 100% of $f_{NTRM,max}$); and (c) development of average and maximum crack width

4.4. GENERAL DISCUSSION AND RECOMMENDATIONS

4.4.1. Interrelationship between natural fibres, yarns, textiles

Tests at multiple scales are required to obtain information on the basic material properties and assess the effect of yarn geometry as well as weaving characteristics on the performance of the textile and on the stress-transfer mechanisms. This information is required to optimise the design of textiles for TRM strengthening applications and to quantify the exploitation of the basic material properties. In addition, the determination of the constitutive relationship of yarns and textiles is of fundamental importance for the development of numerical and analytical models, which will enable further systematic and parametric studies.

Yarns can typically develop higher strains than the individual fibres at lower strength and stiffness. The linear density and the level of twist of the individual fibres within the bundle have a

marked effect on the yarn structural performance. Yarns of lower linear density and higher twist level exhibit superior mechanical properties. The performance of high linear density yarns can be limited by the development of a pronounced shear lag effect, which can result in a reduction in both strength and stiffness of up to 74%.

The tensile properties of the textiles are dependent on the yarn geometry and weave characteristics. Local phenomena (e.g. friction at warp-weft intersection, non-uniform activation of the yarns and yarn's filaments) can also affect their overall response. For the same reinforcement material (flax), the woven textile (F2) was characterised by similar stiffness to that of the corresponding yarn, however the interlacing of warp and weft yarns caused local stress concentrations, resulting in a loss of strength and ultimate strain of approximately 20%. On the other hand, the largely spaced and stitched flax textiles (F1) were characterised by an increased ultimate strain and reduced stiffness, yet maintaining a strength similar to that of their constituent yarns.

Although the mechanical and physical properties of natural fibres are affected by a large inherent variability, textile properties are less variable and can be accounted for in a similar manner as for existing TRM systems.

4.4.2. Critical parameters and recommendations for the design of NTRM composites

The NTRM composite performance is strongly affected by the reinforcement ratio, the textile characteristics and the bond performance at the fibre/mortar interface.

The use of mechanical reinforcement ratios greater than 3%, provided that the capacity of the reinforcement exceeds the mortar cracking strength, results in composites failing due to rupture of the reinforcement (either of filaments or individual yarns), characterised by multiple distributed cracking and high ductility. An increase in reinforcement ratio through the addition of NTRM layers does not affect significantly the mechanical properties of the composites, but can ensure a more uniform stress distribution and a better composite action. Although the application of thicker mortar overlays results in a reduction in reinforcement ratio, this is not detrimental to the mechanical properties of the system, as long as the critical reinforcement ratio is provided.

The poor penetrability of high linear density yarns may promote telescopic failure and impede the full exploitation of the textile within the composite (up to 45%). On the contrary, the use of twisted yarns of lower linear density improves the mechanical interlock between textile and mortar and can ensure composite action with high exploitation of the textile tensile strength (77%).

Existing provisions for the characterisation of the stiffness developed by the TRM composite should be re-evaluated to represent the actual contribution of natural reinforcement. The development of the crack initiation or crack stabilization stages is dependent upon the amount and type of textile, as well as the fibre-matrix interaction. The design stiffness value for each of these stages should be determined as the slope of the best-fit line within an appropriate strain range, rather than the secant value within predefined stress levels.

4.5. CONCLUSIONS

This experimental study examines the tensile performance of flax- and jute-TRM with a view of assessing their potential as strengthening solutions for masonry structures. A multi-scale approach was adopted and detailed characterisation of fibres, yarns, textiles and composites was carried out. The effect of key design aspects, including the number of NTRM layers, the textile geometry and the mortar overlay thickness was investigated. Based on the results and foregoing discussion, the following conclusions can be made:

- Both flax and jute fibres exhibit mechanical properties suitable for structural applications, with strengths equal to 560 MPa for jute and ranging from 680 to 865 MPa for flax. Stiffness values range from 25 to about 40 GPa.
- Among the tested composites, Flax-TRM developed the highest strength (80 to 200 MPa) and elongation capacity (4 to 8%).
- The good interaction between the denser flax textile comprising low linear density yarns and the lime mortar enables the formation of multiple cracks and more uniform stress distribution in the composite, thus making it suitable for strengthening applications.
- The increase in the number of NTRM layers leads to an almost directly proportional increase in load capacity and to a more ductile behaviour. However, the maximum stress sustained by the textiles and the ultimate strain developed by the composites does not increase significantly (up to 20% on average).
- For the Flax-TRM tested in this study the critical mechanical reinforcement ratio is 3%.
- For the tested Jute-TRM, the weak fibre-matrix interaction did not result in a structurally acceptable composite behaviour, even at the higher reinforcement ratios examined.
- Thicker mortar overlays do not necessarily improve the mechanical performance of the composite and can be detrimental when low mechanical reinforcement ratios are provided.

Overall, flax textiles embedded in lime-based mortar offer high deformation capacity, along with a reasonably good strength and excellent environmental credentials, thus making them a promising solution as externally bonded systems for masonry structures. Further studies are required to examine the effect of different textile architectures and fibre provenance, and to examine the interaction between NTRM systems and masonry substrate, as well as their effectiveness as strengthening solutions.

Acknowledgments

The lime-based mortar was gratefully provided by Vimark S.r.L. The authors would also like to thank L. Barilli, G. Martinelli and S.L. Meghwar for their assistance in the experimental programme.

5. BOND OF FLAX TEXTILE-REINFORCED MORTARS TO MASONRY

N. Trochoutsou, M. Di Benedetti, K. Pilakoutas, M. Guadagnini, Bond of Flax Textile-Reinforced Mortars to Masonry, *Constr. Build. Mater.* 284 (2021) 122849.

doi: 10.1016/j.conbuildmat.2021.122849

Abstract

This paper investigates the structural performance of Flax-TRM (FTRM) systems bonded to a masonry substrate. Single-lap shear bond tests were carried out to assess the influence of bond length, number of TRM layers and bond width on the behaviour of two flax textiles of different architecture embedded in lime-based mortar. Conventional and non-contact measuring methods (DIC) were employed to gain additional insights into the development of stress transfer mechanisms and load-slip behaviour at the global and local scale. It was found that textile architecture significantly affects overall bond performance, with smaller diameter and twisted yarns arranged in a denser mesh utilising the fibre strength to a higher degree. The effective bond length for the tested single-layer systems is between 150 and 210 mm and failure is dominated by fibre rupture. A high variation in stress distribution was seen in multilayer specimens with a wider bond width, and this can lead to premature delamination. Finally, recommendations for testing in line with the existing RILEM experimental methodology are given to account for the high variability and unique failure modes observed in natural fibre TRM. This work aims to provide design guidelines for sustainable and effective structural strengthening solutions, which are particularly suitable for less developed countries.

This chapter consists of a stand-alone journal paper and includes the associated reference list at the end of the chapter. Additional information and further test results are presented in Appendix B.

5.1. INTRODUCTION

The international drive towards sustainable construction materials is currently fuelling research into the use of natural fibres as reinforcement for composite systems. Natural fibres are not only carbon neutral and cost-effective, but they also possess good mechanical properties at low specific gravity [30].

Owing to the many advantages offered by TRM over more traditional solutions, various commercial systems using advanced textiles have already been developed for both reinforced concrete and masonry structures using cement or lime-based mortars [25,48,49]. However, the high strength and stiffness of the advanced textiles currently used can rarely be fully utilised when applied to masonry substrates, due to vastly different strength and stiffness characteristics. In addition, their high cost discourages their use in less favoured economies. The rationale of using natural fibres with mortars is based on the hypothesis that the lower stiffness of these materials makes them more compatible with masonry substrates, as they can accommodate large strains without imposing high bond stresses.

Although the literature on NTRM systems is still in its infancy, several studies already examined the potential of using natural fibre textiles, such as flax, sisal, jute, hemp and cotton, in combination with lime-based mortars [69,86,98-102,116,141,142]. Nonetheless, rather than bond, these studies mainly focus on mechanical characterisation of the composites and their constituents [69,98-102, 141,100], durability [98,142,116] or methods to improve the fibre-to-mortar adhesion [86,100]. A study by Olivito et al. [104] has provided some preliminary encouraging evidence that adequate bond behaviour can be developed in flax-TRM systems bonded to masonry, with the flax textiles being able to develop their ultimate tensile capacity.

The complexity of the bond behaviour of advanced TRM/masonry systems has been highlighted in previous studies [34] and it is generally accepted that shear stress transfer mechanisms govern overall performance and that the tensile capacity of the textile reinforcement cannot be always effectively exploited. Additionally, mortar impregnation of the yarn cross-section can only be achieved to a limited degree and “telescopic” failures dominate the performance of some systems [139]. The inherent variability of natural fibres increases the complexity of these issues even further as both mechanical and physical properties can vary considerably along the length and width of the textile and affect the interaction between the textile and the mortar.

Test methods for the bond characterisation of TRM/masonry systems have been recently published by RILEM TC 250-CSM [54]. As the failure modes of natural fibre textiles may be different from those of advanced textiles, the suitability of the existing test methods for the characterisation of this new family of TRMs is yet to be assessed. Irrespective of the adopted test set-up, accurate measurements of strain along the textile reinforcement are essential for the development of reliable interfacial shear stress/strain relationships, but this has proven to be a very complex task [143]. Furthermore, as a result of specimen manufacture and alignment in test rigs, a

non-uniform strain distribution along the composite width is almost inevitable [144] as each yarn may be strained differentially leading to variations in recorded strain values along the width of up to 50% [145]. In some studies, strain gauges were attached to the textile in predefined locations by leaving openings in the mortar layer [27,146]. However, the openings themselves and the strain gauge adhesive interfere with stress transfer [31,147] and it is unlikely that the yarn strain can be quantified accurately in this manner. Optical contactless methods, such as Digital Image Correlation (DIC), were proven to provide better insight into the strain distribution of the unbonded textile as well as into the crack initiation and development throughout the top mortar layer [132].

One of the key design parameters for externally bonded strengthening systems is their effective bond length [27,148-150], typically defined as the minimum bond length required for the development of the maximum debonding force [150]. Crediting the unique shear transfer mechanisms developed in different TRM systems, some studies show that an increase in load carrying capacity can be developed for bond lengths longer than the effective length, albeit not significant [34]. Different bond lengths are also known to trigger different failure modes, with longer bond lengths in general causing a shift from debonding to fibre rupture (filaments or yarns) [148,150]. Other critical design parameters that can significantly affect the bond performance of TRM systems, such as the number of TRM layers, textile architecture and bond width, have received very limited attention and existing studies report contradictory results. In particular, although similar or higher axial stress values than the corresponding single-layer specimens are expected in multi-layer specimens [46,111,151], the addition of TRM layers may result in decreased ductility and premature debonding from the substrate [46,151,152]. The textile geometry is also very important, as it was shown that, for the same reinforcement ratio, denser meshes can result in lower bond properties [111,112]. Current studies on the effect of bond width on the bond performance of TRM systems ([111,149] against [147]) provide contradictory evidence and hence this parameter requires further investigation.

This paper addresses the aforementioned gaps in knowledge by investigating the bond behaviour of flax-reinforced lime-based composites (hereafter referred to as FTRM) applied to masonry substrates and contributes to the development of design guidelines for the strengthening or retrofitting of unreinforced masonry structures. Single-lap shear bond tests were performed on FTRM comprising two different types of flax textile to examine the effect of bond length, number of FTRM layers, textile architecture and bond width. The tests were monitored using a comprehensive set of experimental measurements with a combination of contact and non-contact methods (DIC). This study identifies the key parameters for the design of FTRM systems and, along with a previous study by the authors [141], enables a critical assessment of their potential as strengthening solution for masonry structures. The overall aim of this work is to provide design guidelines for sustainable and effective structural strengthening solutions, which are particularly suitable for less developed countries.

5.2. EXPERIMENTAL PROGRAMME

Fifty-one single-lap shear tests were carried out on single and multi-layer flax-TRM (FTRM) systems bonded to masonry prisms to investigate their bond performance. The examined parameters include: textile architecture (**Fig. 5.1**), bond length (from 65 to 260 mm), number of FTRM layers (from one to three) and bond width (50 and 100 mm). All textiles were embedded in the same lime-based mortar.

The characterisation of each constituent material and the FTRM composite is reported in the following sections, along with details of specimen preparation and experimental setup.

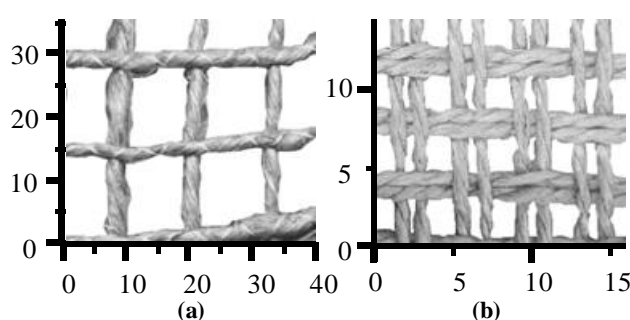


Fig. 5.1 Flax textile reinforcements adopted in the present study: (a) Flax1 (F1) and (b) Flax2 (F2). Scale in mm.

5.2.1. Masonry

Each masonry prism comprised commercial engineered solid clay bricks, measuring 215 x 102.5 x 65 mm and 10-mm thick mortar joints. A general purpose mortar was developed to achieve a low compressive strength (equivalent to class M2 according to EN 998-2 [153]), containing cement, hydrated lime and sand in proportions 1:2:9 by volume. The water/mortar ratio was 0.21, resulting in a fresh mortar flow value equal to 175 mm, according to EN 1015-3 [154].

The tests performed to characterise the masonry included: i) compression tests on 5 single brick units (following RILEM LUMA1 [155]); ii) flexural and compression tests on 39 mortar specimens (following EN 1015-11 [125]); iii) compression tests on 4 masonry prisms (following RILEM LUMB1 [156]). Linear variable displacement transducers (LVDT) of 5 mm stroke were installed on the opposite sides of each brick and masonry specimen to determine their elastic modulus. The average values of the mechanical properties of brick units, mortar and masonry prisms, are presented in **Table 5.1** in terms of flexural strength (f_{fl}), compressive strength (f_c), and Young's modulus (E), along with the associated number of tests (n) and their coefficient of variation (CoV).

Table 5.1 Mechanical properties of masonry prisms and their constituents. CoV in parentheses.

Specimen Type	n	f_n (MPa)	f_c (MPa)	E (MPa)
Brick Unit	5	-	124.3 (5%)	-
Masonry Mortar	13	0.7 (13%)	-	1290 (30%)
	26	-	2.3 (7%)	-
Masonry Prism	4	-	30.5 (2%)	1970 (5%)

5.2.2. FTRM

Flax textiles of different geometry (mesh size, yarn diameter), physical properties and weave characteristics (**Fig. 5.1**) were combined with a lime (NHL2)-based mortar, typically used in the field of restoration and repair of historic masonry structures. All textiles were balanced bidirectional, with equal mesh openings along the two orthogonal directions. The mechanical properties of the reinforcement (at a yarn and textile level), the mortar and the resulting composites were experimentally determined by the authors in a previous study [141] and they are summarised in **Table 5.2**, in terms of tensile strength (f_t), Young's modulus (E_f), strain at maximum stress (ϵ_{max}), and compressive strength (f_c), along with the corresponding cross-sectional area (A_f).

Table 5.2 Tensile properties of FTRM constituents and coupons [5] (CoV in parentheses).

Property	F1					F2					Lime-based mortar
	Yarn	Textile	Coupon			Yarn	Textile	Coupon			
			1L	2L	3L			1L	2L	3L	
f_t (MPa)	212.6 (9%)	196.4 (11%)	82.2 (15%)	83.0 (11%)	89.3 (15%)	377.9 (7%)	289.0 (6%)	177.8 (12%)	208.9 (8%)	205.0 (5%)	2.8 (15%)
E_f (GPa)	10.1 (12%)	7.1 (13%)	2.0* (15%)	2.1* (13%)	2.0* (43%)	14.4 (12%)	13.6 (7%)	3.0* (9%)	3.9* (9%)	3.8* (11%)	3.42 (18%)
ϵ_{max} (%)	3.6 (11%)	4.2 (10%)	4.1 (22%)	4.4 (11%)	4.7 (10%)	4.9 (5%)	3.8 (4%)	7.3 (14%)	7.9 (8%)	7.5 (%)	-
f_c (MPa)	-										7.7 (15%)
A_f (mm ²)	1.11	3.33	3.33	6.66	9.99	0.22	4.32	4.32	8.64	12.96	-

* cracked stiffness

5.2.3. Bond Specimen Preparation

Fifty-one stack-bonded masonry prisms (3 replicates per FTRM configuration) were manufactured using two to four bricks and 10 mm thick mortar joints. The prisms measured 215 x 102.5 x 1 mm (nominal dimensions), where 1 was dictated by the bond length under investigation. Five different bond lengths (BL varying from 65 to 260 mm) were examined at a constant bond width equal to 100 mm, corresponding to 7 and 40 yarns in the width direction for specimens reinforced with F1 and F2 textiles, respectively. The effect of multiple FTRM layers and bond width was

examined only for specimens of bond length equal to 260 mm to ensure adequate stress transfer between FTRM and substrate. The number of layers varied from 1 to 3. Bond widths (BW) of 50 mm and 100 mm were considered only for the specimens reinforced with single and multiple FTRM. All of the configurations examined as part of this test programme are shown in **Fig. 5.2** along with the associated number of tested specimens.

Prior to the application of the FTRM, all masonry prisms were kept damp under a wet hessian cloth for 7 days and then stored in standard laboratory conditions (20 °C and RH < 70%) for at least 21 days. The FTRM was applied following the recommendations of RILEM TC 250-CSM [54]. A bespoke timber frame was glued to the masonry substrate, which was previously thoroughly brushed and water saturated to avoid absorbing moisture from the mortar. The FTRM was applied on one side of the masonry following a hand lay-up procedure, including: a) the application of a first mortar layer, b) the manual embedment of the reinforcing textile into the mortar and c) the application of the top mortar layer. The same procedure was repeated for the specimens fitted with multiple FTRM layers. All mortar overlays were 3 mm thick, resulting in composites of total thickness varying from 6 to 12 mm. Special care was taken to ensure a uniform thickness across the bonded area. The bonded area in all specimens started 30 mm away from the front face of the prism to avoid stress concentrations, and was positioned centrally width-wise. The unbonded textile was 600 mm long. Specimens were kept damp for a total period of 28 days, whilst protecting the unbonded textile against humidity, and were subsequently stored in standard laboratory conditions until testing.

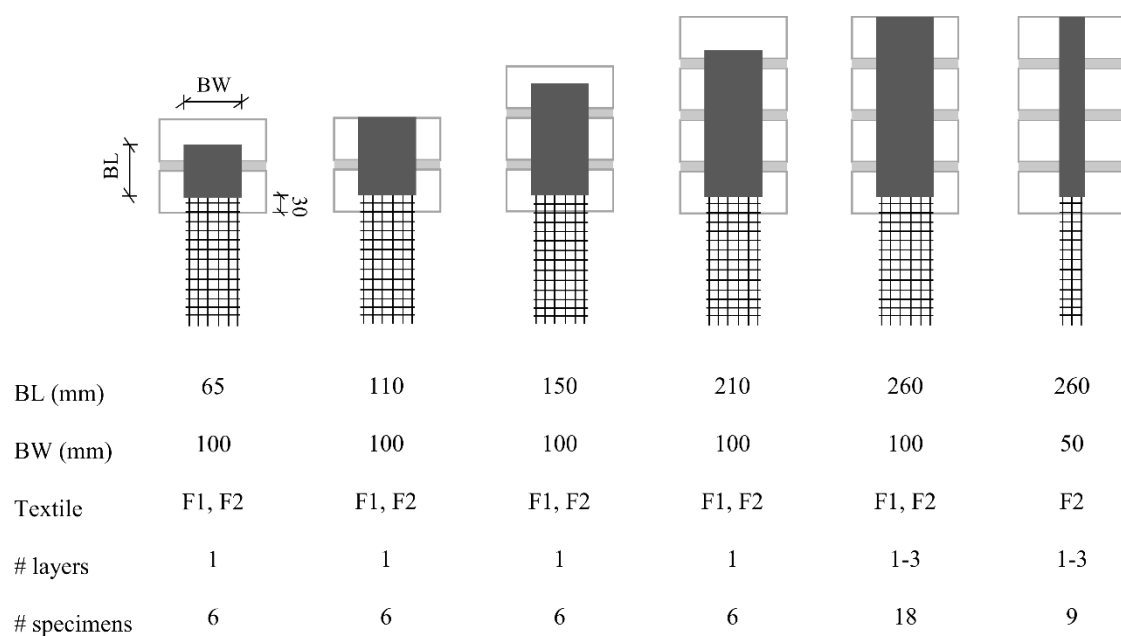


Fig. 5.2 FTRM strengthening configuration (all dimensions in mm).

5.2.4. Experimental Set-up

The bond behaviour of the examined FTRM systems was investigated by employing a single-shear pull-push set-up (**Fig. 5.3**). Single-lap test setups are easier to implement and provide more reliable information on post-peak response that is not normally possible in double-lap tests, since in double-lap tests, after the initiation of debonding, there is loss of symmetry. The masonry components of the specimens were fixed horizontally in a reaction steel frame bolted to a rigid support to avoid rotations during the test. A transversal steel element was bolted to the two sides of the reaction frame and was used to constrain the rear end of the specimen and to prevent overturning.

The tests were performed in displacement control at a rate of 0.5 mm/min. A triptych of measures was implemented to mitigate any potential misalignment of the applied load: a) a levelling plate was placed under each specimen; b) an additional plate equipped with a spherical seating was placed between the reaction frame and the masonry prism; and c) a long length (of 600 mm) was employed for the unbonded textile. Prior to testing, 150 mm long aluminium tabs were epoxy-bonded to the loaded end of the textile to ensure adequate load transfer and prevent slippage within the gripping area. For the specimens with multiple FTRM layers, additional plates (3 mm thick) were placed in between the textile layers to ensure alignment.

A pretension load of 100 N was applied prior to the installation of the instrumentation to eliminate any potential slack in the textile and avoid spurious measurements.

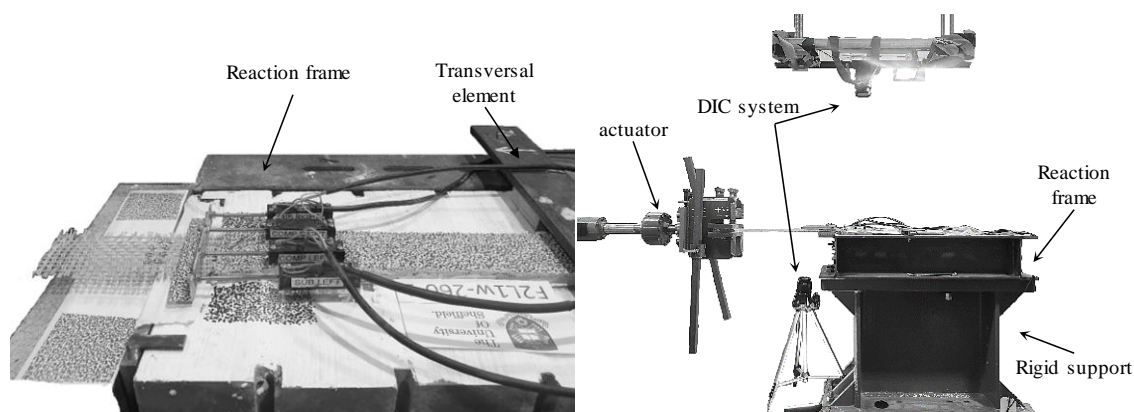


Fig. 5.3 Experimental test setup and instrumentation.

5.2.5. Instrumentation

Both conventional instrumentation and a non-contact optical measuring system (DIC) were used to monitor the slip of the textile and the slip of the FTRM with respect to the masonry support (**Fig. 5.3, Fig. 5.4**).

5.2.5.1. Conventional measurements

Four linear potentiometers of 10 mm stroke length were mounted on the FTRM/masonry system (**Fig. 5.4**): i) two on the substrate (POT_{IS}), on either side of the bonded area, to measure the slip

between the textile and the substrate, and ii) two on the composite ($POT_{i,c}$), on either side of the bonded width, to measure the slip between the textile and the composite. The subscript i indicates the side of the specimen being monitored, with L or R standing for left or right, respectively. A thin aluminium L-shaped plate was attached to the flax reinforcement at the beginning of the unbonded area and served as a reaction point for the potentiometers.

5.2.5.2. Non-contact measurements

A 2D-DIC setup was employed to obtain displacement and strain measurements on the surface of the masonry prism and the FTRM composite and gain additional information on crack initiation and development. The surface of the masonry was whitewashed to provide sufficient contrast for the identification of the speckle pattern, while the white lime mortar did not require any additional preparation. The speckle pattern was manually applied on both masonry and FTRM across the region of interest, which included the total length of the masonry prism and part of the unbonded textile extending from the loaded end. A computer-generated speckle pattern was affixed to both the reaction plate and the optical targets positioned at selected locations along the unbonded length of the longitudinal yarns (**Fig. 5.4b**). The optical targets were used to quantify the strain development across the textile of all specimens. Both top and bottom textile layers were monitored in the case of multi-layer FTRM systems to identify strain differences.

Virtual extensometers ($POT_{i,v}$) were created alongside the potentiometers and used to obtain additional displacement and slip measurements (**Fig. 5.4c**). DIC was also employed to obtain local displacements and strains along individual yarns across the width of the unbonded textile as well as to measure their global slip (**Fig. 5.4d**).

A single camera positioned 0.5 m above the specimen was used for all tests on single-layer FTRM, while a second camera, positioned 0.3 m below the unbonded textile, was used to monitor the displacement of the bottom textile layer of the multi-layer FTRM systems (**Fig. 5.3**).

Images were acquired with CMOS digital cameras having a 4272×2848 pixel resolution and the measurement surface was uniformly illuminated by led lights. During the test, the shutter was remotely triggered every 3 seconds by the data acquisition system. The acquired images were processed with GOM Correlate [133] and a subset and step size of 50 and 10 pixels, respectively, were chosen for the analysis. The displacement and the strain resolution obtained from the DIC analysis were $1.25 \mu\text{m}$ and approximately $100 \mu\epsilon$, respectively.

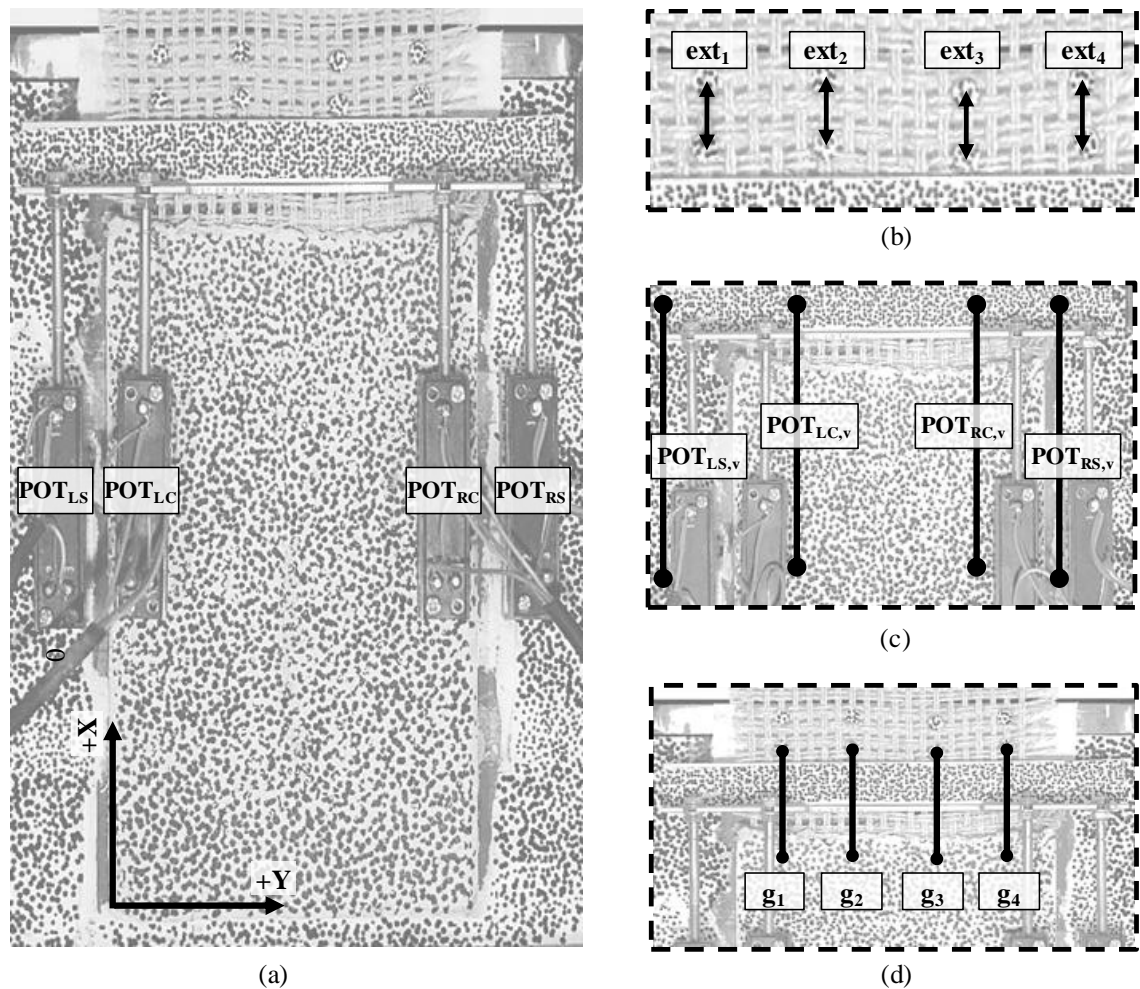


Fig. 5.4 (a) Instrumentation layout and typical speckle pattern for non-contact measurements; (b) location of optical targets; (c) virtual extensometers alongside the potentiometers and (d) virtual extensometers for slip measurements of individual yarns.

5.3. RESULTS AND DISCUSSION

5.3.1. Introductory Remarks

The overall performance of the specimens tested was derived based on the following assumptions: a) the cross-sectional area of the yarns is constant during the test; b) the stress distribution is uniform across the composite width and across the individual filaments of each yarn as well as between the multiple FTRM layers; c) the elongation of the unbonded textile is uniform across the width; d) the slip of the textile is uniform across the width of the composite. Although these assumptions enable a comparative analysis with published data for different FTRM systems, their correctness will be assessed and discussed in the following sections.

The results obtained from the single-lap shear tests on the FTRM systems bonded to masonry prisms are summarised in Table 5.3-5.6, grouped per flax type and bond length (Tables 4.3 and 4.4), number of FTRM layers (Table 5.5) and bond width (**Table 5.6**). Both average values and CoV are presented.

The specimen ID follows the format XY-BL-BW-n, where X denotes the type of textile reinforcement (F1 or F2); Y is the number of FTRM layers (L1, L2 or L3); BL is the bond length (65 to 260 mm); BW is the bond width (50 or 100 mm) and n is the replicate number of the specimen (1 to 3). For instance, F2L3-260-100-2 identifies the second replicate with three layers of Flax2 textiles bonded over an area measuring 260 mm in length and 100 mm in width.

Table 5.3 Experimental results for single F1-TRM of 100 mm bond width (CoV in parentheses)

Specimen ID	no. layers	BL (mm)	$P_{b,max}$ (N)	$f_{b,max}$ (MPa)	τ_{max} (MPa)	$g_{t,max}$ (mm)	η_t (%)	η_{TRM} (%)	μ_{gt}	μ_G	Failure Mode
F1L1-65-100-1*			271	34.8	0.04	1.06	18	42	2.0	2.2	T, D
F1L1-65-100-2	1	65	228	29.3	0.04	0.61	15	36	3.1	3.2	T, D
F1L1-65-100-3			160	20.6	0.02	0.73	11	25	12.3	15.4	T, D
AVG			220	28.3	0.03	0.80	14	34	5.8	7.0	
CoV			(25%)	(25%)	(25%)	(29%)	(25%)	(25%)	(97%)	(106%)	
F1L1-110-100-1*			351	45.2	0.03	3.04	23	55	2.8	3.6	T, D
F1L1-110-100-2*	1	110	371	47.7	0.03	2.42	24	58	4.0	5.2	T, D
F1L1-110-100-3			284	36.9	0.03	1.56	15	35	-	-	T, D
AVG			315	40.5	0.03	2.34	21	49	2.3	4.4	
CoV			(26%)	(26%)	(26%)	(32%)	(27%)	(27%)	(91%)	(26%)	
F1L1-150-100-1			554	72.0	0.04	1.55	37	88	3.8	2.7	T, D, E
F1L1-150-100-2*	1	150	358	46.5	0.02	1.63	24	57	1.2	1.3	T, D, E
F1L1-150-100-3*			584	75.8	0.04	2.67	39	92	1.7	2.0	T, D, E
AVG			499	64.8	0.03	1.95	33	79	2.2	2.0	
CoV			(25%)	(25%)	(25%)	(32%)	(25%)	(25%)	(62%)	(36%)	
F1L1-210-100-1			331	43.0	0.02	2.94	22	52	1.6	1.8	T, D, E
F1L1-210-100-2	1	210	616	80.1	0.03	5.72	41	97	1.1	1.2	T, D, E
F1L1-210-100-3			606	78.7	0.03	5.50	40	96	1.1	1.2	T, D, E
AVG			518	67.3	0.02	4.72	34	82	1.3	1.4	
CoV			(31%)	(31%)	(31%)	(33%)	(31%)	(31%)	(22%)	(26%)	
F1L1-260-100-1*			268	34.4	0.01	1.17	18	42	1.0	1.1	T, D, E
F1L1-260-100-2	1	260	360	46.3	0.01	3.85	24	56	2.0	2.0	T, D, E
F1L1-260-100-3			204	26.3	0.01	1.61	13	32	1.0	1.0	T, D, E
AVG			278	35.7	0.01	2.21	18	43	1.3	1.4	
CoV			(24%)	(24%)	(24%)	(86%)	(24%)	(24%)	(41%)	(42%)	

*results derived from DIC analyses; Failure mode: T = telescopic; D and E as described in Fig. 5.7.

Table 5.4 Experimental results for single F2-TRM of 100 mm bond width (CoV in parentheses).

Specimen ID	no. layers	BL (mm)	$P_{b,max}$ (N)	$f_{b,max}$ (MPa)	τ_{max} (MPa)	$g_{t,max}$ (mm)	η_t (%)	η_{TRM} (%)	μ_{gt}	μ_G	Failure Mode
F2L1-65-100-1			1044	120.8	0.16	2.11	42	68	3.1	4.7	C, D
F2L1-65-100-2	1	65	993	115.0	0.15	2.57	40	65	2.2	2.8	C, D
F2L1-65-100-3 [†]			355	41.1	0.05	1.63	14	23	-	-	C, D
AVG			1019	117.9	0.16	2.34	41	66	2.6	3.8	
CoV			(4%)	(4%)	(4%)	(14%)	(4%)	(4%)	(24%)	(35%)	
F2L1-110-100-1 [†]			474	54.9	0.04	6.99	19	31	-	-	C, D
F2L1-110-100-2 [†]	1	110	474	54.8	0.04	3.35	19	31	-	-	C, D
F2L1-110-100-3 [†]			782	90.5	0.07	3.69	31	51	-	-	C, D
AVG			-	-	-	-	-	-	-	-	
CoV			-	-	-	-	-	-	-	-	
F2L1-150-100-1			1490	172.4	0.10	6.71	60	97	1.1	1.2	B, C, D
F2L1-150-100-2 [†]	1	150	1109	128.4	0.07	7.67	44	72	-	-	B, C, D,
F2L1-150-100-3			1555	180.0	0.10	6.95	62	101	1.1	1.2	B, C, D, E
AVG			1522	176.2	0.10	6.83	61	99	1.1	1.2	
CoV			(3%)	(3%)	(3%)	(2%)	(3%)	(3%)	(0%)	(0%)	
F2L1-210-100-1*			1799	208.2	0.09	6.71	72	117	1.1	1.1	D, E
F2L1-210-100-2	1	210	1923	222.6	0.09	7.21	77	125	1.2	1.3	D, E
F2L1-210-100-3*			1889	218.6	0.09	6.21	76	123	1.1	1.1	D, E
AVG			1870	216.5	0.09	6.71	75	122	1.1	1.2	
CoV			(3%)	(3%)	(3%)	(7%)	(3%)	(3%)	(5%)	(9%)	
F2L1-260-100-1			1728	200.1	0.07	6.77	69	113	1.2	1.3	D, E
F2L1-260-100-2 [†]	1	260	1193	138.1	0.05	5.47	48	78	-	-	D, E
F2L1-260-100-3			1870	216.4	0.07	9.93	75	122	1.1	1.2	D, E
AVG			1799	208.2	0.07	8.35	72	117	1.2	1.2	
CoV			(6%)	(6%)	(6%)	(27%)	(6%)	(6%)	(1%)	(1%)	

*results derived from DIC analyses; [†]excluded from discussion and average values

Table 5.5 Experimental results for multi-layer FTRM with 260 mm bond length and 100 mm bond width (CoV in parentheses).

Specimen ID	no. layers	$P_{b,max}$ (N)	$f_{b,max}$ (MPa)	τ_{max} (MPa)	$g_{t,max}$ (mm)	η_t (%)	η_{TRM} (%)	μ_{gt}	μ_G	Failure Mode
F1L2-260-100-1 [†]		583	47.5	0.02	8.68	19	45	-	-	T, E
F1L2-260-100-2*	2	1607	103.3	0.06	5.06	53	124	1.2	1.2	T, E
F1L2-260-100-3*		1030	66.2	0.04	2.79	34	80	1.2	1.3	T, E
AVG		1319	84.8	0.05	3.93	43	102	1.2	1.3	
CoV		(31%)	(31%)	(31%)	(41%)	(31%)	(31%)	(3%)	(5%)	
F1L3-260-100-1		1515	64.9	0.06	5.07	33	74	1.9	2.1	T, E
F1L3-260-100-2 [†]	3	330	14.2	0.01	3.78	7	16	-	-	T, E
F1L3-260-100-3		1415	60.6	0.05	10.54	31	68	1.1	1.2	T, E
AVG		1465	62.8	0.06	7.80	32	70	1.5	1.6	
CoV		(5%)	(5%)	(5%)	(50%)	(5%)	(5%)	(34%)	(41%)	
F2L2-260-100-1*		2753	159.3	0.11	6.70	55	76	1.1	1.1	C, D, E
F2L2-260-100-2	2	3183	184.2	0.12	7.30	64	88	1.1	1.2	C, D, E
F2L2-260-100-3 [†]		1573	91.0	0.06	7.64	31	44	-	-	C, D, E
AVG		2968	171.8	0.10	7.00	59	82	1.1	1.1	
CoV		(10%)	(10%)	(10%)	(6%)	(10%)	(10%)	(3%)	(6%)	
F2L3-260-100-1		1798	69.4	0.07	6.06	24	34	1.1	1.2	C, D, E
F2L3-260-100-2*	3	1733	66.9	0.07	11.26	23	33	-	-	C, D, E
F2L3-260-100-3*		2126	82.0	0.08	5.09	28	40	1.3	1.5	C, D, E
AVG		1886	72.8	0.07	7.47	25	35	1.2	1.3	
CoV		(11%)	(11%)	(11%)	(44%)	(11%)	(11%)	(9%)	(14%)	

*results derived from DIC analyses; [†]excluded from discussion and average results.

Table 5.6 Experimental results for F2-TRM with 260 mm bond length and 50 mm bond width (CoV in parentheses).

Specimen ID	no. layers	$P_{b,max}$ (N)	$f_{b,max}$ (MPa)	τ_{max} (MPa)	$g_{t,max}$ (mm)	η_t (%)	η_{TRM} (%)	μ_{gt}	μ_G	Failure Mode
F2L1-260-50-1*	1	789	182.7	0.06	6.05	63	103	1.1	1.2	D, E
F2L1-260-50-2		840	194.5	0.06	4.22	67	109	1.2	1.3	D, E
F2L1-260-50-3		912	211.2	0.07	3.15	73	119	1.2	1.3	D, E
AVG		847	196.1	0.07	4.32	68	110	1.2	1.3	
CoV		(7%)	(7%)	(7%)	(28%)	(7%)	(7%)	(3%)	(4%)	
F2L2-260-50-1*	2	1738	201.1	0.13	4.15	70	96	1.4	1.6	D, E
F2L2-260-50-2*		1511	174.8	0.12	6.74	60	84	1.1	1.1	D, E
F2L2-260-50-3		1678	194.2	0.13	4.68	67	93	1.4	1.6	D, E
AVG		1642	190.1	0.13	5.19	66	91	1.3	1.4	
CoV		(7%)	(7%)	(7%)	(26%)	(7%)	(7%)	(13%)	(19%)	
F2L3-260-50-1	3	2177	168.0	0.17	5.51	58	82	1.9	2.6	D, E
F2L3-260-50-2		2462	190.0	0.19	6.50	66	93	1.1	1.2	D, E
F2L3-260-50-3		2565	197.9	0.20	5.70	68	97	1.1	1.2	D, E
AVG		2401	185.3	0.18	5.90	64	90	1.4	1.7	
CoV		(8%)	(8%)	(8%)	(9%)	(8%)	(8%)	(43%)	(47%)	

* results derived from DIC analyses.

For each specimen, maximum load ($P_{b,max}$), maximum axial strength ($f_{b,max}$), maximum shear strength (τ_{max}) and corresponding global slip of textile to masonry ($g_{t,max}$) are reported. The axial strength was calculated by dividing the maximum load by the textile area ($A_t = n_l n_y A_y$), where n_l is the number of layers (1-3), n_y is the number of yarns in a single layer (7 for F1, 40 along a 100-mm bond width or 20 along a 50 mm bond width for F2) and A_y is the yarn cross-sectional area (as given in **Table 5.2**). The maximum shear strength was calculated at the FTRM/substrate interface as the maximum load divided by the bonded area. Three types of global slip measurements were recorded during each test: textile to masonry, g_t ; textile to FTRM, g_c ; and FTRM to masonry, $g_{TRM} = g_c - g_t$. The values g_t and g_c were calculated from the average measurements recorded by the two potentiometers placed on the masonry or mortar, respectively, and subtracting the elongation of the unbonded textile. It should be kept in mind that in the present study, the term global slip refers to the relative displacement between two reference points, and may include, as it will be discussed in the following sections, additional displacement caused by damage mechanisms that cannot be easily decoupled from the slip due to pure debonding.

The efficiency of each FTRM system is also assessed through exploitation ratios (**Tables 5.3-5.6**), which are calculated as ratios of tensile strength from bond tests to the tensile strength of the corresponding dry textiles (η_t), or corresponding FTRM coupons (η_{TRM}). Global slip (μ_{gt}) and energy absorption (μ_G) ductility ratios are also reported, calculated using values from the end of the elastic load-slip response and at a load degradation of 20%.

5.3.1.1. Instrumentation and Measurements

For some of the specimens, the potentiometers failed to capture the initiation of slip and the response of the corresponding virtual extensometers $POT_{i,v}$ (derived by DIC) was used in all subsequent analyses. **Fig. 5.5** shows the load-slip response of two different specimens as obtained by both contact (POT) and non-contact (POTv) instrumentation. In one case (**Fig. 5.5a**), the slip determined by DIC shows an almost exact match with that obtained by the potentiometers. However, in the second case (**Fig. 5.5b1**) DIC seems to capture the initiation of slip more accurately (earlier) than the physical potentiometers. **Fig. 5.5b2** provides a more detailed analysis of the different displacement readings recorded by all physical potentiometers (thin lines) and corresponding virtual extensometers (thicker lines) during the initial phases of loading (see **Fig. 5.4c** for location of measurements). It can be observed that the potentiometers are “activated” late and in a sequence that does not match their physical position, thus suggesting that the movement of some of the potentiometers was somehow restrained/delayed. DIC measurements typically show a more linear variation in displacement across the width of the specimen, consistent to small in-plane rotation and, hence, can be considered to yield more reliable results. Henceforth, for specimens exhibiting similar issues with the data acquired from potentiometers, the response obtained through DIC was used to calculate slip.

The elongation of the textile that had to be subtracted in order to determine global slip values was derived using two different methods: 1) using the non-linear tensile stress-strain behaviour of the dry textiles as obtained by the authors [141] (**Fig. 5.6**) and analytically described by Eqs. (5-1) and (5-2); 2) using the average of the strains measured by the virtual extensometers (ext_i) on the individual yarns.

$$f = \frac{E_f - E_i}{2\varepsilon_f} \varepsilon^2 + E_i \varepsilon \quad \text{for } \varepsilon \leq \varepsilon_f \quad (5-1)$$

$$f = \frac{E_f}{2(\varepsilon_f - \varepsilon_{\max})} \varepsilon^2 - \frac{E_f \varepsilon_{\max}}{\varepsilon_f - \varepsilon_{\max}} \varepsilon + \left(\frac{E_f + E_i}{2} \varepsilon_f + \frac{2E_f \varepsilon_{\max} \varepsilon_f^2 - E_f \varepsilon_{\max} \varepsilon_f}{2(\varepsilon_f - \varepsilon_{\max})} \right) \quad \text{for } \varepsilon \geq \varepsilon_f \quad (5-2)$$

where E_i and E_f are the initial and apparent stiffness values of the textile, respectively, and ε_f and ε_{\max} are the strain values corresponding to the initiation of fibre rupture and maximum stress, respectively. These values were determined experimentally from direct tensile tests [141]. Note that Eq. (1) can also be used to describe the behaviour of yarns if E_i and E_f are taken as the corresponding stiffness values for an individual yarn and $\varepsilon_f = \varepsilon_{\max}$.

The failure modes observed for each specimen are also reported in the relevant Tables, adopting the classification proposed by RILEM [54] as illustrated in **Fig. 5.7**. Failure within the masonry substrate (cohesive debonding) did not occur in any of the tested specimens.

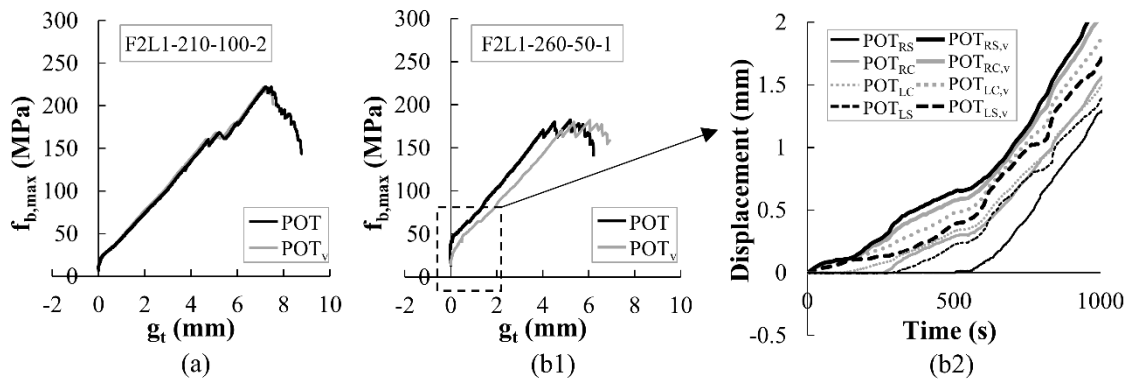


Fig. 5.5 Comparison between physical (POT) and virtual (POT_v) potentiometers on the basis of load-slip response: (a) for a typical specimen, (b1) for a specimen with unreliable potentiometer data and (b2) initiation displacement measurements for different instrumentation positions for the specimen shown in b1.

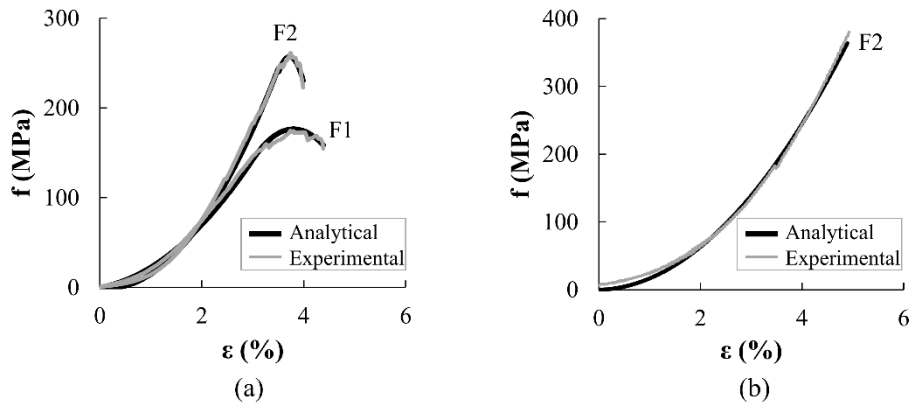


Fig. 5.6 Average tensile stress-strain relationship used in the analyses for (a) F1 and F2 textiles; (b) F2 yarns.

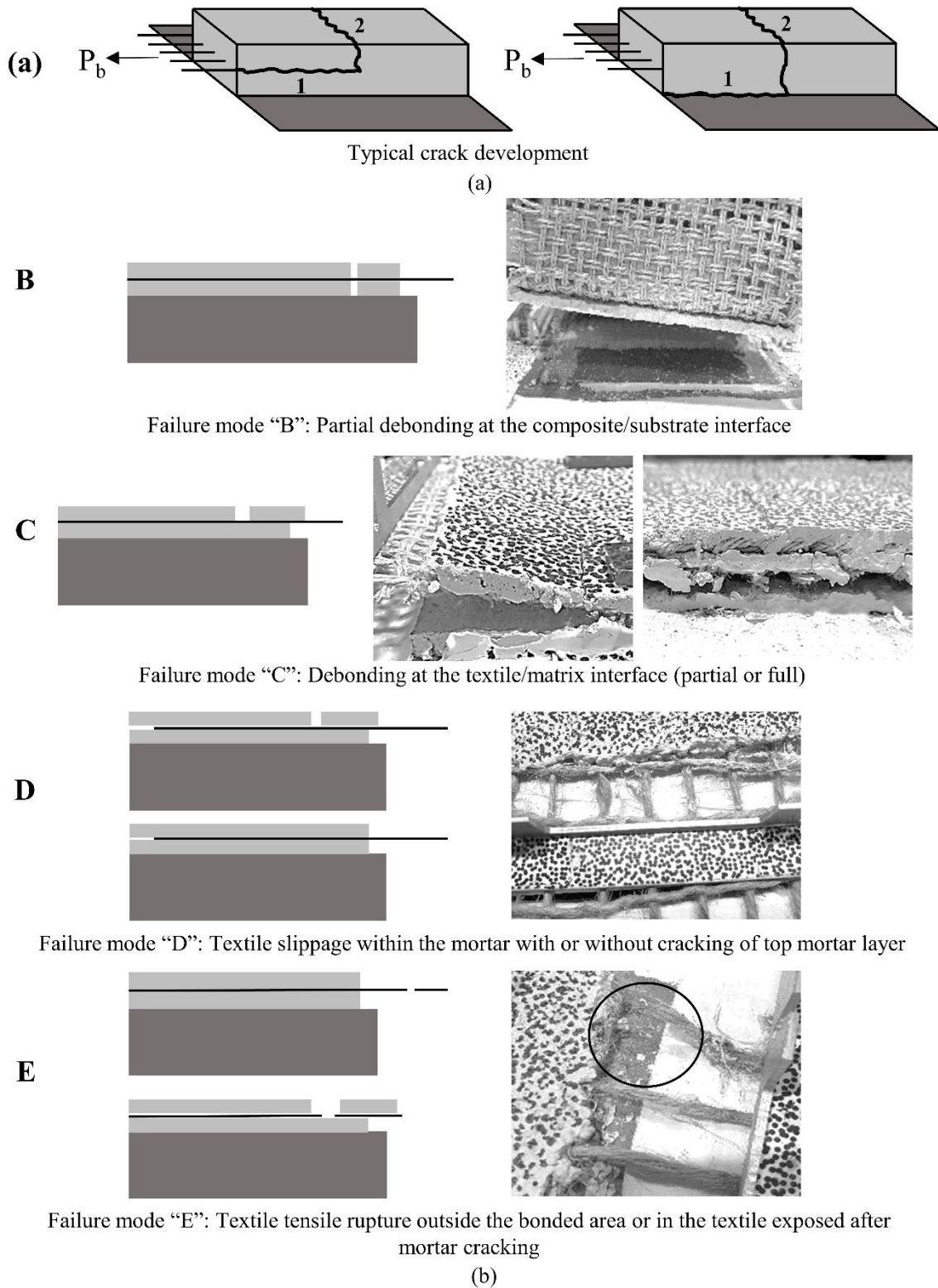


Fig. 5.7 (a) Typical crack development and (b) failure modes in single-lap shear bond tests (adapted from RILEM TC-250 CSM).

5.3.2. Bond-slip Behaviour of Single-Layer FTRM and Effect of Bond Length

The load-global slip ($P_b - g_t$) response curves of single-layer F1- and F2-TRM bonded to masonry prisms over a bond width of 100 mm are shown in **Fig. 5.8** and **Fig. 5.9**, respectively, while Tables 3 and 5 summarise the corresponding results.

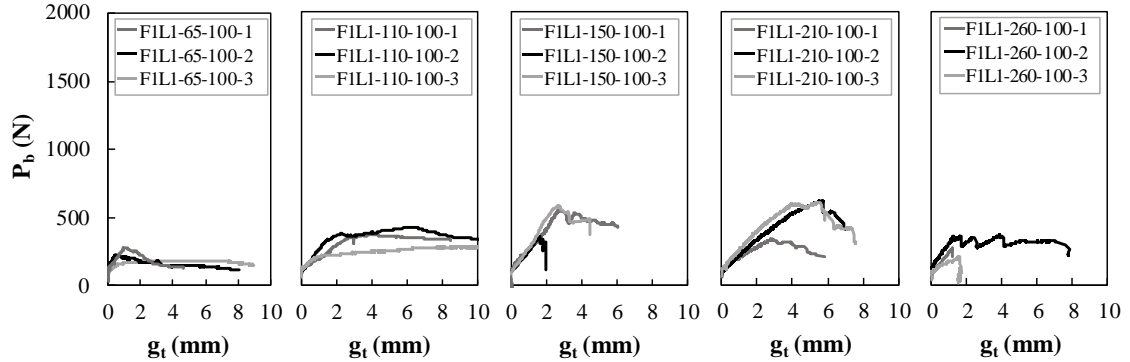


Fig. 5.8 Load-slip response curves of F1-TRM specimens for all bond lengths investigated.

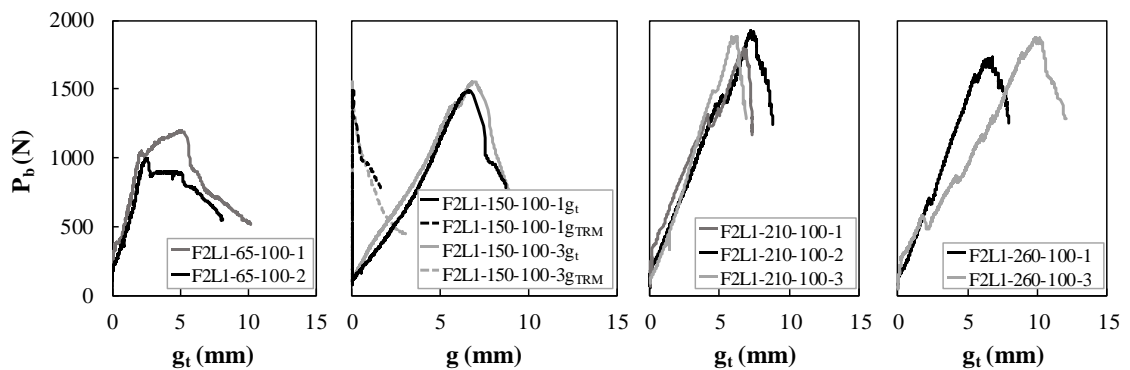


Fig. 5.9 Load-slip response curves of F2-TRM specimens for all bond lengths investigated.

For all bond lengths investigated, the F1L1-TRM series exhibited significant relative slip between textile and substrate, which can be mainly attributed to the observed telescopic type of failure of the yarns (denoted as “T” in the tables) rather than slip of the textile along the bonded length. No cracking of the mortar along the bonded area occurred, and no debonding at the textile/matrix or matrix/substrate interfaces was observed. Most F1L1-TRM systems exhibited an almost linear response up to the peak load, while distinctive post-peak stages were observed for increasing bond lengths. In particular, for bond lengths ≤ 110 mm, the behaviour was almost elasto-plastic. In specimens with a bond length of 65 mm, the maximum load coincided with the initiation of textile slip within the mortar.

Specimen F1L1-65-100-3 and all specimens with a bond length of 110 mm developed high slip values with no significant loss in bond capacity. The observed higher total relative textile-to-substrate displacement and pseudo-ductile behaviour of these specimens, evidenced by the high μ_{gt} and μ_G ductility values, are the result of slip between the core of the yarn and the outer filaments, which are sufficiently bonded to the surrounding mortar. It should be noted that the tests on the F1-TRM specimens of this group were halted when the travel of the potentiometers was reached and no further

increase in the sustained load was observed. For bond lengths ≥ 150 mm, a post-peak softening stage developed as a result of the progressive rupture of the individual filaments outside the bonded area, and less commonly of the individual yarns, coupled with telescopic failure. The η_t exploitation ratio of the F1-TRM specimens ranged between 10-40%, highlighting the poor degree of mortar penetration through the F1 filaments, which prevented the activation of the full capacity of the textile despite achieving rupture of some of the filaments/yarns in the specimens with a bond length ≥ 150 mm. Nonetheless, the tensile capacity of the F1L1-TRM system can be fully exploited when sufficient bond length is provided, as evidenced by the high values of the η_{TRM} exploitation ratios.

A different bond performance was observed for the F2-TRM specimens, which all developed higher load capacity compared to their F1-TRM counterparts. The failure of the specimens within this group occurred at the textile/matrix interface at relatively large values of slip. However, the global slip measurements taken also include any additional elongation of the textile along the progressively increasing unbonded length following cracking and initial debonding, which cannot be easily decoupled from the actual slip.

Specimens with bond length ≥ 210 mm developed a single crack in the proximity of the loaded end, while the specimens with a shorter bond length either developed one single crack in the middle of the bonded region, or a more distributed crack pattern. As shown in **Fig. 5.7a**, cracks initiated as interlaminar cracks at the textile/mortar or mortar/substrate interface (1), and propagated transversally through the top mortar layer (2).

In specimens with a bond length of 65 mm, an almost linear behaviour was observed up to the occurrence of the first crack (at first drop in load). The development of the first crack also marks the initiation of debonding at the textile/matrix interface. The behaviour of specimen F2L1-65-100-1, following the crack formation, was characterised by an increase in load and significant slip between the textile and the mortar up to the peak load. The other specimen of the same group (F2L1-65-100-2) experienced an almost “plastic” behaviour after reaching the peak load and developing the first crack, during which more cracks developed in the top mortar layer and the load was carried primarily through friction between fibres and mortar. The failure mode observed for this bond length was partial detachment of the textile and top mortar layer. The composite beyond the cracks remained intact and well bonded to the masonry.

The behaviour of the specimens with a bond length of 150 mm was characterised by an almost linear uncracked stage up to the peak load, accompanied by cracking in the mortar and partial debonding of the textile. Some of the cracks initiated at the location of the potentiometers and propagated along the top mortar layer, causing the top mortar layer to move towards the loaded end along with the instrumentation mounted on it. As a result, an apparent relative movement of the composite with respect to the masonry substrate was recorded (non-zero g_{TRM} in **Fig. 5.9**). Ultimately, the failure mode of the specimens in this group was characterised by partial interlaminar shear failure followed by rupture of some of the yarns and partial debonding between the mortar and the substrate.

Debonding of the composite from the substrate occurred only within the region close to the loaded end, possibly caused by the development of a fracture Mode III.

The behaviour of specimens with a bond length ≥ 210 mm was characterised by the formation of one single crack and slip of the textile within the mortar, followed by the progressive rupture of the yarns, indicating that the provided bond length was sufficient to effectively anchor the textile. In all such specimens, the bottom mortar layer remained well bonded to the masonry support.

The exploitation ratios, η_i and η_{TRM} , of F2L1-TRM systems were significantly higher than those of F1L1-TRM, indicating an overall better composite behaviour due to a higher degree of bond and mechanical interlock between the textile and the lime-based mortar. Although the axial stress never exceeded the tensile strength of the textile (η_i values up to 75%), possibly due to a certain degree of degradation of the flax fibres when embedded into the lime-based mortar, values of η_{TRM} greater than 100% were recorded for specimens with a sufficient anchorage length, which ultimately failed due to fibre rupture. A lower efficiency (about 65%) was recorded for specimens characterised by different failure modes (see **Table 5.4**).

Overall, the difference in the failure modes observed for the two FTRM systems can be mainly attributed to textile architecture. Although the larger mesh openings of F1 textiles ensured adequate penetration of the mortar and a good bond between the mortar layers, a poor composite action between yarns and mortar was observed. The large diameter straight yarns could not be effectively impregnated, thus resulting in relative slip between inner and outer filaments, which led to the development of significant textile-to-substrate relative displacement (global slip) and highly scattered values ($CoV \gg 30\%$). On the contrary, telescopic failure was not observed for the F2L1-TRM series and despite the small mesh size, which could have hindered the adequate impregnation of the textile (as discussed in Section 5.3.3), the twisted and smaller diameter yarns in F2 textiles ensured a good mechanical interlock between the fibres and the surrounding mortar. The same conclusion was reached for F2-TRM systems under direct tension [141].

A good shear stress transfer within the composite was observed for all specimens, with the exception of those in the F2L1-110-100 series and F2L1-150-100-2, which failed due to complete delamination at the textile/mortar interface at relatively low load values. This failure mode may be attributed to problems during manufacture that might have resulted in poor impregnation of the textile and promoted the subsequent loss of adhesion between the two mortar layers. The possible misalignment between the applied load and the embedded textile may have also generated significant stresses perpendicular to the direction of loading and facilitated the detachment at the weakest interface. Although specimen F2L1-65-100-3 failed in a similar manner as its replicates, it exhibited a significantly lower bond performance (by more than 70%), possibly due to problems related to bending phenomena during the test and/or poor manufacture. Specimen F2L1-260-100-2 suffered significant rotation in the unbonded textile during the test, which was evidenced by the large difference in the slip values recorded by the potentiometers mounted on the opposite sides of the

specimen, and the development of a diagonal crack at a relatively low load value. These specimens are excluded from further discussion and are not taken into account in the derivation of average results.

Fig. 5.10a shows the variation of the maximum resisted load with bond length. Such graphs can be used to identify the effective anchorage length as the length corresponding to a negligible increment in load capacity. An effective bond length of 150 mm can be assumed for the F1-TRM systems at a maximum debonding force equal to 0.5 kN. The shift in failure mode from telescopic to filament or yarn rupture at bond lengths equal or longer than 150 mm reinforces this finding. The decrease in the maximum resisted load at a bond length of 260 mm (by approximately 45%) may be due to the variability of the tensile properties of the textile, as well as the degree of mortar impregnation of the yarns. Although for F2-TRM systems the results of Fig. 10a would suggest an effective bond length of 210 mm, a shift in failure mode was already observed for one of the specimens with 150 mm bond length, indicating that the effective bond length lies between 150 and 210 mm at a maximum force of about 1.8 kN.

The effect of the bond length on the global slip g_t at maximum load is shown in **Fig. 5.10b**. For F2-TRM composites the slip tends to stabilise for bond lengths larger than 150 mm. For F1-TRM composites, however, it is difficult to correlate slip values with maximum load levels due to the telescopic failures of yarns. Hence, it is difficult to draw direct conclusions on effective bond length based only on the results of bond slip.

Specimens with shorter bond lengths exhibited higher average ductility ratios, μ , (**Fig. 5.11a** and c). These ratios decreased with increasing bond length to minimum values ranging from 1.1 to 2, for bond lengths higher than the effective bond length. The high ductility indexes of F1-TRM systems are due to their pseudo-ductile behaviour, resulting from the pronounced telescopic failure mechanism.

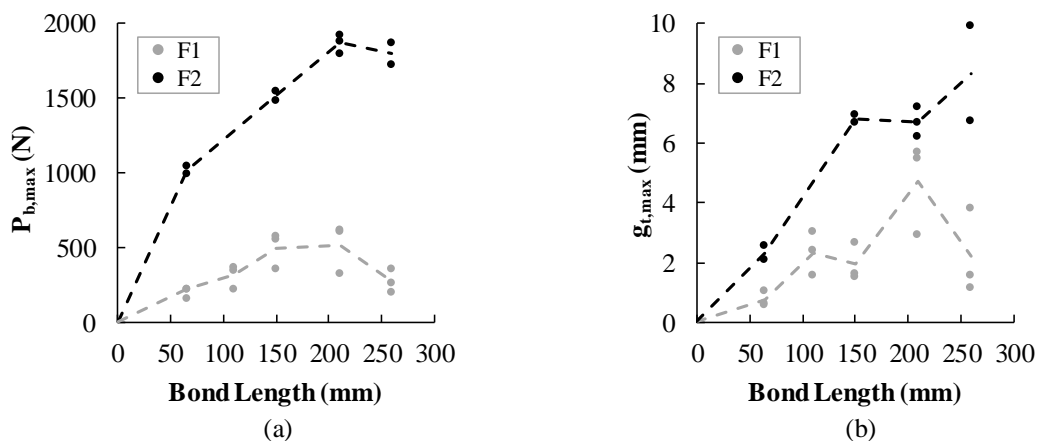


Fig. 5.10 Effect of bond length on (a) the ultimate load/strength and (b) slip at the textile/masonry developed by single-layer F1- and F2-TRM.

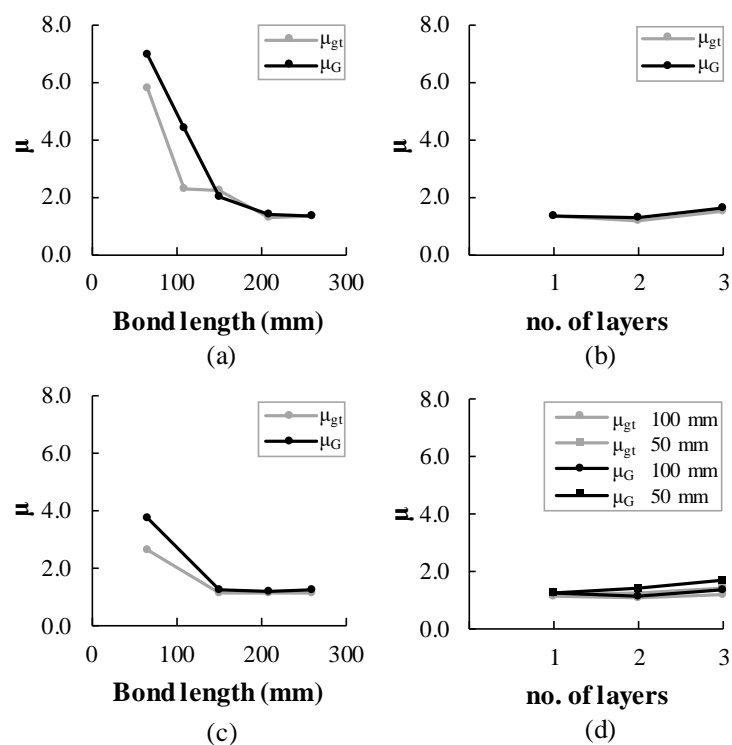


Fig. 5.11 Ductility of FTRM systems with respect to: (a,c) the bond length and (b,d) the number of TRM layers, for F1 and F2-TRM specimens respectively.

5.3.3. Effect of Multiple FTRM Layers

The results on multiple layer FTRM systems are summarised in **Table 5.5**, while their load-slip behaviour is presented in **Fig. 5.12**, along with a typical response of the corresponding single-layer FTRM system. Increasing the number of F1-TRM layers did not result in a change of failure mode. Similarly to the specimens with one layer, no cracking of the mortar occurred along the bonded area and no delamination was observed between textile layers and mortar. The poor impregnation of the yarns, also observed in single-layer specimens, prevented the effective transfer of forces from the yarns to the matrix. This resulted in substantial telescopic behaviour in all specimens and large deformation/slip of the textile, followed by the rupture of single filaments within the yarns or the rupture of individual yarns. This progressive failure mode resulted in the pseudo-ductile post-peak load-slip response shown in Fig. 12a.

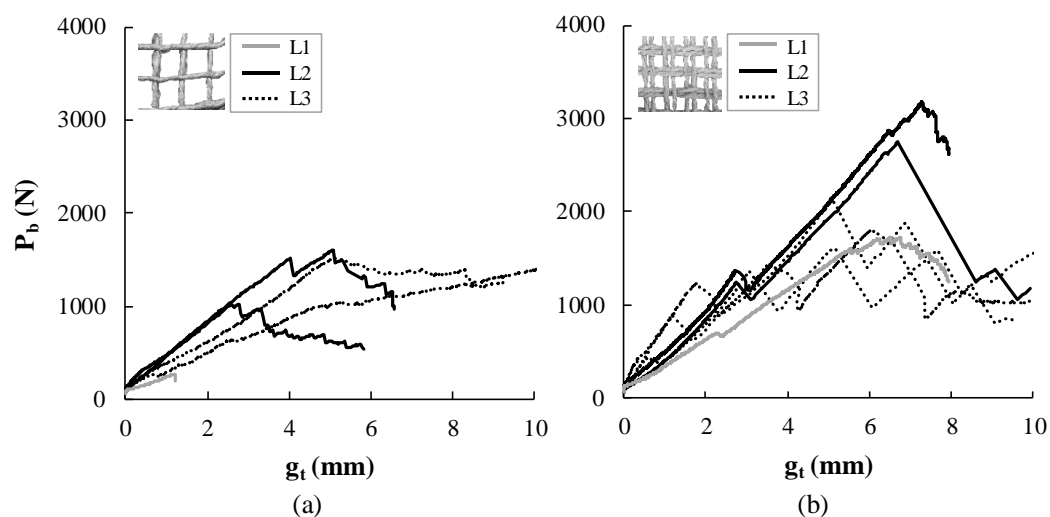


Fig. 5.12 Load-slip behaviour of specimens with multiple (a) F1- and (b) F2-TRM layers.

In terms of mechanical performance, a significantly higher load capacity was achieved with the increase in the number of F1-TRM layers, with specimens with 2 and 3 layers resisting on average a load 5 or 6 times higher than that of the corresponding single-layer FTRM system ($P_{XL1,b,max}$), as shown in **Fig. 5.13a**. This non-proportional increase in load carrying capacity is attributed to the better distribution of stress within the composite as a result of the more uniform distribution of yarns within the matrix.

The behaviour of specimens with multiple F2-TRM layers was characterised by the development of multiple cracks within the mortar matrix (as evidenced by the successive drops in load seen in **Fig. 5.12b**). The observed cracking pattern is indicative of the more effective interaction between the textile and the mortar in comparison to F1-TRM. A shift in failure mode was observed with the increase in the number of TRM layers and failure of F2-TRM specimens typically occurred due to delamination between the textile layers and rupture of the filaments/yarns. Delamination was promoted by the non-uniform stress distribution across the different textile layers and across the width of the composite, and in some cases extended to all textile/mortar interfaces. The bottom mortar layer remained always well bonded to the masonry surface, indicating that the employed bond length (260 mm) was indeed sufficient.

The specimens with two layers of F2-TRM developed higher maximum load capacity than their single-layer counterparts (by up to 160%), resulting in comparable values of axial stresses. However, only a slight increase in relative load capacity was observed for specimens with three layers of F2-TRM (**Fig. 5.13a**). This may be possibly attributed to the increase in the number of weak textile/mortar interfaces, as well as the development of higher bond stresses along these interfaces due to the relatively higher stiffness ratio of the reinforcement. Specimens with multiple TRM layers exhibited comparable average slip values to those of single-layer composites, although characterised by high scatter (**Table 5.5**).

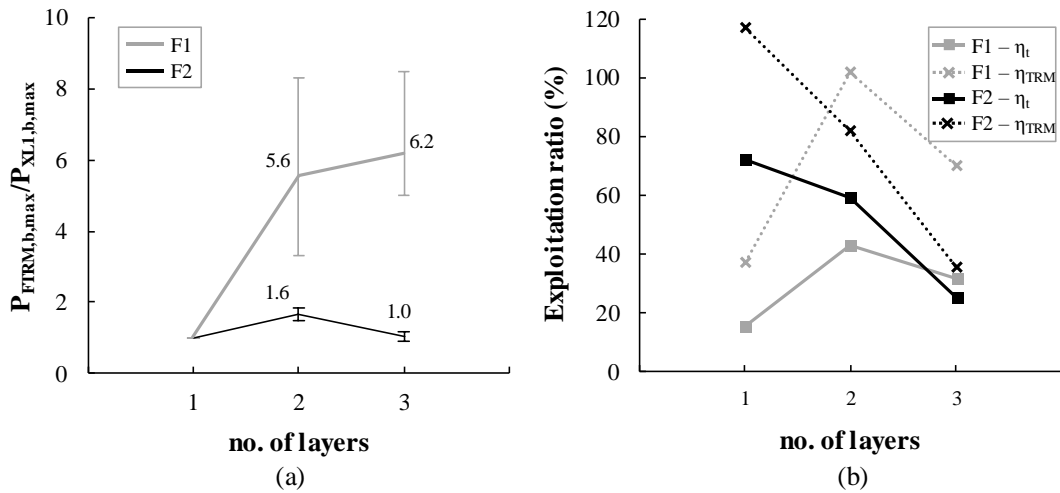


Fig. 5.13 Effect of number of FTRM layers on (a) normalised load capacity and (b) exploitation ratio.

As indicated earlier, the experimental response observed for some of the specimens may have also been affected by setup and manufacturing errors. Specimen F2L2-260-100-3, the failure of which was characterised by the complete detachment of the top mortar layer at a very low load level, was considered to be an outlier and the corresponding experimental values were excluded from the calculation of the average results presented in this paper.

The effect of the number of FTRM layers on the exploitation ratios for both systems is shown in **Fig. 5.13b**. It can be observed that η_t values for F1 textiles were low and varied between 20-40%, highlighting the poor interaction between the yarns and the mortar and the unfavourable effect of the telescopic mode of failure. Values of η_{TRM} , however, increased in multi-layer composites, indicating a slightly better stress distribution within the composite. With respect to F2-TRM systems, a reduction in both η_t (from 75% to 25%) and η_{TRM} (from 120% to 35%) values is observed as a result of the mobilisation of more complex failure modes, including tensile and interlaminar shear failure modes. Rupture of the textile did not occur simultaneously in all textile layers and, although some stress redistribution took place after the initial fibre rupture (see section 5.3.6), the development of high local shear stresses compromised the overall performance and resulted in the lower exploitation ratios.

The ductility of the FTRM systems (μ_{gt} and μ_G) was not significantly affected by the addition of multiple TRM layers (**Fig. 5.11b** and d), as the primary failure mode in all specimens was governed by the rupture of some of the fibres.

5.3.4. Effect of Bond Width

The effect of bond width on the overall performance and failure mode of single- and multi-layer F2-TRM systems was examined using two bond widths. Specimens with 50 mm bond width were provided with the same reinforcement ratio as their 100 mm counterparts, ranging from 1.4 % (single-layer) to 2.2 % (three-layer composites). **Table 5.6** summarises the results obtained from the single-

lap shear tests on 50 mm wide TRM strips, while the results on the corresponding 100 mm wide strips are included in **Tables 5** and **6**.

The typical failure mode of the specimens with 50 mm wide TRM included textile slippage within the mortar, the formation of one crack parallel to the loaded end, and ultimately the progressive rupture of the yarns in one or more textile layers, which resulted in the post-peak softening load-slip response shown in **Fig. 5.14a**. In contrast with the wider F2-TRM systems, the failure mode did not change with the addition of multiple TRM layers. No interlaminar shear failure or detachment from the substrate occurred, indicating adequate bond strength between the mortar layers and the textile, and the reinforcement was exploited to the same degree, regardless of the number of TRM layers (64-68% and 90-110% for η_t and η_{TRM} , respectively).

The effect of bond width on the normalised maximum axial strength capacity of single- and multi-layer F2-TRM systems (with respect to the resistance of the specimens with TRM strips of 50 mm bond width - $f_{b,max,BW=50}$) is shown in **Fig. 5.14b**. In the case of single-layer composites, similar values of axial stress were obtained, and the same failure mode between the specimens with different bond widths was observed. However, a significant bond width effect was observed for multi-layer TRM, with the specimens with wider TRM strips exhibiting a decrease in the maximum axial strength up to 60% in the case of three-layer TRM systems. It should be kept in mind that the dominant failure mode for specimens with 100 mm wide multiple TRM layers was interlaminar shear, which prevented the full exploitation of the flax reinforcement. The different performance of these specimens can also be due to inadequate textile alignment and penetration of the mortar through the mesh openings, which are more difficult to control in wider specimens and can result in different anchorage conditions among the yarns and the loss of bond between the mortar layers. The alignment of wider multi-layer TRM within the test rig can also be more difficult to ensure, thus increasing the probability of some yarns to be more highly stressed than others and resulting in localised failures. In contrast, a more uniform stress distribution in the specimens with 50 mm bond width was typically achieved both across the textile width and among the different textile layers as confirmed by DIC (Section 5.3.6). This more uniform load distribution also led to slightly higher ductility (**Fig. 5.11d**) and lower scatter of results (CoV values less than 10% excluding slip values).

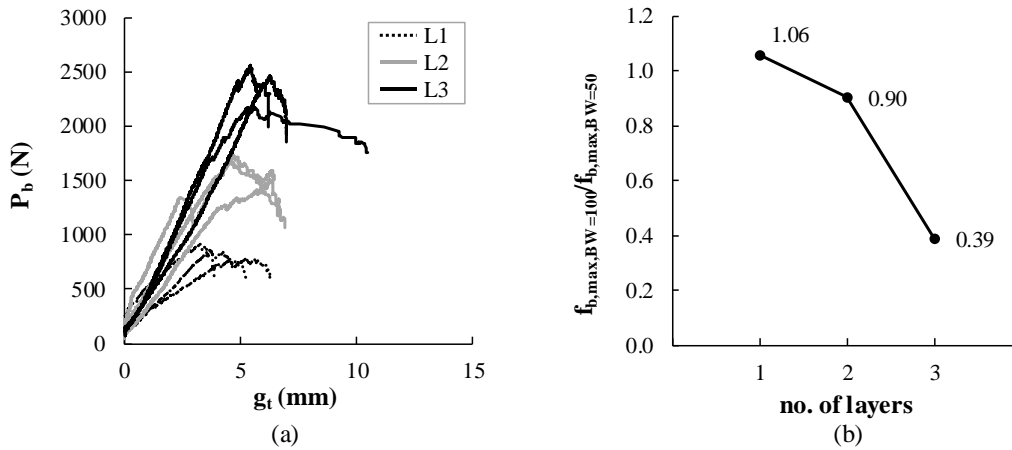


Fig. 5.14 (a) Load-slip response curves of single and multi-layer F2-TRM systems of 50 mm bond width; (b) axial strength capacity normalised over bond width as a function of the number of F2-TRM layers.

5.3.5. Crack Initiation and Development

The data obtained for F1-TRM are not discussed herein as failure of these specimens always occurred outside the bonded region without mobilising significant bond-related mechanisms.

Crack development was best monitored through post-processing of DIC displacement measurements, and the number of cracks, sequence of occurrence and crack width and location were determined. For example, the initiation and location of the crack that developed in specimen F2L1-210-100-3 can be easily determined through the analysis of the displacement profile (d_x) obtained along the centreline of the specimen (**Fig. 5.15b**).

Virtual extensometers (w_i) spanning each crack (see **Fig. 5.15a**) were created along the direction of loading and their corresponding measurements were used to calculate the average crack width at failure ($w_{80\%}$). In specimens characterised by the formation of multiple cracks, only the crack with the maximum crack width is considered. The development of $w_{80\%}$ with bond length and number of F2-TRM layers for the two bond widths examined is presented in **Fig. 5.15c** and **Fig. 5.15d**, respectively. From these results, it can be seen that the use of an adequate bond length (i.e. longer than the effective bond length – see Section 3.2) promotes the development of larger cracks through the mortar as a result of the progressive debonding along the yarns and textile slippage within the mortar matrix. For bond lengths shorter than the effective bond length, crack widths at failure ranged from 0.37 to 3.55 mm.

Increasing the number of TRM layers (**Fig. 5.15d**) decreases maximum crack widths, as also observed in tensile tests on the same system [141]. The more significant decrease in crack width observed in specimens with 100 mm bond width, which failed due to delamination at relatively low load values, was mainly due to the formation of multiple cracks. Specimens with 50 mm bond width had overall smaller crack widths, at larger axial stress, due to a more even stress distribution.

Although DIC can be used to obtain full-field strain measurements, the lack of a stereo-vision system renders these measurements inaccurate. However, they can be used for a qualitative analysis of the crack pattern, and cracks can be identified by high strain concentration zones (peaks) along the length (Fig. 5.15b). A more detailed quantitative analysis would be of limited use as: i) only the displacement of the top mortar layer can be tracked, making it impossible to get any information on the strain in the embedded textile; ii) the mortar cracking strain (approximately equal to $35 \mu\epsilon$) is significantly lower than the strain accuracy of the DIC setup employed in this study ($100 \mu\epsilon$).

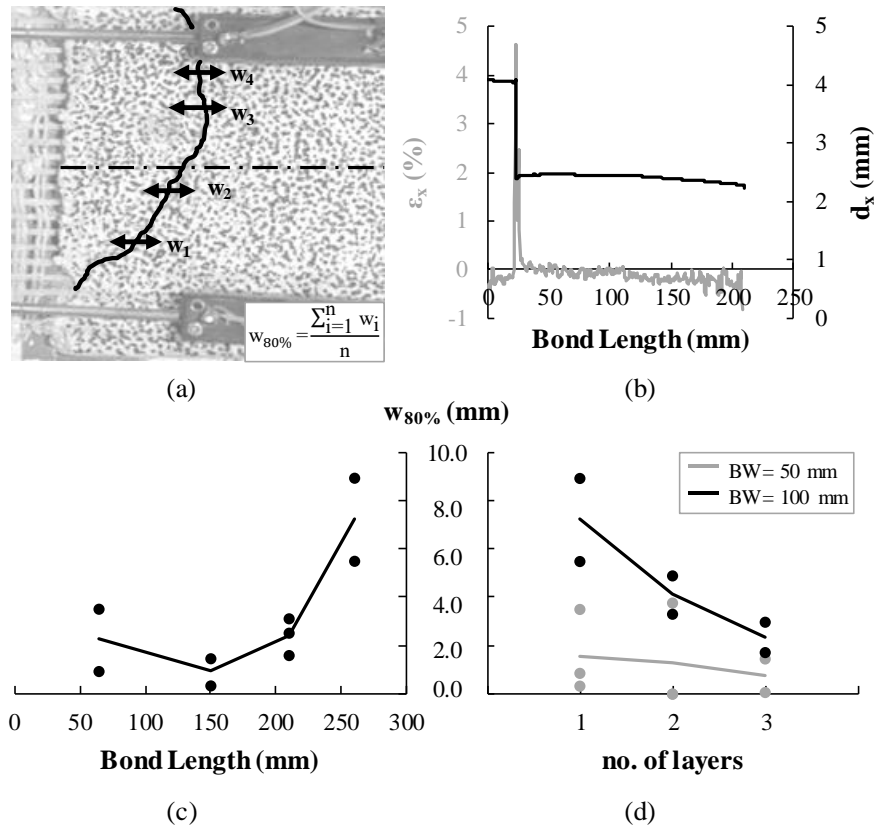


Fig. 5.15 (a) Calculation of crack width for a typical specimen (F2L1-210-100-3); (b) displacement and strain profile along the centreline; (c) development of maximum crack width with the bond length and (d) the addition of multiple F2-TRM layers.

5.3.6. Stress-Strain Distribution

The virtual extensometers (ext_j) shown in Fig. 5.4a were used to measure the strain values (ϵ_j) along the unbonded part of the textile at increasing levels of applied load.

The strain distribution across the width of the textile for a representative specimen with a bond length shorter than the effective length (F2L1-65-100-1) is presented in Fig. 5.16a, while that for a specimen of sufficient bond length (F2L1-210-100-2) is shown in Fig. 5.16b, along with the average ultimate tensile strain of the textile (dashed line) and of the yarn (dotted line). It can be seen that

strain levels along the yarns of specimens with insufficient bond length (e.g. **Fig. 5.16a**) fall below the ultimate yarn strain, confirming that the debonding mechanism did not involve yarn rupture. On the contrary, strain values even higher than the average ultimate tensile strain of the textile and of the yarn were developed in specimens with sufficient bond length (e.g. F2L1-210-100-2 in **Fig. 5.16b**) at levels of load as low as 40% of $P_{b,max}$. The local loss of yarn stress did not immediately lead to global failure at this load level, as other yarns still had sufficient strain/stress capacity to enable an increase in overall load capacity. Such localised failures resulted in varying degrees of stress redistribution that enabled the progressive engagement and eventual rupture of the yarns.

Fig. 5.16c and **d** show the strain distribution across the width at the top and bottom of the unbonded textile for typical multi-layer F2-TRM specimens. A significant difference in strain distribution between top and bottom textile layer can be seen in the specimen with a wide TRM strip (**Fig. 16c**), possibly as a result of the different level of pre-tension developed in the textile layers during the installation of the end tabs. The top textile layer did not share the strain, and that led to the rupture of the bottom layer. On the contrary, a more uniform strain distribution is observed for the narrower strips (**Fig. 5.16d**). The negative strains recorded at low load levels by some of the virtual extensometers placed on the top textile layer indicate a local loss in the initial pre-tension load as a result of rotation of the textile. Ultimately, this specimen failed due to rupture of the top textile layer, at strains approaching the average ultimate tensile strain of the textile.

The non-uniform strain distribution between textile layers is more clearly shown in **Fig. 5.17**, which summarises the ratio between the average strain ($\epsilon_{avg,max}$) recorded in the top and bottom textile layer of all multi-layer F2-TRM specimens at maximum load. It is confirmed that the narrower TRM strips have a more uniform strain distribution (ratios close to unity). **Fig. 5.16c** and **d** show the strain distribution across the width at the top and bottom of the unbonded textile for typical multi-layer F2-TRM specimens. A significant difference in strain distribution between top and bottom textile layer can be seen in the specimen with a wide TRM strip (**Fig. 5.16c**), possibly as a result of the different level of pre-tension developed in the textile layers during the installation of the end tabs. The top textile layer did not share the strain, and that led to the rupture of the bottom layer. On the contrary, a more uniform strain distribution is observed for the narrower strips (**Fig. 5.16d**). The negative strains recorded at low load levels by some of the virtual extensometers placed on the top textile layer indicate a local loss in the initial pre-tension load as a result of rotation of the textile. Ultimately, this specimen failed due to rupture of the top textile layer, at strains approaching the average ultimate tensile strain of the textile.

The non-uniform strain distribution between textile layers is more clearly shown in **Fig. 5.17**, which summarises the ratio between the average strain ($\epsilon_{avg,max}$) recorded in the top and bottom textile layer of all multi-layer F2-TRM specimens at maximum load. It is confirmed that the narrower TRM strips have a more uniform strain distribution (ratios close to unity).

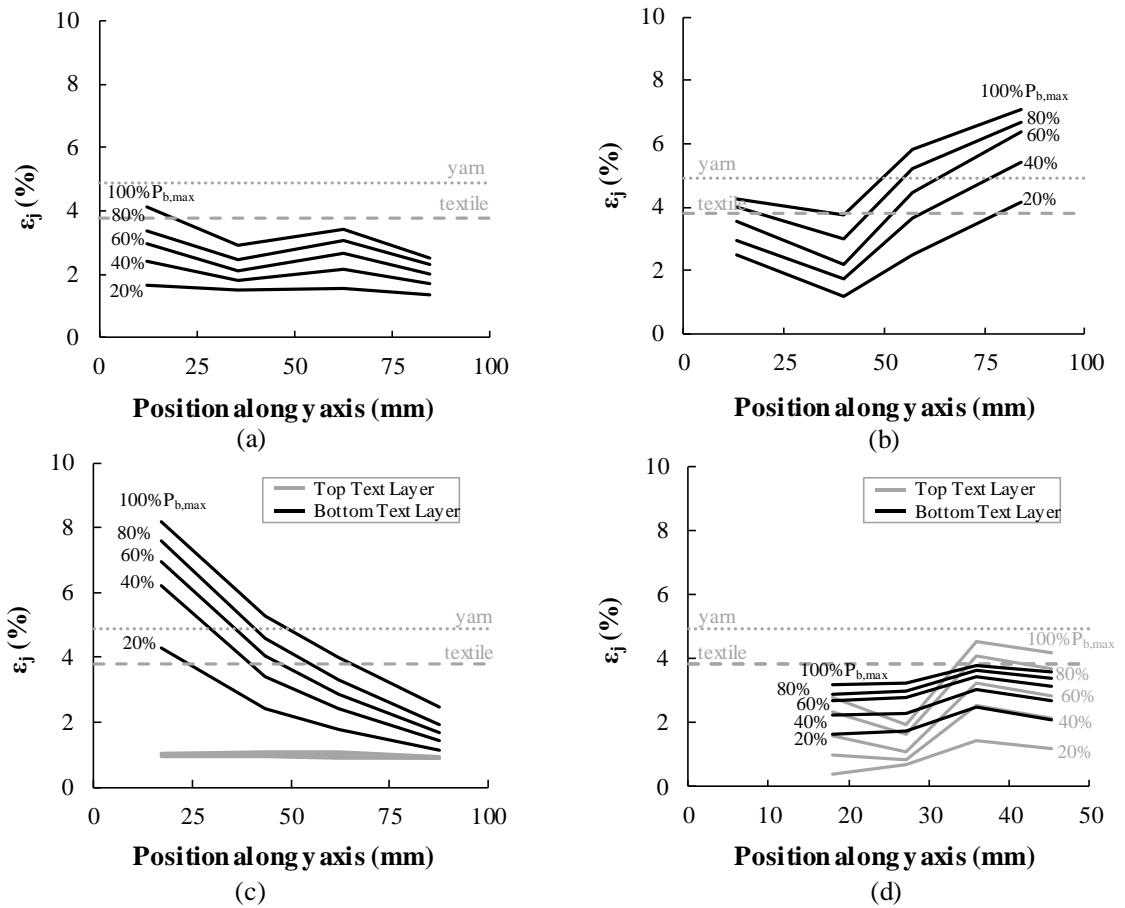


Fig. 5.16 F2-TRM systems. Strain profile across the width of the unbonded textile at different loading stages for a typical specimen with: (a) insufficient bond length (F2L1-65-100-1); (b) sufficient bond length (F2L1-210-100-2); (c) three TRM layers of 100 mm bond width (F2L3-260-100-2); (d) two TRM layers of 50 mm bond width (F2L2-260-50-1). Note: the dashed and the dotted line correspond to the textile and yarn strain at failure, respectively.

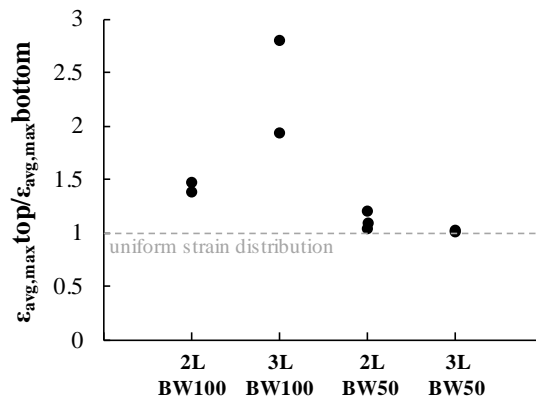


Fig. 5.17 Ratio of average strain at maximum load between top and bottom textile layer in multi-layer F2-TRM systems.

5.3.7. Load-slip Response of Individual Yarns

The load-slip response of individual yarns was examined using local strain and slip values obtained from DIC measurements. The load in the yarns instrumented with the optical targets was determined based on the constitutive law developed from tensile tests on the same reinforcing materials [141] as described by Eq. (1) and shown in **Fig. 5.6b**. The global slip of the individual yarns (g_j) was calculated through the implementation of virtual extensometers as shown in Fig. 4d and accounting for the elongation of the yarn.

Fig. 5.18a,c show the development of the load resisted by each individual yarn, P_j (grey thin lines), the average load resisted by the yarns, P_{avg} (grey thick line), and the average applied load per yarn (load from actuator/number of yarns), P_b (black line), with time, for a typical specimen with a short bond length (F2L1-65-100-1) and one with sufficient bond length (F2L1-210-100-2), respectively. The corresponding load-slip responses (i.e. global P_b - g_t , average P_{avg} - g_{avg} and local P_j - g_j) for the same specimens are shown in **Fig. 5.18b,d**.

The different load-slip behaviour observed for each of the individual yarns (**Fig. 5.18b,d**) is the result of load redistribution during the test and upon individual yarn failure, with every yarn reaching the corresponding maximum load at different levels of slip g_j . Yarns well anchored (e.g. yarn 4 in **Fig. 5.18d**) resist significantly higher loads at relatively low slip values, while the remaining yarns can undergo extensive slip (e.g. yarn 2 in **Fig. 5.18d**) before they pick up any load.

In the specimen with a short bond length (65 mm, **Fig. 5.18a**), all yarns exhibit an almost elastoplastic behaviour, despite the loss in global load capacity. The high shear bond stresses that develop at the yarn/mortar interface cause local debonding and the progressive increase in unbonded length, which for short bond lengths results in slip followed by partial detachment. On the contrary, the progressive debonding of the yarns in specimens with sufficient bond length (210 mm, **Fig. 5.18c**) does not compromise the ability of the yarns to develop their full capacity along the remaining bonded length. As a result, the yarns in specimens with a sufficient bond length (≥ 210 mm) appear to develop a total load capacity significantly higher than the externally applied load. As the strain readings are correct, this can be the result of an overestimation of the cross-sectional area of the yarn that is effectively carrying load, due to failure of some of the fibres in the yarn. The number of fibres failing depends on the degree of mortar penetration and available anchorage length at increasing stress levels. It should be noted that, although strains higher than the average ultimate tensile strain were measured on individual yarns ($\epsilon_{max}=4.9\%$), the yarns were assumed to carry load only up to ϵ_{max} . Strain values exceeding ϵ_{max} can be attributed to the additional elongation caused by the increase of the effective length of the remaining yarn filaments, which is directly related to the degree of mortar impregnation along the bond length, as well as the inherent variability of the yarns.

The analysis of the load-slip behaviour of individual yarns has provided useful insights into the local yarn/matrix stress transfer mechanisms, highlighting the significance of key aspects on the average global load-slip behaviour of NTRM systems, namely the variability in mortar impregnation

of the yarns along the embedded length, and the percentage of yarn cross-sectional area that is effectively mobilised. Further research is needed to quantify these aspects as they are critical for the optimal design of bonded TRM systems.

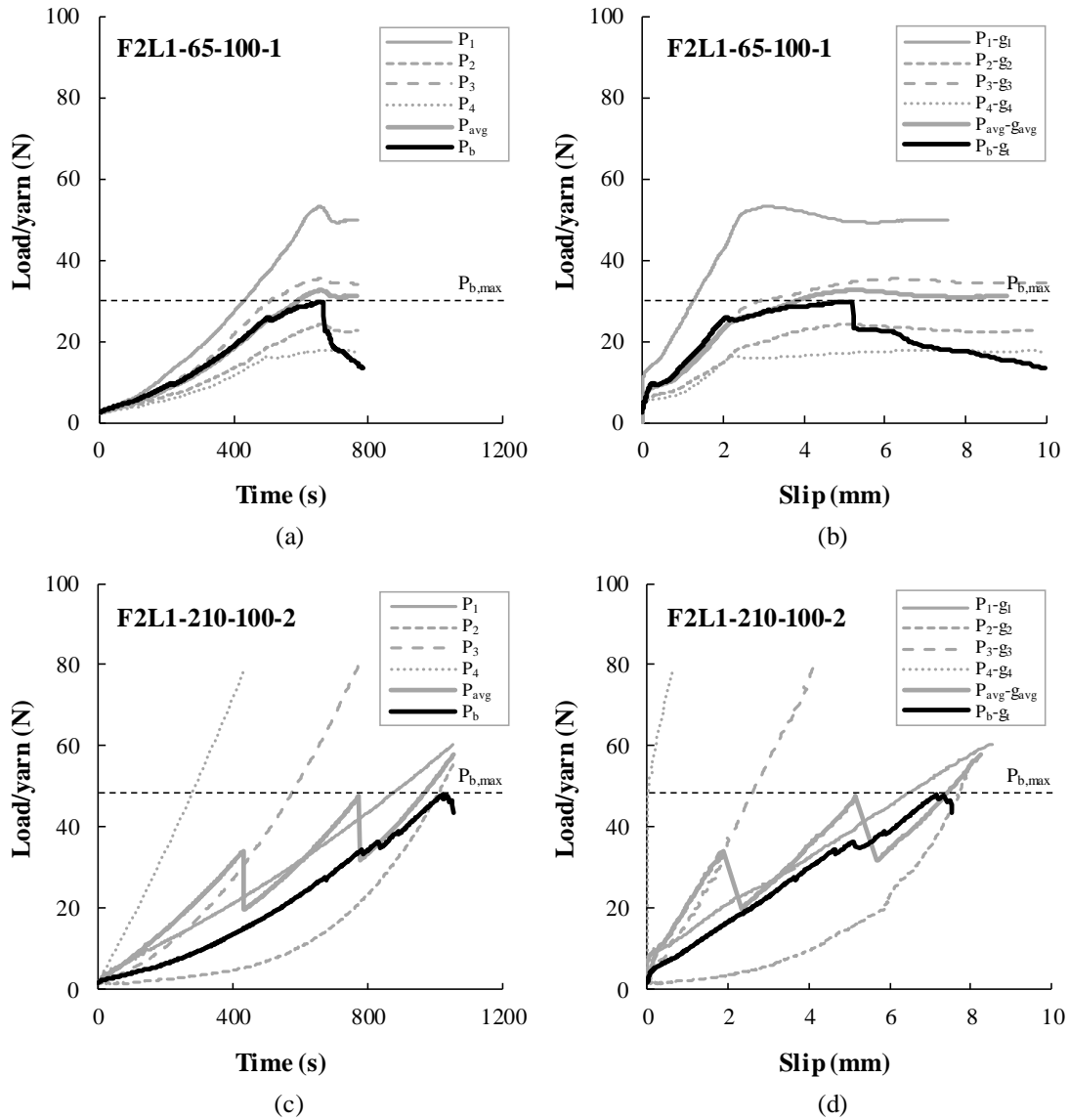


Fig. 5.18 (a,c) Global and local load development with time per individual yarn; (b,d) Global (P_{b-g_i}) and local (P_{j-g_j}) load-slip response of individual yarns.

5.4. GENERAL DISCUSSION AND RECOMMENDATIONS

5.4.1. Experimental Procedures and Measurements

Tests on natural fibre TRMs are clearly very challenging. The characterisation of the TRMs cannot rely on simple tests on the constituent materials (mortar, filaments, yarns or even fabrics) and evidence shows that the strength of individual yarns cannot be fully mobilised in TRMs. This poses a serious issue for the development of design guidelines. The main challenges in experimental procedures and measurements include:

- i. Loading of the specimens invariably leads to eccentricities.
- ii. The measurement of strains/slips is difficult due to abrupt large deformation development, hidden strains due to debonding and telescopic fibre movement, and difficulty in measuring strains along the natural fibres embedded in mortar.
- iii. Large variability in material geometry and mechanical characteristics.

These challenges are discussed in the following.

5.4.1.1. Load eccentricities

Despite the best attempts to ensure good alignment by using rigid attachment of the fabric to the actuator and applying a prestress to the fabric prior to testing, severe load eccentricity and uneven stress distributions were still found. These issues arise due to the natural fibre fabric architecture and the manufacturing process of the composite.

5.4.1.2. Natural Fibre architecture

The basic component of a textile is the yarn, which is weaved or stitched together to make the textile. It is clear from this work that yarn manufacture plays an important role in the ability of fibres to be mobilised in tension and shear.

The maximum tensile stress that can be developed in the yarns depends on their embedment length, and the quality of their anchorage at the force application ends. Large diameter yarns with a very gentle (or no) twist (like the yarns of F1) are likely to exhibit telescopic failures. Furthermore, if not all fibres are perfectly aligned and stressed during manufacture, the loose fibres will be mobilised only after other fibres carry already a significant amount of load, or even fail. A larger twist in the fibre, or even twisting smaller yarns together (as yarns of F2) can increase friction between individual fibres and result in higher tensile strength.

Similar issues arise with bond strength. In a gentle twist yarn, only few fibres remain near the surface, which means that the fibres inside the yarn are not bonded to the mortar and hence cannot be effectively mobilised as the shear stress transfer within the yarn is very small. As a result, most of the force is carried by the outer filaments of the yarns, which break prematurely. The sectional area of the yarn effectively bonded, depends not only on fibre twist, but also on yarn diameter and linear density. Mortars are more likely to penetrate yarns with smaller diameter and lower linear density.

Textile architecture is also important. If individual yarns are not perfectly straight during the manufacture of the textile, some of them will remain loose, and eventually attract less force, causing in plane and out of plane eccentricities. Woven textiles can also increase bond stress transfer in TRMs, whilst simple stitching is unlikely to offer much resistance to relative movement.

In conclusion, textiles for TRMs should be made of woven textiles and preferably twisted yarns of small diameter, to enable the maximum number of fibres to reach the surface over a given length (less than half the effective bond length).

5.4.1.3. Composite Manufacture

The textiles in TRMs need to remain straight to be able to develop their strength. Hence, textiles should be stretched uniformly during the manufacture of the composite. To avoid delamination, the fabric ends should be secured at the ends during the curing process.

The surface of the substrate needs to be clean and moist to enhance bond characteristics. The TRM layers, need to be uniform in thickness to avoid eccentric strength and stiffness. Furthermore, the layers need to be placed in quick succession, to avoid issues of drying and consequent differential shrinkage in the materials.

5.4.1.4. Measurements

Bonding conventional foil strain gauges on yarns is practically impossible, as the glue and foil are likely to exceed the strength and stiffness of individual fibre filaments. In addition, it is impossible to know the direct strain development along the portion of the yarn embedded in mortar. Surface measurements, either through foil strain gauges or glued potentiometers will only reflect the mortar strain, but will also span cracks or suffer rigid body movement when the mortar becomes cracked and/or partially or fully delaminated.

DIC systems, when properly used, are much better at monitoring all surface movements (yarn, fabric and composite), including crack width and slip. However, as the cracking strains of mortars are very low, a system with a resolution of at least $5 \mu\epsilon$ is required.

5.4.1.5. Material Variability

The variability in material properties and mechanical characteristics amplifies the load eccentricities during testing, and as such, a significant number of tests is required to get accurate and meaningful results. Test procedures similar to those published by RILEM TC 250-CSM [54] and modified according to the recommendations proposed in Section 5.4.2, can be implemented for NTRM.

5.4.2. Recommendations for Testing and Design

It is clear from the above discussion that yarn and textile architecture are important in maximising the yarn, textile and composite tensile and bond strengths. With poor yarn architecture, exploitation of the textile may be well below 50% and characteristic TRM strengths may be as low as 10-20% of the dry textile strength. On the other hand, good architecture enables high exploitation of the textile (e.g. 75% in the case of F2), with characteristic values around 70% of the dry textile strength.

The RILEM TC 250-CSM testing procedure needs to be modified to enable a more reliable characterisation of natural fibre TRM. Given the high uncertainty in material properties, and accounting for the time required to prepare the specimens, a minimum of 9 samples need to be tested to obtain design characteristic values with a precision of $\pm 15\%$ at a confidence level of 95%. Specimens experiencing a failure mode different from that characterising the group series should be treated as outliers.

Particular attention shall be paid during textile installation to account for the high flexibility of natural fibre textiles and ensure a good alignment of the textile reinforcement along the bond length and across the bond width of the composite. An axial pre-stress force shall be applied during manufacture and curing of the composite to promote alignment of the yarn filaments and exploit the full stiffness of the textile. This prestress level accounts for the initial stiffening of the yarns and shall be determined based on direct tensile tests on dry textiles. This will enable a more uniform stress distribution during testing. DIC shall be employed to monitor the crack development along the bonded length, quantify the strain distribution in the unbonded textile (using pairs of optical targets bonded to individual yarns), and determine local bond-slip relationships.

NTRM systems should be designed to maximise the exploitation of the mechanical properties of the textile. The effective bond length of an NTRM system should be taken as the minimum length that prevents debonding from the substrate before fibre rupture occurs.

The textile architecture (e.g. weaving and mesh size) can limit the number of layers that can be applied, and consequently the overall strengthening potential. When multiple NTRM layers are required to meet performance targets, the use of two rather than three layers of NTRM is recommended, and the degree of ductility of the corresponding failure modes should be taken into account.

Though it is tempting to use the entire textile width in strengthening applications, keeping wide textiles uniformly stretched is a big challenge. As the effective bond strength has been shown to decrease severely in wider multi-layer NTRM (see **Fig. 5.13b**), it is recommended that natural fibre fabrics are applied in narrow strips, in quick succession to avoid moisture transfer issues, with some mild prestress to keep the yarns well aligned.

5.5. CONCLUSIONS

This paper presents the results obtained from single-lap shear bond tests on flax lime-based composite systems bonded to masonry prisms made of clay bricks. The effect of key design parameters on the bond characteristics of the flax-TRM/masonry systems was investigated, focusing on the bond length, the number of FTRM layers, the textile architecture and the bond width. The strain distribution across the width of the textile and between the textile layers was also examined in detail. Based on the results and the discussion above, the following conclusions can be drawn.

- The effective bond length for the tested single-layer FTRM/masonry systems is between 150 and 210 mm and failure is dominated by fibre rupture.
- The increase in the number of F1-TRM layers from 1 to 3 did not cause a change in failure mode and resulted in a significant increase in load carrying capacity (up to 600%). On the contrary, delamination occurred in multi-layer F2-TRM systems with moderate increase in load carrying capacity (up to 60% in 2-layer F2-TRM). The ductility of both systems was not affected by the number of layers.
- When multiple NTRM layers are required to meet performance targets, the use of two rather than three layers of NTRM is recommended.
- Textile architecture plays a major role in the overall bond performance. The large mesh size of the F1 textile ensured a good bond between the mortar layers, but the inadequate penetration of the mortar within the large diameter yarn compromised the development of the full textile capacity (only up to 35%). On the other hand, the twisted and smaller diameter yarns of the F2 textile ensured a good mechanical interlock with the mortar, enabling a high utilisation (up to 75% of the dry textile strength), but their dense mesh resulted in poor mortar penetration and delamination when multiple layers were used.
- The performance of single-layer F2-TRM systems does not seem to be affected by the width of the bonded composite. However, the more pronounced non-uniform load distribution in multi-layer specimens with wider TRM strips, resulted in a 60% loss of their axial strength when three layers were provided.
- The analysis of load-slip behaviour at both the global and local scale revealed that the performance of NTRM systems is significantly affected by the variability in mortar impregnation of the yarns along the embedded length and the percentage of yarn cross-sectional area that can be effectively mobilised.

More research and development work should be carried out in collaboration with natural-fibre textile manufacturers to optimise the yarn and textile architecture in accordance with the recommendations given in this study.

Acknowledgments

The authors gratefully acknowledge Vimark S.r.L for providing the lime-based mortar, S. Basso for his assistance in the experimental programme and the technical staff in the Heavy Structures Laboratory at The University of Sheffield for their help in manufacturing the bespoke experimental test setup.

6. IN-PLANE SEISMIC PERFORMANCE OF MASONRY WALLS RETROFITTED WITH FLAX-TRM

N. Trochoutsou, M. Di Benedetti, K. Pilakoutas, M. Guadagnini, In-Plane Seismic Performance of Masonry Walls Retrofitted with Flax-TRM (*under preparation*) (xxxx).

Abstract

This paper investigates the performance of Flax Textile-Reinforced Mortars (FTRM) as a seismic retrofitting solution for unreinforced masonry. Six single-wythe medium-scale unreinforced masonry walls were subjected to quasi static in-plane reverse cyclic shear loading. Four of the specimens were retrofitted on both sides with one or two layers of flax textiles embedded in lime-based mortar. One bare wall and one wall strengthened only with lime-based mortar were examined as reference samples. The FTRM-retrofitted specimens were able to sustain up to 113% higher shear load, and developed improved deformability, ductility and energy dissipation capacity. The mortar overlays contributed to increasing the shear cracking capacity, while the flax textiles increased peak capacity and promoted a more uniform damage distribution. Near collapse, the flax textile ensured the integrity of the wall and controlled the development of brittle failure modes, a property of utmost importance in seismic strengthening applications. The shear contribution of the NTRM system is examined in detail and the experimental evidence is used to assess the underlying philosophy of current shear design provisions. In general, existing models overestimate the stress that can be developed in the flax textile reinforcement. A more rational limiting strain value is proposed along with a simplified design model that accounts for the contribution of the mortar and the unique mechanical performance of FTRM systems.

This chapter consists of a stand-alone journal paper and includes the associated reference list at the end of the chapter. Additional information and further test results are presented in Appendix C.

6.1. INTRODUCTION

Time and time again, post-earthquake reconnaissance reports highlight the high vulnerability of unreinforced masonry structures (URM) to seismic actions, with structural failures and partial or global collapses causing high death tolls and severe economic losses, in both developed and developing countries [3]. Such failures are the result of poor structural performance of URM walls under in-plane and out-of-plane loading [6]. While the latter can be avoided if sufficient wall-diaphragm connections are ensured [37,157], the overall seismic performance is governed by the ability of the walls to effectively transfer the in-plane loads and provide the required stability to avoid collapse [158]. Inadequate construction practices, material deterioration, lax or non-efficient enforcement of seismic codes and/or non-compliance of old buildings with current seismic requirements are some of the major reasons for the seismic deficiency of much of the existing masonry building stock [4]. Hence, the implementation of reliable assessment strategies and retrofitting methods are critical to preserving existing structures and promoting more sustainable construction [5,7].

Textile-Reinforced Mortars (TRM), comprising structural textiles/grids embedded in inorganic matrices, have been employed successfully to increase the in-plane performance of URM walls. TRM have plethora of structural benefits including: i) high strength and stiffness at low weight and ii) ease and speed of application with minimal change to the structure's geometry. More conventional techniques (e.g. reinforced concrete jacketing, shotcrete overlays) can provide increased strength, but at the expense of deformation capacity [10] and a significantly higher cost and disruption of use.

The inorganic nature of the TRM matrix also imparts other desirable characteristics, especially in restoration of heritage buildings or in applications where cost and environmental impact are primary concerns, such as vapour permeability, recyclability, compatibility with masonry substrates and ability to conduct post-earthquake damage assessment [159].

Several studies [25] have demonstrated the potential benefits of TRM systems in applications where deformation capacity and improved ductility are desirable. Experimental tests on walls strengthened with TRM reinforcement have shown that TRM can delay initial cracking [160], ensure structural integrity even without the use of mechanical anchorages [107] and promote more distributed cracking, as well as increased energy dissipation capacity and strength [161]. When both sides of the wall can be accessed, double-sided configurations are preferable as they can help avoid problems due to load eccentricity [162]. Furthermore, full coverage of walls is preferred as it can limit damage caused by out-of-plane bending [49]. The superior mechanical properties of the advanced textiles currently used in TRM systems, however, can remain largely unexploited as the performance of such systems is often governed by premature debonding [27].

Given the limited utilisation of advanced textiles in some strengthening applications and the urgent need for more sustainable structural solutions, recent studies have started to examine the use of plant fibres as structural reinforcement in TRM systems, as they combine excellent environmental

credentials with good mechanical properties, and offer a cost-effective solution against the high cost of advanced textiles [72]. Although literature on the topic is still rather scarce, a considerable amount of work has already been undertaken to examine the mechanical characterisation of natural fibre TRM (NTRM) systems comprising flax [86,98,99,101,141], jute [69,141], hemp [69,100], sisal [98-100,102], cotton [100] textiles and lime-based mortars. Flax textiles are reported to be the most suitable for strengthening applications [98,99,141] and have been shown to develop good composite action when embedded in a lime-based mortar [99,141], especially if twisted yarns of low linear density are used [141,163]. Studies on NTRM bonded to masonry substrates have also shown that when a sufficient bond length is provided, a good structural performance can be achieved and, ultimately, failure is dominated by textile rupture with high utilisation of the textile strength [104,108,164]. However, a study performed by the authors on small scale bond tests [164] has shown that the use of two or more flax textile layers may result in delamination when large bond widths are provided.

Available studies have relied mainly on results from small scale testing and only limited work has examined the performance of NTRM at the structural level. Cevallos et al. [165] were the first to examine the behaviour of masonry elements strengthened with flax-TRM systems under eccentric compressive loading and compared their behaviour to that of their PBO counterparts. Although both systems improved strength and deformability, the stiffness compatibility of the flax-TRM with the masonry prevented debonding and resulted in a more ductile failure mode. A later study by Menna et al. [109] confirmed that significant improvement in terms of ductility could be achieved by applying a resin-treated Hemp-TRM system on both brick and tuff masonry panels subjected to diagonal compression tests, with no premature debonding and an in-plane shear strength increase similar to that provided by commercially available advanced TRM systems. An additional study on masonry panels strengthened with one and two layers of Flax-TRM and subjected to diagonal compression has shown that superior ductility can be developed, especially when using a two-layer configuration, leading to textile rupture without any debonding [108]. Although an increase in capacity was not achieved when using two layers of Flax-TRM, other studies on advanced TRM have shown that the shear strength can be increased with the increase in the number of layers [11,16].

Diagonal compression tests are easier to perform than in-plane lateral loading tests and provide useful information on shear strength/strain and modulus of rigidity [106]; however, they do not enable the examination of all the critical in-plane shear resistance mechanisms, which are highly dependent on wall geometry, boundary conditions, magnitude of vertical loads, as well as masonry characteristics [37]. As a result, the suitability of a strengthening system to improve seismic performance is best assessed on wall specimens subjected to in-plane reversed load cycles [105].

Finally, as the properties of natural fibres differ considerably from those of engineered advanced textiles, the suitability of design models included in available guidelines for the prediction of the shear capacity of TRM-retrofitted walls needs to be assessed. Current approaches estimate the

contribution of the TRM system based on bond performance, either using bond strength directly or imposing an equivalent effective strain limit, while neglecting the contribution of the mortar [56]. This approach, however, might not be applicable to mortars reinforced with natural-fibre textiles, as the textile can undergo relatively large deformations at low stress levels and the relative contribution of the mortar can be substantial when paired with the lower stiffness of the fibres.

The present study investigates for the first time the effectiveness of flax-reinforced lime-based composite systems (FTRM) as a seismic retrofitting solution for unreinforced masonry walls using in-plane shear tests under quasi-static cyclic loading. The predictions of available design models are compared with the experimental results and commented upon. Based on the analysis of the strain evolution in the FTRM retrofitted walls, the contributions of the mortar layer and textile reinforcement are estimated and a new design model is proposed. The results presented herein complement previous studies by the authors on the development of sustainable and cost-effective seismic retrofitting solutions for unreinforced masonry structures [141,164].

6.2. EXPERIMENTAL PROGRAMME

A total of six single-wythe medium-scale masonry walls, nominal size of 1,125 x 1,115 mm, were built. Four of the walls were retrofitted on both sides with FTRM including one or two textile layers, while one bare wall and one wall retrofitted only with lime-based mortar were used as control specimens. Material properties and details of the tests are given in the following sections.

6.2.1. Material Characterisation

6.2.1.1. Masonry

All specimens were manufactured using commercial fired clay single-frog bricks, measuring 215 x 102 x 65 mm with net loaded area equal to 35% of the bed face, and a general-purpose masonry mortar. The cement: lime: sand proportions used in the mortar were 1:2:9 by volume, and the water/solid ratio was 0.27 by weight. The masonry constituents were selected to replicate low strength masonry typical of residential buildings in less developed countries [166]. Detailed mechanical characterisation was performed on the masonry constituents and on masonry assemblages, including:

- i) flexural tests on 160 x 40 x 40 mm mortar prisms, followed by compressive tests on the resulting halves;
- ii) compressive tests on single bricks;
- iii) compressive tests on masonry wallettes with nominal dimensions of 440 x 102 x 515 mm (length x width x height).

Tests ii) and iii) were performed in both directions parallel and perpendicular to the bed joints, and a normal strength cement mortar was used for capping the surface in contact with the loading plates to ensure a uniform stress distribution. Linear variable displacement transducers (LVDT) of 5

mm stroke were installed on the opposite sides of each mortar prism and wallette specimen, to determine their elastic modulus.

The results obtained from the tests are summarised in **Table 6.1** in terms of average compressive strength (f_c), average flexural strength (f_n), and average elastic modulus (E), along with the number of test repetitions (n), the loading rate and the associated standards according to which the tests were performed. Coefficient of variation (CoV) values are given in parentheses.

The difference in the properties of the masonry constituents in the two directions resulted in slightly different properties of the masonry wallettes, which experienced, nevertheless, similar failure mode. When specimens were tested in compression perpendicular to the bed joints, vertical cracks were formed parallel to the loading direction, crossing through the bricks and mortar joints and eventually leading to brick crushing. For compression parallel to the bed joints, cracks ran mainly along the mortar joints and led to the crushing of the outer only bricks. Good agreement was found between the experimental compressive strength of the masonry perpendicular to bed joints and the corresponding theoretical value (5.9 MPa) estimated according to Eurocode 6 [167].

Table 6.1 Masonry properties. CoV values are given in parentheses.

Specimen Type		n	Loading Rate	f_c (MPa)	f_n (MPa)	E (GPa)	Reference Standard
Brick	⊥	3	0.15 MPa/s	24.4 (13%)	-	-	EN 772-1 [168]
	//	3		17.3 (11%)	-	-	
Masonry	flexure	28	0.5 mm/min	-	0.6 (6%)	1.1 (16%)	EN 1015-11 [125]
Mortar	compression	56	100 N/s	2.1 (8%)	-	-	
Masonry Wallette	⊥	3	0.25 mm/min	6.0 (2%)	-	2.4 (7%)	EN 1052-1 [169]
	//	3		6.8 (5%)	-	2.9 (2%)	

In addition, shear tests were performed on masonry triplets with nominal dimensions of 215 x 102 x 215 mm to determine the initial shear strength of the masonry. Three series of three specimens each were prepared and tested at three pre-compression levels varying from 0.2-1 MPa, following EN 1052-3 [170]. The characteristic initial shear strength after linear regression was found to be 0.13 MPa. This is in close agreement with the EC6 provisions of 0.1 MPa for clay masonry units with M1-M2 general purpose mortar [167].

6.2.1.2. Textile-Reinforced Mortar

The strengthening system comprised commercially available balanced bi-directional flax textiles (**Fig. 6.1**) embedded in lime-based mortar. The mortar used in the TRM system was a commercial product consisting of NHL2, short cellulose fibres to mitigate shrinkage, and siliceous and calcareous aggregates with a maximum size of 2mm. A water/solid ratio of 0.23 by weight was used as per supplier's instructions. The mechanical properties of the mortar were determined through a series of thirty flexural and sixty compressive tests following EN 1015-11 [125]. The flexural tests were

performed in displacement control at a rate of 0.5 mm/min, while the compressive tests were carried out in load control at a rate of 400 N/s. The mortar had an average flexural strength of 2.7 MPa (CoV: 5%), average elastic modulus of 3.8 GPa (CoV: 12%) and average compressive strength of 6.8 MPa (CoV: 7%).

The mechanical properties of the textile and TRM systems with one and two layers of flax reinforcement were determined experimentally [141] and the results are summarised in **Table 6.2**, along with the physical properties of the textile as provided by the manufacturer.

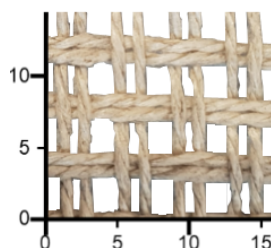


Fig. 6.1 Flax textile used for TRM retrofitting. Scale in mm.

Table 6.2 Physical and mechanical properties of textile and composites. CoV values are given in parentheses.

Property	Textile	TRM	
		1 layer	2 layers
Mesh size (mm)	4	-	-
Weight (g/m ²)	300	-	-
Cross-sectional area (mm ² /mm)	0.01	-	-
Tensile strength (MPa) ^a	289.0 (6%)	177.8 (12%)	208.9 (8%)
Ultimate tensile strain (%) ^a	3.8 (4%)	7.3 (14%)	7.9 (8%)
Tensile elastic modulus (GPa) ^a	13.6 (7%)	3.0 ^b (9%)	3.9 ^b (9%)
Bond strength (MPa) ^c	-	208.1 (6%)	171.8 (10%)

^atested according to AC434 [51] in a study previously conducted by the authors [141].

^bcracked stage.

^ctested according to RILEM TC 250 [54] on specimens with 260 mm bond length, 100 mm bond width [164].




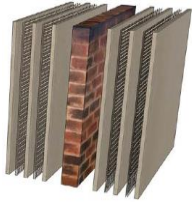
6.2.2. Specimen Preparation

The six single-wythe unreinforced masonry walls were constructed in a running bond pattern, comprising bed and head mortar joints of approximately 10 mm in thickness. The first course of each wall was laid directly into a steel channel, which was designed to be bolted to the strong floor and provide continuous restraint to the wall. A rapid hardening high strength fibre-reinforced cement grout was used to fill the steel channel and create a bonded joint of adequate strength along the entire length of the wall. The compressive, tensile and adhesion strength of the grout were 55 MPa, 10 MPa, and 2 MPa, respectively, according to the manufacturer's datasheet. The same high strength grout was used to bond the top course of bricks to an additional steel channel, which served as capping system and loading beam. The top and bottom steel channels were also equipped with side

brackets to allow the positioning of threaded rods and the application of a mild prestressing force to ensure safe handling of the specimens. The specimens were cured under wet hessian cloth for the first 7 days and then stored in standard laboratory conditions for at least 21 days.

With the exception of wall (BW), which was left bare, three different strengthening configurations were examined as detailed in **Table 6.3**: one specimen was strengthened with plain lime-based mortar (LW), two specimens were strengthened with one layer of flax-TRM (FL1W) and the remaining two with two layers of flax-TRM (FL2W). Specimens BW and LW served as control specimens and enabled a direct assessment of the effectiveness of the flax-TRM retrofitting solutions. Before strengthening, the wall surfaces were brushed thoroughly and then water saturated to avoid moisture uptake from the mortar. A layer of lime-based mortar was trowelled on the entire wall surface (full covering) and the flax textile was manually stretched and embedded slightly into the mortar by applying hand pressure. The TRM application was completed with an additional mortar layer while the previous layer was still in its fresh state and finished to ensure a uniform surface. An additional layer of textile and mortar were applied on specimens strengthened with 2 layers of flax-TRM. The same procedure was repeated on both sides of the strengthened specimens. All mortar overlays were approximately 3 mm thick, resulting in a total thickness of 6 mm and 9 mm per side for FL1W and FL2W series, respectively. Specimen LW was strengthened with 6-mm thick mortar overlays on both sides to enable a direct comparison with single-layer TRM-retrofitted specimens (FL1W). After strengthening, the specimens were cured under wet hessian cloth for the first two days and then stored in standard laboratory conditions (20 °C and RH < 70%) until the day of testing. The different phases of construction and TRM application are illustrated in **Fig. 6.2**.

Table 6.3 Specimens' configuration

Specimen ID				
	BW	LW	FL1W	FL2W
Configuration	-	1 layer of mortar	1 layer of FTRM	2 layers of FTRM
Repetition(s)	1	1	2	2

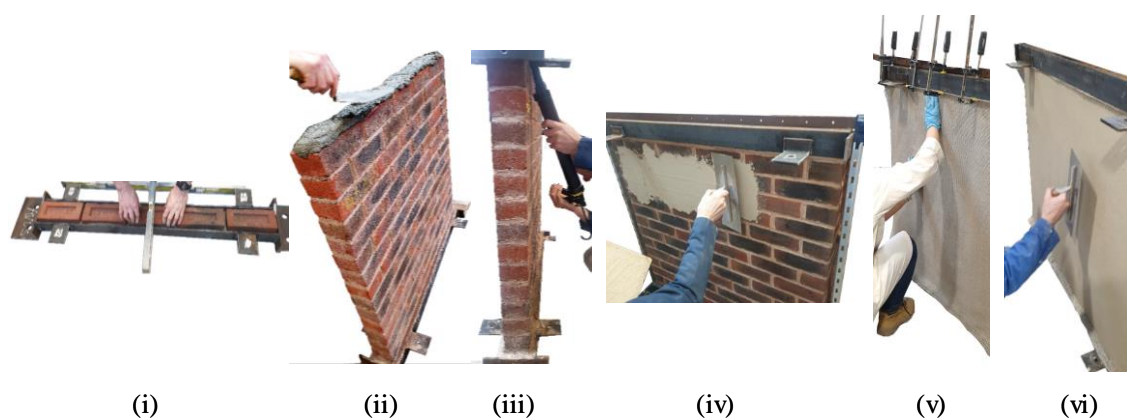


Fig. 6.2 i) Laying of first course in the steel channel; ii) application of rapid-hardening high strength grout; iii) positioning of capping system and use of injection guns for grout filling; iv) application of first mortar layer; v) embedment of flax textile; vi) application of top mortar layer and finishing.

6.2.3. Experimental Setup

The wall specimens were subjected to in-plane shear compression tests, under quasi-static cyclic loading up to near collapse state. An overview of the experimental setup is presented in **Fig. 6.3**.

The horizontal load was applied using a servo-hydraulic actuator with a stroke of ± 75 mm and fitted with a load cell of 250 kN capacity. The actuator was coupled to one end of the loading beam by means of stiff steel plates and four threaded rods. The coupling plates were machined with pass through slotted holes for horizontal and vertical adjustments so as to accommodate any deviation in the actual geometry of the specimens from their nominal dimensions. The two ends of the bottom channel of each wall were mounted to the reaction frame using two 16-mm 8.8 grade bolts.

A vertical compressive load was applied to the top channel via a spreader beam on rollers to simulate the gravity load imposed by upper storeys. The vertical load was transferred under a mixed force-displacement controlled mode by means of a pair of hydraulic actuators, the pressure of which was adjusted and monitored through a pressure gauge. The load remained constant throughout the test and updated dynamically to keep the spreader beam horizontal. The concurrent control of the applied vertical load and imposed vertical displacement was imposed in an attempt to minimise the effect of bending and shear sliding and force a shear-dominated deformation behaviour. Under these conditions, the masonry is free to translate in the push-pull direction and restrained to deflect in the vertical direction. Nevertheless, at the higher levels of load that developed during the tests on specimens retrofitted with two FTRM layers, rotation of the spreader beam was unavoidable, but only after the specimens underwent significant damage and exhibited extensive shear diagonal cracking (see Section 6.3.1.4).

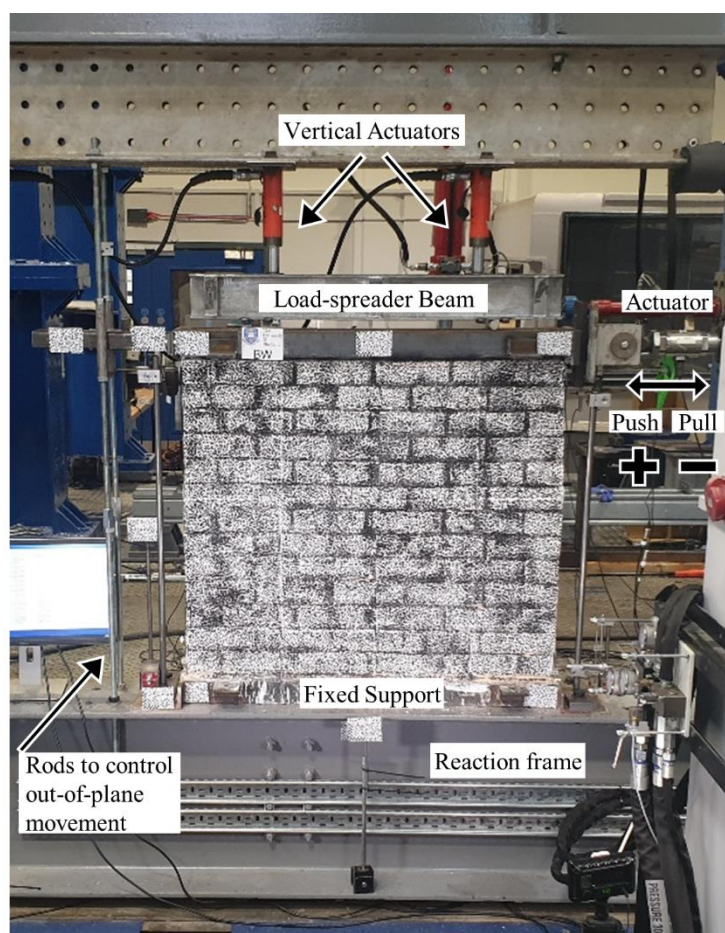


Fig. 6.3 Test setup

6.2.3.1. Loading protocol

A total vertical pre-compression load of 70 kN, equivalent to approximately 10% of the masonry compressive strength, was applied to each specimen before initiating the in-plane loading sequence. The tests were performed in displacement control under quasi-static conditions to capture the post-peak softening stage and the associated damage accumulation phenomena. All specimens were subjected to the same in-plane reverse cyclic loading regime (push and pull) shown in **Fig. 6.4a**. The first two cycles were performed at a target displacement of ± 0.5 mm and ± 1 mm to capture the elastic response of the masonry wall (**Fig. 6.4b**), while the subsequent cycles were performed at increasing target displacement amplitudes of 1 mm in both directions. As summarized in **Fig. 6.4b**, a slower loading rate was used for the bare specimen to better capture the expected, more brittle hysteretic response, and the transition between the various limit states. Each test was terminated after a strength degradation of about 20% was observed, level at which the element was considered to have reached its near-collapse limit state [171].

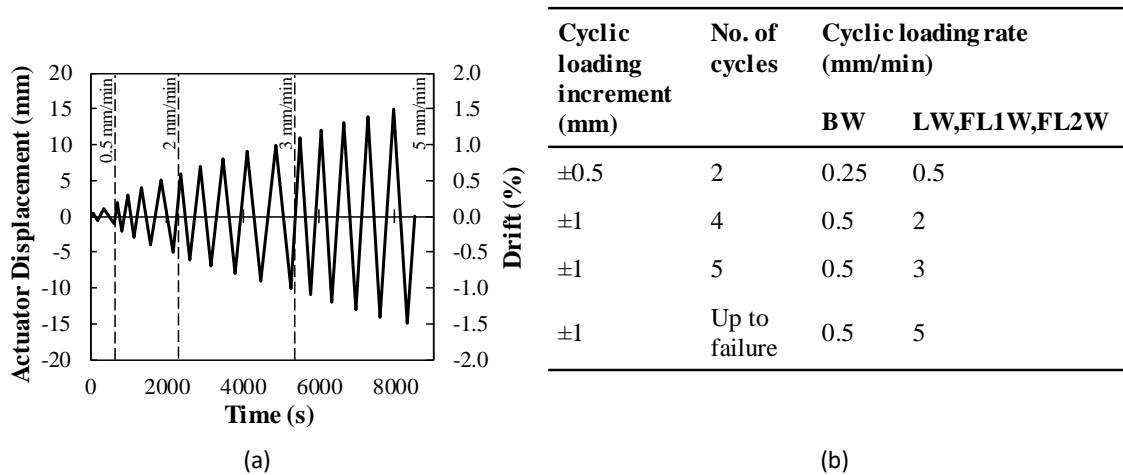


Fig. 6.4 (a) Displacement history for retrofitted specimens (LW, FL1W, FL2W); (b) Adopted loading regime for all wall specimens.

6.2.3.2. Instrumentation

6.2.3.2.1 Conventional measurements

The global and local behaviour of the specimens were monitored using 11 LVDTs as shown in **Fig. 6.5**. The LVDTs measured: (1) the horizontal displacement at the top of the wall; (2) and (3) the horizontal displacement of the top and bottom second brick courses, respectively; (4) and (5) the vertical displacement of the opposite sides of the top channel; (6) and (7) the relative vertical displacement between the bottom second brick course and the footing; (8) and (9) the relative vertical displacement between the top second brick course and the top channel. In addition, any rocking or uplift of the footing from the strong frame was measured through LVDT (10), while LVDT (11) was used to monitor any out-of-plane movement. All data were acquired at a frequency of 5 Hz.

6.2.3.2.2 Digital Image Correlation

A bespoke 2D-DIC setup was employed to obtain the displacement field of the entire specimen's surface and gain additional information on crack initiation and development.

The surface of the bare wall was whitewashed to provide sufficient contrast for the identification of the speckle pattern, while the lime mortar layer of the retrofitted specimens provided a suitable surface and did not require any additional preparation. Stencils with a random pattern of 3-mm diameter speckles were laser cut onto adhesive paper and attached to the wall surface, which was then sprayed with a matt black paint. The adhesive paper was subsequently removed, leaving a high-quality speckle pattern throughout the region of interest (**Fig. 6.6**).

Images were acquired with a single Sony IMX183 CMOS camera having a 5,472x3,648pixel resolution (BFS-U3-200S6M-C USB 3.1 Blackfly® S, Monochrome Camera) and equipped with a fixed lens of 18 mm focal length. The camera was positioned approximately 3 m away from the monitored surface and led lights were used to provide uniform light distribution over the region of

interest. The acquired images were processed with GOM Correlate [133]. A subset size of 50 pixels was chosen to contain a minimum of 3×3 speckles [131], while a step size of 15 pixel was selected to provide a high spatial resolution. Based on the field of view and the camera resolution, the magnification factor was equal to 2.4 pixels/mm.

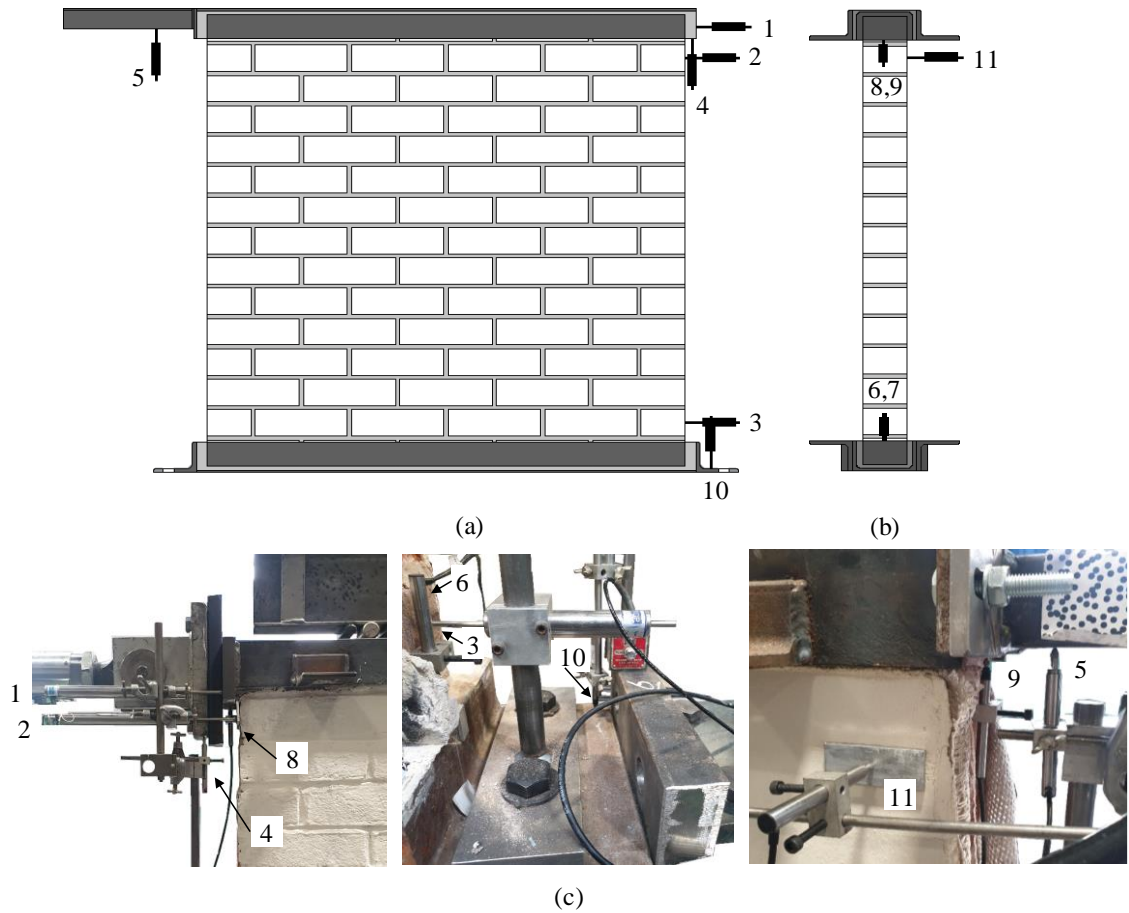


Fig. 6.5 Instrumentation layout: (a) front view; (b) side view; (c) mounting details

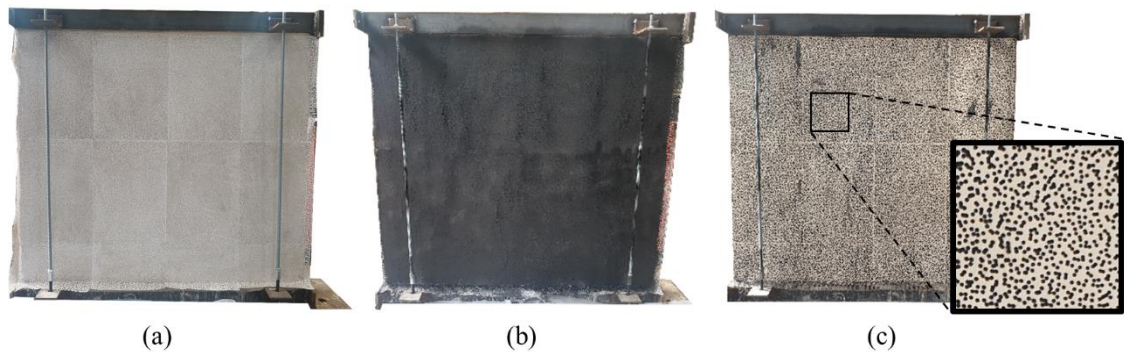


Fig. 6.6 Specimen preparation for DIC analyses: (a) wall fitted with laser cut stencils; (b) application of a matt black paint; (c) detail of speckle pattern after removal of stencils.

6.3. RESULTS AND DISCUSSION

The main experimental results for both push (+) and pull (-) directions are summarised in **Table 6.4** in terms of maximum shear load (V_{\max}), lateral drift corresponding to the maximum shear capacity ($\delta_{v\max}$) and lateral drift corresponding to 20% strength degradation (δ_u). The drift values were obtained by normalising the displacements recorded by LVDT1 (**Fig. 6.5**) by the specimens' actual height (given in the first column). The predominant failure mode is also reported along with the loading direction in which failure was deemed to have occurred. The specimen ID shown in **Table 6.4** follows the notation X-n, where X denotes the retrofitting configuration as given in **Table 6.3**, and n is the replicate number (1 or 2).

Table 6.4 Experimental results of in-plane cyclic tests.

Specimen ID	H (mm)	V_{\max} (kN)		$\delta_{v\max}$ (%)		δ_u (%)		Failure Mode
		(+)	(-)	(+)	(-)	(+)	(-)	
BW	1085	45.1	-46.4 ^a	0.48	-0.61 ^a	0.80	-0.61 ^b	Diagonal Shear (-)
LW	1150	83.7	-75.2	0.82	-0.62	1.15	-0.87	Diagonal Shear/Toe crushing (+)
FL1W-2	1100	90.1	-84.1	0.92	-0.76	1.15	-0.76 ^b	Diagonal Shear/Toe crushing/local TRM debonding (+)
FL2W-1	1120	93.7	-95.1	0.96	-0.93	1.15	-1.26	Diagonal Shear (-)
FL2W-2	1075	102.6	-102.1	1.25	-1.12	1.38	-1.49	Diagonal Shear (+)

^aderived from first cyclic test.

^bfailure in the push direction occurred before any load degradation in the pull direction; δ_u is taken here equal to $\delta_{v\max}$.

6.3.1. Hysteresis Response and Failure Modes

Fig. 6.7a-e show the load versus drift hysteresis response of each specimen, while **Fig. 6.7f** shows the backbone curves (experimental envelopes) of the tested walls, in both positive and negative loading directions. The drift capacity estimated according to EC8 and corresponding to the limit states of Significant Damage (SD) and Near Collapse (NC) [171] are also plotted for reference (grey dashed lines). The crack patterns captured by DIC at the maximum drift (δ_u) imposed in the direction of loading that induced failure are presented in **Fig. 6.8**, along with the percentage of the cracked/uncracked portion of the wall, as well as close-up photos of the observed failures.

The inherent heterogeneity of the masonry and the imperfections introduced during the manufacture and retrofitting stages (e.g. variations in walls' dimensions, lack of symmetry in the application of lime or FTRM retrofitting layers) resulted in the development of non-symmetrical damage during the reverse loading cycles and in a non-symmetrical hysteresis response in the two directions of loading. Overall, the response of the specimens is characterised by a linear behaviour up to the occurrence of the first cracks, followed by cycles displaying varying degrees of pinching, especially in the low drift cycles performed in the pull direction (S-shaped loops) for specimens BW, LW and FL1W-2, indicating the presence of rigid body movements, such as rocking and/or failure at the bed joints. The difference between the maximum strength values recorded in the two directions

was up to 11% (LW), while the corresponding drift ratios varied up to approximately 30%. The behaviour of the specimens retrofitted with two layers of FTRM were characterised by a more symmetrical response, with only about 1.5% and 10% difference in terms of strength and corresponding drift values, respectively. All specimens experienced diagonal shear cracking (**Fig. 6.8**), with the major cracks connecting the two bottom corners of the walls to the points of application of the vertical load, thus suggesting that bending effects were not completely eliminated. No significant uplift of the footing was recorded for any of the specimens ($\ll 0.01$ mm).

The following sections include a detailed analysis of the behaviour of each specimen and the associated failure mechanisms.

6.3.1.1. BW

The bare wall specimen experienced a linear response in both directions up to the appearance of horizontal cracks at the interface of the first mortar bed joints and the footing. Cracks initiated from the bottom end corners and propagated during the subsequent cycles along the full length of the wall. Some degree of rocking was observed soon after, as reflected by the change in stiffness of the load-drift response, which resulted in additional compression of the bottom mortar joints in the toe regions of the wall. The first diagonal shear cracks opened along the diagonal in the push direction at load levels close to the maximum shear force, followed by additional cracks along the opposite diagonal after load reversal. The lack of symmetry in loading between the push and pull directions was also reflected in the crack pattern, with a wider and less inclined diagonal crack being induced by the load in the push direction. A brittle shear-dominated failure developed at an ultimate drift δ_u of 0.8% (8.7 mm) that was characterised by two major diagonal shear cracks partly passing through the bricks (**Fig. 6.8a**).

The specimen was able to sustain a drift higher than that corresponding to NC limit state (**Fig. 6.7f**), exceeding it by approximately 28% in the 9th cycle. Given the long test duration due to the slow loading rate, the test had to be halted and resumed the next day. An additional loading cycle was performed (indicated as cyclic test no2 and plotted in grey in **Fig. 6.7a**), starting from the pull direction. Accidentally, a much faster loading rate was applied (0.5 mm/s against 0.5 mm/min), resulting in peak load and corresponding drift values of -56 kN and -0.85%, respectively. These values are not considered in the discussion of the results and do not form the basis of any comparison for the analysis and assessment of the TRM retrofitting technique presented herein. The correct loading protocol was resumed after the target drift of 10 mm was achieved in the pull direction and the specimen was loaded in the push direction, during which ultimate failure (20% drop in load) occurred, before any load degradation was observed in the pull direction. For the two loading directions, the maximum base shear force recorded was -46.4 kN/+45 kN at corresponding drift ratios of -0.61 %/0.48 %.

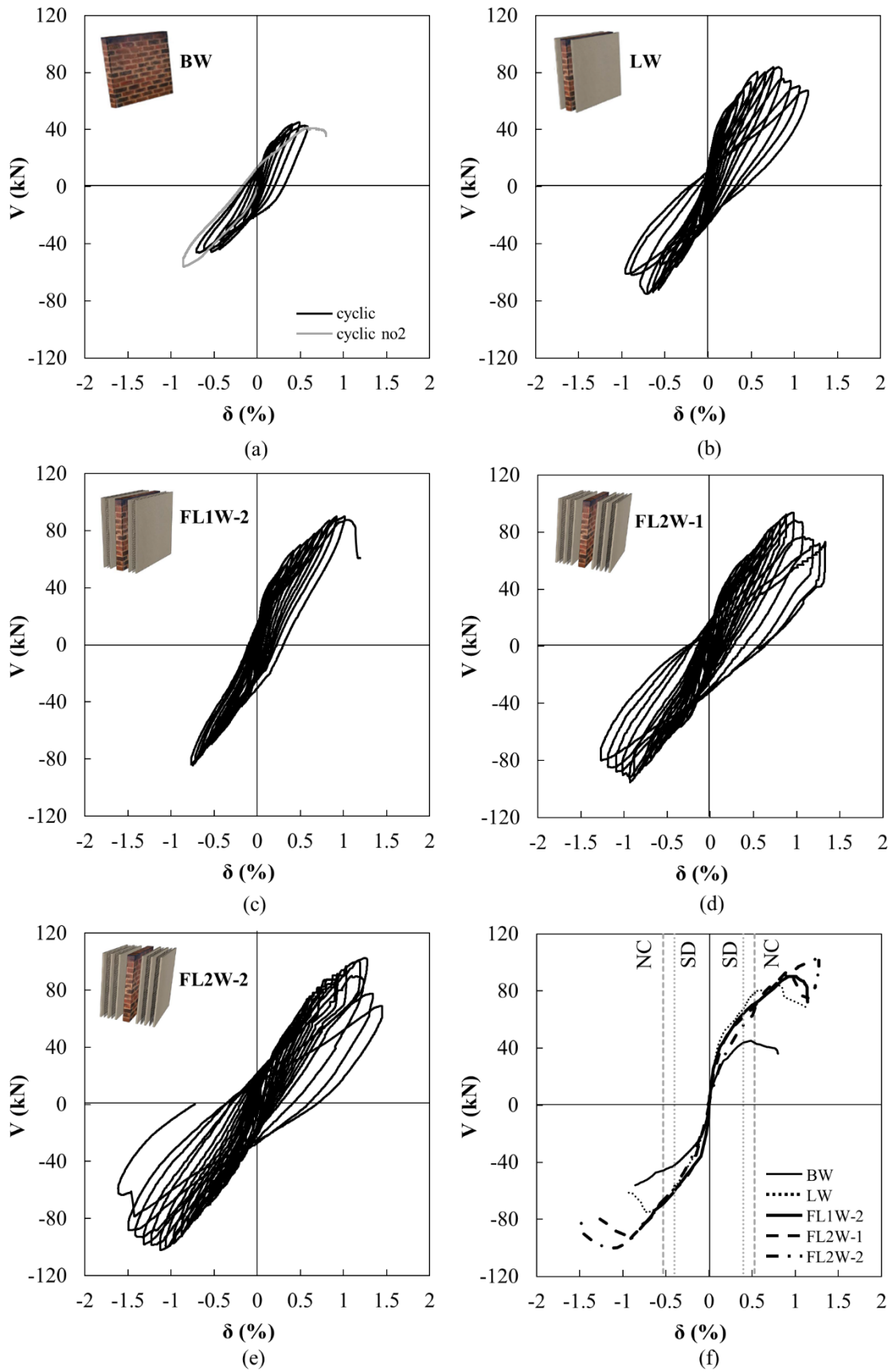


Fig. 6.7 a-e) Load-drift hysteresis responses of the wall specimens; (f) Experimental envelopes.

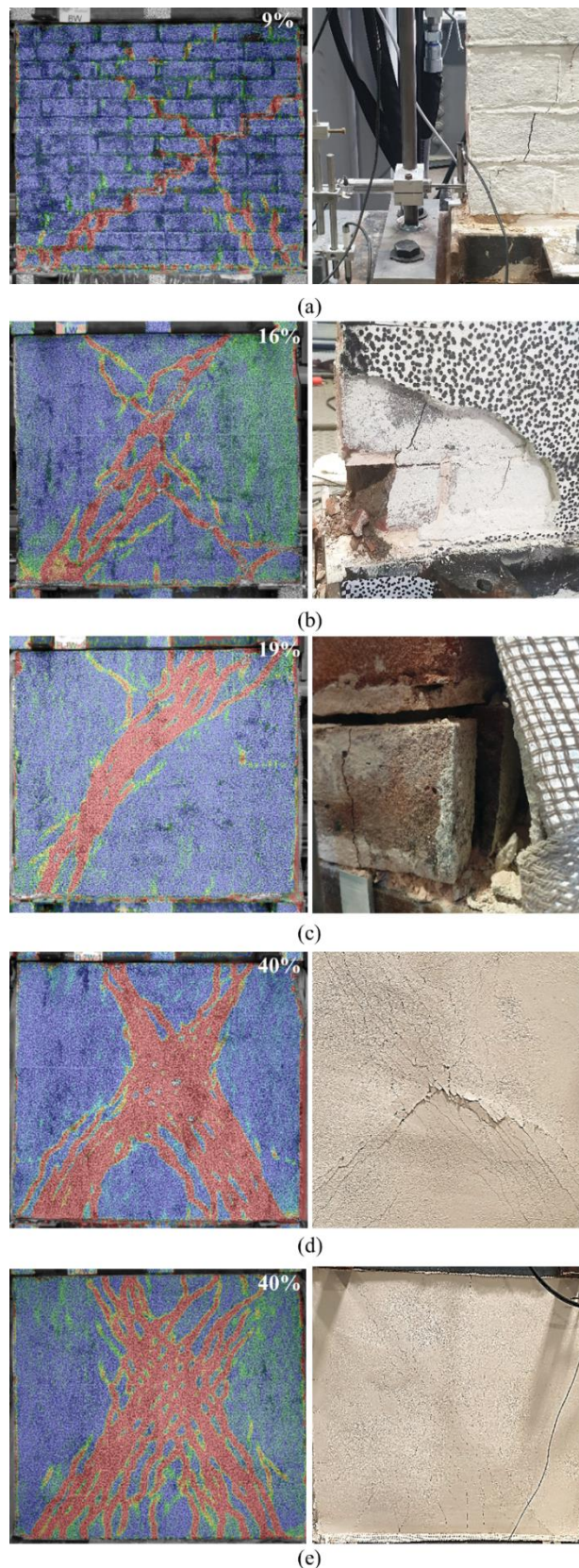


Fig. 6.8 Crack patterns and failure mode details at maximum drift for: (a) BW; (b) LW; (c) FL1W-2; (d) FL2W-1; and (e) FL2W-2. Note: Percentages correspond to the ratio of cracked/uncracked portion of wall.

6.3.1.2. LW

The specimen retrofitted only with a layer of lime mortar on both sides (**Fig. 6.7b**) exhibited higher strength and deformability than the bare wall. Failure initiated with cracks along the horizontal mortar joints near the base, followed by the development of two major diagonal cracks at higher target drift cycles (approximately 0.7%). After the maximum peak load was achieved (+83.7 kN, drift 0.82%), the behaviour of the wall in the push direction exhibited a more gradual strength degradation than in the pull direction as a result of the widening of existing cracks and opening of additional parallel diagonal cracks followed by progressive toe crushing. The test was continued until a maximum drift of 1.15% was attained, and was halted after substantial damage was observed, including detachment of the lime mortar layer in both bottom corner regions of the wall and crushing of the masonry bricks in the bottom left corner (**Fig. 6.8b**). No significant shear sliding ($<\pm 1$ mm) was observed during the initial cycles of the test and up to the peak load; however, a 4-mm horizontal movement of the bottom brick course was recorded in the pulling direction upon failure.

6.3.1.3. FL1W

Although two walls were tested with one layer of FTRM, subsequent DIC analysis of the images taken during the test performed on specimen FL1W-1 revealed an excessive rigid translation of the footing along the push-pull direction (up to 6 mm), which compromised the actual load and deformation response of the specimen. Hence, the experimental behaviour of FL1W-1 is not discussed further and is not considered in the overall assessment of this strengthening scheme.

Specimen FL1W-2 achieved higher load and drift capacity than the wall retrofitted with only lime (see **Table 6.4**). It should be noted that the mortar layer of these specimens had the same nominal thickness so a comparison of their performance can yield useful insights into the role of the textile reinforcement. A horizontal crack formed at the two bottom ends and propagated towards the centre of the wall along the bed joints during the initial cycles, followed by the opening of cracks along both diagonals and the development of additional multiple diagonal cracks of smaller width upon the attainment of the maximum load. Ultimate failure occurred due to toe crushing and limited local detachment of the FTRM from the substrate at the two bottom corners (**Fig. 6.7c**). No rupture of flax yarns was observed and strains in the FTRM were controlled by the presence of the embedded textile, which promoted strain redistribution and multiple crack formation (**Table 6.5**).

6.3.1.4. FL2W

Specimens strengthened with two layers of FTRM were characterised by higher strength and ultimate displacement capacity than their single-layer counterparts (see **Table 6.4**). No flexural cracks or shear sliding were observed for any of the specimens in this group during the initial cycles. Visible cracking was only observed upon the attainment of the peak load, with the formation of multiple cracks spreading along the diagonals of the walls during subsequent cycles. The post-peak

response of these specimens was characterised by high energy dissipation capacity, albeit with rapid strength degradation. While clear signs of damage were visible on FL2W-1 when the test was halted at the target strength degradation, the test on FL2W-2 was continued beyond the 20% load degradation threshold as cracking appeared to be better controlled and there were no other signs of critical damage. Eventually, failure of FL2W-2 occurred due to extensive diagonal cracking, followed by toe crushing and shear sliding. Both specimens in this series developed a higher ultimate drift capacity (-1.26% and 1.38% for FL2W-1 and FL2W-2, respectively) and dissipated a significant amount of energy through progressive diagonal cracking (cracking extended to about 40% of the wall surface - **Fig. 6.7d** and **e**), thus highlighting the contribution of the flax reinforcement to energy dissipation and in controlling the development of brittle failure modes. As in the single-layer FTRM-retrofitted specimen, no rupture of flax yarns was observed. A post-test inspection of the specimens enabled the detection of localized TRM debonding near the centre of the wall and at the intersection of the two diagonal crack bands; however, the accurate identification of the interface at which it occurred could not be located, as the integrity of the wall, in both specimens, was maintained till the end of the tests.

6.3.1.5. Diagonal crack initiation and development

The contour maps of the principal strains obtained from DIC analysis were used to identify the initiation and development of the entire crack pattern (**Fig. 6.8**). This information was then used to evaluate the crack width evolution of critical diagonal cracks by applying virtual transducers perpendicular to the crack direction at different locations. The horizontal cracks that developed along the base of the wall due to flexural deformation were excluded from this analysis. In specimens characterised by the development of wide crack bands, namely FTRM-retrofitted walls, a minimum of 20 representative cracks across the crack band were considered for the analysis. The values of maximum crack width at peak load ($w_{V_{max}}$) and at ultimate state (w_u) obtained for each of the specimens were then used to assess the performance of the tested strengthening schemes (**Table 6.5**).

The localised strain around the crack openings (ϵ_{max}) was also calculated as the change in length of the virtual extensometers divided by their initial length and can be used as an estimate of the level of strain developed in the flax textile. Additional virtual extensometers spanning the entire crack band width along the two diagonals were also created to estimate average strain values, ϵ_{avg} . The values of ϵ_{max} and ϵ_{avg} associated with the maximum load attained during the tests are reported in **Table 6.5**.

Table 6.5 Maximum crack widths and average and maximum strains, as measured by DIC.

Specimen ID	W_{\max} (mm)		ϵ_{avg} (%)	ϵ_{\max} (%)
	$W_{V_{\max}}$	W_u		
BW	2.93	2.93*	-	-
LW	0.36	3.79	-	-
FL1W-2	1.12	1.28	2.00	3.52
FL2W-1	0.21	0.58	0.29	2.34
FL2W-2	0.09	0.81	0.16	0.79

* w_u is taken here equal to $w_{V_{\max}}$, as no strength degradation occurred in the failing direction (pull).

Although the use of FTRM did not lead to the development of strength values significantly higher than those of specimen retrofitted only with lime, the maximum crack width was considerably reduced at NC limit state in specimens with flax reinforcement (by more than 50% for specimens with 1 layer of textile), which exhibited a larger number of more distributed cracks. As expected from experience gained from bond and tensile tests conducted on the same FTRM system [141][164], the addition of FTRM layers helped in controlling maximum crack widths, confirming that higher amounts of flax reinforcement can effectively promote strain redistribution. The maximum crack width at ultimate load was generally small for all specimens (except for FL1W-2), as the diagonal cracks only formed at a load value very close to the peak load resistance.

The evolution of maximum crack width with maximum applied load and drift at each cycle (up to the last value of drift commonly exhibited by all specimens) is plotted in **Fig. 6.9a** and **b**, respectively. Both diagrams highlight the ability of the FTRM to delay cracking and control crack opening at any given level of drift. The level of load corresponding to the initiation of diagonal shear cracking was in the range of 88-91% of V_{\max} for specimens with two FTRM layers, and between 70-80% for specimens BW, LW and FL1W-2. In an attempt to quantify damage, the percentage of the cracked over uncracked area of the wall was measured through DIC and plotted as a function of load (**Fig. 6.9c**). As evidenced, the use of one layer of FTRM experienced the same degree of damage as the LW, albeit at higher loads and as a result of finer cracks. A significantly different behaviour was exhibited by the specimens retrofitted with two FTRM layers, where a favourable combination of damage accumulation (indicating strain redistribution) and smaller crack widths was observed.

The strain values estimated to have been developed in the textile reinforcement confirm that no rupture occurred, as strain values were significantly smaller than either the ultimate textile strain (**Table 6.2**) or the strain corresponding to bond failure (**Section 4**).

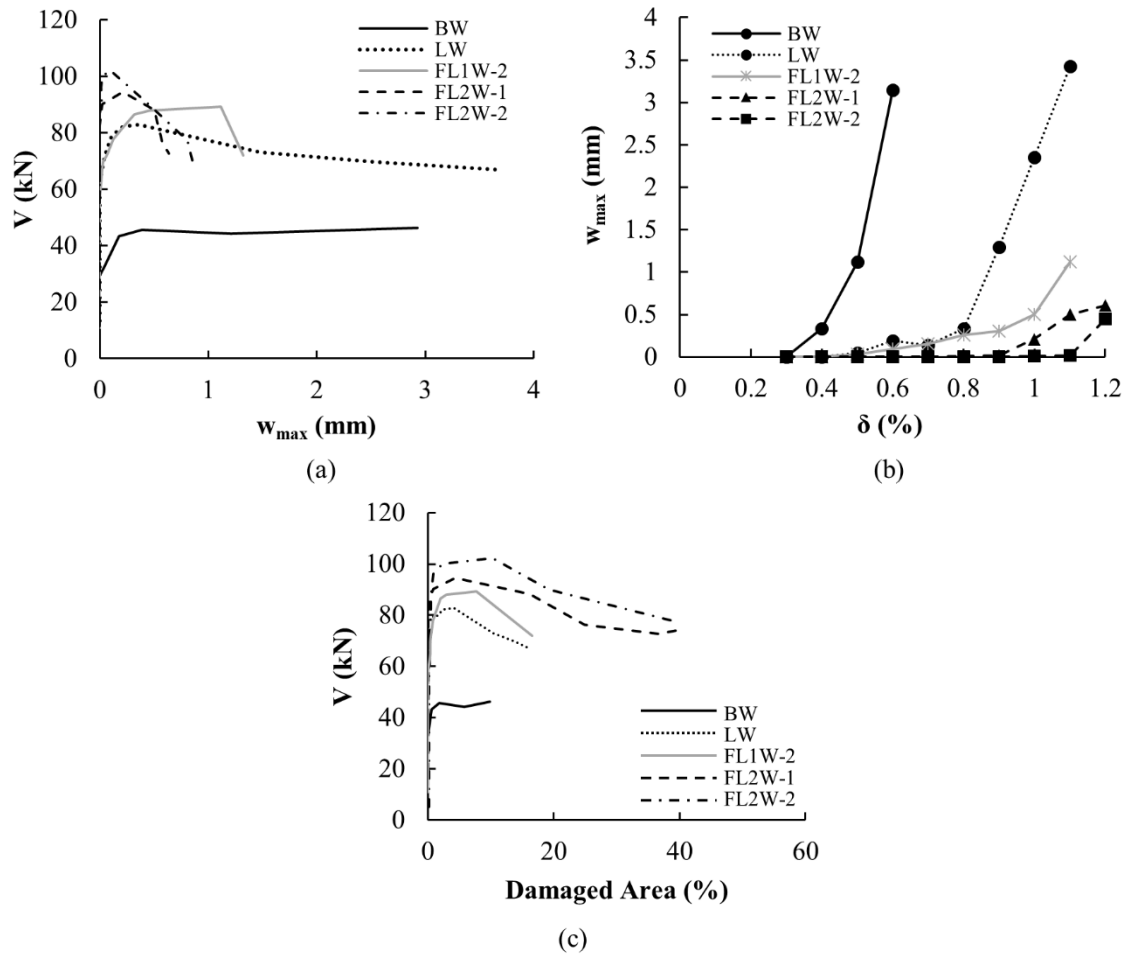


Fig. 6.9 Development of maximum crack width with: (a) load and (b) drift; (c) Load versus damage evolution until Near Collapse.

6.3.2. Stiffness Degradation

The analysis of the progressive stiffness degradation of the tested specimens due to cracking and damage accumulated throughout the loading history can provide additional insights into the effectiveness of the examined strengthening schemes. The lateral secant stiffness (K_{eff}) of the bare and retrofitted specimens versus drift is shown in **Fig. 6.10**, where the stiffness of each hysteresis cycle i is calculated according to Eq. (6-1) [51]. K_{eff} is calculated up to the last full cycle of each test.

$$K_{eff,i} = \frac{|V_i^+| + |V_i^-|}{|\delta_i^+| + |\delta_i^-|} \quad (6-1)$$

From **Fig. 6.10**, it can be seen that during the first initial cycle, when the specimens are still uncracked, a higher initial stiffness is displayed by the retrofitted specimens with respect to that of the bare wall. Hence, the strengthening layers are acting compositely with the masonry.

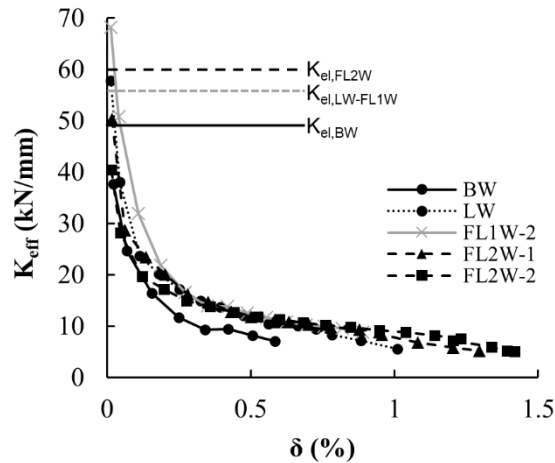


Fig. 6.10 Stiffness degradation versus drift for bare and retrofitted specimens.

In all specimens, the lateral initial stiffness degrades at increasing drift ratios following a nearly hyperbolic trend, with a high stiffness degradation rate during the first low drift cycles and up to approximately 0.3% drift, followed by a slower, nearly linear decay. Comparable stiffness degradation is exhibited by the retrofitted specimens at drift values ranging from approximately 0.35% to 0.75%, resulting in an effective damaged stiffness of approximately 15 kN/mm, which translates into an 80% stiffness loss for the specimen with one FTRM layer, 75% loss for the specimen with only lime mortar, and 67% loss for the specimens with two FTRM layers. However, after 1% drift the lime mortar is unable to sustain larger drifts and specimen LW fails, whilst the double textile reinforcement becomes activated. Specimens retrofitted with two layers of FTRM exhibited the highest drift capacity at NC limit state, and a residual stiffness of approximately 5 kN/mm.

6.3.3. Bilinear Idealization of the Experimental Envelopes

The idealised bilinear (elastoplastic) resistance envelopes [6,37] of the masonry walls was also determined in line with current international standards [172,173]. The three parameters that need to be obtained to fully describe the elastoplastic behaviour include: 1) the effective lateral stiffness (K_e), i.e. the elastic stiffness of the bilinear curve, taken as the secant stiffness at crack limit and calculated as the ratio of the experimental cracking load (V_{cr}) over the corresponding displacement (d_e); 2) the maximum load resistance (V_u); 3) the ultimate displacement (d_u).

Different approaches are proposed in the literature to identify the crack limit: Eurocode 8 [172] suggests the use of a cracking load equal to 70% of the maximum experimental load (V_{max}), FEMA [173] considers the first crack to develop at 60% of V_{max} , while a more conservative ratio of 40% is assumed for the determination of the shear resistance of masonry walls by ASTM [174]. In absence of experimental data, current codes [171] suggest to take an effective stiffness equal to 50% of the elastic value. If K_e and d_u are known, then V_u can be computed by imposing that the energy

dissipation capacity of the cyclic response (circumscribed area, A_{env}) is equal to that of the idealized elastoplastic response (Eq. (6-2) [6]).

$$V_u = K_e \left(d_u - \sqrt{d_u^2 - \frac{2A_{env}}{K_e}} \right) \quad (6-2)$$

The elastic stiffness K_{el} was calculated according to Timoshenko beam theory (Eq. (6-3)):

$$K_{el} = \frac{1}{\frac{H^3}{aEI} + \frac{H}{\kappa AG}} \quad (6-3)$$

where:

- E and G are the elastic and shear modulus of the masonry, respectively
- H and A are the height and the cross-sectional area of the wall, respectively
- κ is the shear coefficient (= 5/6 for rectangular sections)
- a is the coefficient accounting for the type of boundary conditions (3 for fixed-free ends and 12 for fixed-fixed ends)

The elastic modulus of the masonry, E, was determined from experimental data (**Table 6.1** and direction parallel to the bed joints), while the shear modulus, G, was taken equal to 10% of E [175]. Fixed-fixed boundary conditions were assumed, as they represent more closely the experimental boundary conditions. The elastic stiffness of the lime- and FTRM-retrofitted specimens was estimated based on the properties of a transformed section, which was determined by transforming the thickness of lime or FTRM in an equivalent thickness of masonry using their modular ratio and assuming a perfect bond between masonry and retrofitting material. The elastic stiffness of the wall specimens was also determined through a linear elastic finite element analysis to verify the validity of the assumptions made when adopting Eq. (6-3). A simplified macro-modeling approach was adopted for the masonry, which was treated as a homogeneous anisotropic continuum material with smeared properties equal to those derived experimentally. As in the uncracked stage the textile is not mobilised and does not contribute to the overall stiffness, the external TRM layers were modelled using a continuum material with elastic properties as derived from the experimental characterisation of the lime-based mortar. One layer with a thickness of 6mm or 9mm was fully bonded on either side of the masonry wall to model the elastic response of specimens FL1W and FL2W, respectively. The top and bottom capping steel beams were also modelled to mimic the experimental setup and ensure a more realistic distribution of stresses along the boundaries of the masonry panel. After the application of the vertical load, the vertical translation of the capping beam at the loading points was either restrained or left unrestrained to examine the influence of the boundary conditions on the initial response of the specimens (**Fig. 6.11**). The values of elastic stiffness derived from the analytical model and the numerical analyses are summarised in **Table 6.6** along with the experimentally determined initial stiffness, K_{in} , which is taken as that corresponding to the first loading cycle and

computed as discussed in Section 6.3.2. The discrepancies between the experimental and theoretical values can be attributed to the difficulty in replicating the idealised boundary conditions during the experiments and the variability in the geometry of the specimens. The values derived from Eq. (6-3) seem to approximate well the expected initial elastic stiffness of the specimens and can be more easily implemented in design, hence these are adopted in all subsequent analyses.

K_{eff} was also determined according to both Eurocode 8 [171] and ASTM [174] (**Table 6.6**) for the sake of comparison. EC8 yields the most conservative estimates of K_e (ranging between 22-27% of K_{in}) due to the adoption of a load value higher than the expected cracking load, at which the tested specimens had already incurred a significant amount of damage (**Section 6.3.2**).

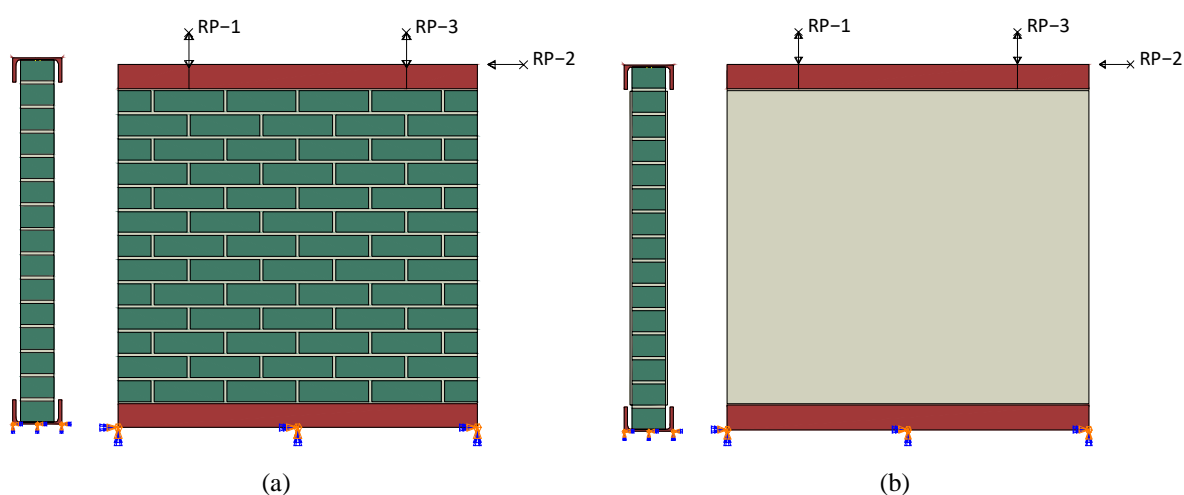


Fig. 6.11 Geometry and boundary conditions adopted in the FE model to estimate the elastic stiffness of (a) the bare wall and (b) the retrofitted walls

Table 6.6 Experimental and theoretical values of initial, elastic and effective stiffness for the tested specimens (kN/mm)

Specimen ID	K_{in}	K_{el}	$K_{\text{el_FEM}}$		K_e EC8	K_e ASTM
			Unrestrained	Restrained		
BW	38	49	41	58	14	23
LW	58	56	45	62	16	30
FL1W	68	56	45	62	15	34
FL2W	50	60	46	64	12	24

From the above discussion, it is clear that the determination of the effective stiffness is very sensitive to the various assumptions made and can introduce significant uncertainty in the assessment of the structural performance of URM and retrofitted walls at both serviceability limit state [176], and ultimate (V_u is a function of K_e).

The idealised bilinear response of the tested specimens, taken as the average of the response observed in the two loading directions, is shown in **Fig. 6.12**, adopting the theoretical elastic stiffness

(Eq. (6-3)) of the tested specimens and represent more accurately their actual behaviour. Key structural parameters, such as displacement ductility (μ) and behaviour factor (q), which reflect the ability of a structure to withstand deformations beyond its elastic limit (d_e), and dissipate energy, have also been estimated as shown in Eq. (6-4) and Eq. (6-5), respectively.

$$\mu = \frac{d_u}{d_e} \quad (6-4)$$

$$q = \sqrt{2\mu - 1} \quad (6-5)$$

The values characterising the end of each stage, i.e. load and displacement at the end of the elastic and perfectly plastic stage, as well as the μ and q factors of the structural systems, are summarised in **Table 6.7**. The ratio between the ultimate (bilinear) and maximum (experimental) lateral load (given in parentheses in **Table 6.7**) ranged between 0.72-0.76 for the FTRM-retrofitted specimens and was equal to 0.80 and 0.93 for LW and BW, respectively. These latter values are in line with the average value of 0.90 that has been proposed based on the analysis of a large database of unreinforced masonry walls failing in shear [177]. Despite the apparent high ductility of the bare wall ($\mu = 8.6$), this was achieved at a relatively low level of drift and energy dissipation (0.7%, 280J) in comparison to the retrofitted specimens. Specimens retrofitted with 2 layers of FTRM developed higher ductility with respect to the lime-only retrofitted specimen, while the single textile reinforcement layer in specimen FL1W-2 does not seem to have contributed to the overall deformability of the system, possibly because failure was dominated by the toe crushing mechanism.

The values of the behaviour factor of the retrofitted specimens ranged between 4.1 - 4.8, while the bare wall was characterised by a q factor equal to 4.0. It should be noted that the values of q suggested by EC8 are between 1.5-2.5 for URM buildings designed against seismic actions and 1.5 for URM buildings not complying with specific seismic provisions [172].

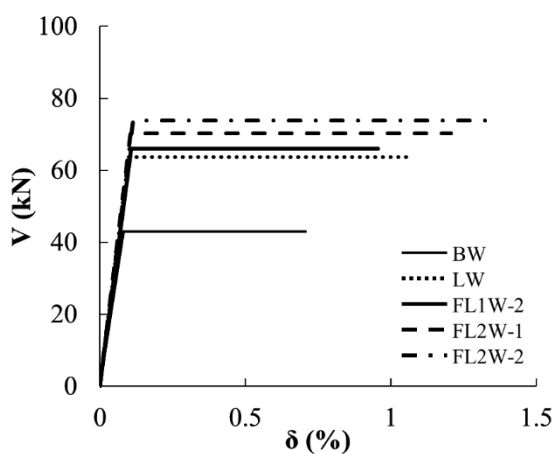


Fig. 6.12 Bilinear idealised response of bare and retrofitted wall specimens.

Table 6.7 Bilinear idealised response parameters, ductility and behaviour factors based on K_{el}

Specimen ID	V_u (kN)	δ_e (%)	δ_u (%)	μ	q
BW	43.0 (0.94 V_{max})	0.08	0.71	8.7	4.0
LW	63.7 (0.80 V_{max})	0.10	1.06	10.7	4.5
FL1W-2	66.0 (0.76 V_{max})	0.11	0.96	9.0	4.1
FL2W-1	70.3 (0.74 V_{max})	0.10	1.21	11.5	4.7
FL2W-2	73.8 (0.72 V_{max})	0.11	1.35	11.8	4.8

6.3.4. Energy Dissipation

The cumulative energy dissipation capacity of all specimens (E_D), calculated as the area enclosed within the hysteresis load-top displacement cycles (illustrated in **Fig. 6.13a**) is plotted against increasing drift (taken as the average drift of the push and pull directions) in **Fig. 6.14**.

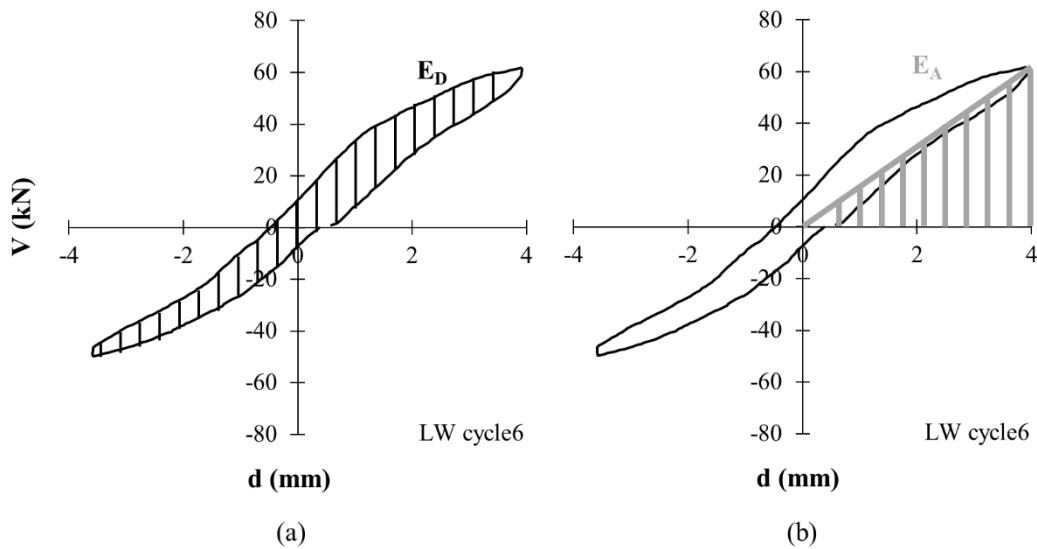


Fig. 6.13 Method of evaluation of (a) dissipated and (b) absorbed energy capacity.

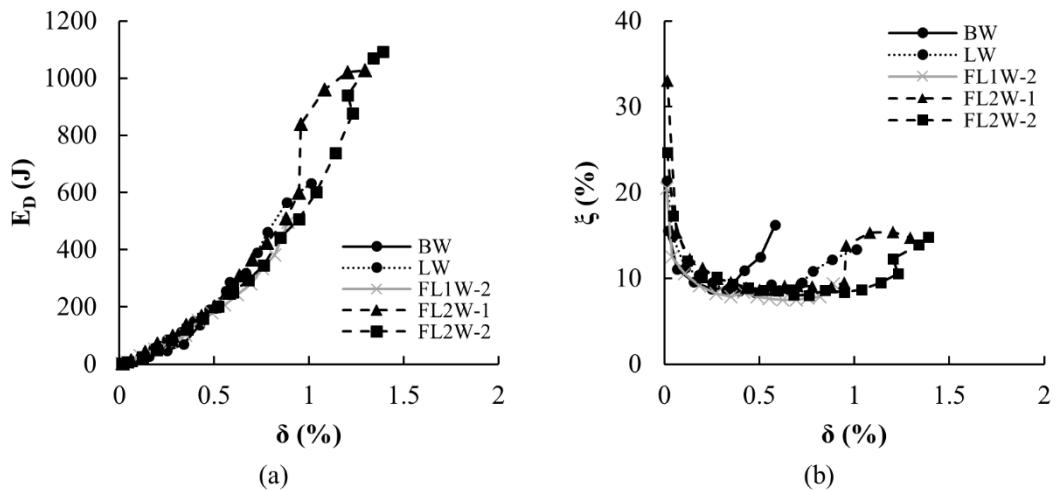


Fig. 6.14 (a) Energy dissipation and (b) equivalent damping ratio versus drift for bare and retrofitted specimens.

All specimens exhibit a similar energy dissipation capacity up to approximately 0.5% drift, with the lowest energy being dissipated by the bare wall. Thereafter, higher hysteresis energy was dissipated by the lime and the specimens retrofitted with two-layers of FTRM. On the contrary, the specimen with one FTRM layer failed to dissipate any more energy than its lime-only counterpart, indicating the limited contribution of the reinforcement, despite enabling a better damage distribution at similar drift levels. Owing to their comparatively high deformation capacity, the specimens with two FTRM layers were able to dissipate the highest amount of energy.

The dissipated hysteretic energy can be expressed through the equivalent damping coefficient (ξ) determined according to Eq. (6-6) [178]:

$$\xi = \frac{E_D}{4\pi E_A} \quad (6-6)$$

where E_A is the absorbed energy, calculated based on the equivalent linear system as illustrated in **Fig. 6.13b**.

Fig. 6.14b compares the evolution of the equivalent damping coefficient of the tested walls over the range of examined drift ratios. For all retrofitted specimens, the damping coefficient stabilises around a value of 9-10% at a drift of approximately 0.35%, which corresponds to the initiation of diagonal cracking in the bare wall. The increase in ξ is associated with the development of additional dissipative frictional mechanisms because of shear failure and the progressive opening of diagonal cracks. The minimum equivalent damping coefficient for all specimens, and regardless of the retrofitting configuration is approximately 9%, which is in line with observations by Magenes and Calvi [37] on brick masonry walls exhibiting diagonal shear failure modes.

6.3.5. Assessment of the FTRM Retrofitting Technique

The performance of the bare wall was significantly improved by the application of any of the examined retrofitting solutions (lime-only or FTRM), both in terms of strength and deformability. The retrofitted specimens exhibited a notable enhancement in ultimate drift capacity beyond the NC limit state, along with only a moderate increase in lateral stiffness. Compared to the bare wall, an 80% strength increase was achieved by applying only one layer of lime mortar on both sides, while the strength of specimens retrofitted with one and two FTRM layers increased by 95% and 113%, respectively. The lowest drift increase at NC was observed in the specimens retrofitted with one FTRM layer (35%) and lime-only (43%), while a significant 107% increase in ultimate drift capacity was developed by the two-layer FTRM retrofitted specimens.

From this study, it was observed that the lime mortar layer significantly contributes to enhancing both strength and deformability. This can be mainly attributed to the excellent compatibility of the lime mortar with the substrate and its ability to enable a certain degree of strain redistribution upon cracking of the masonry units due to the presence of short dispersed fibres, which in turn improves the post-cracking behaviour and enhances the overall ductility of the strengthened masonry [109].

Although an apparent higher ductility was developed by the bare and the lime-only walls, the higher ultimate drift was accompanied by severe discrete cracking, which would have significantly compromised the specimen's integrity. The flax textile effectively promoted strain redistribution upon mortar cracking (smaller crack widths were measured in FTRM-retrofitted specimens - see **Table 6.5**) and successfully increased the energy dissipation capacity of the structural system. Only minor localised debonding of the top mortar layer of the FTRM was observed in some of the tests, and it only occurred after the governing failure mode (diagonal shear or toe crushing) was fully developed. Although the development of damage under increasing drift values is inevitable, the inclusion of textile layers prevented the detachment of large portions of mortar and controlled crushing of the lime/masonry system.

6.4. PREDICTIVE MODELS

All available national and international design documents evaluate the shear resistance of TRM-retrofitted elements based on the truss analogy and on the assumption that the total shear resistance is the sum of the contribution of masonry and of the strengthening system [179], similarly to what is assumed for the design of reinforced concrete members and FRP-strengthened elements. It is also considered that the TRM system is activated only after masonry cracking [180]. In this study, the shear capacity of the bare masonry wall is estimated according to the provisions given in EC6 [167], EC8 [171,172], ACI 549 [47] and the Italian Building Code (NTC18 [181]), while the capacity of the retrofitted specimens is determined based on ACI 549.4R [47] and its newest version ACI549.6R [56], CNR 215 [182], as well as two alternative methodologies proposed by Triantafillou [183], and Thomoglou et al. [184].

The experimental results obtained from this study are used to assess the suitability of these design models to predict the contribution of NTRM systems to the overall shear resistance of masonry walls. The main parameters governing the design of the retrofitting solution are identified, and the performance of the examined models is critically assessed in terms of both ultimate predicted load capacity and failure mode. All materials and load factors are taken equal to unity, while the material properties are taken as obtained from the material characterisation presented in Section 6.2.1. The actual geometry of each wall is considered for the evaluation of the ultimate capacity. Detailed step-by-step calculations for the case of the bare wall and the specimen with a single layer of FTRM, as well as the used nomenclature can be found in Appendix C.

6.4.1. Shear Contribution of Masonry, V_m

Table 6.8 presents the analytical formulations adopted in each of the examined standards, while the predicted values are summarised in **Table 6.9**. EC8 and NTC identify three failure modes, namely rocking failure with crushing of the compressed toe, shear sliding and diagonal shear cracking, while ACI 549 (which relies on the approach given in FEMA 356 [173,185]) differentiates rocking from

toe crushing. In all three models, the shear capacity of the unreinforced masonry is determined as the minimum resistance associated with the different possible failure modes. Conversely, EC6 considers the shear strength of the masonry as the dominant design parameter, thus implicitly considering shear sliding as the governing failure mechanism [175].

Similar predictions are obtained from the examined models, but the European codes approximate better the experimentally determined capacity of the bare wall, with relative errors of around 6-8% for EC6, EC8 and NTC, and approximately 25% for ACI. The minimum capacity according to all codes is associated with a shear sliding mechanism, while a diagonal tension failure was observed on the tested specimen. It should be noted, however, that the predicted shear capacity for shear sliding and diagonal cracking are only marginally different.

Table 6.8 Analytical predictions - Shear resistance of URM (V_m)

Type of failure	EC6	EC8* [171,172]	ACI 549 [47,173,185]	NTC 18* [181]
Shear Resistance		$V_m = \min(V_f, V_s, V_d)$	$V_m = \min(V_f, V_s, V_d, V_{tc})$	$V_m = \min(V_f, V_s, V_d)$
Rocking		$V_f = \frac{LN_d}{2h_o} (1-1.15v)$	$V_f = 0.9aN_d \left(\frac{L}{H}\right)$	$V_f = \frac{L^2 t \sigma_d}{2} \left(1 - \frac{\sigma_d}{0.85f_{wc}}\right) \frac{2}{H}$
Shear sliding	$V_m = f_{vd} t L$	$V_s = d' t \left(f_{v0} + \frac{\mu N_d}{d' t}\right)$	$V_s = v_{mc} A_n$	$V_s = f_{vd} t L$
Diagonal cracking		$V_d = \frac{d t}{b} \left(\frac{f_{vko}}{1+\mu_j \phi} + \frac{\mu_j}{1+\mu_j \phi} \sigma_d\right)$	$V_d = f_{dt} A_n \beta \sqrt{\left(1 + \frac{\sigma_d}{f_{dt}}\right)}$	$V_d = L t \frac{1.5f_{vko}}{b} \sqrt{1 + \frac{\sigma_d}{1.5f_{vko}}}$
Toe crushing	-	-	$V_{tc} = aN_d \left(\frac{L}{H}\right) \left(1 - \frac{\sigma_d}{0.7f_{wc}}\right)$	-

*an equivalent rectangular stress block of depth equal to 0.87 and 0.85 is assumed in the analysis, for EC8 and NTC18, respectively.

Table 6.9 Theoretical in-plane resistance of specimen BW associated with possible failure modes (in kN).

Type of failure	EC6	EC8	ACI 549	NTC 18	$V_{m,exp}$
Rocking		65.6	66.8	65.4	
Shear sliding	43.0	42.7	35.0	43.0	
Diagonal cracking		44.3	38.4	45.6	46.4
Toe crushing	-	-	63.5	-	
V_m	43.0	42.7	35.0	43.0	

6.4.2. Shear Contribution of FTRM, V_{TRM}

The four models examined in this study were chosen as they exemplify the different approaches that can be taken to estimate the shear contribution of external TRM. The models are summarised in **Table 6.10**, while their underlying philosophy is presented and discussed in the following subsections. All models rely on the main following assumptions:

- uniform spatial distribution of the textile reinforcement along the length of the wall (for full coverage strengthening configurations);
- the tension is carried only by the TRM system; the tensile strength of the masonry is ignored;

- the contribution of the inorganic mortar is neglected;
- the dowel action and the shear stiffness of the fibres is negligible;
- perfect bond at the fibre/matrix and at TRM/masonry interfaces;
- arching effects and any interaction between normal and shear stresses in the ultimate shear resistance of the element are neglected;
- the shear resistance provided by the TRM is computed as the sum of the forces resisted by the textile reinforcement parallel to the direction of the horizontal loading, intersecting a diagonal shear crack of 45° inclination.

With respect to the shear contribution of masonry, the models proposed by Triantafillou [183] and Thomoglou et al. [184] adopt the value predicted by EC6 and EC8, respectively.

Table 6.10 Comparison between different design approaches to estimate the shear contribution of TRM.

ACI 549.4R [47]	$V_{Rd} = \min(V_m + V_{TRM}, 1.5V_m)$ $V_{TRM} = 2nA_f H f_{fv}$
ACI 549.6R [56]	$V_{Rd} = V_m + V_{TRM}$ $V_{TRM} = nA_f E_f \varepsilon_{fd}$
Triantafillou [183]	$V_{Rd} = \min(V_m + V_{TRM}, V_{Rd,max})$ $V_{TRM} = 0.9H n t_f f_{td}$
CNR 215 [182]	$V_{Rd} = V_m + V_{TRM}$ $V_{TRM} = n t_f H \alpha_t \varepsilon_{fd} E_f$
Thomoglou et al. [184]	$V_{Rd} = V_m + (V_f + V_{mortar}) \cdot k$ $V_f = 2nA_f H E_f \varepsilon_{ffd}$ $V_{mortar} = A_{mortar} E_{mortar} \varepsilon_{tm}$

6.4.2.1. ACI 549.4R [47]

The ACI design approach adopts a similar philosophy to that adopted for the design of FRP strengthened elements and is based on the implementation of a limiting effective strain of 0.4% (Eq. (6-7)). This limiting strain is then used to determine the effective stress that is mobilised in the TRM, according to Eq. (6-8):

$$\varepsilon_{fv} = \min(\varepsilon_{fu}, 0.004) \quad (6-7)$$

$$f_{fv} = \varepsilon_{fv} E_f \quad (6-8)$$

where, ε_{fu} and E_f are the tensile strength and cracked stiffness of the employed TRM system (derived from tensile tests on TRM coupons).

The shear contribution of TRM is then given by Eq. (6-9):

$$V_{TRM} = 2nA_f H f_{fv} \quad (6-9)$$

where, strengthening of both sides is assumed (factor 2), n is the number of TRM layers, A_f the area of the textile reinforcement per unit width, and H the height of the wall.

The total shear contribution V_{Rd} (sum of the shear components of masonry and TRM) shall not exceed 50% of the capacity of the bare masonry to limit the total force per unit width transferred to the substrate of the masonry [160]. For design values, a strength reduction ϕ_v equal to 0.75 (for shear) is applied to V_{Rd} .

6.4.2.2. ACI 549.6R [56]

A unified document for the repair and strengthening of masonry structures using externally bonded FRM/SRG was developed as the result of a joint effort between ACI committee 549 and RILEM TC 250-CSM and provides side-by-side comparison of the design equations adopted in both American and European regulations.

The shear contribution of TRM according to both ACI and RILEM is given by Eq. (6-10):

$$V_{TRM} = n A_f E_f \varepsilon_{fd} \quad (6-10)$$

where n is number of wall sides strengthened with FRM/SRG and A_f the area of the fabric reinforcement effective in shear.

The approach followed by ACI is similar to the one provided in ACI549.4R and imposes the same limit for the effective strain (0.004), however, a higher strain limit can be used for design if experimental evidence is provided. In Eq. (6-10), E_f and ε_{fd} are the cracked stiffness and axial strain of the employed TRM system, respectively. For the retrofitted specimens tested in this study and from results obtained from the mechanical characterisation of the employed Flax-TRM system [141], the effective strain was taken equal to 7.3% and 7.9% for single and double-layer FTRM, respectively, and no limit was applied.

In contrast, there is no strain limit imposed by RILEM and the design strain (ε_{fd}) is taken as in Eq. (6-11), where ε_{fb} and ε_{tk} are the maximum tensile strain in the fabric attained through bond tests and direct tensile tests on bare textiles, respectively, taken as the corresponding strength values divided by the stiffness of the bare textile. The coefficients a_1 and a_2 have been experimentally calibrated and are equal to 1.5 and 1.0, respectively. E_f in Eq. (6-10) accounts for the stiffness of the bare textile.

$$\varepsilon_{fd} = \min\left(a_1 \varepsilon_{fb}, \frac{\varepsilon_{tk}}{a_2}\right) \quad (6-11)$$

In this study, ε_{fb} values were derived from the debonding strength attained during the tests and implementing the constitutive law of the textile as given in Eqs. (5-1) and (5-2).

6.4.2.3. Triantafillou [183]

The model proposed by Triantafillou [183] adopts the principles of current European shear design models, with the contribution of TRM given by the following equation (Eq. (6-12)):

$$V_{TRM} = 0.9 H n t_f f_{td} \quad (6-12)$$

where, H is the height of the wall, n is the number of sides strengthened with the TRM system of design thickness t_f . When multiple layers of TRM are used, the design thickness is the product of the number of layers and the design thickness of a single layer.

The stress that the TRM is allowed to develop (f_{td}) accounts for both its tensile properties and its bond performance and is taken as the minimum of the tensile strength (f_t) (from tests performed on TRM coupons) and bond stress at the onset of debonding (f_{tbd}) (from shear bond tests performed on TRM/masonry substrate), as described in Eq. (6-13):

$$f_{td} = \min\left(\frac{f_{tk}}{\gamma_t}, f_{tbd}\right) \quad (6-13)$$

The total shear resistance (sum of the shear contributions of masonry and TRM) is limited by the compression strength of the struts computed according to the truss analogy [183].

6.4.2.4. CNR DT 215 [63]

The model proposed in the Italian standards was informed by the design procedures developed by RILEM TC 250 [54] and relies on the use of an effective strain, which is taken as the strain that is developed in the textile when the debonding strength is attained. The value of the effective strain can be increased through the use of an amplification factor α equal to 1.5 to account for the higher strain that can be developed in the textile when local debonding is expected to occur at intermediate regions of an element. If the resulting effective stress falls within the crack development stage, however, $\alpha=1$. In any case, the value of the effective stress cannot be higher than the tensile strength of the TRM [54]. The shear contribution of the TRM is evaluated through Eq. (6-14), in which a reduction factor α_i is also considered ($=0.8$ in the absence of experimental results) to account for the reduction of the textile strength when subjected to shear:

$$V_{TRM} = nt_f H \alpha_i \varepsilon_{fd} E_f \quad (6-14)$$

where, n is the total number of reinforcement layers on the sides of the wall and t_f is the equivalent thickness of a layer of the fibres arranged in the direction parallel to the shear force.

The constitutive law of the textile was used to derive the effective strain that corresponds to the debonding strength. For the FTRM systems in this study, the effective strain was equal to 3.24% and 2.96% for single and double-layer FTRM, respectively, falling within stage II of the tensile response [164]. Hence, no amplification factor is needed and the product $\varepsilon_{fd} E_f$ can be taken equal to the debonding strength. The factor α_i was taken equal to 0.8 as suggested in the guidelines.

6.4.2.5. Thomoglou et al. [184]

In contrast with the three models presented above, which do not explicitly consider the shear strength provided by the mortar overlays, Thomoglou et al. [184] account separately for the shear contribution of the mortar (V_{mortar} - Eq. (6-15)) and the textile (V_f). These are then added together to yield the contribution of the TRM and subsequently multiplied by a factor k (Eq. (6-16)), which has

been calibrated based on an experimental database and depends on the type of TRM system and masonry substrate. The effective strain that the textile is assumed to develop at shear failure is taken equal to the debonding strain of the textile (derived from shear bond tests).

$$V_{\text{mortar}} = A_{\text{mortar}} E_{\text{mortar}} \varepsilon_{\text{tm}} \tag{6-15}$$

$$V_{\text{Rd}} = V_m + (V_f + V_{\text{mortar}}) \cdot k \tag{6-16}$$

where ε_{tm} is the tensile strain of the mortar at the transition between uncracked and crack development stage in the TRM tensile response and depends on the adopted type of TRM system.

Eq. (6-15) and (6-16) were implemented in this study by taking the experimental values of ε_{mt} (0.057% and 0.07% for 1 and 2 layers of FTRM, respectively), while the calibration factor k was taken equal to 0.55 (as suggested for Glass-TRM/clay brick masonry systems, which represents more closely the stiffness of the tested NTRM system).

6.4.3. Assessment of Predictive Models for V_{TRM}

The comparison between the analytical and experimental results is shown in **Fig. 6.15**, in terms of V_{TRM} , with the experimental contribution of the FTRM computed as the difference between the capacity of FTRM retrofitted specimens and that of the bare wall. **Table 6.11** presents the analytical values of masonry contribution (V_m), shear contribution of the FTRM system (V_{TRM}) and total shear in-plane resistance of the strengthened element (V_{Rd}), for each specimen examined in this study.

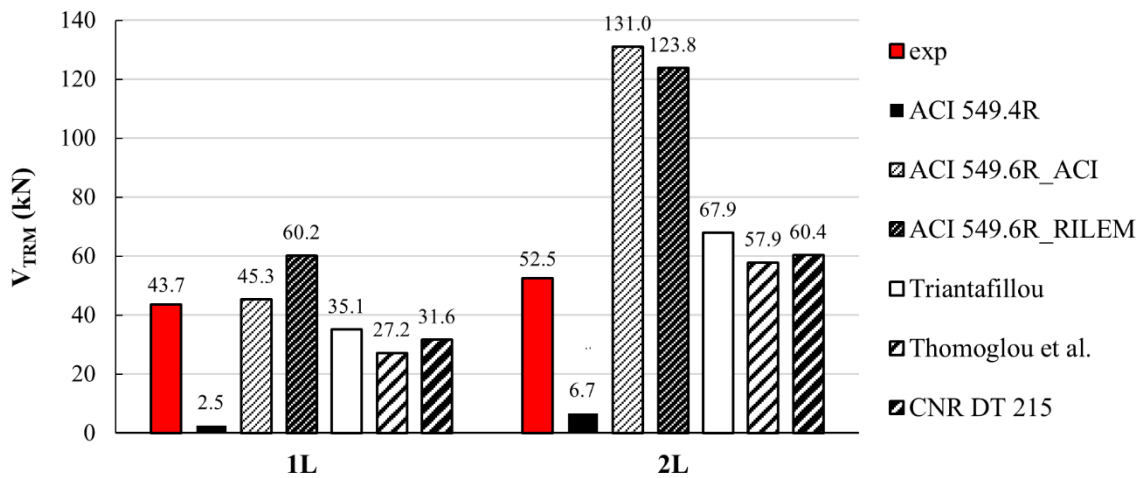


Fig. 6.15 Comparison of experimental and analytical predictions of the shear contribution provided by 1 (1L) and 2 (2L) layers of FTRM.

Table 6.11 Predicted in-plane shear capacity of retrofitted specimens (in kN).

Specimen ID	ACI549.4R			ACI549.6R_ACI549.6R_RILEM [56]			ACI549.6R_RILEM			Triantafillou[183]			Thomoglou et al. CNR 215					
	V _m	V _{TRM}	V _{Rd}	V _m	V _{TRM}	V _{Rd}	V _m	V _{TRM}	V _{Rd}	V _m	V _{TRM}	V _{Rd}	V _m	kV _{TRM}	V _{Rd}	V _m	V _{TRM}	V _{Rd}
LW	35.0	-	-	35.0	-	-	43.0	-	-	43.0	-	-	41.8	-	-	43.0	-	-
FL1W-2	35.0	2.5	37.5	35.0	45.3	80.3	42.5	60.2	102.5	42.3	35.1	77.4	40.9	27.2	69.1	42.5	31.2	73.7
FL2W-1	35.0	6.9	41.9	35.0	136.1	171.1	143.0	128.6	171.7	43.0	69.3	112.3	42.7	59.5	102.1	43.0	61.6	104.6
FL2W-2	35.0	6.4	41.4	35.0	125.9	160.9	94.2	119.0	161.5	42.5	66.5	109.0	42.7	56.2	98.9	42.5	59.1	101.6

Although all of the models examined in this study are based on the same fundamental assumptions, the different limitations imposed on the strain and associated stress that is allowed to develop in the textile at shear failure can lead to substantially different predictions. The limiting effective strain of 0.4% recommended by ACI549.4R is extremely conservative and constitutes only a fraction of the strain that the FTRM system used in this study can develop before tensile rupture (7.3% and 7.9% for single and double layer systems, respectively [141]) or before debonding (approximately 4% [164]). In addition, a strain equivalent to 0.4% would lie within the crack development stage of the FTRM and the associated stress determined using the cracked stiffness would largely underestimate the stress in the composite. Moreover, although conservative in nature, the use of a constant strain would imply the same contribution for each of the composite layers, regardless of the reinforcement ratio, which is in contrast with findings from previous studies by the authors [164]. The removal of the 0.4% strain limit in the newest ACI approach (ACI549.6R), however, results in a predicted shear capacity that is in very close agreement (+4%) with the experimental value for the specimens retrofitted with a single-layer on both sides. When the RILEM procedure included in the same guideline document [56] is implemented, the performance of single-layer FTRM-retrofitted specimens is overestimated by approximately 40%. Both RILEM and ACI guidelines overestimate the performance of double-layer FTRM-retrofitted specimens by 2.3-2.5 times. The difference between the two approaches lies within the mechanical behaviour assumed in the TRM system, which is highly dependent on the boundary conditions imposed during mechanical testing and those expected in the field. The design properties used in the ACI approach are based on the tensile characterisation of TRM coupons subjected to direct tension, while the RILEM approach implements design strain values that are obtained indirectly from shear bond tests through the stiffness of the dry textile and limited by the tensile strain of dry textiles (Section 6.4.2.2). With respect to the latter approach, a larger strain can be considered to be developed in the textile at debonding to account for differences between tests in laboratory environment and field conditions, through the use of the factor a_1 (see Eq. (6-11)). Although the RILEM approach acknowledges the lack of sufficient experimental data to accurately calibrate the a_1 factor, it should be noted that this data is derived from diagonal compression tests on high-strength TRM/masonry systems, where the inherent boundary conditions and the level of stress/state in the retrofitting material significantly differ from those induced in in-plane shear compression tests. Hence, the proposed value of 1.5 needs to be re-evaluated. The model proposed by Triantafillou provides reasonable estimates of the

experimental values, but underestimates the contribution of the FTRM in the case of single layer specimens (-20%) and overestimates that of the 2-layer FTRM system (+30%). The main advantage of the model by Triantafillou lies in its simplicity.

The model by Thomoglou et al. provides a conservative estimate of the capacity of the wall with 1 layer of FTRM (-25%) and can predict more accurately the average capacity of the specimens retrofitted with 2 layers of FTRM (+10%). The good correlation achieved with Thomoglou et al. model highlights the significant role of the mortar overlays in contributing to the overall shear resistance. Further work should be carried out to develop a more in-depth understanding of the relative contribution of the mortar overlay and the embedded textile and to assess the need of a calibration factor k and its physical role.

The difference in the values predicted according to CNR DT 215 and Triantafillou is only due to the implementation of the factor α_t to account for the reduced strength exploitation of the textile subjected to combined tension and shear ($=0.8$). In fact, both models rely on an effective stress being developed in the textile equal to the minimum of the tensile and bond strength. However, the use of the reduction factor α_t should not be required if a design by testing approach is implemented, as debonding strength values from experimental tests already account for the reduced performance of fibres loaded in shear. On the other hand, a reduction factor is indeed needed to account for the different failure modes that can be observed in TRM-retrofitted elements. The observed differences in the predicted values obtained by implementing the CNR DT 215 and the RILEM approach given in ACI 549.6R are due to the use of the calibrated parameter a_1 , as well as the reducing factor a_t . CNR DT 215 recommends that a_1 is not to be used when the debonding strains lie within the crack development stage, which was the case for the specimens examined in this study, thus providing a better estimate. However, in the RILEM approach, the use of a_1 results in a debonding strain higher than that of the dry textile in tension, with the latter eventually governing the contribution of the FTRM system to the total shear capacity. In this study, no textile rupture was observed, and local debonding phenomena occurred only at high levels of drift, indicating that much lower average strains than the textile failure strain were developed in the reinforcement. Interestingly, although an increase of only 9% in capacity was observed between the walls retrofitted with 1 and 2 FTRM layers, all available models predict an increase in the V_{TRM} of 93-115% between single and double-layer FTRM systems, indicating that an increase in the reinforcement ratio does not result in a proportional increase in the overall shear capacity. This is in line with what was observed in [108], when testing similar FTRM systems under diagonal compression and may be attributed to the inherent variability of the natural fibres across the length and width of the textile and the different degree of mortar impregnation that can be developed, which can result in an uneven strain distribution.

The shear contribution of the mortar layer can be estimated using Eq. (6-15), substituting the product $E_{mortar} \epsilon_{mt}$ with the shear strength of the mortar, which can be taken equal to its tensile strength

multiplied by 1.5 [186]. This results in a shear capacity $V_{\text{lime}} = 23.8$ kN, thus providing a conservative estimate of the experimental value ($V_{\text{LW}} - V_{\text{BW}} = 37.3$ kN).

6.4.4. Proposed Model

Overall, the models proposed by ACI549.6R, Triantafyllou, Thomoglou et al. and CNR estimate the contribution of the TRM/textile based on the effective stress that can be developed in the textile at debonding (or at tensile failure), which is either determined directly or indirectly via an equivalent limiting strain value corresponding to a debonding type of failure (or fracture). However, the mechanical performance of the FTRM systems tested in this study was not governed by debonding or rupture and the experimental evidence confirms that the maximum average strain values that developed in the textile across the cracks were relatively low (about 3.5% as reported in **Table 6.5**).

The average strain values estimated from DIC analyses on the three FTRM retrofitted specimens (FL1W-, FL2W-1 and FL2W-2) were used to attempt a decomposition of the resisting mechanisms and estimate the relative contribution of the masonry, lime-based mortar layer and textile (**Fig. 6.16**). In this analysis, the contribution of the textile was estimated based on the derived experimental strains and the constitutive model proposed in [164]. The external mortar layer was assumed to start contributing to the total shear resistance from a load equivalent to that initiating cracking in the masonry wall (taken as the cracking load of specimen BW) and reach its maximum contribution (V_{mortar}) when the embedded textile starts to be mobilised (i.e. when cracking initiates in the retrofitted specimen). The mortar contribution is then gradually reduced to account for the development of cracks and the consequent limited ability of the cracked mortar layer to effectively transfer stresses. A simple linear degradation has been assumed in this analysis (shown with a dashed line in **Fig. 6.16**).

Although the average strain level is such that only a limited strength contribution is offered by the textile layers (given the relative low stiffness), the natural fibre textiles can effectively redistribute strain within the mortar layer and the underlying masonry, thus progressively activating undamaged areas of the wall. Hence, this analysis suggests that a shear resistance greater than that mobilised by the bare specimen can be developed in the masonry when externally bonded TRM is used as retrofitting solution. The additive nature of the individual shear contributions should be revisited and the development of the resisting mechanisms should be estimated based on the strain level induced in the materials and the degree of strain redistribution that can be achieved.

The adoption of a limiting effective strain to estimate the design shear contribution of TRM systems, however, seems reasonable provided that an adequate strain level is considered so that the integrity of the shear resisting mechanisms is maintained and excessive cracking is prevented. It is clear that the strain level suggested in ACI 459.4R is too conservative, while the strain levels used in the model by CNR and Thomoglou et al., though reasonable, tend to overestimate the stress in the reinforcement as this is computed using the stiffness of the dry textile or the cracked stiffness of the

composite. Based on the analysis of the experimental response of the walls observed in this study, and the behaviour of the NTRM obtained from material characterisation, an effective limiting strain equivalent to that corresponding to the end of the crack development stage would provide an appropriate upper limit for design. At this level of strain, cracking in the TRM is still effectively controlled by the embedded textile and a good strain redistribution within the underlying masonry can still be assumed. The resulting contribution of the FTRM can be derived from its tensile response, which can be easily written as the sum of the contribution provided by the mortar and that of the fibres, as proposed in Eq. (6-17).

$$V_{Rd} = V_{\text{mortar}} + n t_f H \varepsilon_{II} E_{II} \quad (6-17)$$

where, $n t_f$ is the total thickness of TRM as defined in Eq.(6-12), and ε_{II} and E_{II} are the strain at the end of the crack development stage and elastic modulus that characterises the same stage, respectively. The properties corresponding to the crack development stage of the NTRM systems used in this study can be found in [141]. The shear capacity of the mortar can be evaluated as described in Section 6.4.3.

The use of Eq. (6-17) yields a total shear capacity for the single-layer FTRM systems equal to 31.4 kN (against 43.7 kN), while for two-layer FTRM systems this is 43.9 kN (against 52.5 kN). The conservative estimate provided by the proposed model can be attributed to use of conservative strain values derived from average surface strain measurements, as well as the underestimation of the contribution of the underlying masonry wall, as discussed above.

The proposed model is simple and yields acceptable predictions for the systems tested in this study. Further work is needed to validate the model against experimental results on elements using both natural and advanced TRM systems of different configuration and fibre provenance, and to examine in more depth the evolution and deterioration of shear resisting mechanisms in masonry walls subjected to in-plane shear.

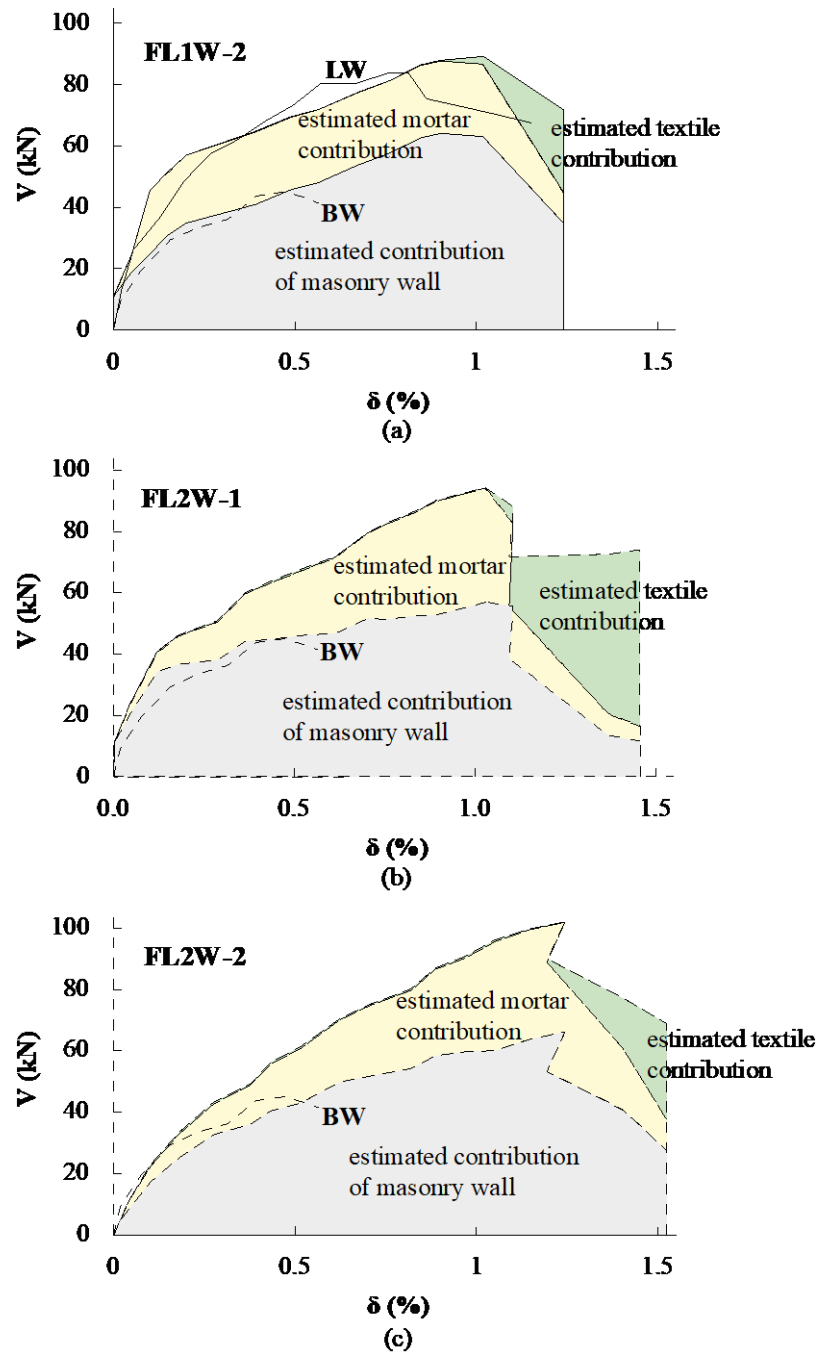


Fig. 6.16 Estimated contribution of masonry, mortar layers and textile to total shear resistance for (a) FL1W-2; (b) FL2W-1; and (c) FL2W2 specimens

6.5. CONCLUSIONS

This paper presents and discusses the results of a series of in-plane cyclic shear-compression tests on URM walls retrofitted with Flax-TRM composites. The performance of the adopted strengthening solutions is examined in terms of strength, ductility, and energy dissipation enhancement. The shear contribution of the NTRM system is examined in detail and the experimental evidence is used to

assess the underlying philosophy of current shear design provisions and propose a new design model. Based on the results and the discussion above, the following conclusions can be drawn:

- Although all shear walls failed predominantly due to diagonal shear, the bare and lime-only retrofitted walls experienced significant damage at relatively low drift levels. The presence of the flax reinforcement ensured the integrity of the wall and controlled the development of brittle failure modes.
- FTRM retrofitting can significantly improve the in-plane seismic performance of unreinforced masonry walls, in terms of strength gain (up to 113%), ultimate drift (107%) and energy dissipation capacity. In parallel, it does not add significant stiffness to the structure (even when placed in two-layer configurations).
- All retrofitted specimens showed comparable stiffness degradation and were characterised by an average equivalent damping coefficient of 9%, before additional dissipative mechanisms took place.
- Although the inclusion of one FTRM layer did not result in further strength or drift enhancement, it ensured good strain redistribution and contributed to maintaining the structural integrity.
- The use of two FTRM layers enabled the development of additional strength and deformability and promoted a more effective distribution of strains across the wall surface as well as higher energy dissipation capacity.
- The increase in the provided reinforcement ratio did not result in a directly proportional increase in in-plane shear strength (9%) but offered some enhancement in terms of deformability (20%).
- The analysis of the shear contribution of the NTRM systems highlights the complexity of the development of shear resisting mechanisms in retrofitted masonry walls and suggests that the additive nature of the individual contributions, though adequate for design, should be revisited.
- Current design models overestimate the stress that can be developed in the flax textile reinforcement. A more rational limiting strain value is proposed along with a simplified design model that accounts for the contribution of the mortar and textile reinforcement.

The results of this study highlight the promising potential of FTRM systems to be used as seismic retrofitting solution for unreinforced masonry structures. More research work should be carried out to examine the complex nature of shear resisting mechanisms in URM retrofitted walls and validate the proposed design model.

7. CONCLUSIONS

7.1. SYNOPSIS

The aim of this research was to develop an efficient, cost-effective and sustainable seismic retrofitting solution for URM structures using natural fibre textiles embedded in lime-based mortars, and provide design recommendations.

An extensive experimental programme was designed to investigate the performance of NTRM systems at composite and structural level and develop a comprehensive understanding of the shear stress transfer mechanism between fibres, mortar and parent material. A detailed multi-scale characterisation of the NTRM constituents and composites examined in this study was followed by an in-depth analysis of their bond performance to masonry substrates. The small-scale testing was complemented by structural tests on medium scale walls to assess the effectiveness of NTRM systems for in-plane seismic retrofitting of URM walls. The shear contribution of the NTRM system was examined in detail, both experimentally and analytically, and the experimental evidence was used to evaluate the underlying philosophy of current shear design provisions. Global deformation and energy dissipation analyses were coupled with extensive 2D - DIC analyses to gain valuable insights on the crack behaviour and strain distribution across the NTRM.

The results of this study highlighted the potential of Flax-TRM as a seismic strengthening solution for unreinforced masonry structures. Good mechanical properties, high deformability, ductility and energy dissipation capacity, together with high exploitation of the textile tensile strength, can be achieved when suitable textile architectures and sufficient reinforcement ratios are provided.

This Chapter summarises the main conclusions drawn from the present study and provides recommendations for testing and design of NTRM systems, as well as directions for future research. All research objectives set in Chapter 1 were achieved.

7.2. CONCLUSIONS

7.2.1. On the Mechanical Performance of NTRM

Flax and jute fibres, yarns, textiles and the resulting TRM composites were tested in direct tension to assess the effect of textile architecture, number of NTRM layers and mortar overlay thickness. The main conclusions of this study are the following:

- At fibre level, both flax and jute exhibit mechanical properties suitable for structural applications, with strengths ranging from 680 to 865 MPa and equal to 560 MPa, respectively. Stiffness values range from 25 to approximately 40 GPa.
- Flax-TRM are characterised by a ductile behaviour, high strength (80 to 200 MPa) and elongation capacity (4 to 8%), thus making them a promising retrofitting solution for masonry.

- The textile architecture has a marked effect on the NTRM composite performance and crack development. Low linear density, twisted yarns arranged in denser meshes can: ensure better composite action with the lime mortar; enable multiple crack formation and a more uniform stress distribution in the composite; and ensure a high exploitation of the textile tensile strength (77%).
- An increase in the number of NTRM layers leads to a proportional increase in load capacity and to a more ductile behaviour, without significantly affecting the maximum stress sustained by the textiles, the ultimate strain developed by the composites or the failure mode.
- Tensile rupture of the reinforcement after the development of multiple distributed cracking and high ductility was observed in NTRM with mechanical reinforcement ratios greater than 3%.
- The weak fibre-matrix interaction in Jute-TRM did not result in a structurally acceptable composite behaviour, even at high reinforcement ratios.
- An increase in the thickness of mortar overlays does not affect the composite mechanical performance but can be detrimental when lower than critical mechanical reinforcement ratios are provided.

7.2.2. On the Bond Performance of NTRM/Masonry

The performance of Flax-TRM bonded to clay brick masonry prisms was investigated through single-lap shear tests. The effect of textile architecture, number of FTRM layers, bond length and bond width were assessed. The main conclusions of this study are the following:

- The effective bond length for the single-layer FTRM/masonry systems is between 150 and 210 mm and failure is dominated by fibre rupture.
- Textile architecture critically affects the overall bond performance. The large mesh size of the F1 textile ensured good bond between the mortar layers, but the inadequate penetration of the mortar within the large diameter yarn compromised the development of the full textile capacity (only up to 35%). On the other hand, the twisted and smaller diameter yarns of the F2 textile ensured a good mechanical interlock with the mortar, enabling a high utilisation (up to 75%) of the textile strength.
- The effect of the number of FTRM layers is coupled with the effect of the textile architecture. The use of multiple F1-TRM layers did not cause a change in failure mode and resulted in a significant increase in load carrying capacity (up to 600%). On the contrary, the dense mesh of F2-TRM systems resulted in poor mortar penetration within the textile layers and delamination in multi-layer systems. A moderate increase in load carrying capacity was achieved (up to 60% in 2-layer F2-TRM).
- The use of different bond widths can affect the results obtained from single lap shear tests, especially for multi-layer TRM systems, as wider strips can promote the development of a non-uniform load distribution within the composite and trigger delamination failure modes.

Systems comprising three F2-TRM layers bonded over a larger width developed a significantly lower axial strength (by up to 60%).

- The analysis of local load-slip behaviour at the yarn scale revealed the variability in mortar impregnation of the yarns along the embedded length. This affects the percentage of yarn cross-sectional area that can be effectively mobilised and significantly affects the global load-slip behaviour of NTRM systems.

7.2.3. On the In-plane Seismic Performance of URM Walls Retrofitted with NTRM

The effectiveness of FTRM as a seismic retrofitting solution for masonry structures was investigated through in-plane cyclic shear-compression tests on medium scale single-wythe walls. The underlying philosophy of current shear design provisions was assessed. A new design model is proposed based on the analysis of the shear contribution of the FTRM and masonry system. The main conclusions of this study are the following:

- The presence of the flax reinforcement ensured the integrity of the wall and controlled the development of the brittle failure modes otherwise experienced by the bare and lime-only retrofitted walls.
- FTRM retrofitting provided a substantial increase in strength (up to 113%), ultimate drift (82%) and energy dissipation capacity, without significantly affecting the stiffness of the reference bare wall (even when using a two-layer FTRM system).
- Although no further strength or drift enhancement was offered by the single-layer FTRM system compared to its lime counterpart, the inclusion of flax reinforcement ensured good strain redistribution and maintained the structural integrity.
- The use of two FTRM layers enabled the development of additional strength and deformability and promoted a more effective strain distribution across the wall surface as well as higher energy dissipation capacity.
- An increase in the number of FTRM layers does not result in a proportional increase in in-plane shear strength (9%) but can offer a more significant enhancement in terms of deformability (20%).
- The analysis of the shear contribution of the FTRM and masonry components highlights the complexity of shear resisting mechanisms and indicates that the additive nature of the individual contributions, though adequate for design, should be revisited.
- A simplified design model that accounts for the contribution of the mortar and textile reinforcement is proposed based on the use of a limiting strain, which reflects the ability of the FTRM system to control crack development (equivalent to the strain developed at the end of the crack development stage in uniaxial tensile tests).

7.3. RECOMMENDATIONS FOR TESTING AND DESIGN OF NTRM SYSTEMS

Based on the outcome of Phases 1 - 2, yarn and textile architecture are the most important parameters affecting the yarn, textile and composite tensile and bond strength. Recommendations for testing and design of NTRM systems were provided, the most important of which are reported below:

- The use of high linear density yarns may cause poor mortar penetrability. As a result, telescopic failure modes may be promoted, significantly limiting the exploitation of the textile strength (well below 50%).
- The use of low linear density twisted yarns improves the mechanical interlock between the textile and mortar and ensures good composite action with high exploitation of the textile strength (between 70-80%).
- Largely spaced textile meshes enable good bond between the mortar layers when used in composites.
- Denser meshes may result in poor mortar penetration within the textile layers and delamination when multiple layers are used.
- The critical mechanical reinforcement ratio for NTRM systems is 3%.
- When multiple FTRM layers are required to meet performance targets, the use of two layers of FTRM is recommended, as they provide significant deformability enhancement and energy dissipation capacity, as well as maintain a good composite behaviour.
- NTRM should be preferably applied in narrow strips, to alleviate problems related to non-uniform strain distribution during loading.
- During textile installation, special care should be given in ensuring good alignment of the textile reinforcement along the bonded area. An axial prestress level should be applied during manufacture and curing stages to ensure uniform stress and strain distribution.
- A minimum of 9 samples is needed for statistical validation accounting for the high uncertainty in the natural fibre material properties and consequent problems related to load eccentricities during testing.

7.4. RECOMMENDATIONS FOR FUTURE RESEARCH

Given the novelty of NTRM systems, significant amount of experimental, numerical and analytical work still needs to be carried out to optimise their performance and to develop more reliable testing protocols and design models. Possible directions are given below:

At composite level:

- Given the significant role of the textile architecture to the overall tensile and bond performance, further experimental work should focus on the mechanical and bond characterisation of NTRM systems comprising textiles of different layouts, and natural fibre provenance.

- The value of critical mechanical reinforcement ratio of 3% determined in Phase 1 needs to be validated with more experimental results on NTRM composites. A range of reinforcement ratios, either through the addition of subsequent textile layers or through alterations of the same textile geometry should be investigated.
- The use of complementary analytical techniques, including SEM and XRD, should be used alongside mechanical testing to quantify the degree of mortar impregnation along the yarn/textile embedment length and determine the effective yarn cross-sectional area that can be mobilised when subjected to tension and shear.
- Variability in mechanical properties along the length and across the width of the textile when embedded in the composite should be determined and considered in design recommendations, through the implementation of design factors.
- Durability studies need to be performed to assess the long-term performance of NTRM and identify methods to improve it, possibly through surface coatings using bio-resins not to affect the environmental credentials of the NTRM.
- More research and development work should be carried out in collaboration with natural-fibre textile manufacturers to optimise the yarn and textile architecture in accordance with the recommendations given in this thesis.
- The experimental work recommended above would provide the critical data that is required to develop and validate detailed numerical models, which in turn can be used to optimise the design of next generation NTRM.

At structural level:

- Preliminary analyses on the decomposition of the shear contribution of the NTRM and masonry components highlighted the complex interaction of shear resisting mechanisms in retrofitted masonry walls and showed the necessity to revisit current design guidelines. A similar analysis should be used to identify the shear resisting mechanisms and individual contributions in masonry walls retrofitted with NTRM and advanced TRM systems of different stiffness. Both monotonic and cyclic in-plane shear compression tests should be carried out to examine in detail the progressive development and degradation of shear resisting mechanisms. Numerical models should also be developed and validated against experimental results to carry out further parametric analyses.
- The proposed design analytical model predicting the in-plane shear capacity of FTRM-retrofitted walls needs to be validated against experimental results from tests adopting both natural and advanced TRM strengthening systems. More research is also needed towards the determination of the effective strain that can be developed in the textile, considering the possible failure modes of TRM-retrofitted elements under in-plane shear loading.
- As a more uniform load distribution can be achieved in the textile when embedded into narrow TRM strips, the effect of different NTRM retrofitting configurations should be examined,

including application of NTRM strips at different orientations (e.g. 0/90, 45/45) in a grid-like form. Full coverage of the wall with the orientation of the fibre grid parallel to that of the diagonals should also be explored. In addition, masonry elements of various aspect ratios and of different type of substrate (e.g. stone masonry) need to be examined.

- The effectiveness of NTRM as a strengthening solution should also be explored against out-of-plane loading, which can pose a significant hazard during seismic events, as well as combined in-plane/out-of-plane loading actions.

REFERENCE LIST

- [1] A.W. Coburn, R.J.S. Spence, *Earthquake Protection*, John Wiley & Sons Ltd, Chichester, 2002.
- [2] J. Tumialan, F. Micelli, A. Nanni, *Strengthening of masonry structures with FRP composites*, ASCE, Structures Congress, 2001.
- [3] P. Wallemacq, R. House, UNISDR and CRED report: *Economic Losses, Poverty & Disasters (1998 - 2017)*, United Nations Office for Disaster Risk Reduction (UNISDR) and the Centre for Research on the Epidemiology of Disasters (CRED). <http://www.emdat.be/publications>, 2018 (accessed 2 December 2019).
- [4] A. Ilki, M.N. Fardis, *Seismic Evaluation and Rehabilitation of Structures*, Springer, Berlin, 2014.
- [5] European Commission, Regulation (EU) No 305/2011 of the European Parliament and of the Council of 9 March 2011 laying down harmonised conditions for the marketing of construction products and repealing Council Directive 89/106/EE, *Off. J. Eur. Union* L88 (2011) 5-43.
- [6] M. Tomažević, *Earthquake-Resistant Design of Masonry Buildings*, Imperial College Press, London, 1999.
- [7] P. Luechinger, J. Fischer, *New European Technical Rules for the Assessment and Retrofitting of Existing Structures*, in: S. Dimova, A. Pinto, P. Luechinger, S. Denton (Eds.), *JRC Science and Policy Report*, Publications Office of the European Union, Luxembourg, 2015.
- [8] R. Dunne, D. Desai, R. Sadiku, J. Jayaramudu, *A review of natural fibres, their sustainability and automotive applications*, *J. Reinf. Plast. Compos.* 35 (2016) 1041-1050.
- [9] T.C. Triantafillou, *Strengthening Of Masonry Structures Using Epoxy-Bonded FRP Laminates*, *J. Compos. Constr.* 2 (1998) 96-104.
- [10] S. Raza, M.K.I. Khan, S.J. Menegon, H. Tsang, J.L. Wilson, *Strengthening and Repair of Reinforced Concrete Columns by Jacketing: State-of-the-Art Review*, *Sustainability* 11 (2019) 3208
- [11] C. Papanicolaou, T. Triantafillou, M. Lekka, *Externally bonded grids as strengthening and seismic retrofitting materials of masonry panels*, *Constr. Build. Mater.* 25 (2011) 504-514.
- [12] M. Giaretton, D. Dizhur, E. Garbin, J.M. Ingham, F. da Porto, *In-Plane Strengthening of Clay Brick and Block Masonry Walls Using Textile-Reinforced Mortar*, *J. Compos. Constr.* 22 (2018) 04018028.
- [13] S. Cardamano, F. Crea, A. Iorfida, *Mechanical Characterization of Basalt Fabric-Reinforced Alkali-Activated Matrix Composite: A Preliminary Investigation*, *Appl. Sci.* 10 (2020) 2865.
- [14] T.C. Triantafillou, K. Karlos, P. Kapsalis, L. Georgiou, *Innovative Structural and Energy Retrofitting System for Masonry Walls Using Textile Reinforced Mortars Combined with Thermal Insulation: In-Plane Mechanical Behavior*, *J. Compos. Constr.* 22 (2018) 04018029.

- [15] P.D. Gkournelos, T.C. Triantafillou, D.A. Bournas, Integrated Structural and Energy Retrofitting of Masonry Walls: Effect of In-Plane Damage on the Out-of-Plane Response, *J. Compos. Constr.* 24 (2020) 04020049.
- [16] C.G. Papanicolaou, T.C. Triantafillou, P.R. Fabregat, Increase of load-carrying capacity of masonry with textile reinforced rendering / Erhöhung der Tragfähigkeit von Mauerwerk mit textilbewehrtem Putz. *Mauerwerk*, 19 (2015) 40-51.
- [17] C.G. Papanicolaou, T.C. Triantafillou, K. Karlos, M. Papathanasiou, Textile reinforced mortar (TRM) versus FRP as strengthening material of URM walls: in-plane cyclic loading, *Mater. Struct.* 40 (2007) 1081-1097.
- [18] C.G. Papanicolaou, T.C. Triantafillou, M. Papathanasiou, K. Karlos, K. Textile reinforced mortar (TRM) versus FRP as strengthening material of URM walls: Out-of-plane cyclic loading, *Mater. Struct.* 41 (2008), 143–157.
- [19] S. De Santis, G. de Felice, F. Roscini, Retrofitting of Masonry Vaults by Basalt Textile-Reinforced Mortar Overlays, *Int. J. Archit. Heritage* 13 (2019) 1061-1077.
- [20] V. Alecci, M. De Stefano, F. Focacci, R. Luciano, L. Rovero, G. Stipo, Strengthening Masonry Arches with Lime-Based Mortar Composite, *Buildings* 7 (2017) 49.
- [21] L. Koutas, S.N. Bousias, T.C. Triantafillou, Seismic Strengthening of Masonry-Infilled RC Frames with TRM: Experimental Study, *J. Compos. Constr.* 19 (2015) 04014048.
- [22] M. Minotto, N. Verlato, M. Donà, F. da Porto, Strengthening of In-Plane and Out-of-Plane Capacity of Thin Clay Masonry Infills Using Textile and Fiber-Reinforced Mortar, *J. Compos. Constr.* 24 (2020) 04020059.
- [23] L.N. Koutas, D.A. Bournas, Confinement of masonry columns with textile-reinforced mortar jackets, *Constr. Build. Mater.* 258 (2020) 120343.
- [24] C. Carloni, C. Mazzotti, M. Savoia, K.V. Subramaniam, Confinement of masonry columns with PBO FRCM composites, *Key Eng. Mater.* 624 (2015) 644-651.
- [25] D. Bournas, Strengthening of existing structures: Selected case studies, in: T.C. Triantafillou TC (ed.), *Textile fibre composites in civil engineering*, Woodhead Publishing, Cambridge, pp 389-411, 2016.
- [26] M.R. Valluzzi, F. da Porto, E. Garbin, M. Panizza, Out-of-plane behaviour of infill masonry panels strengthened with composite materials, *Mater Struct* 47 (2014) 2131-2145.
- [27] P.D. Askouni, C.G. Papanicolaou, Experimental investigation of bond between glass textile reinforced mortar overlays and masonry: the effect of bond length, *Mater. Struct.* 50 (2017) 1-15.
- [28] D.B. Dittenber, H.V.S. GangaRao, Critical review of recent publications on use of natural composites in infrastructure, *Compos. Part A* 43 (2012) 1419-1429.
- [29] IPCC, *Climate Change 1995: Impacts, Adaptations, and Mitigation of Climate Change: Scientific - Technical Analyses*. Contribution of working group II to the second assessment

- report of the Intergovernmental Panel on Climate Change (Vol. 39), Press Syndicate of the University of Cambridge, Cambridge, 1996.
- [30] T. Rousakis, Natural fibre rebar cementitious composites, in: M. Fan, F. Fu (Eds.), *Advanced High Strength Natural Fibre Composites in Construction*, Woodhead Publishing, Duxford, 2017, pp. 545–556.
- [31] G. de Felice, S. De Santis, L. Garmendia, B. Ghiassi, P. Larrinaga, P.B. Lourenço, D.V. Oliveira, F. Paolacci, C.G. Papanicolaou, Mortar-based systems for externally bonded strengthening of masonry, *Mater. Struct.* 47 (2014) 2021-2037.
- [32] M. Fan, Future scope and intelligence of natural fibre based construction composites, in: M. Fan and F. Fu (Eds.), *Advanced High Strength Natural Fibre Composites in Construction*, Woodhead Publishing, Duxford, 2017.
- [33] FIB (Federation Internationale du Beton), *Fib bulletin 90 Externally applied FRP reinforcement for concrete structures*, 2019.
- [34] F.G. Carozzi, D. Arboleda, C. Poggi, A. Nanni, Direct Shear Bond Tests of Fabric-Reinforced 843 Cementitious Matrix Materials, *J. Compos. Constr.* 24 (2020) 04019061.
- [35] T-T. Bui, A. Limam, V. Sarhosis, Failure analysis of masonry wall panels subjected to in-plane and out-of-plane loading using the discrete element method, *Eur. J. Environ. Civil Eng.* 2019.
- [36] Triantafillou, T.C., (2006). *Strengthening and Seismic Retrofitting of Concrete and Masonry Structures with Composites*. MSc Lecture Notes, *Advanced Materials & Seismic Retrofit Technologies CIV1507*, University of Patras, Greece.
- [37] G. Magenes, G.M. Calvi, In-Plane Seismic Response of Brick Masonry Walls, *Earthq. Eng. Struct. Dyn.* 26 (1997) 1091-1112.
- [38] K. Karantoni, M.N. Fardis, Effectiveness of Seismic Strengthening Techniques for Masonry Buildings, *J. Struct. Eng.* 118 (1992) 1884-1902.
- [39] M. ElGawady, P. Lestuzzi, M. Badoux, A Review of Conventional Seismic Retrofitting Techniques for URM, in: *proceedings of 13th International Brick and Block Masonry Conference*, 2004.
- [40] E. Mustafaraj, Y. Yardim, Review of Strengthening Techniques and Mechanical Testing for Unreinforced Masonry, *Int. J. Sci. Technol.* 3 (2017) 33-50.
- [41] Y. Korany, R. Drysdale, Rehabilitation of Masonry Walls Using Unobtrusive FRP Techniques for Enhanced Out-of-Plane Seismic Resistance, *J. Compos. Constr.* 10 (2006) 213-222.
- [42] ACI 440.7R-10, *Guide for the Design and Construction of Externally Bonded Fiber-Reinforced Polymer Systems for Strengthening Unreinforced Masonry Structures*, American Concrete Institute, USA, 2010.
- [43] CNR DT 200 R1/2013, *Guide for the design and construction of externally bonded FRP systems for strengthening existing structures*, CNR - Advisory Committee on Technical Recommendations for Construction CNR DT, CNR, Roma, 2013.

- [44] S.M. Rahman, T. Ueda, In-Plane Shear Performance of Masonry Walls after Strengthening by Two Different FRPs, *J. Compos. Constr.* 20 (2016) -1--1.
- [45] F. Micelli, M.S. Sciolti, M. Leone, M.A. Aiello, A. Dudine, Shear behaviour of Fiber Reinforced Mortar strengthened masonry walls built with limestone blocks and hydraulic mortar, in: M. da Porto, A. Valuzzi, (Eds.), *Brick and Block Masonry – Trends, Innovations and Challenges*. Taylor & Francis Group, London, pp. 2137–2145, 2016.
- [46] A. Bilotta, F. Ceroni, E. Nigro, E., M. Pecce, Experimental tests on FRCM strengthening systems for tuff masonry elements, *Constr. Build. Mater.* 138 (2017) 114-133.
- [47] ACI549.4R-13, *Guide to Design and Construction of Externally Bonded Fabric-Reinforced Cementitious Matrix (FRCM) Systems for Repair and Strengthening Concrete and Masonry Structures*, American Concrete Institute, US, 2013.
- [48] L.N. Koutas, Z. Tetta, D.A. Bournas, T.C. Triantafillou, Strengthening of Concrete Structures with Textile Reinforced Mortars: State-of-the-Art Review, *J. Compos. Constr.* 23 (2019) 03118001.
- [49] L.A.S. Kouris, T.C. Triantafillou, State-of-the-art on strengthening of masonry structures with textile reinforced mortar (TRM), *Constr. Build. Mater.* 188: (2018) 1221–33.
- [50] D.A. Pohoryles, D.A. Bournas DA, Seismic retrofit of infilled RC frames with textile reinforced mortars: State-of-the-art review and analytical modelling. *Compos. Part B* 183 (2020) 107702.
- [51] AC434, *Acceptance criteria for masonry and concrete strengthening using fiber-reinforced cementitious matrix (FRCM) and steel reinforced grout (SRG) composite systems*, ICC-Evaluation Service, Whittier, 2016.
- [52] RILEM Technical Committee 232-TDT (Wolfgang Brameshuber), *Recommendation of RILEM TC 232-TDT: test methods and design of textile reinforced concrete Uniaxial tensile test: test method to determine the load bearing behavior of tensile specimens made of textile reinforced concrete*, *Mater. Struct.* 49 (2016) 4923-4927.
- [53] S. De Santis, H.A. Hadad, F. De Caso y Basalo, G. de Felice, A. Nanni, *Acceptance Criteria for Tensile Characterization of Fabric-Reinforced Cementitious Matrix Systems for Concrete and Masonry Repair*, *J. Compos. Constr.* 22 (2018) 04018048.
- [54] G. de Felice, M.A. Aiello, C. Caggegi, et al., *Recommendation of RILEM Technical Committee 250-CSM: Test method for Textile Reinforced Mortar to substrate bond characterization*, *Mater. Struct.* 51 (2018) 95.
- [55] FIB (Federation Internationale du Beton), *Fib bulletin 90 Externally applied FRP reinforcement for concrete structures*, 2019.
- [56] ACI549.6R, *Guide to Design and Construction of Externally Bonded Fabric-Reinforced Cementitious Matrix (FRCM) and Steel-Reinforced Grout (SRG) Systems for Repair and Strengthening Masonry Structures*, Edited by ACI 549-L Committee and RILEM TC 250-CSM, ISBN: 978-1-64195-120-3, 2020.

- [57] O. Onuaguluchi, N. Banthia, Plant-based natural fibre reinforced cement composites: A review, *Cem. Concr. Compos.* 68 (2016) 96-108.
- [58] Z. Magyar, EU plans to reduce GHG emissions with 80% by 2050, available from: https://www.rehva.eu/fileadmin/hvac-dictio/03-2011/EU_plans_to_reduce_GHG_emissions_with_80_by_2050.pdf, 2011 (accessed 17 december 2017).
- [59] United Nations Environment Programme, Buildings and Climate Change, available from: <https://www.unep.org/sbci/pdfs/SBCI-BCCSummary.pdf>, 2013 (accessed 20 march 2016).
- [60] M. B. Ali, R. Saidur, M. S. Hossain, A Review on Emission Analysis in Cement Industries, *Renewable & Sustainable Energy Reviews* 15 (2011) 2252-2261.
- [61] NetComposites, Technology Overview – Biocomposites. Available from: <https://netcomposites.com/media/1211/biocomposites-guide.pdf>, 2014 (accessed 1 June 2017).
- [62] O. Adekomaya, T. Jamiru, R. Sadiku, Z. Huan, A review on the sustainability of natural fiber in matrix reinforcement - A practical perspective, *J. Reinf. Plast. Compos.* 35 (2016) 3-7.
- [63] FAO, Technical Paper No. 56: Discover natural fibres 2009 - Proceedings of the Symposium on Natural Fibres, 2008 (accessed 12 December 2017).
- [64] S.V. Joshi, L.T. Drzal, A.K. Mohanty, S. Arora, S, Are natural fiber composites environmentally superior to glass fiber reinforced composites?, *Compos. Part A* 35 (2004) 371-376.
- [65] P. Wambua, J. Ivens, I. Verpoest, Natural fibres: Can they replace glass in fibre reinforced plastics?, *Compos. Sci. Technol.* 63 (2003) 1259-1264.
- [66] A.N. Netravali, X. Huang, K. Mizuta, Advanced “green” composites, *Adv. Compos. Mater.* 16 (2007) 269–282.
- [67] F.D.A. Silva, B. Mobasher, R.D.T. Filho, Advances in Natural Fiber Cement Composites: A Material for the Sustainable Construction Industry, in: *Proceedings of 4th Colloquium on Textile Reinforced Structures (CTRS4)*, pp. 377–388, 2017.
- [68] M.S. Salit, *Tropical Natural Fibre Composites*, Springer Science & Business Media, Singapore, 2014.
- [69] R. Codispoti, D.V. Oliveira, R.S. Olivito, P.B. Lourenço, R. Figueiro, Mechanical performance of natural fiber-reinforced composites for the strengthening of masonry. *Compos. Part B*, 77 (2015) 74-83.
- [70] M.P.M. Dicker, P.F. Duckworth, A.B. Baker, G. Francois, M.K. Hazzard, P.M. Weaver, Green composites: A review of material attributes and complementary applications, *Compos. Part A* 56 (2014) 280–289.
- [71] L. Yan, B. Kasal, L. Huang, A review of recent research on the use of cellulosic fibres, their fibre fabric reinforced cementitious, geo-polymer and polymer composites in civil engineering, *Compos. Part B: Eng.* 92 (2016) 94-132.

- [72] T. Sen, H.N. Jagannatha, Strengthening of RC beams in flexure using natural jute fibre textile reinforced composite system and its comparative study with CFRP and GFRP strengthening systems, *Int. J. Sustain. Built Environ.* 2 (2013) 41-55.
- [73] J. Zach, J. Hroudová, J. Brožovský, Z. Krejza, A. Gailius, Development of thermal insulating materials on natural base for thermal insulation systems, *Procedia Eng.* 57 (2013) 1288-1294.
- [74] <http://www.fao.org/faostat/en> (accessed 15 december 2020).
- [75] K.L. Pickering, M.G.A. Efendy, T.M. Le, A review of recent developments in natural fibre composites and their mechanical performance, *Compos. Part A* 83 (2016) 98-112.
- [76] Y. Li, W. Mai, L. Ye, Sisal fibre and its composites: a review of recent developments. *Compos. Sci. Technol.* 60 (2000) 2037-2055.
- [77] D.D. Stokke, W. Wu, G. Han, *Introduction to Wood and Natural Fiber Composites*, John Wiley & Sons Ltd, Chichester, 2014.
- [78] A. Komuraiah, N.S. Kumar, B.D. Prasad, Chemical composition of natural fibres and its influence on their mechanical properties, *Mech. Compos. Mater.* 50 (2014) 359-376.
- [79] A.K. Mohanty, M. Misra, L.T. Drzal, S.E. Selke, B.R. Harte, G. Hinrichsen, Natural fibers, biopolymers and biocomposites: An introduction, in: A.K. Mohanty, M. Misra and L.T. Drzal, (Eds.), *Natural Fibers, Biopolymers and Biocomposites*, CRC Press, London, 2005.
- [80] F.H.M.M. Costa, J.R.M. D'Almeida, Effect of Water Absorption on the Mechanical Properties of Sisal and Jute Fiber Composites. *Polymer-Plastics Technology and Engineering*, 38 (1999) 1081-1094.
- [81] L. Mohammed, M.N.M. Ansari, G. Pua, M. Jawaid, M.S. Islam, A Review on Natural Fiber Reinforced Polymer Composite and Its Applications, *Int. J. Polym. Sci.* (2015) 1-15.
- [82] J.G. Moroz, S.L. Lissel, M.D. Hagel, Performance of bamboo reinforced concrete masonry shear walls, *Constr. Build. Mater.* 61 (2014) 125–137.
- [83] J. Wei, C. Meyer, Degradation mechanisms of natural fibre in the matrix of cement composites. *Cem. Concr. Res.* 73 (2015) 1-16.
- [84] T. Alomayri, I. M. Low, Synthesis and characterization of mechanical properties in cotton fiber-reinforced geopolymer composites. *J. Asian Ceram. Soc.* 1 (2013) 30-34.
- [85] A. Hallonet, L. Michel, E. Ferrier, Investigation of the bond behavior of flax FRP strengthened RC structures through double lap shear testing, *Compos. Part B: Eng.* 100 (2016) 247e256.
- [86] G. Ferrara, M. Pepe, E. Martinelli, R.D. Tolêdo Filho, Influence of Fibres Impregnation on the Tensile Response of Flax Textile Reinforced Mortar Composite Systems, in: P. Serna et al. (Eds.): *BEFIB 2020, RILEM Bookseries* 30, pp. 983–990, 2021.
- [87] H. Danso, D. B. Martinson, M. Ali, J. B. Williams, Mechanisms by which the inclusion of natural fibres enhance the properties of soil blocks for construction. *J. Compos. Mater.* 51 (2017) 3835-3845.
- [88] A.L. Leão, B.M. Cherian, S.F. De Souza, R.M. Kozłowski, S. Thomas, M. Kottaisamy, Natural fibres for geotextiles, *Handbook of Natural Fibres*, 2 (2012) 280-311.

- [89] M.R. Valluzzi, F. da Porto, E. Garbin, M. Panizza, Out-of-plane behaviour of infill masonry panels strengthened with composite materials. *Mater. Struct.* 47 (2014), 2131-2145.
- [90] D. Arboleda, F.G. Carozzi, A. Nanni, C. Poggi, Testing Procedures for the Uniaxial Tensile Characterization of Fabric-Reinforced Cementitious Matrix Composites, *J. Compos. Constr.* 20 (2016) 1-13.
- [91] T. D'Antino, C. Papanicolaou, Mechanical characterization of textile reinforced inorganic-matrix composites, *Compos. Part B: Eng.* 127 (2017) 78-91.
- [92] J. Donnini, V. Corinaldesi, A. Nanni, Mechanical properties of FRCM using carbon fabrics with different coating treatments, *Compos. Part B: Eng.* 88 (2016) 220-228.
- [93] B. Banholzer, T. Brockmann, W. Brameshuber, Material and bonding characteristics for dimensioning and modelling of textile reinforced concrete (TRC) elements, *Mater. Struct.* 39 (2006) 749-763.
- [94] F. Hartig, F. Jesse, K. Schicktanz, U. Haubler-Combe, Influence of experimental setups on the apparent uniaxial tensile load-bearing capacity of textile reinforced concrete specimens. *Mater. Struct.* 45 (2012) 433-446.
- [95] F.G. Carozzi, A. Bellini, T. D'Antino, et al., Experimental investigation of tensile and bond properties of Carbon-FRCM composites for strengthening masonry elements. *Compos. Part B: Eng.* 128 (2017) 100-119.
- [96] M. Malena, G. de Felice, Debonding of composites on a curved masonry substrate: Experimental results and analytical formulation, *Compos. Struct.* 112 (2014) 194-206.
- [97] D. Asprone, M. Durante, A. Prota, G. Manfredi, Potential of structural pozzolanic matrix-hemp fiber grid composites, *Constr. Build. Mater.* 25 (2011) 2867-2874.
- [98] R.S. Olivito, O.A. Cevallos, A. Carrozzini, Development of durable cementitious composites using sisal and flax fabrics for reinforcement of masonry structures. *Mater. Des.* 57 (2014) 258-268.
- [99] O.A. Cevallos, R.S. Olivito, Effects of fabric parameters on the tensile behaviour of sustainable cementitious composites. *Compos. Part B: Eng.* 69 (2015) 256-266.
- [100] L. Mercedes, L. Gil, E. Bernat-Maso, Mechanical performance of vegetal fabric reinforced cementitious matrix (FRCM) composites, *Constr. Build. Mater.* 175 (2018) 161-173.
- [101] G. Ferrara, E. Martinelli, Tensile behaviour of Textile Reinforced Mortar composite systems with flax fibres, in: *Proceedings of the 12th International PhD Symposium in Civil Engineering*, Prague, 2018, pp.1-7.
- [102] C.B. de Carvalho Bello, I. Boem, A. Cecchi, N. Gattesco, D.V. Oliveira, Experimental tests for the characterization of sisal fiber reinforced cementitious matrix for strengthening masonry structures, *Constr. Build. Mater.* 219 (2019) 44-55.
- [103] F.G. Carozzi, D. Arboleda, C. Poggi, A. Nanni, Direct Shear Bond Tests of Fabric-Reinforced Cementitious Matrix Materials, *J. Compos. Constr.* 24 (2020) 04019061.

- [104] R.S. Olivito, R. Codispoti, O.A. Cevallos, Bond behavior of Flax-FRCM and PBO-FRCM composites applied on clay bricks: Experimental and theoretical study, *Compos. Struct.* 146 (2016) 221-231.
- [105] G. Magenes, A. Penna, A. Galasco, M. Da Paré M, In-plane cyclic shear tests of undressed double-leaf stone masonry panels, in: *Proceedings of 8th International Masonry Conference*, 2010.
- [106] J. Donnini, G. Maracchini, S. Lenci, V. Corinaldesi, E. Quagliarini, TRM reinforced tuff and fired clay brick masonry: Experimental and analytical investigation on their in-plane and out-of-plane behaviour, *Constr. Build. Mater.* (in press) 2020. <https://doi.org/10.1016/j.conbuildmat.2020.121643G>.
- [107] A. Prota, G. Marcari, G. Fabbrocino, G. Manfredi, C. Aldea, Experimental In-Plane Behavior of Tuff Masonry Strengthened with Cementitious Matrix–Grid Composites, *J. Compos. Constr.* 10 (2006) 223-233.
- [108] G. Ferrara, C. Caggegi, E. Martinelli, A. Gabor, Shear capacity of masonry walls externally strengthened using Flax-TRM composite systems: experimental tests and comparative assessment, *Constr. Build. Mater.* 261 (2020) 120490.
- [109] C. Menna, D. Asprone, M. Durante, A. Zinno, A. Balsamo, A. Prota, Structural behaviour of masonry panels strengthened with an innovative hemp fibre composite grid, *Constr. Build. Mater.* 100 (2015) 111-121.
- [110] T. D’Antino, C.G. Papanicolaou, Comparison between different tensile test set-ups for the mechanical characterization of inorganic-matrix composites, *Constr. Build. Mater.* 17 (2018) 140-151.
- [111] P.D. Askouni, C.G. Papanicolaou, Textile Reinforced Mortar-to-masonry bond: Experimental 886 investigation of bond-critical parameters, *Constr. Build. Mater.* 207 (2019) 535-547.
- [112] G. Misseri, G. Stipo, S. Galassi, L. Rovero, Experimental Investigation on the Bond Behaviour of 889 Basalt TRM Systems - Influence of Textile Configuration and Multi-Layer Application, *Key Eng. Mater.* 817 (2019) 134-140.
- [113] M. Jawaid, S. Siengchin, Hybrid composites: A versatile materials for future, *Appl. Sci. Eng. Progress* 12 (2019) 223. <http://doi.org/10.14416/j.asep.2019.09.002>.
- [114] K. Van Balen, I. Papayianni, R. Van Hees, L. Binda, A. Waldum, Introduction to requirements for and functions and properties of repair mortars, *Mater. Struct. Constr.* 38 (2005) 781-785. [doi:10.1617/14319](https://doi.org/10.1617/14319).
- [115] J. Lanas, J.I. Alvarez-Galindo, Masonry repair lime-based mortars: Factors affecting the mechanical behaviour, *Cem. Concr. Res.* 33 (2003) 1867-1876. [http://doi.org/10.1016/S0008-8846\(03\)00210-2](http://doi.org/10.1016/S0008-8846(03)00210-2).
- [116] G. Ferrara, B. Coppola, L. Di Maio, L. Incarnato, E. Martinelli, Tensile strength of flax fabrics to be used as reinforcement in cement-based composites: experimental tests under different

- environmental exposures, *Compos. Part B Eng.* 168 (2019) 511-523. <http://doi.org/10.1016/j.compositesb.2019.03.062>.
- [117] J. Hegger, N. Will, O. Bruckermann, S. Voss, Load-bearing behaviour and simulation of textile reinforced concrete, *Mater. Struct. Constr.* 39 (2006) 765-776. <http://doi.org/10.1617/s11527-005-9039-y>.
- [118] S. Babaeidarabad, D. Arboleda, G. Loreto, A. Nanni, Shear strengthening of un-reinforced concrete masonry walls with fabric-reinforced-cementitious-matrix, *Constr. Build. Mater.* 65 (2014) 243-253. <https://doi.org/10.1016/j.conbuildmat.2014.04.116>.
- [119] A. Peled, A. Bentur, Fabric structure and its reinforcing efficiency in textile reinforced cement composites. *Compos. Part A Appl. Sci. Manuf.* 34 (2003) 107-118. [http://doi.org/10.1016/S1359-835X\(03\)00003-4](http://doi.org/10.1016/S1359-835X(03)00003-4)
- [120] M. Wouters, Effects of fibre bundle size and stitch pattern on the static properties of unidirectional carbon-fibre non-crimp fabric composites, Master's thesis, Luleå, Sweden, Luleå University of Technology, 2002.
- [121] EN ISO 1889, Reinforcement yarns - Determination of linear density, European Committee for Standardization, 2009.
- [122] ASTM D8171, Standard Test Methods for Density Determination of Flax Fiber, ASTM International, 2018.
- [123] D.U. Shah, P.J. Schubel, P. Licence, M.J. Clifford, Hydroxyethylcellulose surface treatment of natural fibres: the new 'twist' in yarn preparation and optimization for composites applicability, *J. Mater. Sci.* 47 (2012) 2700-2711. <https://doi.org/10.1007/s10853-011-6096-1>.
- [124] EN 459-1, Building lime - Part 1: Definitions, specifications and conformity criteria, European Committee for Standardization, 2015.
- [125] EN 1015-11, Methods of test for mortar for masonry - Part 11: Determination of flexural and compressive strength of hardened mortar, European Committee for Standardization, 2007.
- [126] FIB (Federation Internationale du Beton), Fib Model Code for concrete structures 2010, 2013.
- [127] J.L. Thomason, J. Carruthers, J. Kelly, G. Johnson, Fibre cross-section determination and variability in sisal and flax and its effects on fibre performance characterisation, *Compos. Sci. Technol.* 71 (2011) 1008-1015. <http://doi.org/10.1016/j.compscitech.2011.03.007>.
- [128] EN ISO 2062, Textiles - Yarns from packages - Determination of single-end breaking force and elongation at break using constant rate of extension (CRE) tester, European Committee for Standardization, 2009.
- [129] EN ISO 13934-1, Textiles - Tensile properties of fabrics Part 1: determination of maximum force and elongation at maximum force using the strip method, European Committee for Standardization, 2013.

- [130] S. De Santis, F.G. Carozzi, G. de Felice, C. Poggi, Test methods for Textile Reinforced Mortar systems, *Compos. Part B Eng.* 127 (2017) 121-132. <http://doi.org/10.1016/j.compositesb.2017.03.016>.
- [131] M.A. Sutton, J. Orteu, H.W. Schreier, *Image Correlation for Shape, Motion and Deformation Measurements*, Springer, Boston, 2009. <http://doi.org/10.1007/978-0-387-78747-3>.
- [132] M. Tekieli, S. De Santis, G. de Felice, A. Kwiecień, F. Roscini, Application of Digital Image Correlation to composite reinforcements testing, *Compos. Struct.* 160 (2017) 670-688. <http://dx.doi.org/10.1016/j.compstruct.2016.10.096>.
- [133] GOM Correlate Evaluation software for 3D testing. <http://www.gom.com/3d-software/gom-inspect.html>, 2017 (accessed 10 January 2017).
- [134] M. Aslan, G. Chinga-Carrasco, B.F. Sørensen, B. Madsen, Strength variability of single flax fibres, *J. Mater. Sci.* 46 (2011) 6344-6354. <http://doi.org/10.1007/s10853-011-5581-x>.
- [135] A.S. Virk, W. Hall, J. Summerscales, Tensile properties of jute technical fibers, *Mater. Sci. Technol.* 25 (2009) 216-228. <https://doi.org/10.1179/174328408X385818>.
- [136] B. Madsen, P. Hoffmeyer, A.B. Thomsen, H. Lilholt, Hemp yarn reinforced composites – I. Yarn characteristics, *Compos. Part A* 38 (2007) 2194-2203. <https://doi.org/10.1016/j.compositesa.2007.06.001>
- [137] J.M.F.A. Blanchard, A.J. Sobey, J.I.R. Blake, Multi-scale investigation into the mechanical behaviour of flax in yarn, cloth and laminate form, *Compos. Part B: Eng.* 84 (2015) 228-235. <http://doi.org/10.1016/j.compositesb.2015.08.086>.
- [138] D. Xue, H. Hu, Mechanical properties of biaxial weft-knitted flax composites, *Mater. Des.* 46 (2013) 264-269. <http://doi.org/10.1016/j.matdes.2012.10.019>
- [139] B. Banholzer, Bond behavior of multi-filament yarn embedded in a cementitious matrix, PhD thesis, Aachen, Germany, Rheinisch-Westfälische Technische Hochschule (RETH) Aachen Univ., 2004.
- [140] B. Madsen, A. Thygesen, H. Lilholt, Plant fibre composites - porosity and volumetric interaction, *Compos. Sci. Technol.* 67 (2007) 1584-1600. <http://doi.org/10.1016/j.compscitech.2006.07.009>.
- [141] N. Trochoutsou, M. Di Benedetti, K. Pilakoutas, M. Guadagnini, Mechanical Characterisation of Flax and Jute Textile-Reinforced Mortars. *Constr. Build. Mater.* 271 (2021) 121564. <http://doi.org/10.1016/j.conbuildmat.2020.121564>.
- [142] C.B. de Carvalho Bello, A. Cecchi, Experiments on natural fibers: durability and mechanical properties. *Adv Mater Proc Technol* (2017), doi: 10.1080/2374068X.2017.1364880
- [143] S. Barducci, V. Alecci, M. De Stefano et al., 2020. Experimental and Analytical Investigations on Bond Behavior of Basalt-FRCM Systems. *J Compos Constr* 24(1), 04019055. [http://dx.doi.org/10.1061/\(ASCE\)CC.1943-5614.0000985](http://dx.doi.org/10.1061/(ASCE)CC.1943-5614.0000985)

- [144] C. Carloni, T. D'Antino, L. Sneed, C. Pellegrino, 2014. Role of the matrix layers in the stress-transfer mechanism of FRCM composites bonded to a concrete substrate. *J Eng Mech* 141(6), 04014165.
- [145] C. Sabau, J.H. Gonzalez-Libreros, L.H. Sneed et al., Use of image correlation system to study the bond behaviour of FRCM-concrete joints. *Mater Struct* 50 (2017) 172. doi:10.1617/s11527-017-1036-4.
- [146] L.H. Sneed, T. D'Antino, C. Carloni, C. Pellegrino, A comparison of the bond behavior of PBO-FRCM composites determined by double-lap and single-lap shear tests. *Cem Con Comp* 64 (2015) 37-38. <http://dx.doi.org/10.1016/j.cemconcomp.2015.07.00723>.
- [147] T. D'Antino, C. Carloni, L.H. Sneed, C. Pellegrino, Matrix-fiber bond behavior in PBO FRCM composites: A fracture mechanics approach. *Eng Fract Mech* 117 (2014) 94-111. <http://dx.doi.org/10.1016/j.engfracmech.2014.01.011>
- [148] F.G. Carozzi, C. Poggi C, Mechanical properties and debonding strength of Fabric Reinforced Cementitious Matrix (FRCM) systems for masonry strengthening. *Compos Part B Eng* 70 (2015) 215-230. doi: 10.1016/j.compositesb.2014.10.056
- [149] L. Ombres, S. Mazzuca, S. Verre, Analysis of the bond between Fabric Reinforced Cementitious Mortar (FRCM) strengthening systems and masonry. In: Euro-American Congress REHABEND, Burgos, Spain, 24-27 May 2016
- [150] A. D' Ambrisi, L. Feo, F. Focacci, Experimental analysis on bond between PBO-FRCM strengthening materials and concrete. *Comp Part B* 44(1) (2013) 524-532. doi:10.1016/j.compositesb.2012.03.011
- [151] A. Younis, U. Ebead, Bond characteristics of different FRCM systems. *Constr Build Mater* 175 (2018) 610-620. <http://dx.doi.org/10.1016/j.conbuildmat.2018.04.216>
- [152] L. Ombres, Analysis of the bond between Fabric Reinforced Cementitious Mortar (FRCM) strengthening systems and concrete. *Compos Part B Eng* 69 (2015)418-426. doi: 10.1016/j.compositesb.2014.10.027
- [153] EN 998-2, Specification for mortar for masonry - Part 2: Masonry mortar, BSI Standards Publication, 2016.
- [154] EN 1015-3, Methods of test for mortar for masonry - Part 3: Determination of consistence of fresh mortar (by flow table), BSI Standards Publication, 1999.
- [155] RILEM TC 76-LUM, LUM A1 Compressive strength of masonry units, in: RILEM Recommendations for the Testing and Use of Constructions Materials, E. & F.N. Spon Ltd, London, 1991, pp.456-458.
- [156] RILEM TC 76-LUM, LUM B1 Compressive strength of small walls and prisms, 1991. In: RILEM Recommendations for the Testing and Use of Constructions Materials, E. & F.N. Spon Ltd, London, 1991, pp.475-477.
- [157] D. Dizhur, J.M. Ingham, Diagonal tension strength of vintage unreinforced clay brick masonry wall panels, *Constr. Build. Mater.* 43 (2013) 418-427.

- [158] E. Mustafaraj, Y. Yardim, In-plane Shear Strengthening of Unreinforced Masonry Walls using GFRP Jacketing, *Period. Polytech. Civil. Eng.* 62 (2019) 330-336.
- [159] T.C. Triantafyllou, C.G. Papanicolaou, P. Zissimopoulos, T. Laourdekis, Concrete Confinement with Textile-Reinforced Mortar Jackets, *ACI Structural Journal* 103 (2016) 28-37.
- [160] S. Babaeiderabad, F. De Caso, A. Nanni, URM Walls Strengthened with Fabric-Reinforced Cementitious Matrix Composite Subjected to Diagonal Compression. *J Compos Constr* 18 (2014) 04013045.
- [161] N. Augenti, F. Parisi, A. Prota, G. Manfredi, In-Plane Lateral Response of a Full-Scale Masonry Subassemblage with and without an Inorganic Matrix-Grid Strengthening System, *J. Compos. Constr.* 15 (2011) 578-590.
- [162] M. del Zoppo, M. Di Ludovico, A. Prota, Analysis of FRM and CRM parameters for the in-plane shear strengthening of different URM types, *Compos. Part B* 171 (2019) 20-33.
- [163] S. Goutianos, T. Peijs, B. Nystrom, M. Skrifvars, Development of Flax Fibre based Textile Reinforcements for Composite Applications, *Appl. Compos. Mater.* 13 (2006) 199–215.
- [164] N. Trochoutsou, M. Di Benedetti, K. Pilakoutas, M. Guadagnini, Bond of Flax Textile-Reinforced Mortars to masonry. *Constr. Build. Mater.* 284 (2021) 122849
- [165] O. A. Cevallos, R. S. Olivito, R. Codispoti, L. Ombres, Flax and polyparaphenylene benzobisoxazole cementitious composites for the strengthening of masonry elements subjected to eccentric loading. *Compos. Part B* 71 (2015) 82–95.
- [166] D. Dizhur, J. Ingham, M. Griffith, D. Biggs, A. Schultz, Performance of unreinforced masonry and infilled RC buildings during the 2015 Gorkha, Nepal earthquake sequence, in: M. da Porto and A. Valuzzi (eds) *Brick and Block Masonry – Trends, Innovations and Challenges*. Taylor and Francis Group, London, pp 2399–2407, 2016.
- [167] EN 1996-1, Eurocode 6 - Design of masonry structures - Part 1: General rules for reinforced and unreinforced masonry structures, European Committee for Standardization, 2013.
- [168] BS EN 772-1, Methods of test for masonry units - Part 1: Determination of compressive strength, European Committee for Standardization, 2000.
- [169] EN 1052-1, Methods of test for masonry - Part 1: Determination of compressive strength, European Committee for Standardization, 1999.
- [170] EN 1052-3, Methods of test for mortar for masonry - Part 3: Determination of initial shear strength, European Committee for Standardization, 2002.
- [171] EN 1998-3, Eurocode 8 - Design of structures for earthquake resistance - Part 3: Assessment and retrofitting of buildings, European Committee for Standardization 2005.
- [172] EN 1998-1, Eurocode 8 - Design of structures for earthquake engineering - Part 1: General rules, seismic actions and rules for buildings, European Committee for Standardization, 2013.

- [173] FEMA 356, Prestandard and Commentary for the Seismic Rehabilitation of Buildings, Federal Emergency Management Agency, Washington DC, 2000.
- [174] ASTM E2126, Standard test methods for cyclic (reversed) load test for shear resistance of vertical elements of the lateral force resisting systems for buildings, ASTM International, Conshohocken PA, 2011.
- [175] M. Tomažević, Shear resistance of masonry walls and Eurocode 6: shear versus tensile strength of masonry, *Mater. Struct.* 42 (2009) 889-907.
- [176] M. Rota, A. Penna, G. Magenes, A framework for the seismic assessment of existing masonry buildings accounting for different sources of uncertainty, *Earthq. Eng. Struct. Dyn.* 43 (2013) 1045-66.
- [177] M. Tomažević, Recent advances in earthquake-resistant design of masonry buildings: European perspective, in: *Proceedings of 11th World Conference on Earthquake Engineering*, Paper No. 2012, 1996.
- [178] L.S. Jacobsen, Damping in composite structures, in: *Proceedings 2nd WCEE*, Tokyo, 1960.
- [179] G.P. Lignola, M. Di Ludovico, A. Prota, et al., Design rules for in-plane shear strengthening of masonry with FRCM, in: *Proceedings of 9th International Conference on Fibre-Reinforced Polymer (FRP) Composites in Civil Engineering (CICE 2018)*, 2018.
- [180] Ö.S. Türkmen, B.T. De Vries, S.N.M. Wijte, A.T. Vermeltoort, In-plane behaviour of clay brick masonry wall panels retrofitted with single-sided fabric-reinforced cementitious matrix and deep mounted carbon fibre strips, *Bull. Earthq. Eng.* 18 (2020) 725–765.
- [181] NTC18, Italian Building Code 2018, D.M. 17/01/2018, Technical code for constructions. Ministry of Transportation and Infrastructures, 2018 (in Italian).
- [182] CNR DT 215, Guide for the Design and Construction of Fiber Reinforced Inorganic Matrix Systems for Strengthening Existing Structures. Italian Council of Research (CNR), 2018.
- [183] T. Triantafillou, Strengthening of existing masonry structures: Design models. in: T.C. Triantafillou (ed) *Textile fibre composites in civil engineering*. Woodhead Publishing, Cambridge, pp 375-388, 2016.
- [184] A.K. Thomoglou, T. Rousakis, D.V. Achillopoulou, A.I. Karabinis (2021) Ultimate Shear Strength Prediction Model for Unreinforced Masonry Retrofitted Externally with Textile Reinforced Mortar, *Earthq. Struct.*, Techno-Press (accepted).
- [185] ASCE 41, Seismic evaluation and retrofit of existing buildings. ASCE, Reston VA, 2013.
- [186] M. Corradi, R. Sisti, A. Borri, Effect of Thin Cement-Based Renders on the Structural Response of Masonry Wall Panels, *Appl. Sci.* 8 (2018) 98.

APPENDIX A -Mechanical Characterisation of Flax and Jute Textile-Reinforced Mortars

Complementary test results and additional information relevant to Chapter 4

A1. YARNS

Figures A.1 - A.3 present the results obtained from the direct tensile tests on single natural fibre yarns. The corresponding mechanical properties are reported in Tables A.1 - A.3.

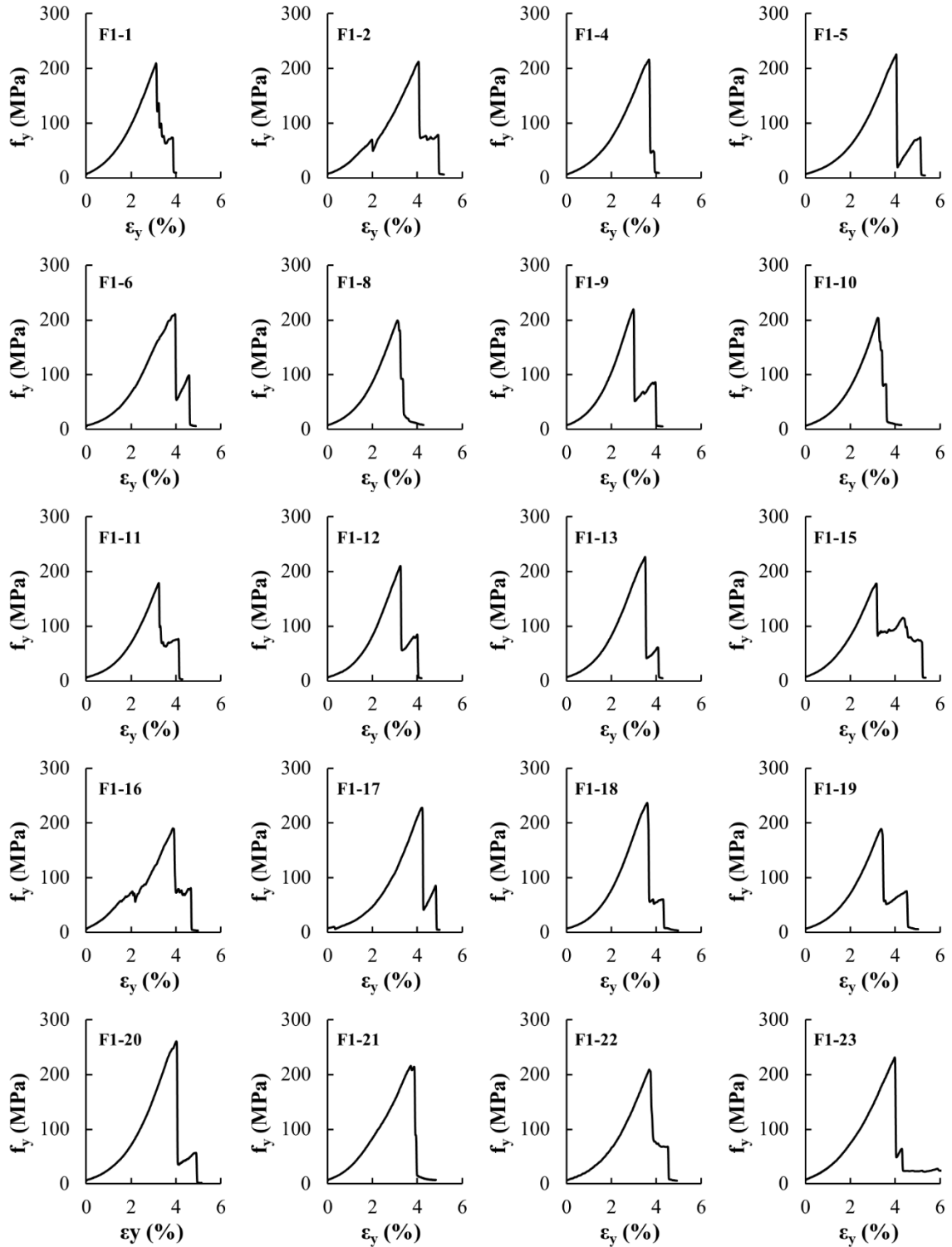


Fig. A. 1 Tensile stress-strain response of F1 yarns.

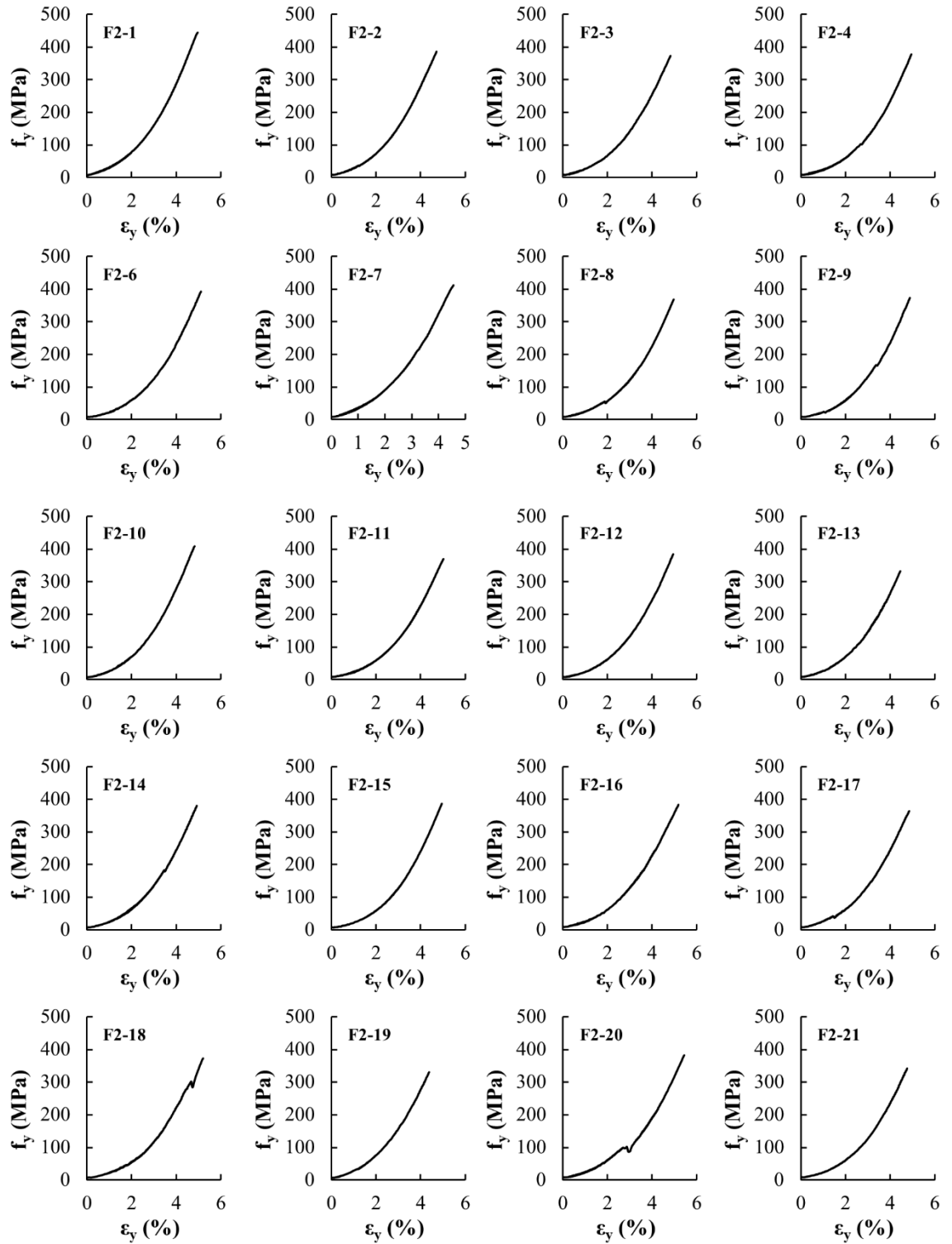


Fig. A. 2 Tensile stress-strain response of F2 yarns.

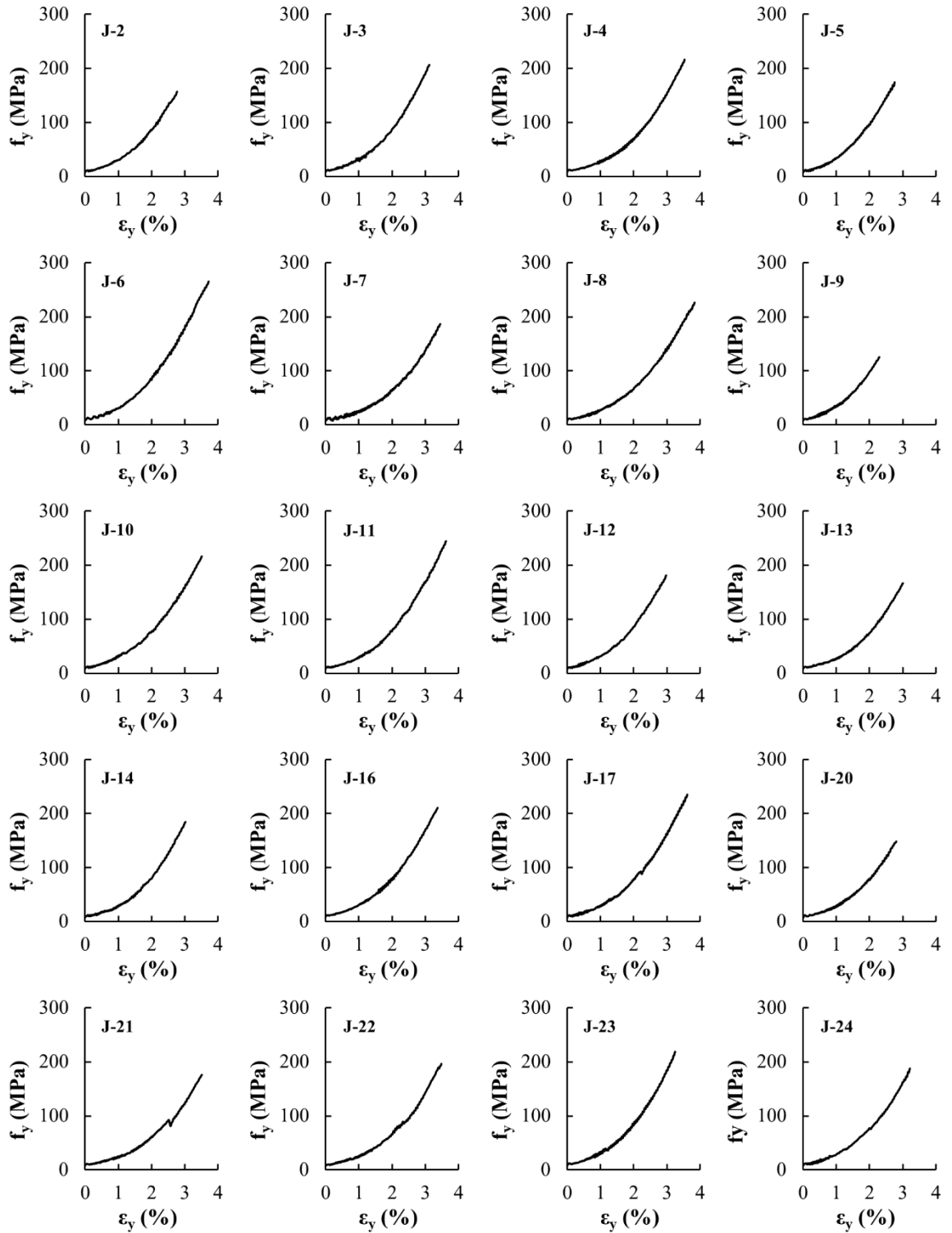


Fig. A. 3 Tensile stress-strain response of J yarns.

Table A. 1 Mechanical Properties of F1 yarns.

Yarn ID	$f_{y,max}$ (MPa)	E_y (GPa)	$\epsilon_{y,max}$ (%)
F1-1	209.4	10.6	3.11
F1-2	212.7	8.7	4.05
F1-4	216.5	9.9	3.68
F1-5	225.8	9.7	4.05
F1-6	211.1	7.9	3.95
F1-8	199.1	10.7	3.12
F1-9	219.5	12.6	2.99
F1-10	203.9	11.4	3.23
F1-11	179.1	9.8	3.23
F1-12	210.1	10.9	3.25
F1-13	226.3	10.6	3.51
F1-15	178.2	9.3	3.17
F1-16	189.8	8.4	3.86
F1-17	227.7	10.6	4.20
F1-18	236.9	11.5	3.61
F1-19	189.4	9.5	3.37
F1-20	260.7	11.5	4.01
F1-21	216.1	8.8	3.71
F1-22	209.1	9.8	3.69
F1-23	231.5	9.1	3.98
AVG (CoV)	212.6 (9%)	10.1 (12%)	3.59 (11%)

Table A. 2 Mechanical Properties of F2 yarns.

Yarn ID	$f_{y,max}$ (MPa)	E_y (GPa)	$\epsilon_{y,max}$ (%)
F2-1	444.7	16.1	4.96
F2-2	385.3	14.4	4.70
F2-3	372.4	13.9	4.84
F2-4	377.0	14.7	4.95
F2-6	392.0	14.2	5.10
F2-7	411.3	15.9	4.55
F2-8	368.5	14.6	4.97
F2-9	372.8	15.1	4.87
F2-10	407.8	20.1	4.82
F2-11	369.2	14.1	5.03
F2-12	383.7	14.2	4.95
F2-13	333.0	13.6	4.45
F2-14	380.2	14.0	4.93
F2-15	386.8	14.9	4.95
F2-16	382.8	12.9	5.19
F2-17	363.9	13.7	4.86
F2-18	372.1	11.6	5.19
F2-19	330.8	13.1	4.38
F2-20	382.4	14.0	5.44
F2-21	342.1	13.4	4.78
AVG (CoV)	377.9 (7%)	14.4 (12%)	4.90 (5%)

Table A. 3 Mechanical Properties of J yarns.

Yarn ID	$f_{y,max}$ (MPa)	E_y (GPa)	$\epsilon_{y,max}$ (%)
JC2	156.6	9.2	2.8
JC3	206.6	11.4	3.1
JC4	216.1	11.0	3.5
JC5	174.2	9.9	2.8
JC6	264.8	12.0	3.7
JC7	186.7	10.0	3.5
JC8	226.4	11.0	3.8
JC9	124.6	8.1	2.3
JC10	216.1	10.1	3.5
JC11	244.1	10.9	3.6
JC12	180.7	9.5	3.0
JC13	166.1	9.6	3.0
JC14	184.9	10.5	3.0
JC16	210.9	10.9	3.4
JC17	234.7	11.3	3.6
JC20	148.5	8.9	2.8
JC21	176.2	9.9	3.5
JC22	196.2	11.0	3.5
JC23	219.1	11.5	3.2
JC24	187.8	9.7	3.2
AVG (CoV)	196.1 (17%)	10.3 (10%)	3.3 (12%)

A2. NTRM COMPOSITES

Figures A.4 - A.12 present the results obtained from direct tensile tests on NTRM coupons. Figures A.13 - A. 22 present the development of crack width as a function of the tensile strength for each specimen, along with the associated number of cracks and location along the free length of the coupon.

A2.1 F1-TRM

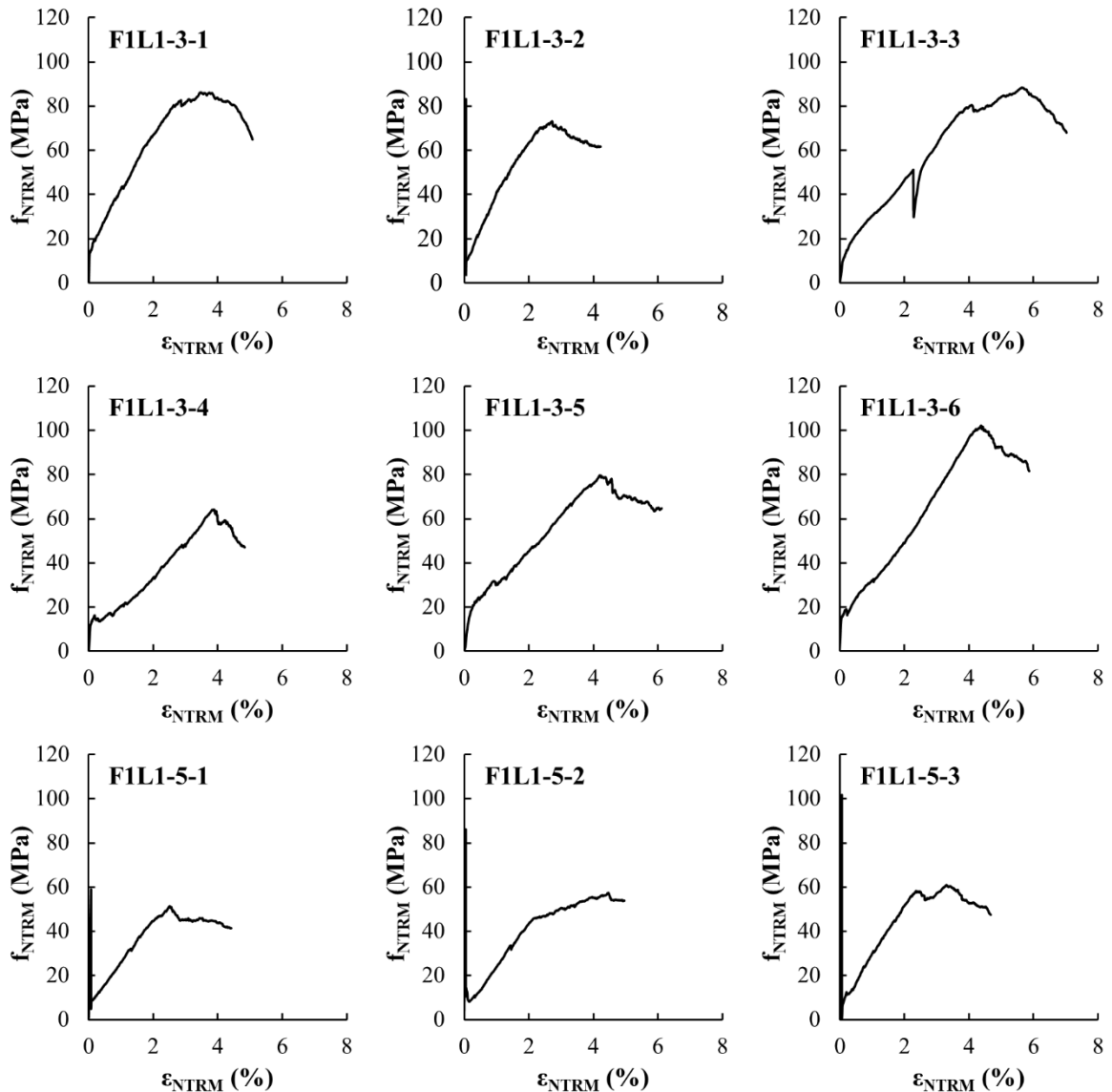


Fig. A. 4 Tensile stress-strain response of single-layer F1-TRM composites.

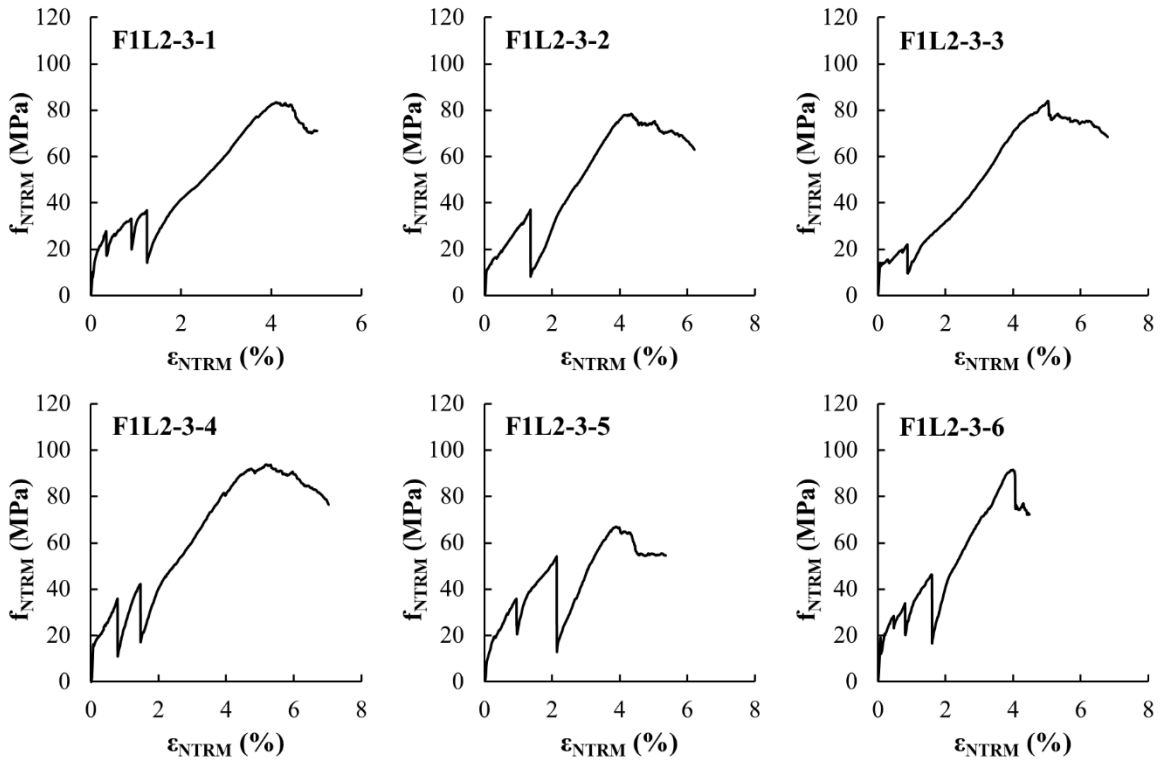


Fig. A. 5 Tensile stress-strain response of two-layer F1-TRM composites.

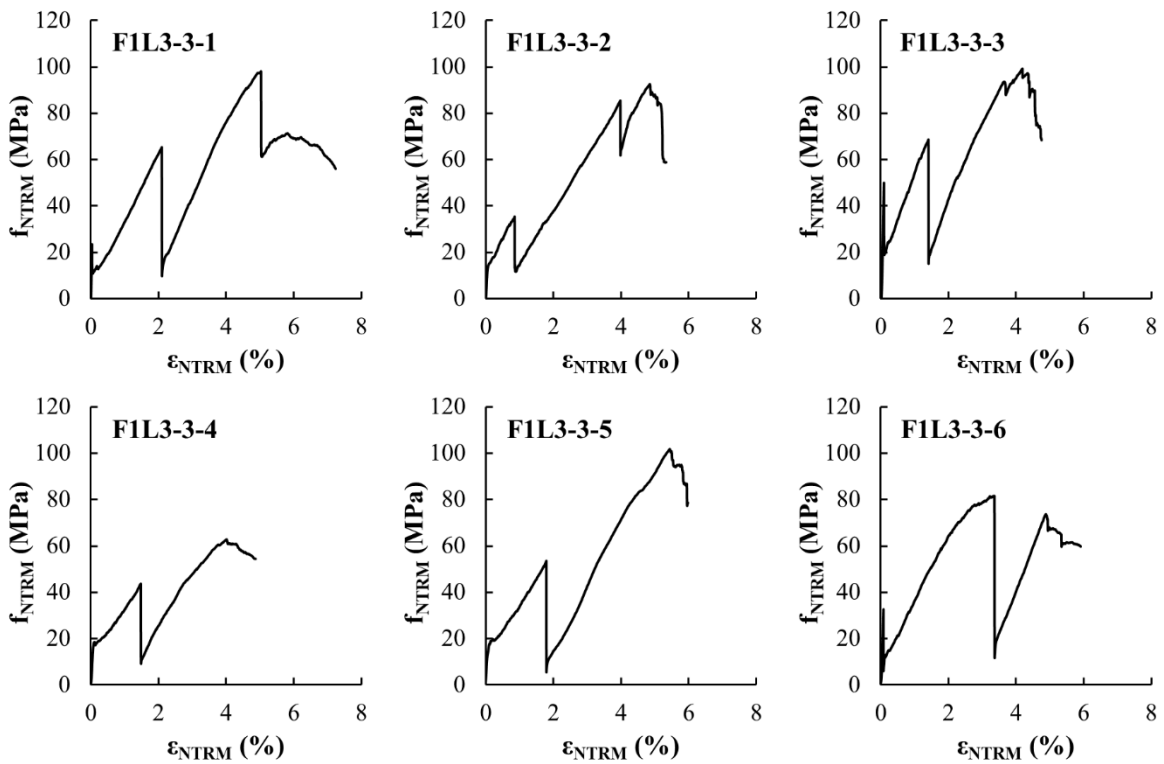


Fig. A. 6 Tensile stress-strain response of three-layer F1-TRM composites.

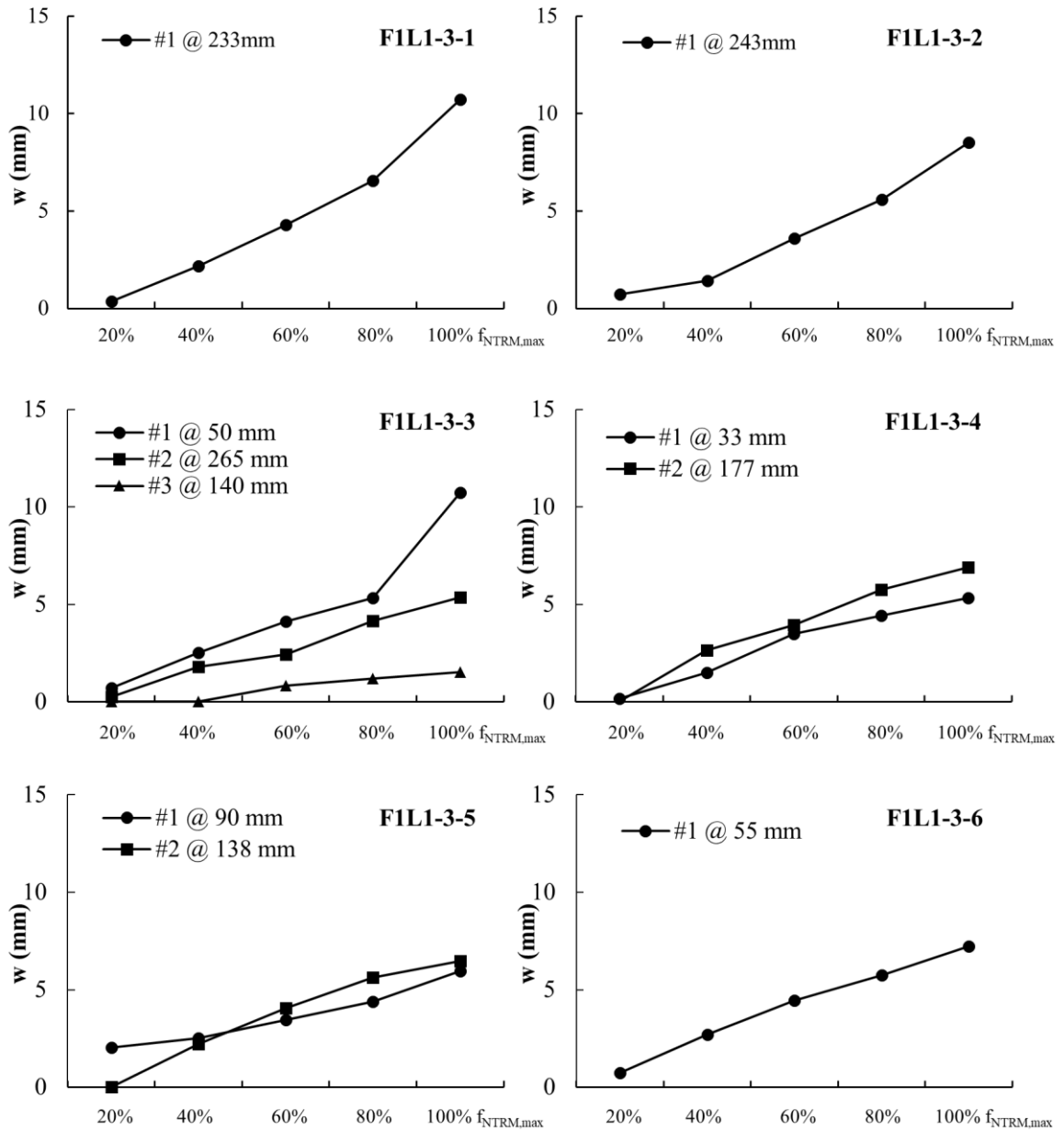


Fig. A. 7 Crack development at different levels of composite strength ($f_{NTRM,max}$), number of cracks and crack location (F1L1-3 group series).

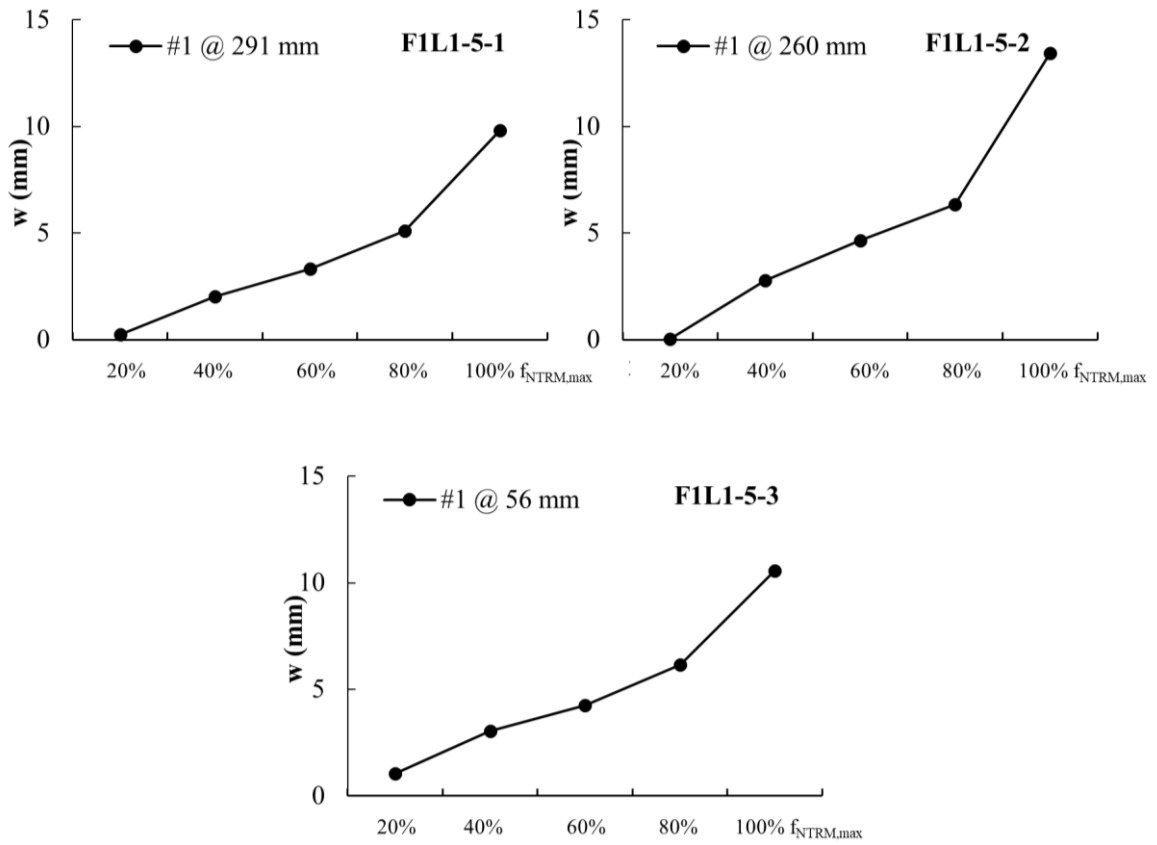


Fig. A. 8 Crack development at different levels of composite strength ($f_{NTRM,max}$), number of cracks and crack location (F1L1-5 group series).

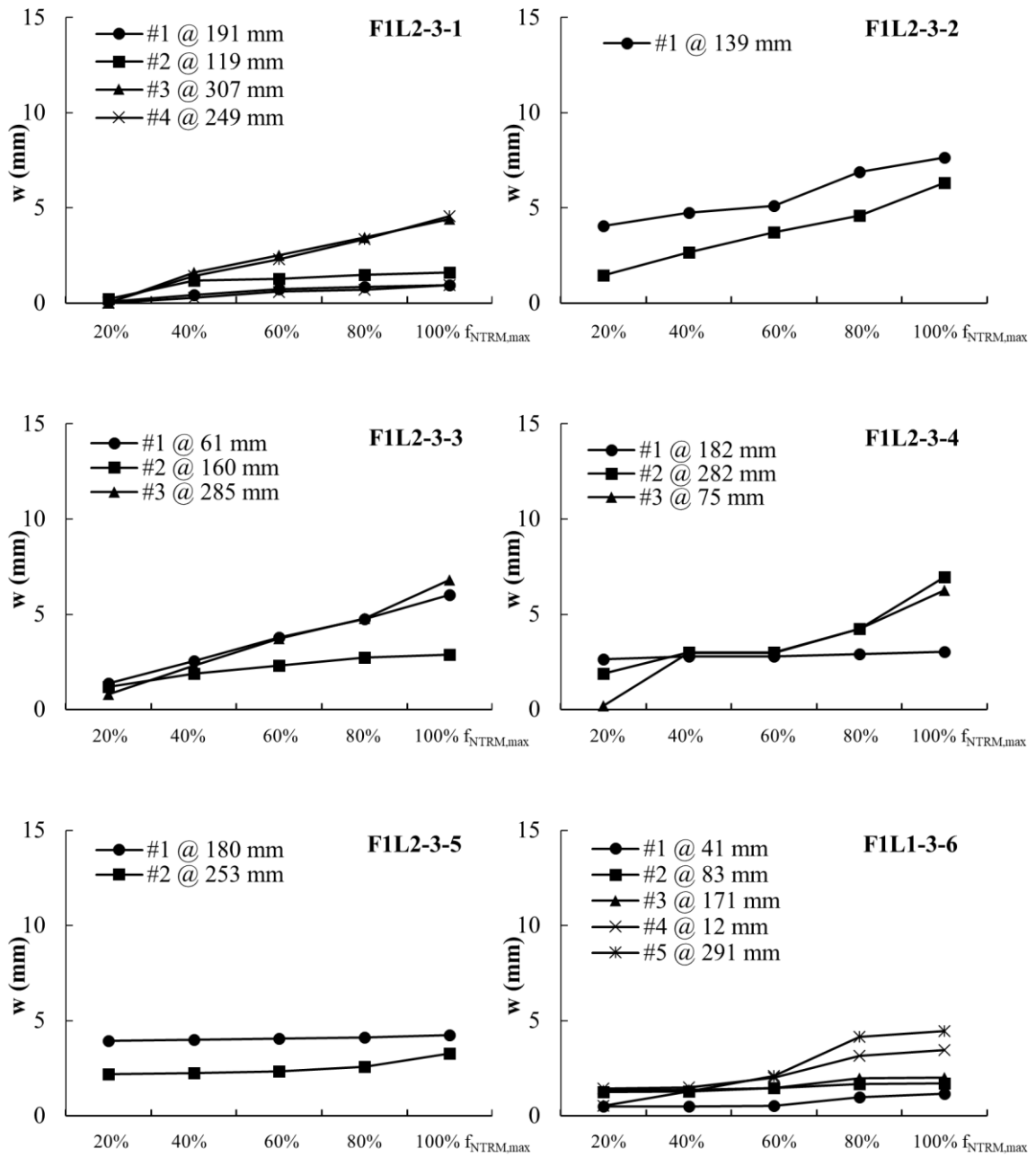


Fig. A. 9 Crack development at different levels of composite strength ($f_{NTRM,max}$), number of cracks and crack location (F1L2-3 group series).

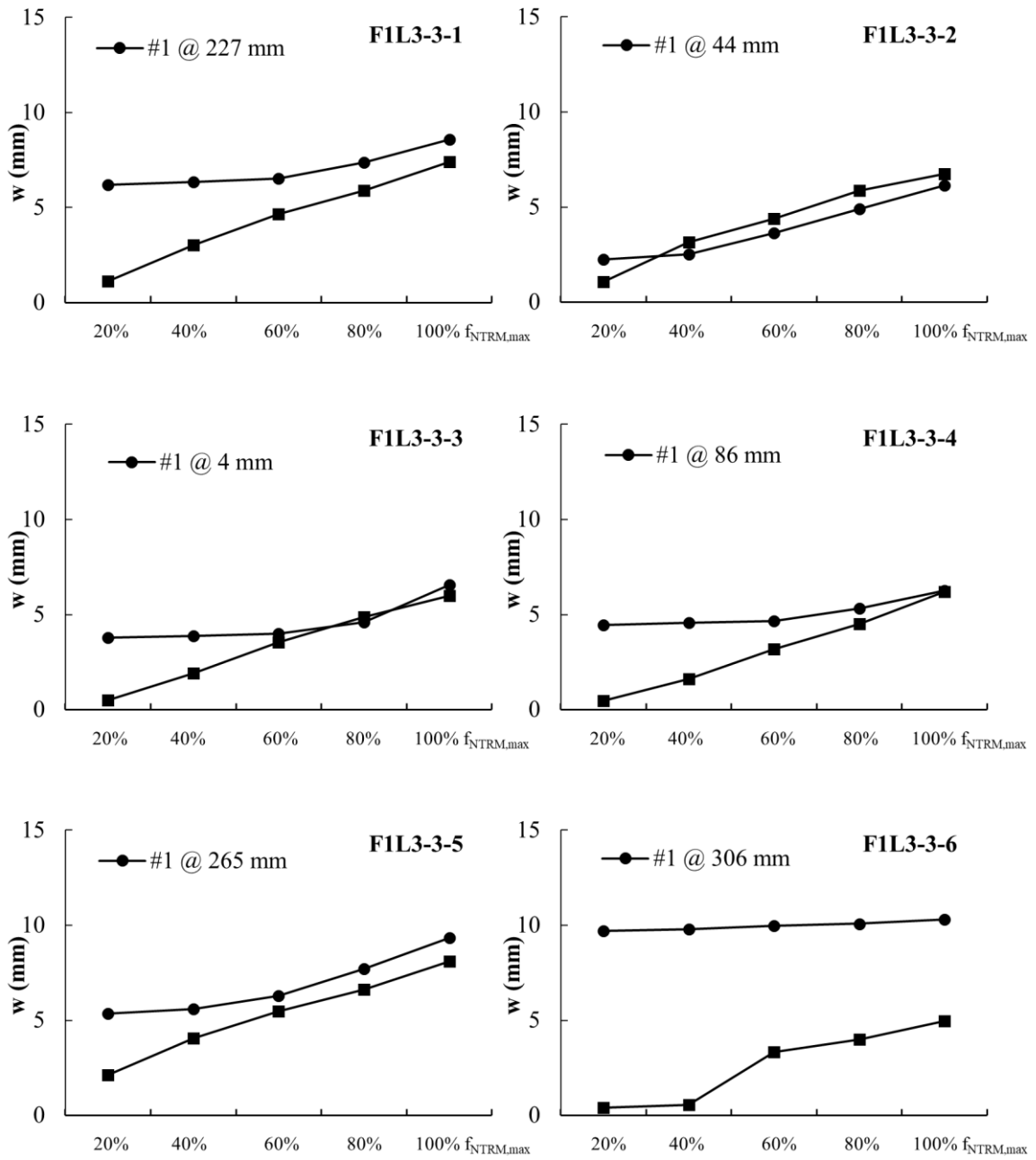


Fig. A. 10 Crack development at different levels of composite strength ($f_{NTRM,max}$), number of cracks and crack location (F1L3-3 group series).

A2.2 F2-TRM

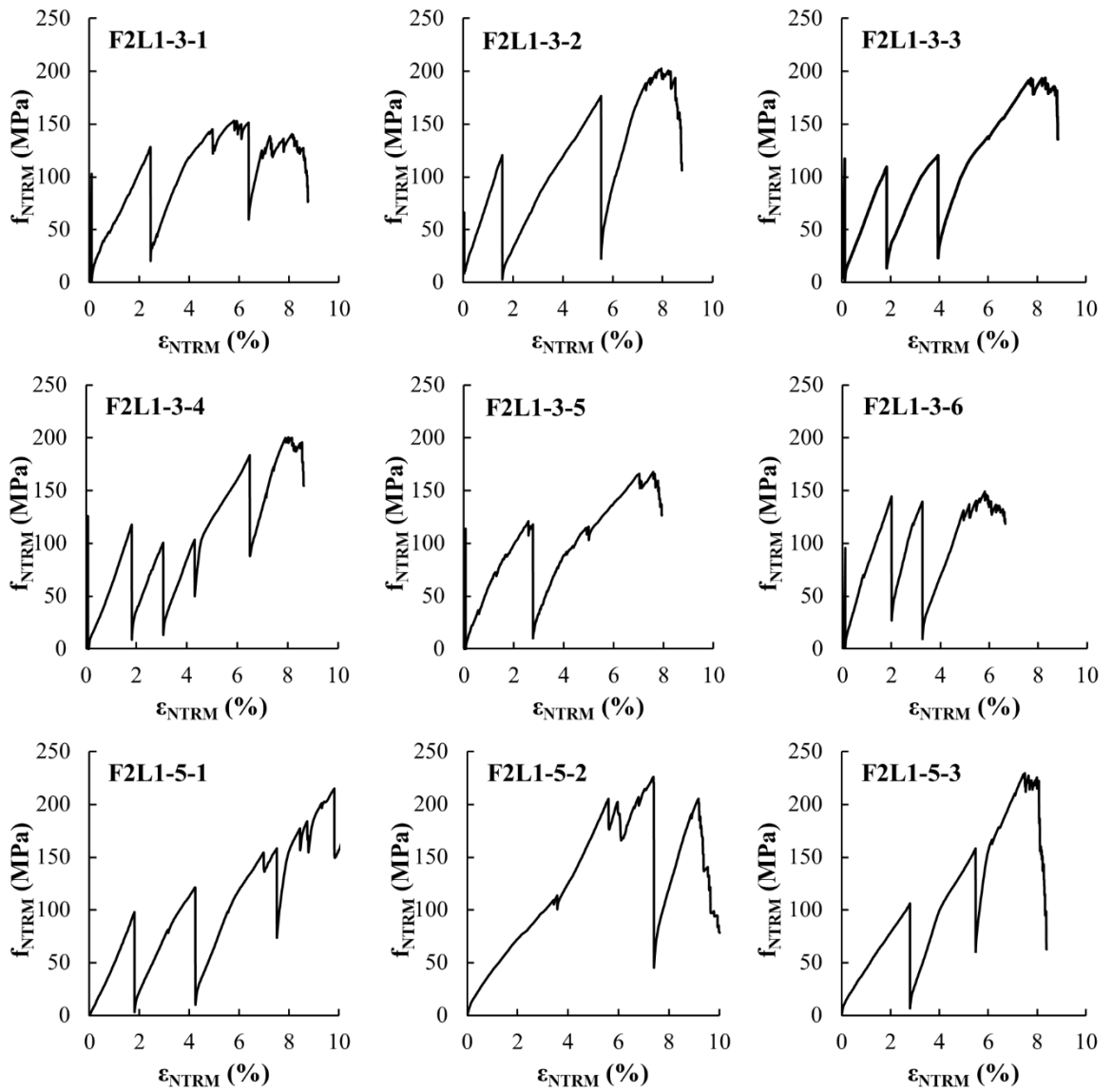


Fig. A. 11 Tensile stress-strain response of single-layer F2-TRM composites.

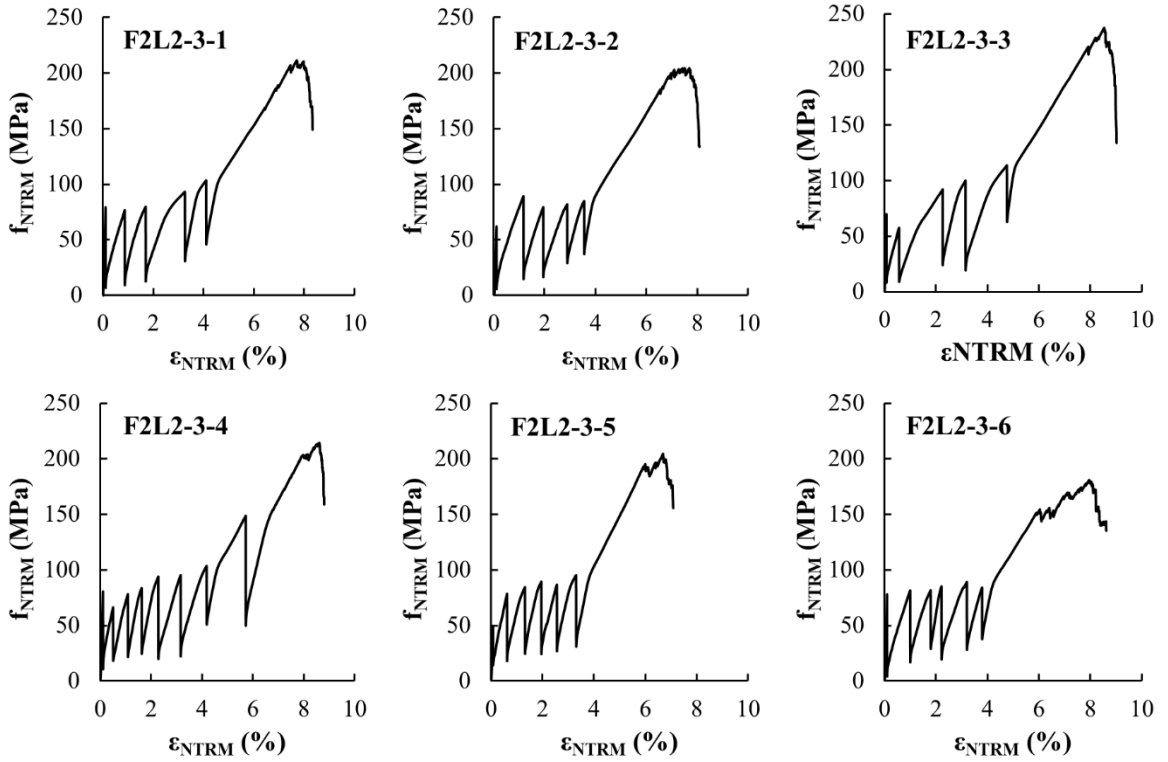


Fig. A. 12 Tensile stress-strain response of two-layer F2-TRM composites.

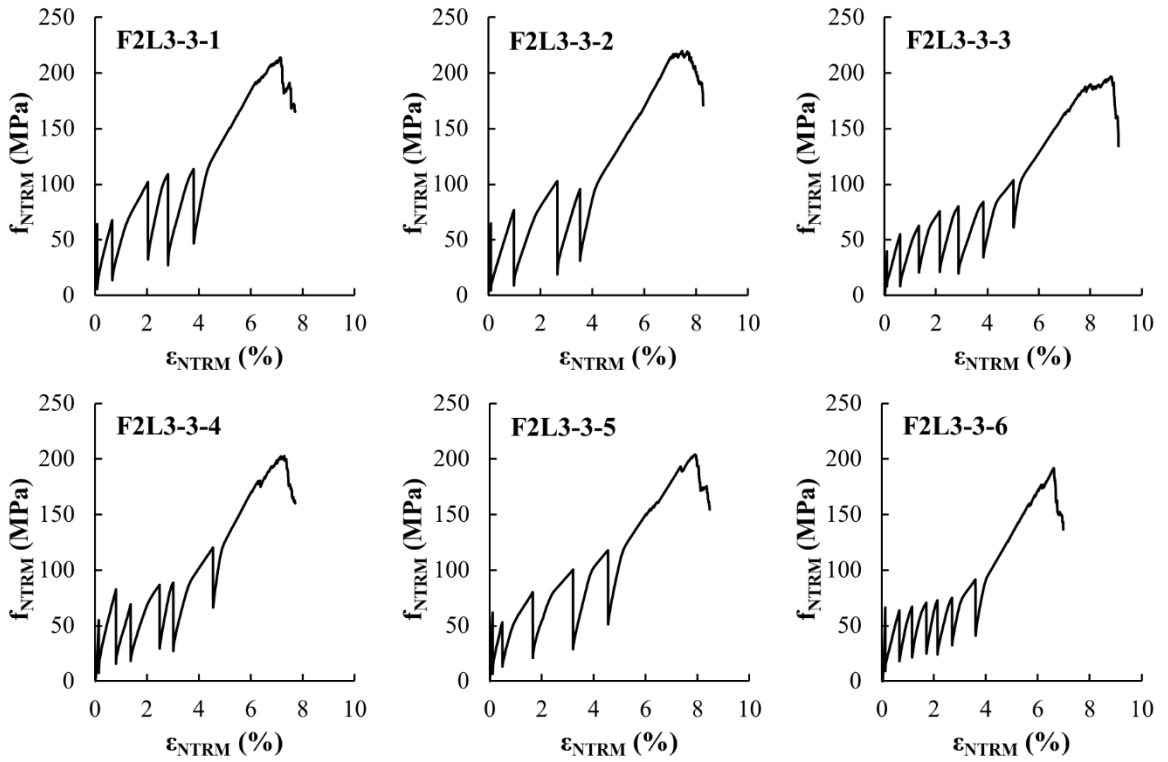


Fig. A. 13 Tensile stress-strain response of three-layer F2-TRM composites.

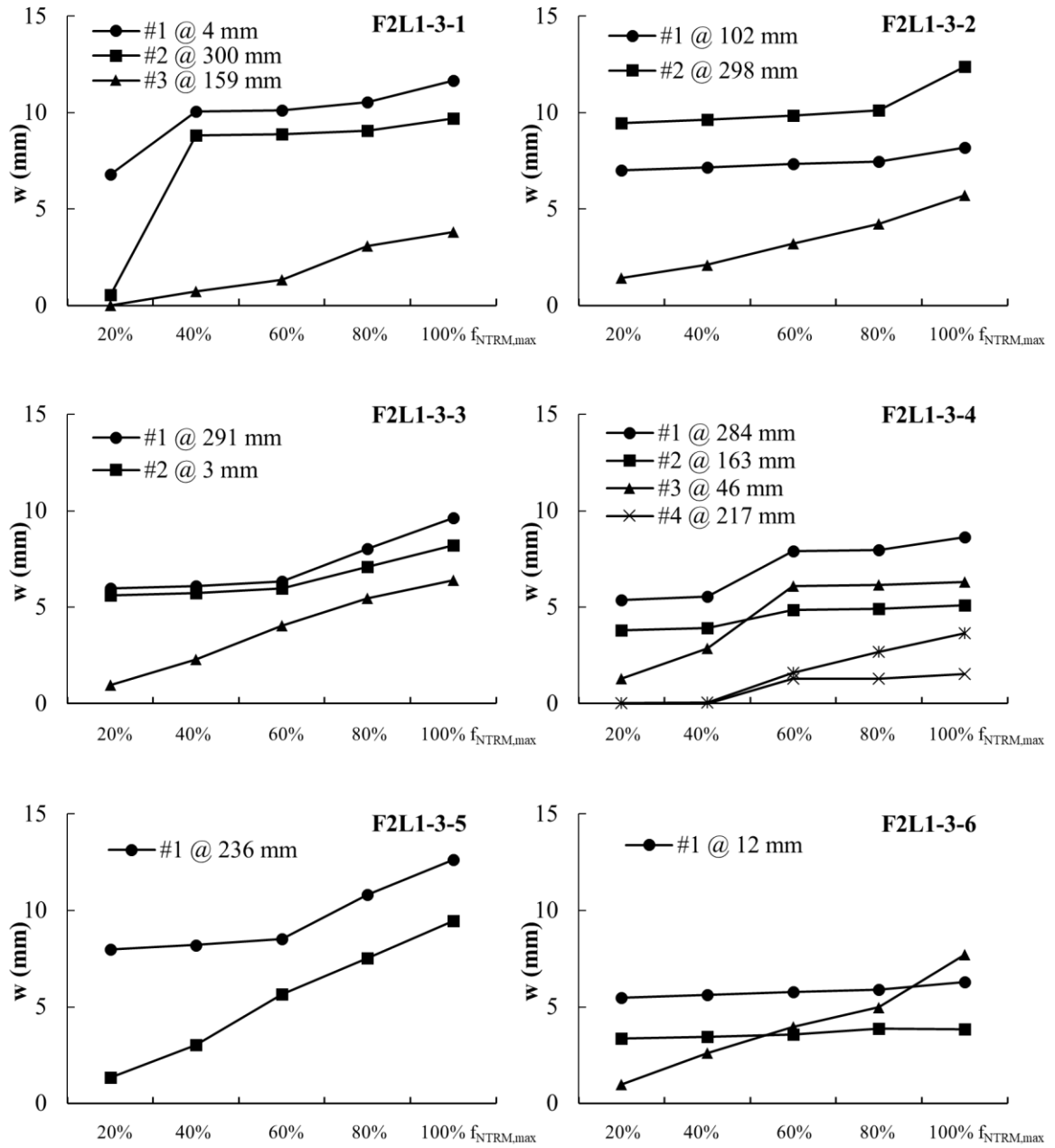


Fig. A. 14 Crack development at different levels of composite strength ($f_{NTRM,max}$), number of cracks and crack location (F2L1-3 group series).

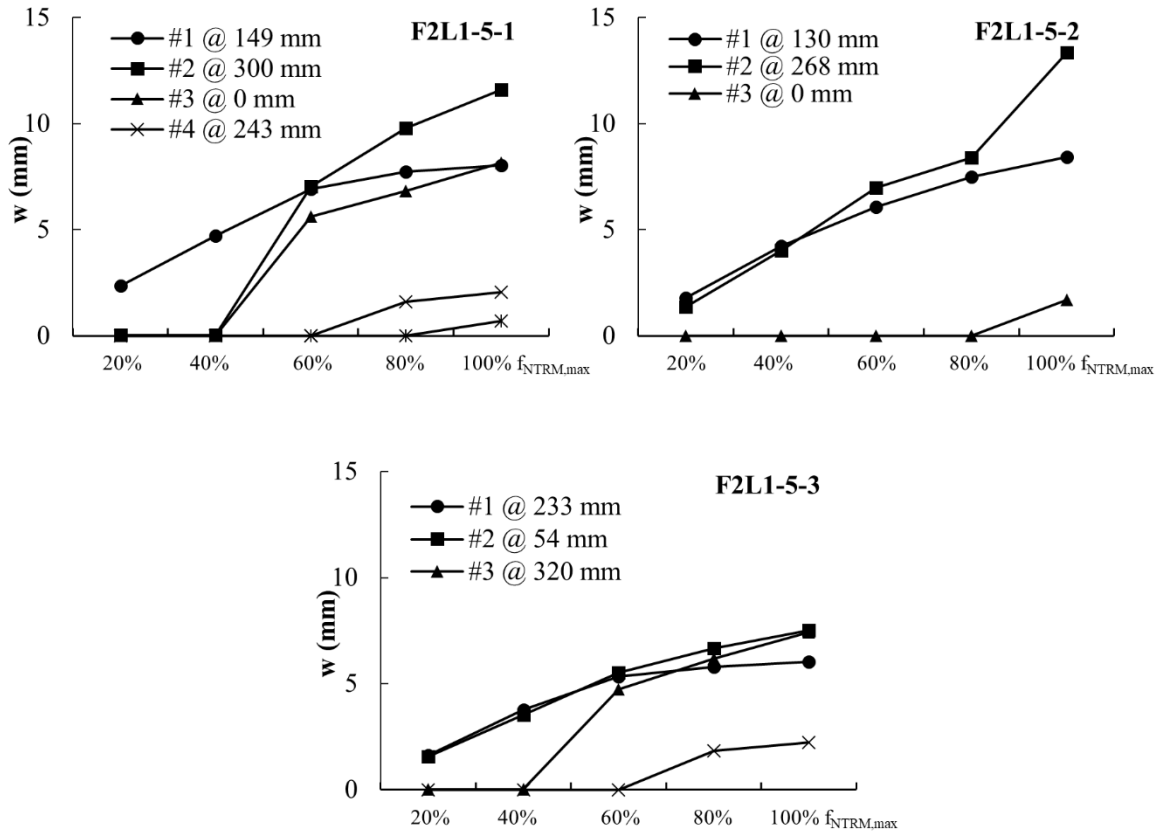


Fig. A. 15 Crack development at different levels of composite strength ($f_{NTRM,max}$), number of cracks and crack location (F2L1-5 group series).

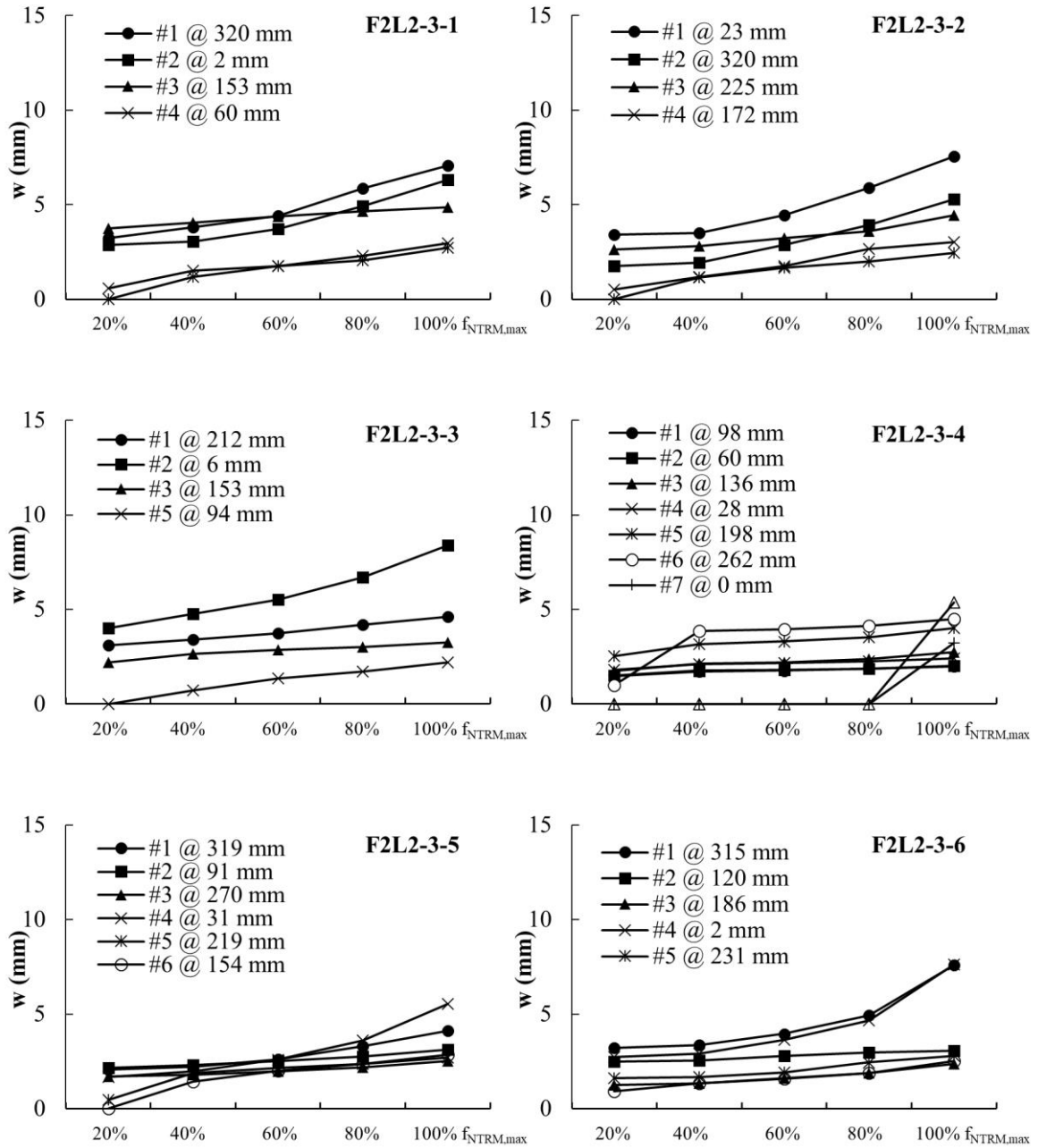


Fig. A. 16 Crack development at different levels of composite strength ($f_{NTRM,max}$), number of cracks and crack location (F2L2-3 group series).

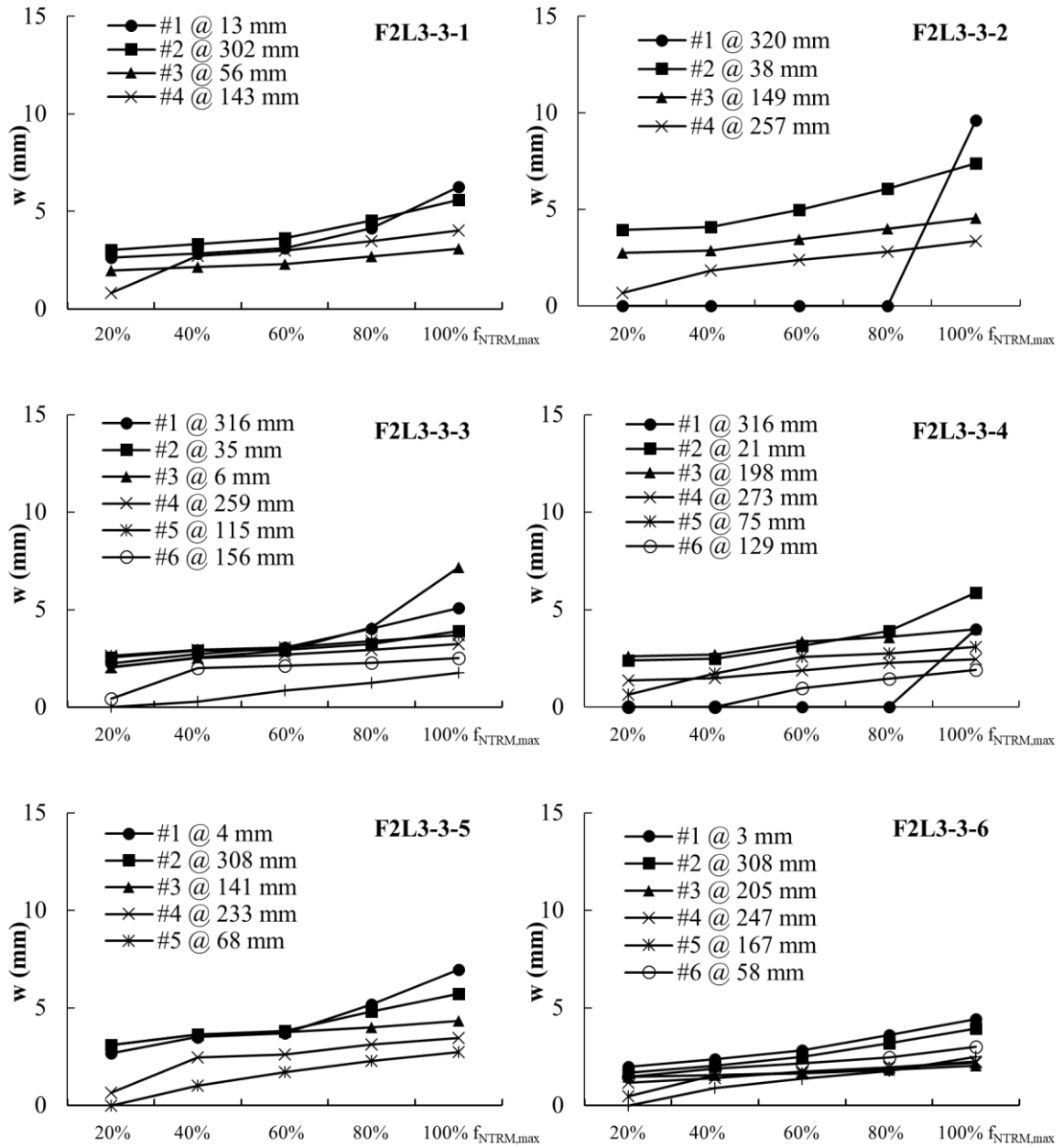


Fig. A. 17 Crack development at different levels of composite strength ($f_{NTRM,max}$), number of cracks and crack location (F2L3-3 group series).

A2.3 J-TRM

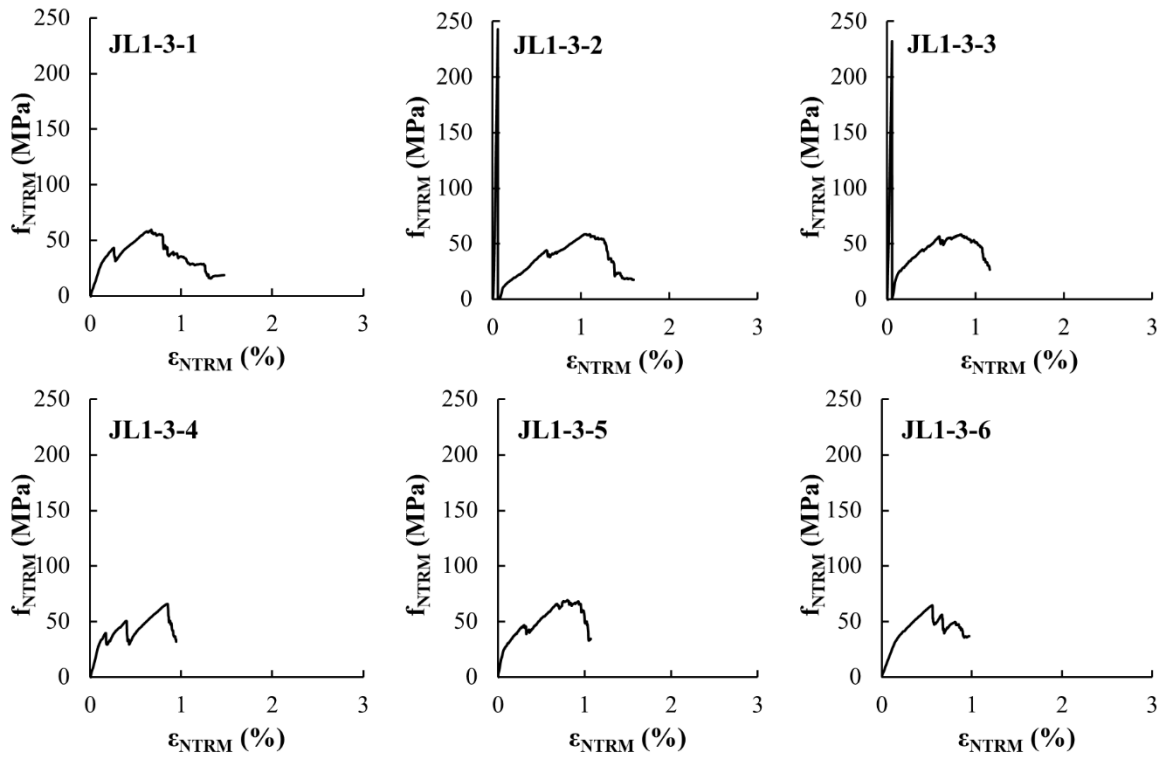


Fig. A. 18 Tensile stress-strain response of single-layer J-TRM composites.

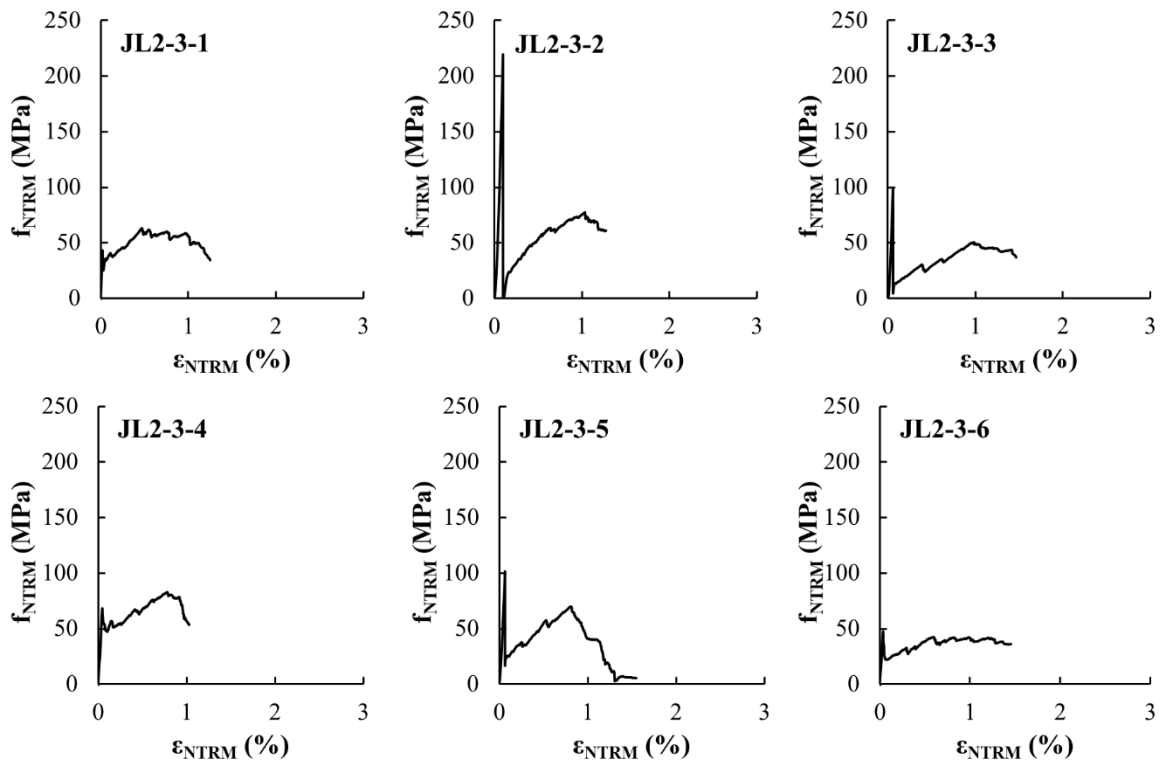


Fig. A. 19 Tensile stress-strain response of two-layer J-TRM composites.

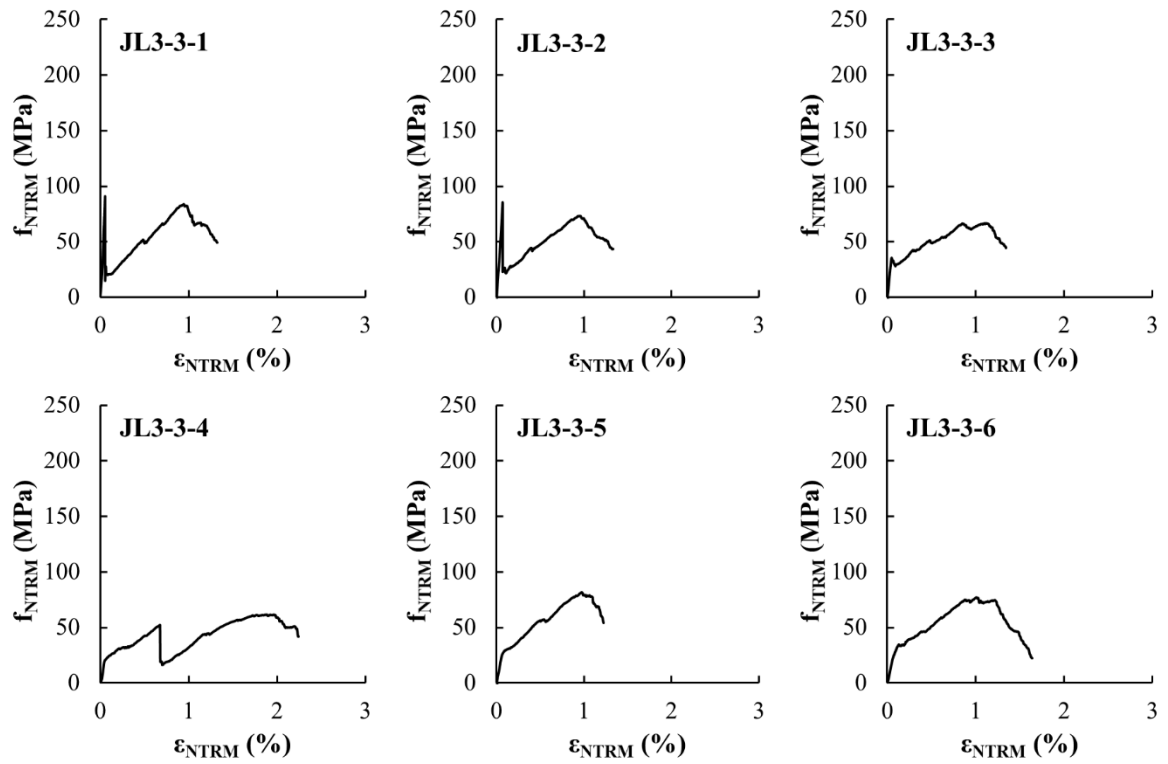


Fig. A. 20 Tensile stress-strain response of three-layer J-TRM composites.

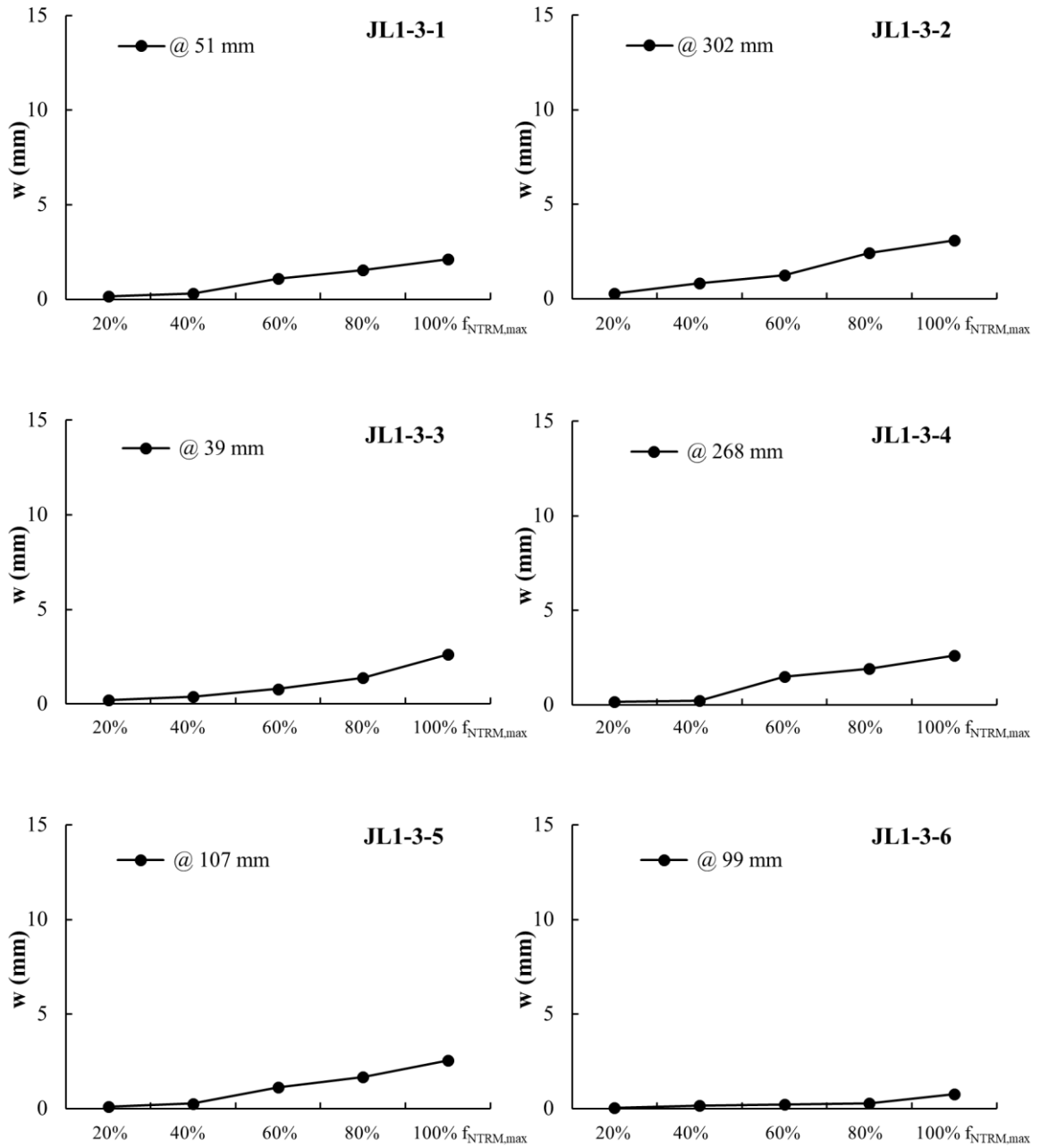


Fig. A. 21 Crack development at different levels of composite strength ($f_{NTRM,max}$), number of cracks and crack location (JL1-3 group series).

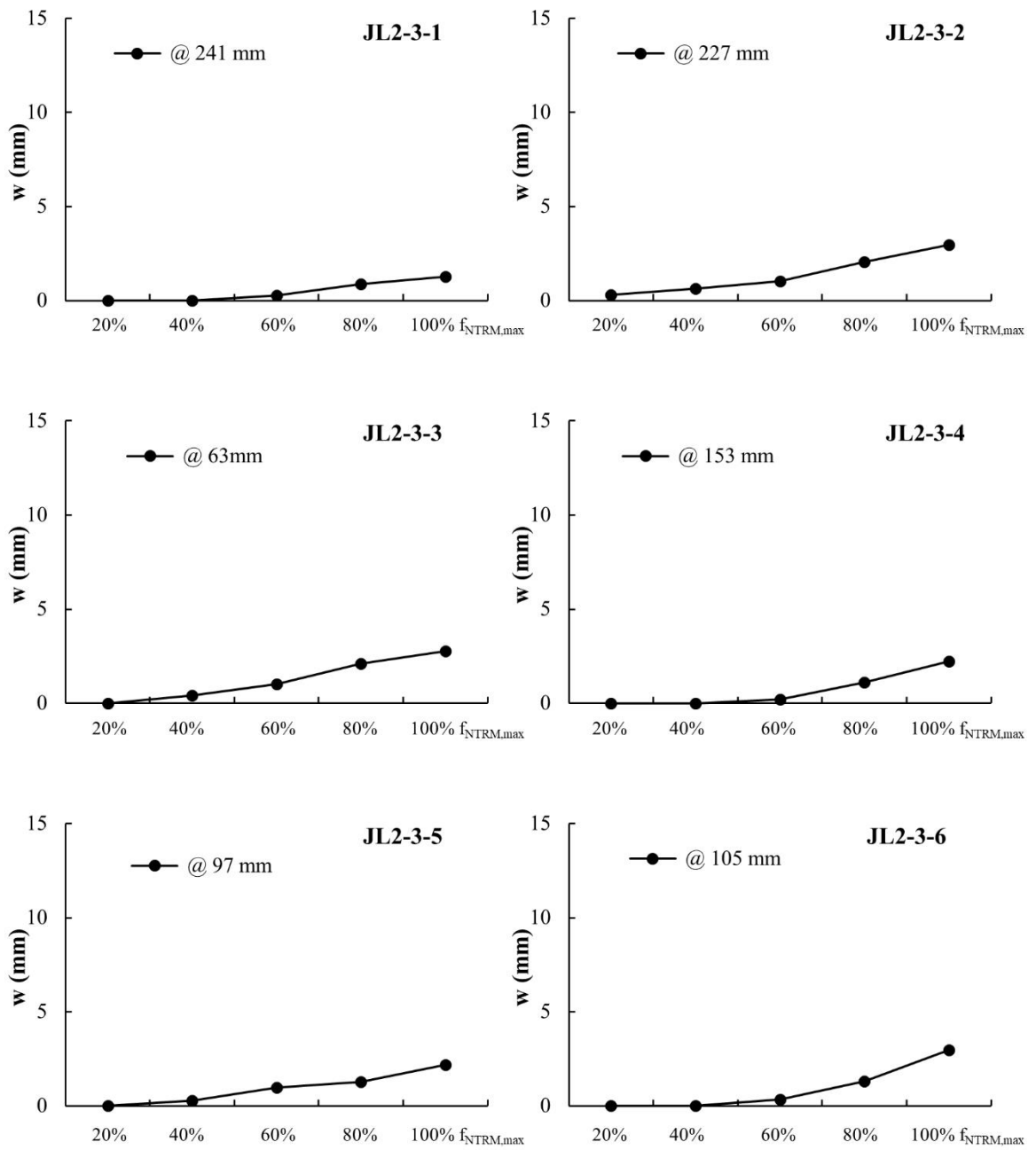


Fig. A. 22 Crack development at different levels of composite strength ($f_{NTRM,max}$), number of cracks and crack location (JL2-3 group series).

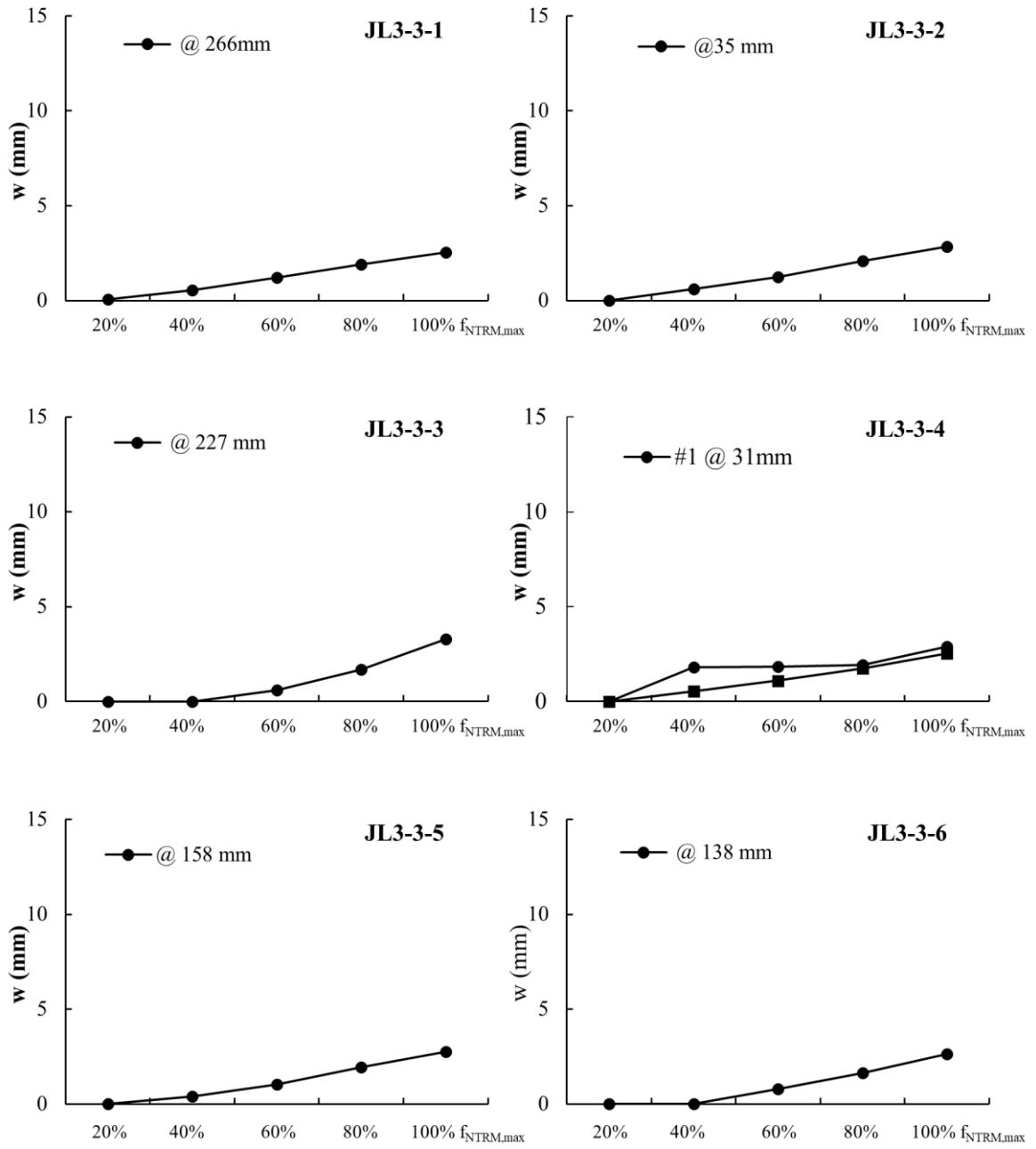


Fig. A. 23 Crack development at different levels of composite strength ($f_{NTRM,max}$), number of cracks and crack location (JL3-3 group series).

A3. CHARACTERISATION OF LIME-BASED MORTAR USED IN THE NTRM COUPONS

The following Tables present the results organised by mortar batch.

Flexure				Compression			
ID	P _{max} (N)	f _{fl} (MPa)	E (MPa)	P _{max,1} (N)	P _{max,2} (N)	P _{max} (N)	f _c (MPa)
29.03.18-1	1167.4	2.7	3798.9	9673.1	12412.3	11042.7	6.9
29.03.18-2	1123.5	2.6	3896.9	12858.3	12160.3	12509.3	7.8
29.03.18-3	1201.8	2.8	4387.5	13354.3	11398.5	12376.4	7.7
AVG (CoV)	1164.2 (3%)	2.7 (3%)	4027.8 (8%)		11976.1 (6%)		7.5 (6%)

Flexure				Compression			
ID	P _{max} (N)	f _{fl} (MPa)	E (MPa)	P _{max,1} (N)	P _{max,2} (N)	P _{max} (N)	f _c (MPa)
06.04.18-1	1090	2.6	3942.2	8937	11190	10064	6.3
06.04.18-2	869	2.0	3952.3	11046	10522	10784	6.7
06.04.18-3	948	2.2	3623.3	10897	10984	10940	6.8
AVG (CoV)	969 (10%)	2.3 (10%)	3839.3 (5%)	10596 (4%)			6.6 (4%)

Flexure				Compression			
ID	P _{max} (N)	f _{fl} (MPa)	E (MPa)	P _{max,1} (N)	P _{max,2} (N)	P _{max} (N)	f _c (MPa)
13.04.18-1	1570	3.7	3701.6	16370	15461	15915	9.9
13.04.18-2	1333	3.1	4388.3	15071	16516	15794	9.9
13.04.18-3	1403	3.3	4482.5	15274	16643	15959	10.0
AVG (CoV)	1436 (7%)	3.4 (7%)	4190.8 (10%)		15889 (0.5%)		9.9 (0.5%)

Flexure				Compression			
ID	P _{max} (N)	f _{fl} (MPa)	E (MPa)	P _{max,1} (N)	P _{max,2} (N)	P _{max} (N)	f _c (MPa)
19.04.18-1	1199	2.8	2793.6	10965	10129	10547	6.6
19.04.18-2	1058	2.5	2867.1	10391	10282	10337	6.5
19.04.18-3	1177	2.8	3481.4	12811	11959	12385	7.7
AVG (CoV)	1144 (5%)	2.7 (5%)	3047.4 (12%)		11090 (8%)		6.9 (8%)

Flexure				Compression			
ID	P _{max} (N)	f _{fl} (MPa)	E (MPa)	P _{max,1} (N)	P _{max,2} (N)	P _{max} (N)	f _c (MPa)
24.04.18-1	975	2.3	3225.6	11496	10346	10921	6.8
24.04.18-2	959	2.2	2891.8	11833	12037	11935	7.5
24.04.18-3	1045	2.4	3136.2	9591	11019	10305	6.4
AVG (CoV)	993 (4%)	2.3 (4%)	3984.6 (6%)		11054 (6%)		6.9 (6%)

Flexure				Compression			
ID	P _{max} (N)	f _{fl} (MPa)	E (MPa)	P _{max,1} (N)	P _{max,2} (N)	P _{max} (N)	f _c (MPa)
09.05.18-1	1031	2.4	2154.0	8764	9492	9128	5.7
09.05.18-2	1146	2.7	2680.5	12394	11392	11893	7.4
09.05.18-3	1093	2.6	2508.4	8304	9080	8692	5.4
AVG (CoV)	1090 (4%)	2.6 (4%)	2447.6 (11%)		9904 (14%)		6.2 (14%)

APPENDIX A

Flexure				Compression			
ID	P_{max} (N)	f_{fl} (MPa)	E (MPa)	$P_{max,1}$ (N)	$P_{max,2}$ (N)	P_{max} (N)	f_c (MPa)
11.05.18-1	1293	3.0	3625.2	13304	13975	13640	8.5
11.05.18-2	1430	3.4	3401.1	12004	12700	12352	7.7
11.05.18-3	1470	3.4	3800.9	16508	15957	16233	10.1
AVG (CoV)	1398 (5%)	3.3 (5%)	3609.1 (6%)	14075 (12%)			8.8 (12%)

Flexure				Compression			
ID	P_{max} (N)	f_{fl} (MPa)	E (MPa)	$P_{max,1}$ (N)	$P_{max,2}$ (N)	P_{max} (N)	f_c (MPa)
17.05.18-1	1041	2.4	-	11919	12574	12246	7.7
17.05.18-2	953	2.2	-	12704	13010	12857	8.0
17.05.18-3	1180	2.8	-	11894	12775	12334	7.7
AVG (CoV)	1058 (9%)	2.5 (9%)	-	12479 (2%)			7.8 (2%)

Flexure				Compression			
ID	P_{max} (N)	f_{fl} (MPa)	E (MPa)	$P_{max,1}$ (N)	$P_{max,2}$ (N)	P_{max} (N)	f_c (MPa)
21.05.18-1	1079	2.5	3125.7	11522	12343	11932	7.5
21.05.18-2	1187	2.8	2936.2	13363	12273	12818	8.0
21.05.18-3	1103	2.6	3064.8	12405	11748	12076	7.5
AVG (CoV)	1123 (4%)	2.6 (4%)	3042.3 (3%)	12276 (3%)			7.7 (3%)

Notation

f_y	tensile stress of yarn
ϵ_y	tensile strain of yarn
E_y	tensile elastic modulus of yarn
$f_{y,max}$	tensile strength of yarn
$\epsilon_{y,max}$	ultimate tensile strain of yarn
w	crack width
$f_{NTRM,max}$	tensile strength of NTRM coupon

APPENDIX B - Bond Performance of FLAX-TRM to Masonry

Complementary testing and additional information relevant to Chapter 5

B.1 SPECIMEN PREPARATION DETAILS

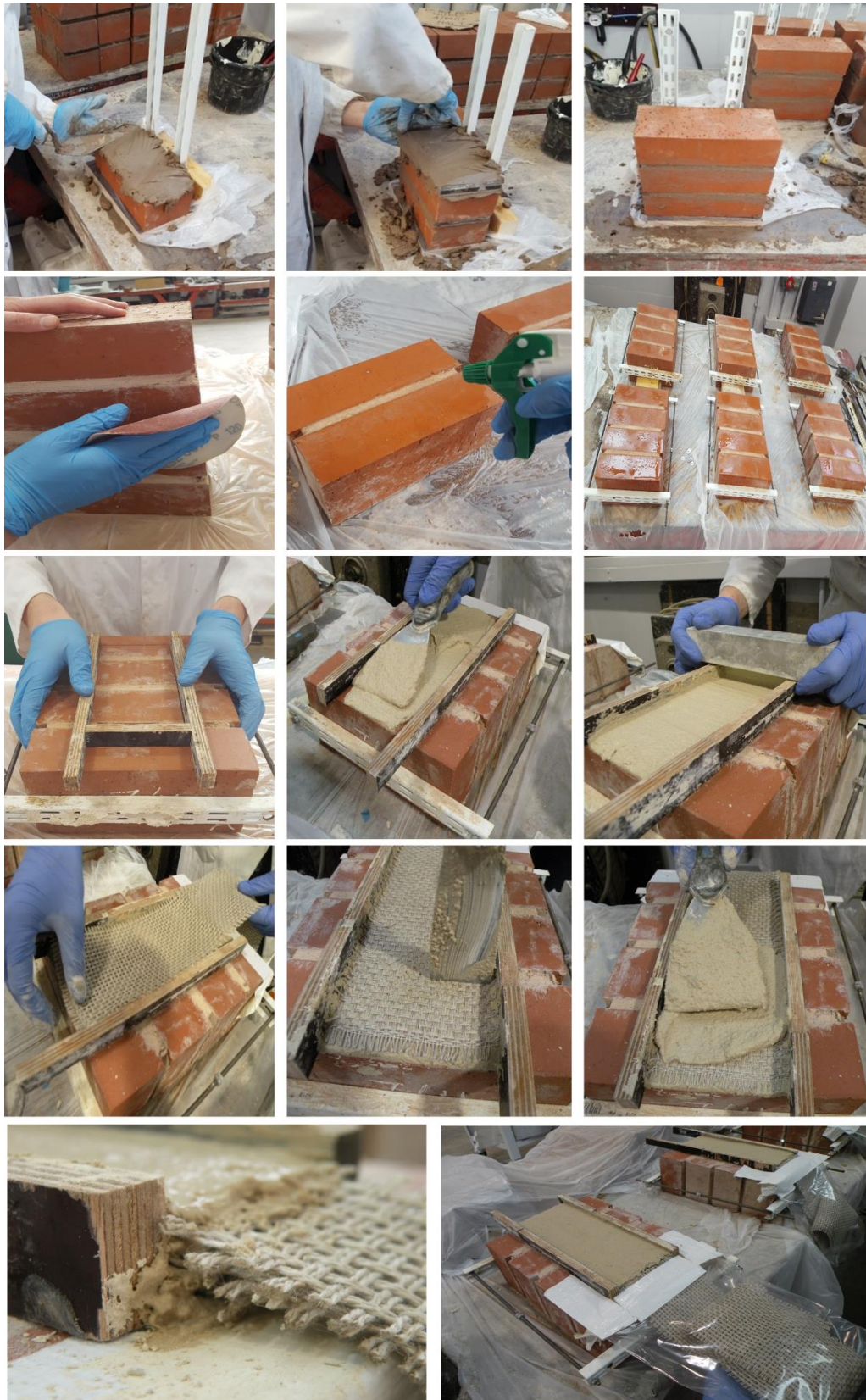


Fig. B. 1 Specimen preparation for shear bond tests.

B2. CHARACTERISATION OF MASONRY MORTAR

The following Tables present the results organised by mortar batch.

Flexure			Compression			
ID	P_{max} (N)	f_{fl} (MPa)	$P_{max,1}$ (N)	$P_{max,2}$ (N)	P_{max} (N)	f_c (MPa)
11.10.17-1	296.4	0.69	3734.6	3734.4	3734.5	2.3
11.10.17-2	248.4	0.58	3406.1	3340.9	3373.5	2.1
11.10.17-3	256.2	0.60	3358.8	3336.3	3347.5	2.1
AVG (CoV)	267.0 (8%)	0.6 (8%)		3485.2 (5%)		2.2 (5%)

Flexure			Compression			
ID	P_{max} (N)	f_{fl} (MPa)	$P_{max,1}$ (N)	$P_{max,2}$ (N)	P_{max} (N)	f_c (MPa)
12.10.17-1	323.7	0.8	3784.8	3633.2	3709.0	2.3
12.10.17-2	354.9	0.8	3505.5	3380.0	3442.7	2.2
12.10.17-3	334.1	0.8	3806.4	3509.1	3657.8	2.3
AVG (CoV)	337.5 (4%)	0.8 (4%)		3603.2 (3%)		2.3 (3%)

Flexure			Compression			
ID	P_{max} (N)	f_{fl} (MPa)	$P_{max,1}$ (N)	$P_{max,2}$ (N)	P_{max} (N)	f_c (MPa)
18.10.17-1	278.6	0.7	3181.7	3420.1	3300.9	2.1
18.10.17-2	262.9	0.6	3469.7	3318.8	3394.3	2.1
18.10.17-3	291.1	0.7	3539.0	3575.4	3557.2	2.2
AVG (CoV)	277.5 (4%)	0.7 (4%)		3417.5 (3%)		2.1 (3%)

Flexure			Compression			
ID	P_{max} (N)	f_{fl} (MPa)	$P_{max,1}$ (N)	$P_{max,2}$ (N)	P_{max} (N)	f_c (MPa)
23.10.17-1	232.6	0.6	3114.2	3041.1	3077.6	1.9
23.10.17-2	260.6	0.6	3480.4	3405.6	3443.0	2.2
23.10.17-3	256.2	0.6	3060.5	3403.1	3231.8	2.0
AVG (CoV)	249.8 (5%)	0.6 (5%)		3250.8 (5%)		2.0 (5%)

Flexure			Compression			
ID	P_{max} (N)	f_{fl} (MPa)	$P_{max,1}$ (N)	$P_{max,2}$ (N)	P_{max} (N)	f_c (MPa)
07.11.17-1	313.6	0.7	3668.0	3180.9	3424.5	2.1
07.11.17-2	274.6	0.6	3482.5	3430.6	3456.6	2.2
07.11.17-3	257.8	0.6	3875.6	3749.0	3812.3	2.4
AVG (CoV)	282.0 (8%)	0.7 (8%)		3564.4 (5%)		2.2 (5%)

Flexure			Compression			
ID	P_{max} (N)	f_{fl} (MPa)	$P_{max,1}$ (N)	$P_{max,2}$ (N)	P_{max} (N)	f_c (MPa)
09.11.17-1	285.5	0.7	3527.1	3322.8	3424.9	2.1
09.11.17-2	239.9	0.6	3680.4	3610.8	3645.6	2.3
09.11.17-3	284.3	0.7	3532.4	3586.1	3559.2	2.2
AVG (CoV)	269.9 (8%)	0.6 (8%)		3543.3 (3%)		2.2 (3%)

Flexure			Compression			
ID	P _{max} (N)	f _{fl} (MPa)	P _{max,1} (N)	P _{max,2} (N)	P _{max} (N)	f _c (MPa)
15.11.17-1	384.0	0.9	3857.8	4042.7	3950.2	2.5
15.11.17-2	372.7	0.9	4098.1	4314.7	4206.4	2.6
15.11.17-3	344.0	0.8	4015.6	4240.8	4128.2	2.6
AVG (CoV)	366.9 (5%)	0.9 (5%)		4094.9 (3%)		2.6 (3%)

Flexure			Compression			
ID	P _{max} (N)	f _{fl} (MPa)	P _{max,1} (N)	P _{max,2} (N)	P _{max} (N)	f _c (MPa)
17.11.17-1	315.9	0.7	3186.1	3058.4	3122.2	2.0
17.11.17-2	310.4	0.7	3119.1	3132.4	3125.7	2.0
17.11.17-3	326.5	0.8	3645.3	3264.0	3454.6	2.2
AVG (CoV)	317.6 (2%)	0.7 (2%)		3234.2 (5%)		2.0 (5%)

Flexure			Compression			
ID	P _{max} (N)	f _{fl} (MPa)	P _{max,1} (N)	P _{max,2} (N)	P _{max} (N)	f _c (MPa)
27.11.17-1	280.4	0.7	3922.3	3890.5	3906.4	2.4
27.11.17-2	242.3	0.6	4151.8	3897.2	4024.5	2.5
27.11.17-3	272.1	0.6	3860.4	4031.0	3945.7	2.5
AVG (CoV)	264.9 (6%)	0.6 (6%)		3958.9 (1%)		2.5 (1%)

Flexure			Compression			
ID	P _{max} (N)	f _{fl} (MPa)	P _{max,1} (N)	P _{max,2} (N)	P _{max} (N)	f _c (MPa)
29.11.17-1	247.2	0.6	3513.0	3789.8	3651.4	2.3
29.11.17-2	272.5	0.6	4084.1	4292.8	4188.5	2.6
29.11.17-3	282.4	0.7	3739.7	4015.8	3877.7	2.4
AVG (CoV)	267.4 (6%)	0.6 (6%)		3905.9 (6%)		2.4 (6%)

Flexure			Compression			
ID	P _{max} (N)	f _{fl} (MPa)	P _{max,1} (N)	P _{max,2} (N)	P _{max} (N)	f _c (MPa)
01.12.17-1	413.1	1.0	4091.2	4056.1	4073.7	2.5
01.12.17-2	295.4	0.7	3606.8	3864.1	3735.4	2.3
01.12.17-3	274.2	0.6	3654.3	3869.1	3761.7	2.4
AVG (CoV)	327.6 (19%)	0.8 (19%)		3856.9 (4%)		2.4 (4%)

Flexure			Compression			
ID	P _{max} (N)	f _{fl} (MPa)	P _{max,1} (N)	P _{max,2} (N)	P _{max} (N)	f _c (MPa)
05.12.17-1	356.4	0.8	3999.0	3977.3	3988.1	2.5
05.12.17-2	330.9	0.8	3856.1	3569.2	3713.0	2.3
05.12.17-3	341.0	0.8	4085.1	4104.6	4094.8	2.6
AVG (CoV)	342.8 (3%)	0.8 (3%)		3932.0 (4%)		2.5 (4%)

Flexure			Compression			
ID	P_{max} (N)	f_n (MPa)	$P_{max,1}$ (N)	$P_{max,2}$ (N)	P_{max} (N)	f_c (MPa)
08.12.17-1A	235.4	0.6	4279.6	4238.6	4259.1	2.7
08.12.17-2A	301.8	0.7	3578.2	3776.4	3677.3	2.3
08.12.17-3A	328.4	0.8	4460.9	4413.3	4437.1	2.8
AVG (CoV)	288.5 (14%)	0.7 (14%)		4124.5 (8%)		2.6 (8%)

Flexure			Compression			
ID	P_{max} (N)	f_n (MPa)	$P_{max,1}$ (N)	$P_{max,2}$ (N)	P_{max} (N)	f_c (MPa)
08.12.17-1B	269.8	0.6	4234.3	4463.9	4349.1	2.7
08.12.17-2B	242.6	0.6	3483.0	3901.9	3692.4	2.3
08.12.17-3B	185.0	0.4	3774.3	3859.8	3817.1	2.4
AVG (CoV)	232.5 (15%)	0.5 (15%)		3952.9 (7%)		2.5 (7%)

B3. CHARACTERISATION OF MASONRY

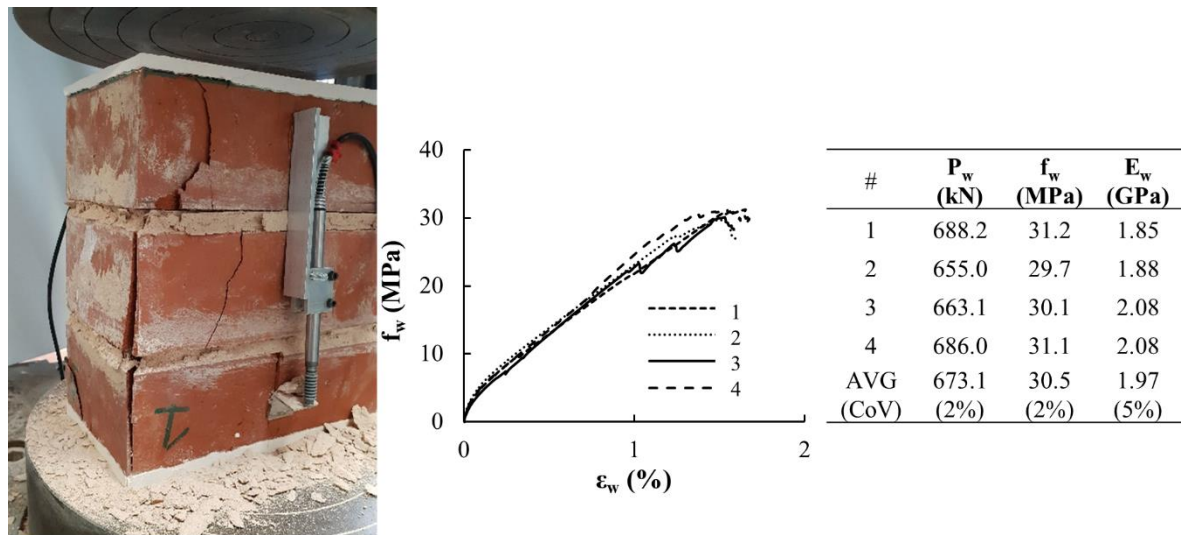


Fig. B. 2 Compression test results on masonry triplets.

B4. BOND TEST RESULTS



Fig. B. 3 Load-slip responses and typical failure mode of excluded F2L1-110-260 group series.

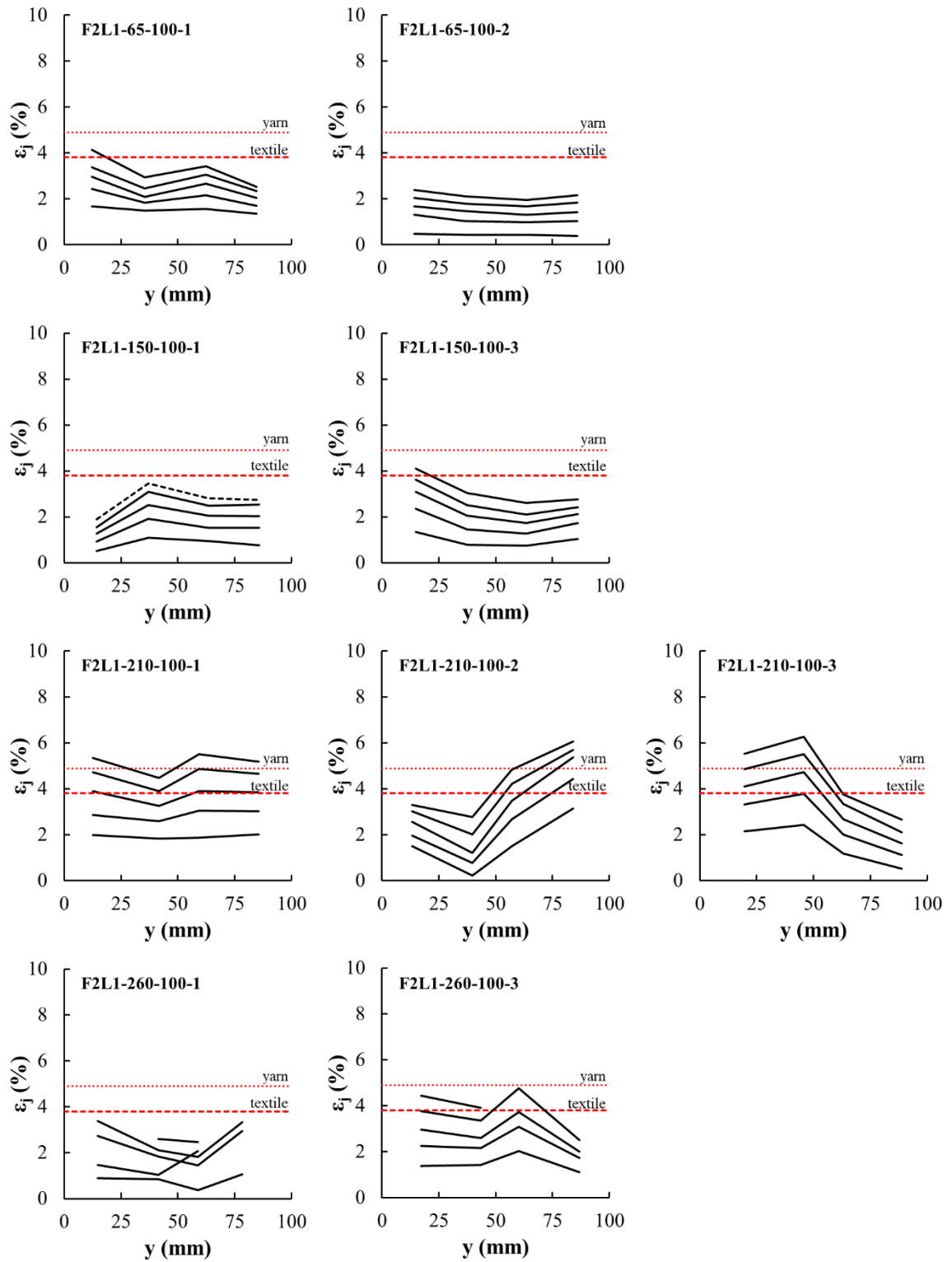


Fig. B. 4 Strain profile across the width of the unbonded textile at different loading stages (F2L1-260-100 group series).

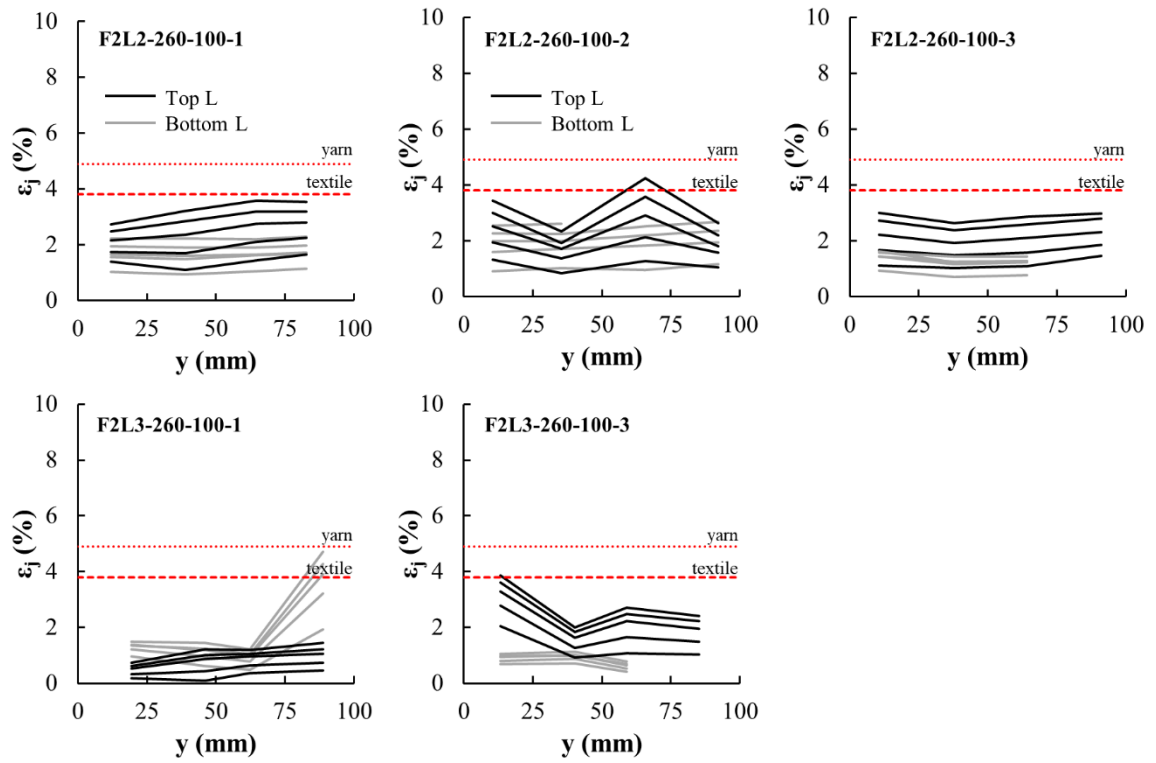


Fig. B. 5 Strain profile across the width of the unbonded textile at different loading stages (F2L2-260-100 and F2L3-260-100 group series).

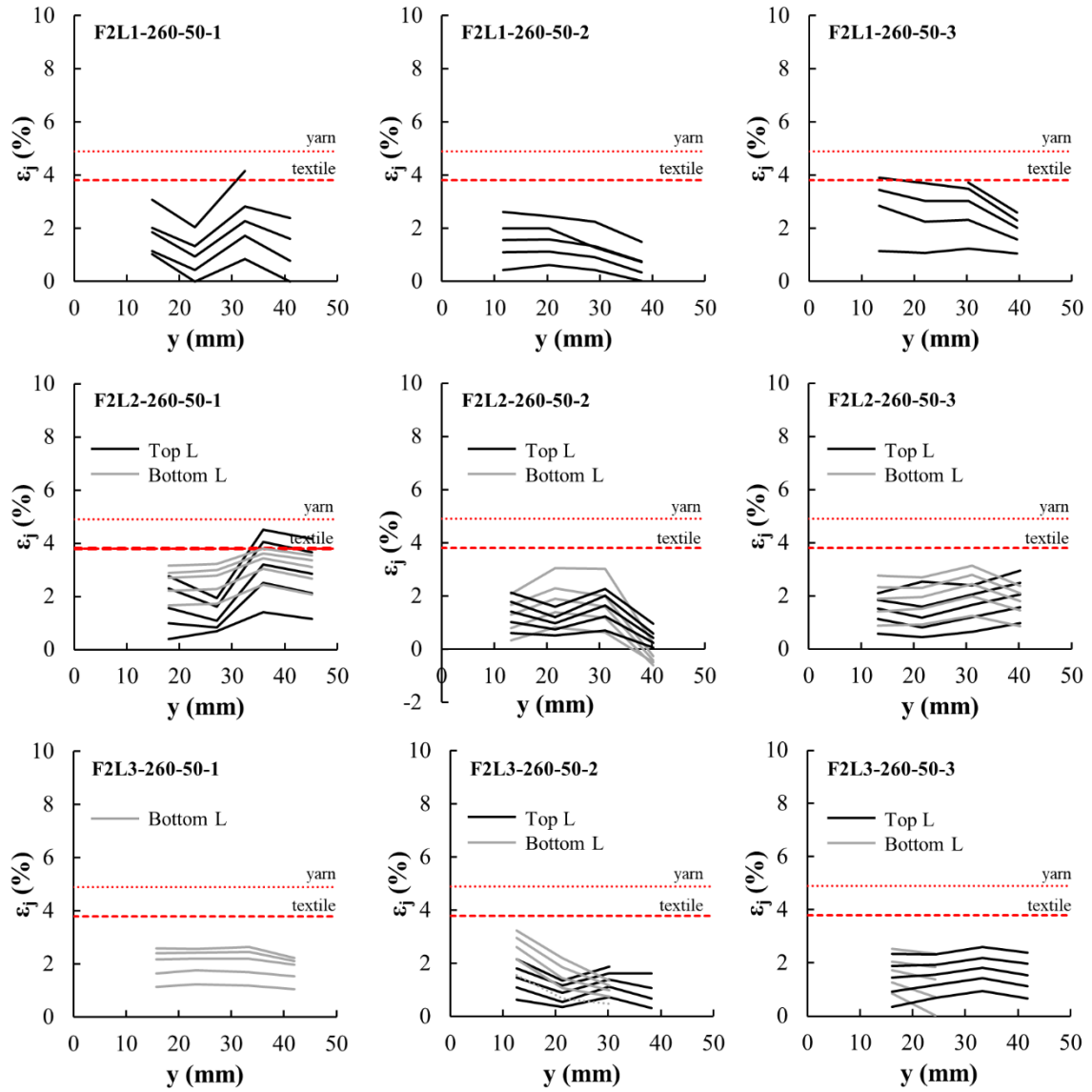


Fig. B. 6 Strain profile across the width of the unbonded textile at different loading stages (F2L1-260-50, F2L2-260-50 and F2L3-260-50 group series).

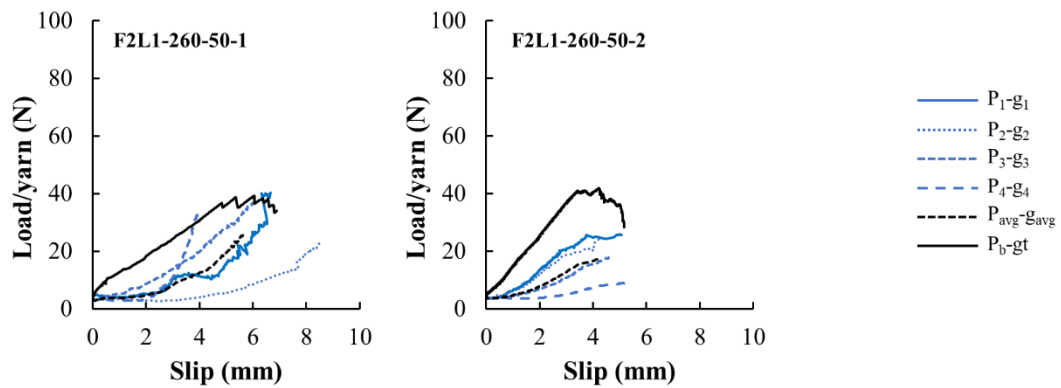


Fig. B. 7 Global (P_b-g_t) and local (P_j-g_j) load-slip response of individual yarns for F2L1-260-50 group series.

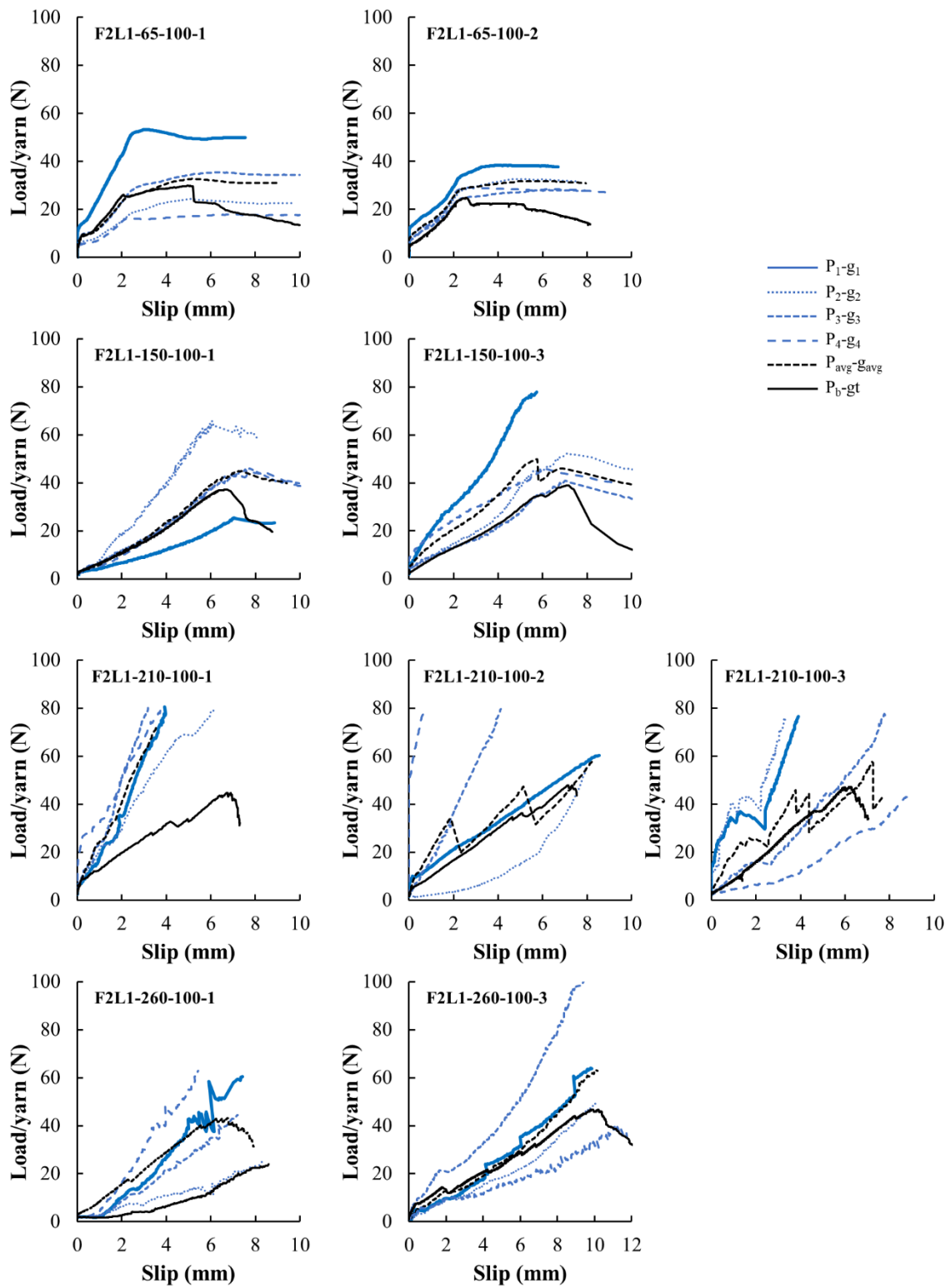


Fig. B. 8 Global (P_{b-g_t}) and local (P_{j-g_j}) load-slip response of individual yarns for F2L1-65-100, F2L1-150-100, F2L1-210-100 and F2L1-260-100 group series.

APPENDIX C - In-Plane Seismic Performance of Masonry Walls Retrofitted with FLAX-TRM

Complementary testing and additional information relevant to Chapter 6

C1. COMPRESSION TESTS ON BRICKS

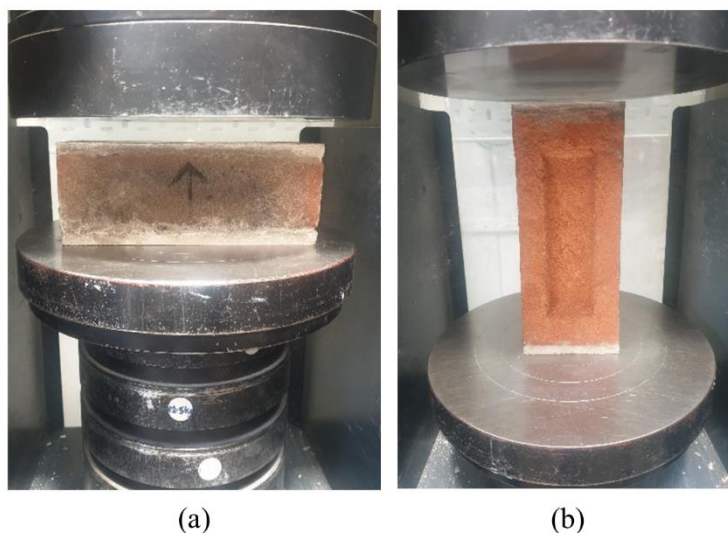


Fig. C. 1 Compression tests on brick units: (a) load perpendicular to bed joints; (b) load parallel to bed joints.

Table C. 1 Experimental results from compression tests on brick units. CoV values in parentheses.

Load direction	Specimen ID	P_{\max} (kN)	f_b (MPa)
⊥ bed joints	B1	555.1	25.3
	B2	439.9	20.1
	B3	607.0	27.7
	AVG (CoV)	534.0 (13%)	24.4 (13%)
// bed joints	B1	99.8	15.1
	B2	130.8	19.7
	B3	113.6	17.1
	AVG (CoV)	114.7 (11%)	17.3 (11%)

C2. FLEXURAL AND COMPRESSION TESTS ON MASONRY AND TRM MORTAR

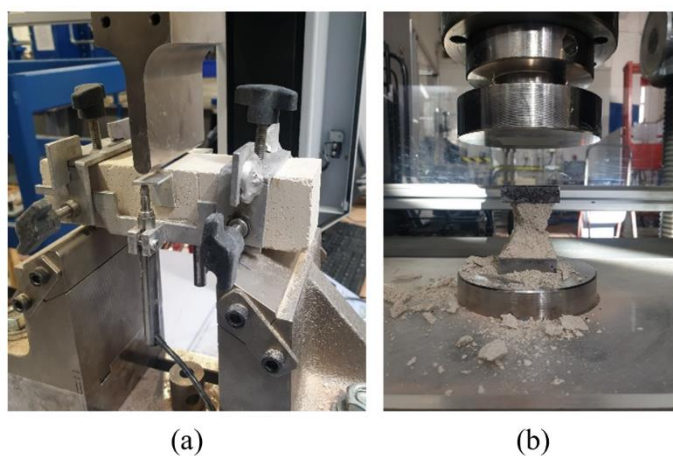


Fig. C. 2 Experimental tests on masonry and TRM mortars: (a) flexural tests on prisms; (b) compression tests on the resulting halves.

- Specimen BW

Table C. 2 Results from flexural tests on mortar prisms and compression tests on the resulting halves. Specimen BW - Masonry Mortar. CoV values in parentheses.

MASONRY MORTAR							
Flexure				Compression			
ID	P_{max} (N)	f_{fl} (MPa)	E (MPa)	P_{max,1} (N)	P_{max,2} (N)	P_{max} (N)	f_c (MPa)
W1-1	294.4	0.7	1098.9	3701.9	3742.4	3722.1	2.3
W1-3	394.6	0.9	1718.3	4151.9	3966.4	4059.2	2.5
W1-4	281.2	0.7	1961.2	3286.9	3098.6	3192.8	2.0
W1-5	224.9	0.5	792.1	2404.5	2431.8	2418.1	1.5
AVG	298.8	0.7	1392.6		3348.1		2.1
(CoV)	(20%)	(20%)	(34%)		(18%)		(18%)

- Specimen LW

Table C. 3 Results from flexural tests on mortar prisms and compression tests on the resulting halves. Specimen LW - Masonry Mortar. CoV values in parentheses.

MASONRY MORTAR							
Flexure				Compression			
ID	P_{max} (N)	f_{fl} (MPa)	E (MPa)	P_{max,1} (N)	P_{max,2} (N)	P_{max} (N)	f_c (MPa)
W6-1	345.6	0.8	757.0	3091.9	3486.3	3289.1	2.1
W6-2	201.0	0.5	736.7	2695.7	3044.1	2869.9	1.8
W6-3	315.2	0.7	1033.7	3504.5	3828.4	3666.4	2.3
W6-4	254.9	0.6	1068.6	3644.2	3183.8	3414.0	2.1
W6-5	220.3	0.5	1184.9	2652.3	2931.1	2791.7	1.7
AVG	267.4	0.6	956.2		3206.2		2.0
(CoV)	(21%)	(21%)	(19%)		(10%)		(10%)

Table C. 4 Results from flexural tests on mortar prisms and compression tests on the resulting halves. Specimen LW - TRM Mortar. CoV values in parentheses.

TRM MORTAR							
Flexure				Compression			
ID	P_{max} (N)	f_{fl} (MPa)	E (MPa)	P_{max,1} (N)	P_{max,2} (N)	P_{max} (N)	f_c (MPa)
W6-1	1079.4	2.5	4185.8	9409.4	9857.7	9633.5	6.0
W6-2	1214.6	2.8	4081.4	10035.1	8634.3	9334.7	5.8
W6-3	1061.9	2.5	4422.0	8616.0	9229.9	8923.0	5.6
W6-4	1096.8	2.6	3907.3	8877.6	9490.0	9183.8	5.7
W6-5	1057.9	2.5	3769.9	9544.9	9504.6	9524.7	6.0
AVG	1045.9	2.5	4027.5		9547.5		6.0
(CoV)	(5%)	(5%)	(5%)		(3%)		(3%)

- Specimen FL1W-1

Table C. 5 Results from flexural tests on mortar prisms and compression tests on the resulting halves. Specimen FL1W-1 - Masonry Mortar. CoV values in parentheses.

MASONRY MORTAR							
Flexure				Compression			
ID	P_{max} (N)	f_{fl} (MPa)	E (MPa)	P_{max,1} (N)	P_{max,2} (N)	P_{max} (N)	f_c (MPa)
W2-1	302.8	0.7	1075.5	3581.6	3527.7	3554.6	2.2
W2-2	277.4	0.7	1045.0	3377.2	3384.3	3380.8	2.1
W2-3	247.7	0.6	1000.9	3994.2	3711.6	3852.9	2.4
W2-4	321.8	0.8	1476.5	3935.1	4255.2	4095.2	2.6
W2-5	321.1	0.8	1146.9	3713.6	3798.2	3755.9	2.3
AVG	287.4	0.7	1149.5		3727.9		2.3
(CoV)	(10%)	(10%)	(17%)		(7%)		(7%)

Table C. 6 Results from flexural tests on mortar prisms and compression tests on the resulting halves. Specimen FL1W-1 - TRM Mortar. CoV values in parentheses.

TRM MORTAR							
Flexure				Compression			
ID	P_{max} (N)	f_{fl} (MPa)	E (MPa)	P_{max,1} (N)	P_{max,2} (N)	P_{max} (N)	f_c (MPa)
W2-I1	1223.6	2.9	3069.4	10661.1	10732.7	10696.9	6.7
W2-I2	1290.9	3.0	4572.4	10380.3	11163.8	10772.0	6.7
W2-I3	977.5	2.3	4725.6	10491.1	9716.2	10103.7	6.3
W2-II1	1172.1	2.7	4056.7	11457.1	11522.3	11489.7	7.2
W2-II2	881.8	2.1	4893.1	10699.2	10145.9	10422.5	6.5
W2-II3	1199.5	2.8	3757.4	10606.9	11426.0	11016.4	6.9
AVG	1124.2	2.6	4179.1		10750.2		6.7
(CoV)	(13%)	(13%)	(15%)		(4%)		(4%)

- Specimen FL1W-2

Table C. 7 Results from flexural tests on mortar prisms and compression tests on the resulting halves. Specimen FL1W-2 - Masonry Mortar. CoV values in parentheses.

MASONRY MORTAR							
Flexure				Compression			
ID	P_{max} (N)	f_{fl} (MPa)	E (MPa)	P_{max,1} (N)	P_{max,2} (N)	P_{max} (N)	f_c (MPa)
W4-1	158.0	0.4	1790.8	3044.6	3715.8	3380.2	2.1
W4-2	278.6	0.7	911.8	3836.5	3857.6	3847.0	2.4
W4-3	256.6	0.6	-	3448.8	3764.5	3606.7	2.3
W4-4	276.8	0.6	861.5	3511.5	3296.2	3403.9	2.1
W4-5	260.5	0.6	1300.0	3488.6	3571.0	3529.8	2.2
AVG	246.1	0.6	1216.0		3553.5		2.2
(CoV)	(18%)	(18%)	(31%)		(5%)		(5%)

Table C. 8 Results from flexural tests on mortar prisms and compression tests on the resulting halves. Specimen FL1W-2 - TRM Mortar. CoV values in parentheses.

TRM MORTAR							
Flexure				Compression			
ID	P_{max} (N)	f_{fl} (MPa)	E (MPa)	P_{max,1} (N)	P_{max,2} (N)	P_{max} (N)	f_c (MPa)
W4-I1	1386.4	3.2	2857.8	11781.7	13504.5	12643.1	7.9
W4-I2	1314.1	3.1	3898.0	13693.5	13507.0	13600.3	8.5
W4-I3	1435.4	3.4	2164.6	13223.0	11130.4	12176.7	7.6
W4-II1	1139.7	2.7	3612.1	10314.2	10059.5	10186.9	6.4
W4-II2	1120.8	2.6	3872.0	10673.2	9929.7	10301.4	6.4
W4-II3	1057.6	2.5	1015.9	8211.5	9610.9	8911.2	5.6
AVG	1242.3	2.9	2903.4		11303.3		7.1
(CoV)	(12%)	(12%)	(36%)		(14%)		(14%)

- Specimen FL2W-1

Table C. 9 Results from flexural tests on mortar prisms and compression tests on the resulting halves. Specimen FL2W-1 - Masonry Mortar. CoV values in parentheses.

MASONRY MORTAR							
Flexure				Compression			
ID	P_{max} (N)	f_{fl} (MPa)	E (MPa)	P_{max,1} (N)	P_{max,2} (N)	P_{max} (N)	f_c (MPa)
W5-1	302.1	0.7	1261.5	2925.6	2728.1	2826.9	1.8
W5-2	265.6	0.6	1036.4	2481.3	3423.1	2952.2	1.8
W5-3	279.3	0.7	1215.0	3470.8	3548.2	3509.5	2.2
W5-4	258.9	0.6	856.1	2886.9	1855.9	2371.4	1.5
W5-5	338.9	0.8	1176.2	3272.1	3221.6	3246.8	2.0
AVG	288.9	0.7	1109.0		2981.4		1.9
(CoV)	(10%)	(10%)	(13%)		(13%)		(13%)

Table C. 10 Results from flexural tests on mortar prisms and compression tests on the resulting halves. Specimen FL2W-1 - TRM Mortar. CoV values in parentheses.

TRM MORTAR							
Flexure				Compression			
ID	P_{max} (N)	f_{fl} (MPa)	E (MPa)	P_{max,1} (N)	P_{max,2} (N)	P_{max} (N)	f_c (MPa)
W5-I1	1268.5	3.0	4234.8	10821.0	11984.7	11402.9	7.1
W5-I2	1061.1	2.5	3893.3	11943.4	11619.0	11781.2	7.4
W5-I3	919.3	2.2	4625.9	11166.5	11687.2	11426.9	7.1
W5-II1	1123.6	2.6	3122.3	9864.4	10022.9	9943.7	6.2
W5-II2	1151.2	2.7	4300.7	9909.7	11321.6	10615.6	6.6
W5-II3	949.0	2.2	4449.2	11910.0	12058.3	11984.1	7.5
AVG	1078.8	2.5	4104.4		11192.4		7.0
(CoV)	(11%)	(11%)	(14%)		(6%)		(6%)

- Specimen FL2W-2

Table C. 11 Results from flexural tests on mortar prisms and compression tests on the resulting halves. Specimen FL2W-2 - Masonry Mortar. CoV values in parentheses.

MASONRY MORTAR							
Flexure				Compression			
ID	P_{max} (N)	f_n (MPa)	E (MPa)	P_{max,1} (N)	P_{max,2} (N)	P_{max} (N)	f_c (MPa)
W3-1	283.6	0.7	1099.3	3475.1	3121.4	3298.3	2.1
W3-2	250.0	0.6	875.0	3101.4	3051.8	3076.6	1.9
W3-3	336.4	0.8	997.8	3360.4	3092.1	3226.3	2.0
W3-4	205.7	0.5	409.9	2742.1	2732.8	2737.4	1.7
AVG	268.9	0.6	845.5		3084.6		1.9
(CoV)	(18%)	(18%)	(31%)		(7%)		(7%)

Table C. 12 Results from flexural tests on mortar prisms and compression tests on the resulting halves. Specimen FL2W-2 - TRM Mortar. CoV values in parentheses.

TRM MORTAR							
Flexure				Compression			
ID	P_{max} (N)	f_n (MPa)	E (MPa)	P_{max,1} (N)	P_{max,2} (N)	P_{max} (N)	f_c (MPa)
W3-I1	931.8	2.2	4697.2	12095.0	11489.7	11792.3	7.4
W3-I2	1044.8	2.4	3516.6	9919.1	8847.0	9383.0	5.9
W3-I3	1141.5	2.7	3774.5	11764.5	12444.4	12104.4	7.6
W3-II1	1276.9	3.0	2750.8	11330.6	11706.6	11518.6	7.2
W3-II2	1184.4	2.8	4301.2	13112.0	13032.6	13072.3	8.2
W3-II3	1230.2	2.9	3937.7	10857.7	11668.5	11263.1	7.0
AVG	1134.9	2.7	3829.7		11522.3		7.2
(CoV)	(10%)	(10%)	(16%)		(10%)		(10%)

C.4 COMPRESSION TESTS ON MASONRY WALLETTES

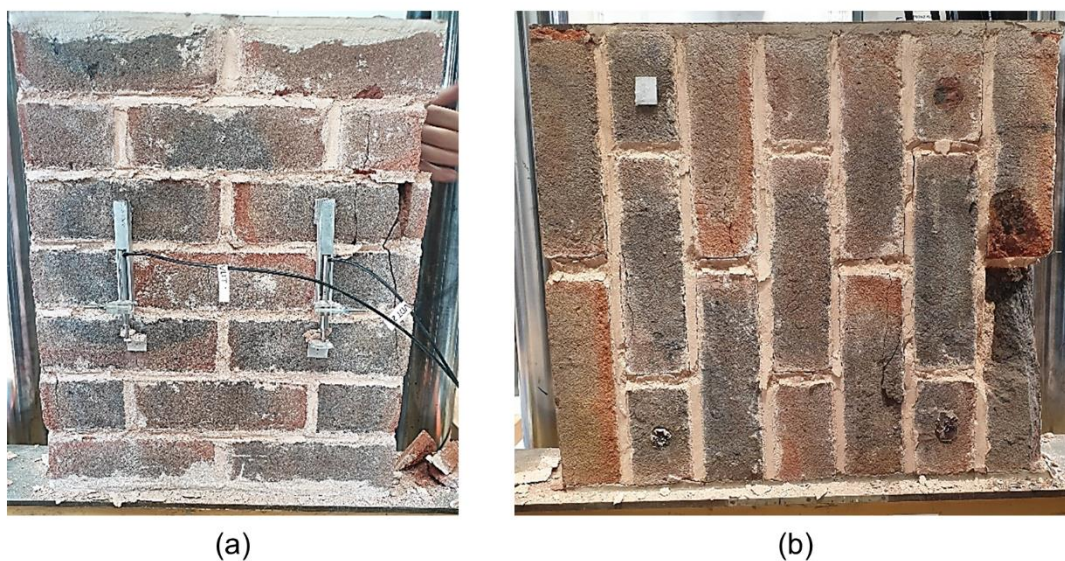


Fig. C. 3 Failure of masonry wallettes in compression: (a) load perpendicular to bed joints (b) load parallel to bed joints.

Table C. 13 Experimental results from masonry compression tests. CoV values in parentheses.

Load direction	Specimen ID	P_{max} (kN)	f_{wc} (MPa)	E_{wc} (GPa)
⊥ bed joints	W1	265.6	5.9	2.34
	W2	278.0	6.2	2.25
	W3	268.9	6.0	2.67
	AVG (CoV)	270.8 (2%)	6.0 (2%)	2.4 (7%)
// bed joints	W1	384.9	7.3	2.87
	W2	354.2	6.7	2.90
	W3	340.4	6.5	2.98
	AVG (CoV)	359.8 (5%)	6.8 (5%)	2.92 (2%)

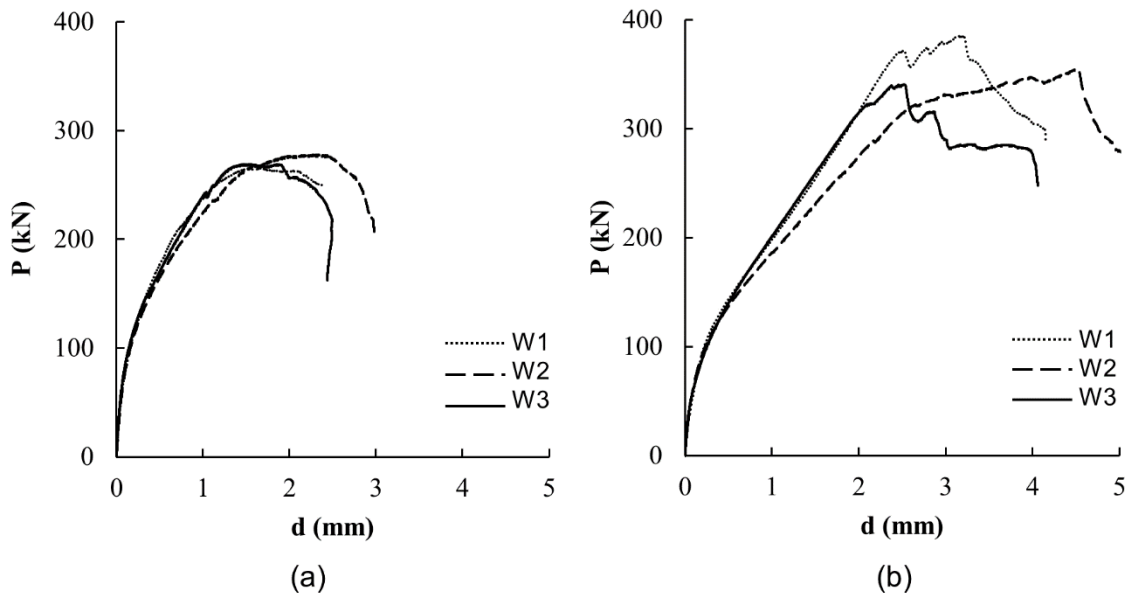


Fig. C. 4 Load-displacement response for masonry wallettes tested in compression for: (a) load perpendicular to bed joints; (b) load parallel to bed joints

C.5. DETERMINATION OF SHEAR STRENGTH OF MASONRY

Table C. 14 Experimental results on shear triplet tests. CoV values in parentheses.

f_{pi} (MPa)	P_{max} (kN)	f_{voi} (MPa)
	17.8	0.41
0.2	15.0	0.34
	19.9	0.45
AVG (CoV)	17.6 (14%)	0.4 (14%)
	37.8	0.86
0.6	31.2	0.71
	30.6	0.70
AVG (CoV)	33.2 (12%)	0.8 (12%)
	54.0	1.23
1	53.1	1.21
	57.8	1.32
AVG (CoV)	54.9 (5%)	1.3 (5%)

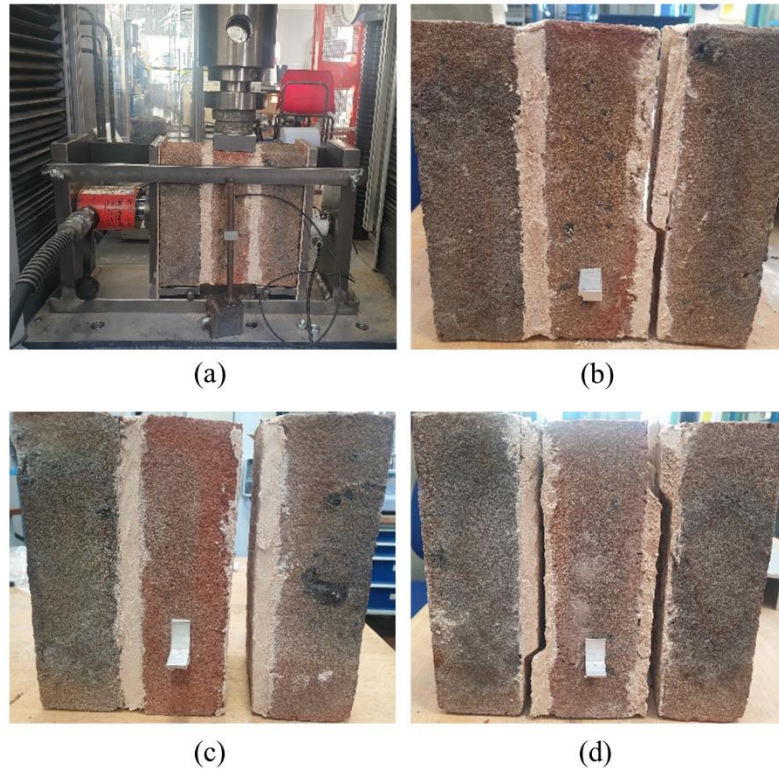


Fig. C. 5 (a) Experimental Setup; (b-d) failure modes of the tested shear triplets (acceptable failure modes “A.1” and “A.2” as per EN1052-3).

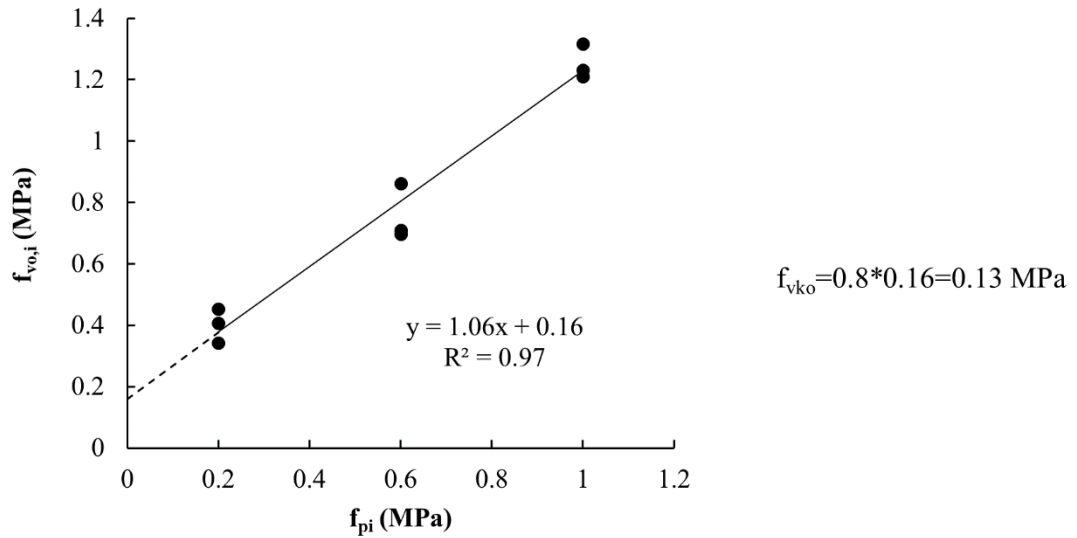


Fig. C. 6 Shear strength $f_{vo,i}$ as a function of precompression stress f_{pi} and final value of characteristic initial shear strength of masonry f_{vko} used in the analytical formulations.

C. 6. In-plane shear tests

- Specimen BW

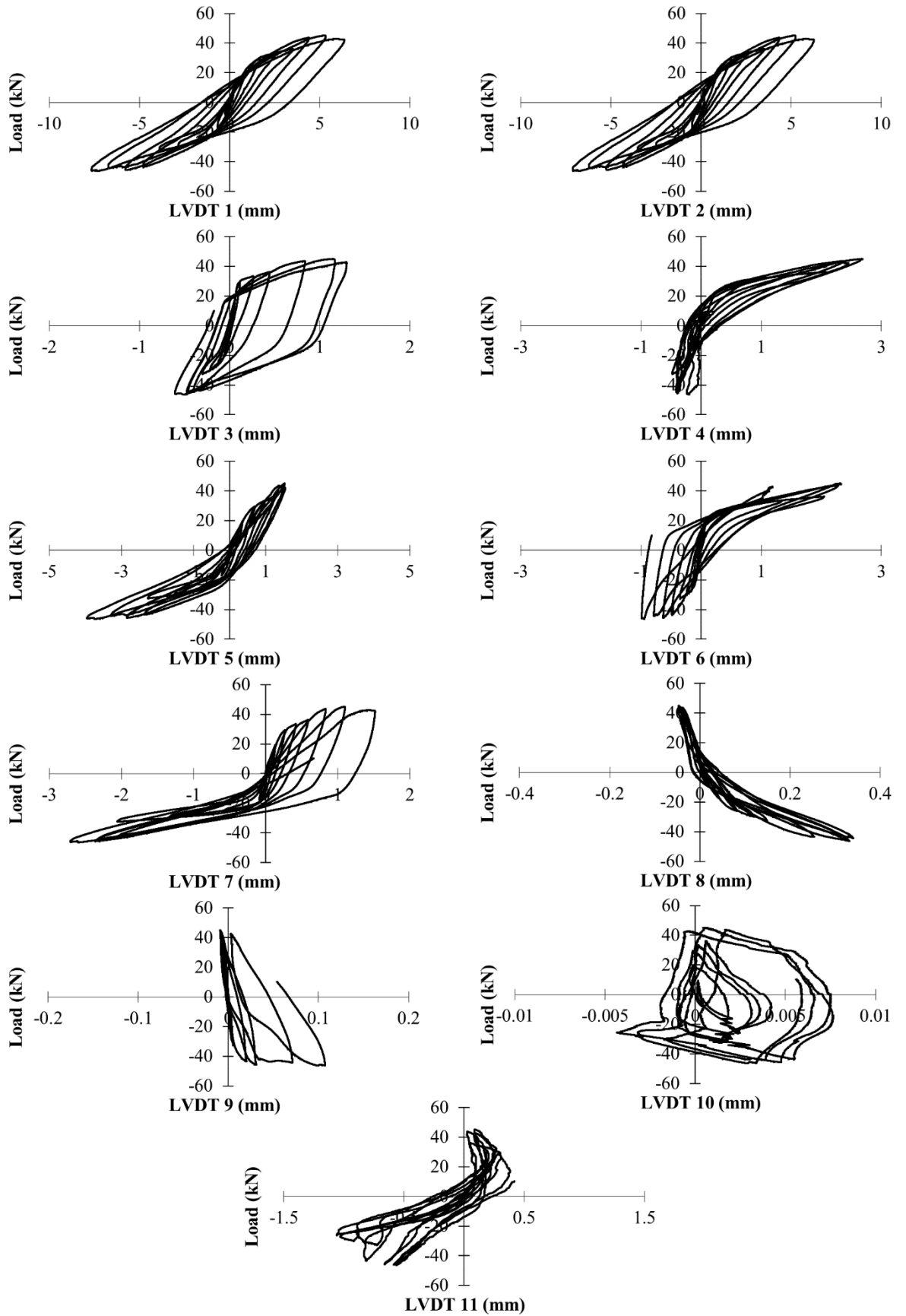


Fig. C. 7 LVDT measurements for specimen BW - cyclic test.

• Specimen LW

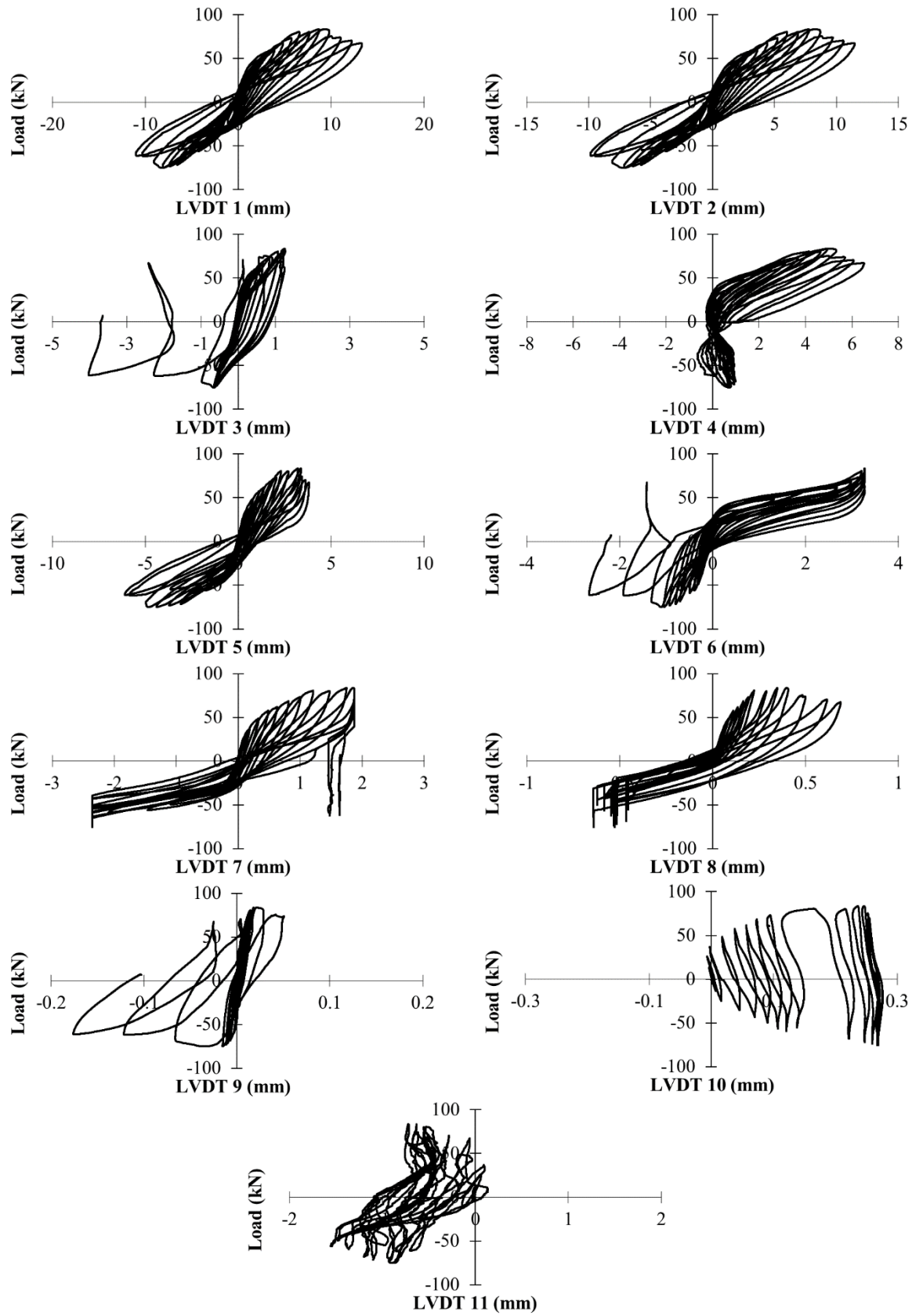


Fig. C. 8 LVDT measurements for specimen LW.

• Specimen FL1W-1

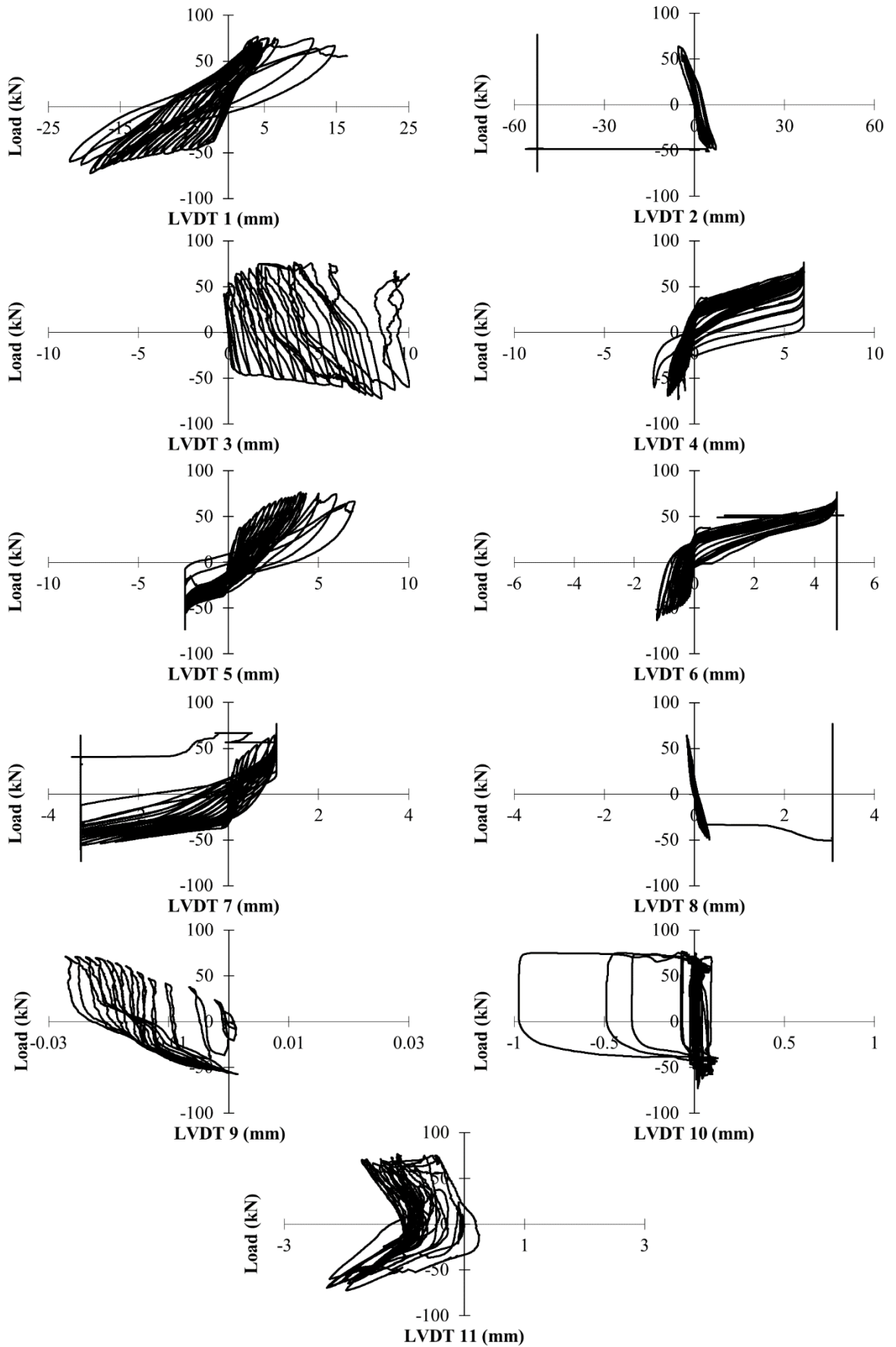


Fig. C. 9 LVDT measurements for specimen FL1W-1.

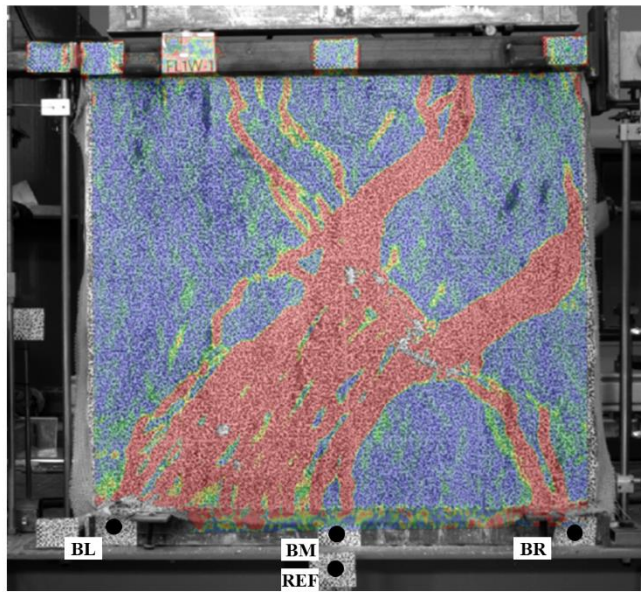
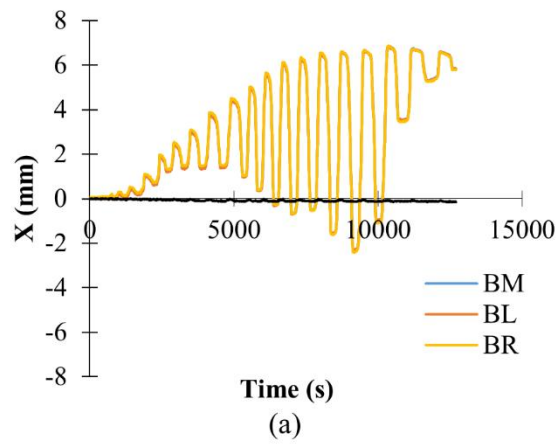


Fig. C. 10 (a) Horizontal Displacement of bottom steel channel, as obtained from DIC analyses. Note: BM, BL, BR stand for the position of the virtual markers as shown in (b); (b) Failure of specimen FL1W-1.

• Specimen FL1W-2

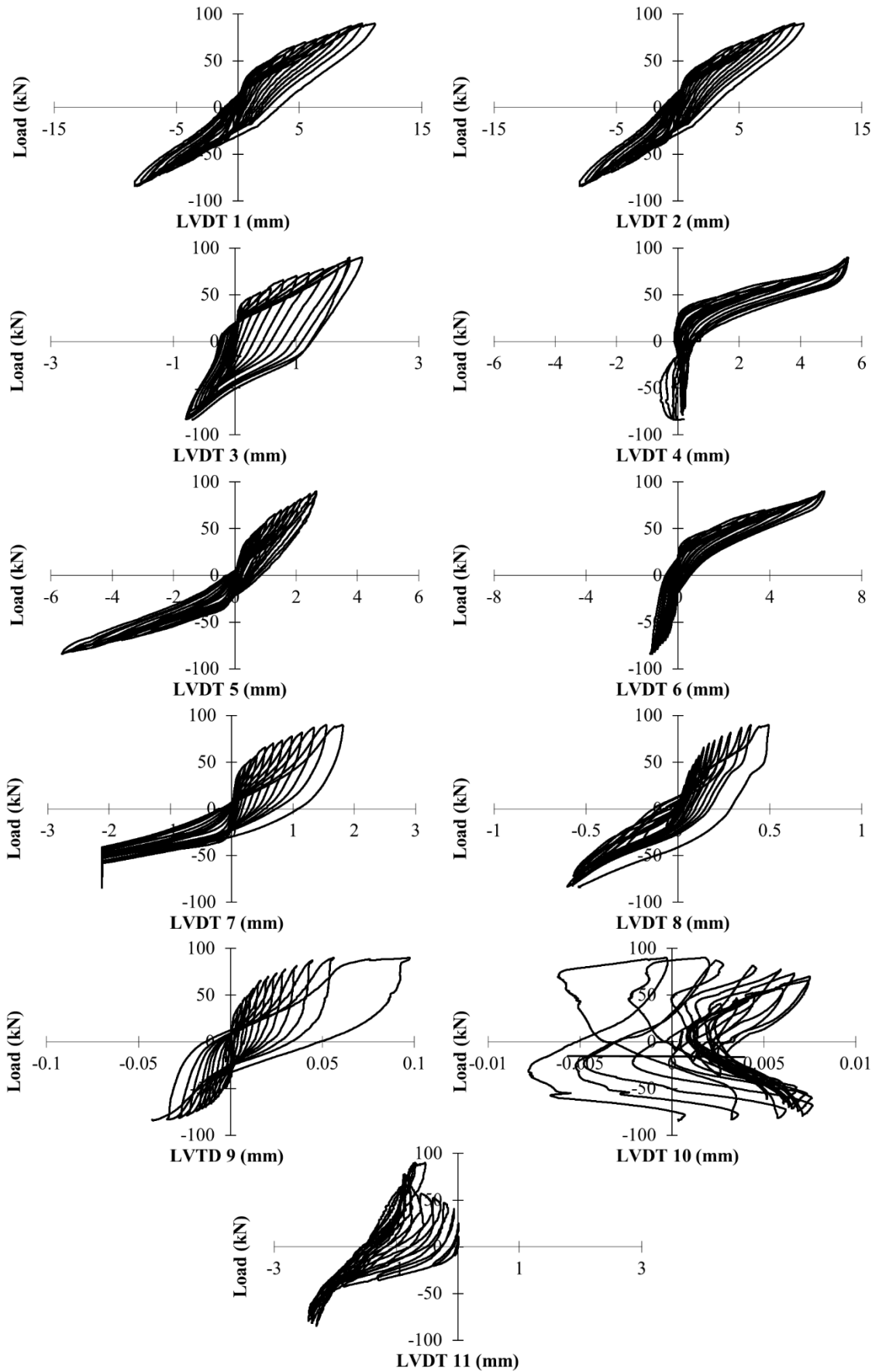


Figure C. 11 LVDT measurements for specimen FL1W-2.

- Specimen FL2W-1

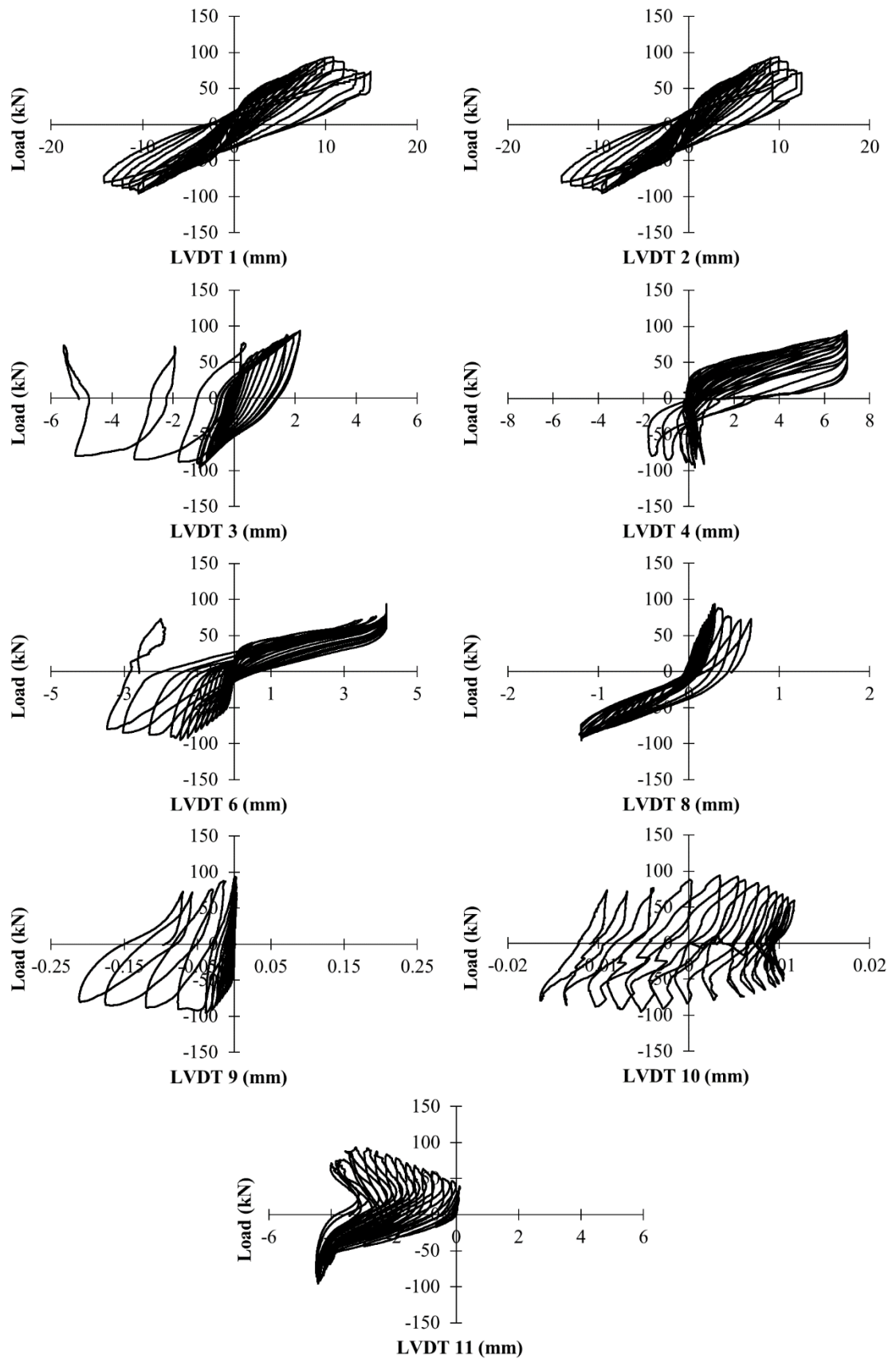


Fig. C. 12 LVDT measurements for specimen FL2W-1.

• Specimen FL2W-2

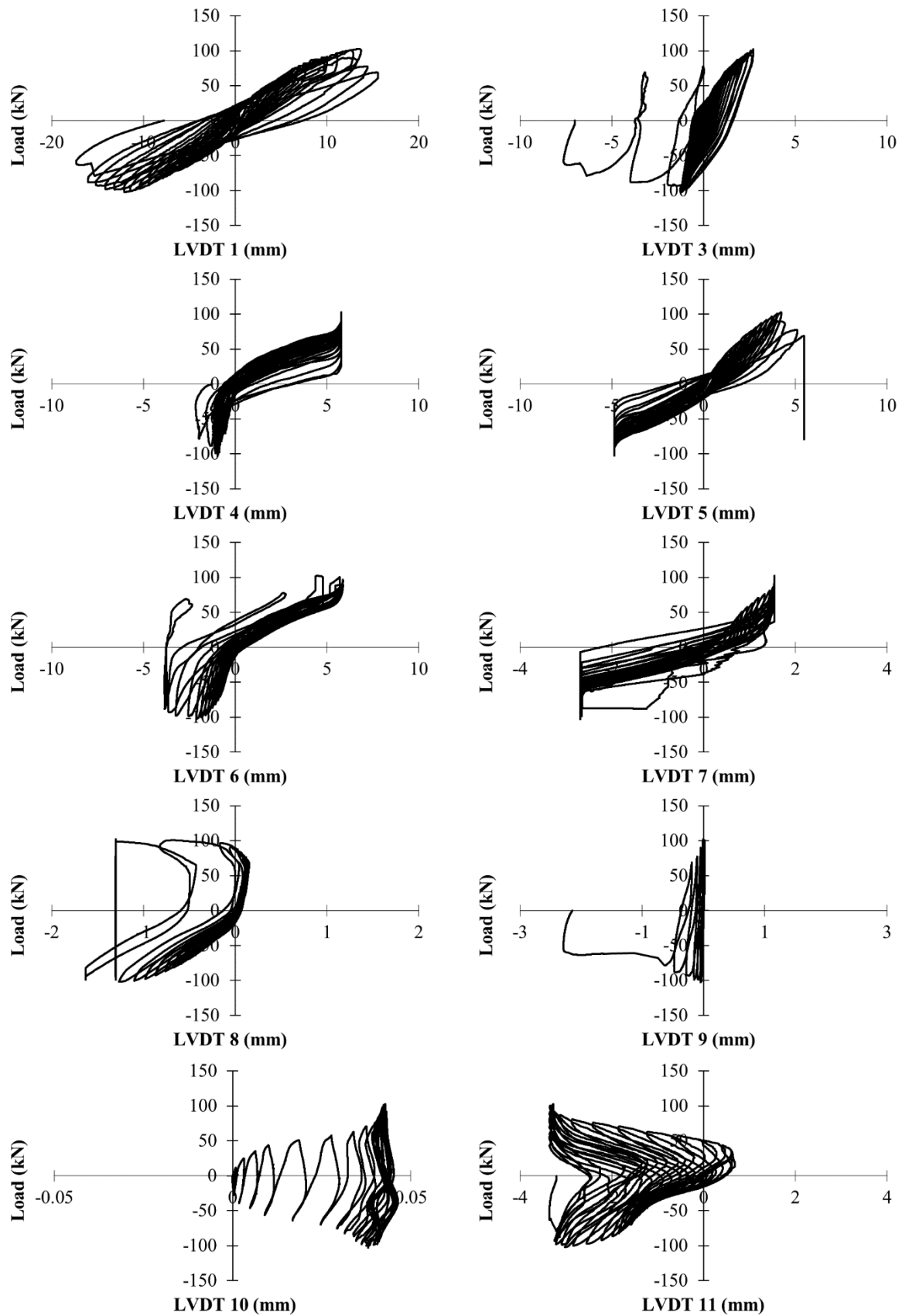


Fig. C. 13 LVDT measurements for specimen FL2W-2.

Table C. 15 Bilinear response details in push direction.

ID	V _{max} (kN)	d _{max} (mm)	d _{vmax} (mm)	K _e (kN/mm)	A _{env} (kNmm)	V _u (kN)	V _u /V _{max}	d _e (mm)	μ
BW	45.1	8.7	5.3	48.7	312.1	37.7	0.84	0.8	11.2
LW	83.7	13.3	9.4	56.3	887.5	70.0	0.84	1.2	10.7
FL1W-2	90.1	12.6	10.1	56.3	856.4	71.6	0.80	1.3	9.9
FL2-W1	93.7	12.9	10.8	60.0	865.2	70.4	0.75	1.2	11.0
FL2-W2	102.6	13.2	13.4	60.0	904.6	71.8	0.70	1.2	11.0

Table C. 16 Bilinear response details in pull direction.

ID	V _{max} (kN)	d _{max} (mm)	d _{vmax} (mm)	K _e (kN/mm)	A _{env} (kNmm)	V _u (kN)	V _u /V _{max}	d _e (mm)	μ
BW	-47.1	-6.7	-9.3	48.7	299.3	-48.3	1.03	-1.0	6.8
LW	-75.2	-11.0	-8.1	56.3	602.2	-57.4	0.76	-1.0	10.8
FL1W-2	-83.5	-8.4	-8.4	56.3	476.6	-60.3	0.76	-1.1	7.9
FL2-W1	-95.1	-14.2	-10.5	60.0	953.9	-70.2	0.74	-1.2	12.1
FL2-W2	-100.2	-15.9	-12.1	60.0	1158.8	-75.9	0.76	-1.3	12.6

C.7 ANALYTICAL PREDICTIONS AND DETAILED STEP-BY-STEP CALCULATIONS

Shear Contribution of URM, V_m (specimen BW)

- EC6

Initial shear strength, f_{vko} :

$$f_{vko} = 0.128 \text{ MPa}$$

Limit to the value of f_{vk} , f_{vlt} :

$$f_{vlt} = 0.065 * f_b = 0.065 * 24.4 = 1.6 \text{ MPa}$$

Vertical stress applied on the wall, σ_d :

$$\sigma_d = \frac{N_d}{tL} = \frac{70 * 1000}{102 * 1085} = 0.60 \text{ MPa}$$

Characteristic shear strength, f_{vk} :

$$f_{vk} = f_{vko} + 0.4 * \sigma_d = 0.128 + 0.4 * 0.60 = 0.37 \text{ MPa} \leq f_{vlt} = 1.6 \text{ MPa} \quad \checkmark$$

Shear resistance of masonry, V_m :

$$V_m = f_{vd} tL = 0.37 * 102 * 1085 = 43.0 \text{ kN}$$

- EC8

i. Rocking

Distance between flexural resistance is attained and the contraflexure point (assuming fixed-fixed conditions),

h_o :

$$h_o = 0.5H = 0.5 * 1085 = 543 \text{ mm}$$

Normalised axial load, v :

$$v = \frac{N_d}{f_{wc} tL} = \frac{70 * 10^3}{5.9 * 102 * 1150} = 0.101$$

Shear force corresponding to flexural failure, V_f :

$$V_f = \frac{N_d L}{2h_o} (1 - 1.15v) = \frac{70 \cdot 10^3 \cdot 1150}{2 \cdot 543} \cdot (1 - 1.15 \cdot 0.101) = 65.6 \text{ kN}$$

ii. Shear sliding

$$V_s = Lt \left(f_{vko} + \frac{0.4N_d}{Lt} \right) = 1150 \cdot 102 \cdot \left(0.128 + \frac{0.4 \cdot 70 \cdot 10^3}{1150 \cdot 102} \right) \cdot 10^{-3} = 42.7 \text{ kN}$$

$$V_{s,units} = 0.065 f_b Lt = 0.065 \cdot 24.4 \cdot 1150 \cdot 102 \cdot 10^{-3} = 181.6 \text{ kN}$$

$$V_s = \min(V_s, V_{s,units}) = \min(42.7, 181.6) = 42.7 \text{ kN}$$

iii. Diagonal Tension

Minimum overlapping length, $l_{overlap,min}$:

$$l_{overlap,min} = \max(0.4 \cdot h_b, 40) = \max(0.4 \cdot 65, 40) = 40 \text{ mm}$$

Actual overlapping length, $l_{overlap}$:

$$l_{overlap} = \frac{l_b}{2} = \frac{215}{2} = 107.5 \text{ mm} > l_{overlap,min}$$

Interlocking coefficient, φ :

$$\varphi = \frac{h_b}{l_{overlap}} = \frac{65}{107.5} = 0.6$$

Local friction coefficient, μ_j :

$$\mu_j = 0.6$$

Correction coefficient accounting for the shear stress distribution in the middle section of the panel and related to the aspect ratio of the panel, b :

$$b = \frac{H}{L} = \frac{1085}{1150} = 0.94$$

Failure of units, $V_{d,lim}$:

$$V_{d,lim} = \frac{Lt f_{bt}}{b \cdot 2.3} \sqrt{1 + \frac{\sigma_o}{f_{bt}}} = \frac{1150 \cdot 102}{0.94} \cdot \frac{0.1 \cdot 24.4}{2.3} \cdot \sqrt{1 + \frac{0.60}{0.1 \cdot 24.4}} \cdot 10^{-3} = 146.9 \text{ kN}$$

where,

$$- f_{bt} = 0.1 f_b \text{ (tensile strength of the unit is 10% of its compressive strength)}$$

Shear strength of regular masonry panels, V_d :

$$V_d = \frac{Lt}{b} \left(\frac{f_{vko}}{1 + \mu_j \varphi} + \frac{\mu_j}{1 + \mu_j \varphi} \sigma_o \right) = \frac{1150 \cdot 102}{1} \left(\frac{0.1}{1 + 0.6 \cdot 0.6} + \frac{0.6}{1 + 0.6 \cdot 0.6} \cdot 0.60 \right) \cdot 10^{-3} = 44.3 \text{ kN}$$

$$V_d = 44.3 \text{ kN} \leq V_{d,lim} = 146.9 \text{ kN} \checkmark$$

• ACI549.4R

i. Rocking

$$V_f = 0.9 a N_d \left(\frac{L}{H} \right) = 0.9 \cdot 1 \cdot 70 \cdot \left(\frac{1150}{1085} \right) = 66.8 \text{ kN}$$

where $a = 1$ for fixed-fixed boundary conditions

ii. Shear sliding (assuming friction only)

$$V_{bjs2} = 0.5 N_d = 0.5 \cdot 70 = 35 \text{ kN}$$

iii. Diagonal Tension

Diagonal tensile strength, f_{dt} :

$$f_{dt}' = 0.75 * \frac{N_d}{1.5A_n} = 0.75 * \frac{70 * 1000}{1.5 * 4080} = 8.58 \text{ MPa}$$

$$V_d = f_{dt}' A_n \beta \sqrt{\left(1 + \frac{\sigma_d}{f_{dt}'}\right)} = 8.58 * 4080 * 1.0 * \sqrt{1 + \frac{0.60}{8.58}} * 10^{-3} = 38.4 \text{ kN}$$

where, $\beta = 1$ (for $L/H > 1$)

iv. Toe crushing

$$V_{tc} = a N_d \left(\frac{L}{H}\right) \left(1 - \frac{\sigma_d}{0.7f_{wc}}\right) = 1 * 70 * \left(\frac{1150}{1085}\right) \left(1 - \frac{0.60}{0.7 * 5.9}\right) = 63.5 \text{ kN}$$

• NTC 18 [[181]]

i. Rocking

$$V_c = \frac{L^2 t \sigma_d}{2} \left(1 - \frac{\sigma_d}{0.85f_{wc}}\right) \frac{2}{H} = \frac{1150^2 * 102 * 0.60}{2} \left(1 - \frac{0.60}{0.85 * 5.9}\right) * \frac{2}{1085} = 65.4 \text{ kN}$$

ii. Shear sliding (same as EC6)

$$V_s = f_{vd} t L = 43.0 \text{ kN}$$

iii. Diagonal Tension

$$V_d = L t \frac{1.5f_{vko}}{b} \sqrt{1 + \frac{\sigma_d}{1.5f_{vko}}} = 1150 * 102 * \frac{1.5 * 0.128}{1} \sqrt{1 + \frac{0.60}{1.5 * 0.1}} * 10^{-3} = 45.6 \text{ kN}$$

where, $b = 1$ for $H/L \leq 1$

Shear capacity of FTRM-retrofitted URM, V_{Rd} (specimen FL1W-2)

• ACI549.4R

$$\phi_v V_{Rd} = \phi_v (V_m + V_{TRM})$$

where $\phi_v = 1.0$ (for prediction purposes)

Contribution of FRCM composite material, V_{TRM} :

$$V_{TRM} = 2nA_f H f_{fv}$$

where,

- $f_{fv} = E_{TRM} \epsilon_{fv}$
- E_{TRM} is the tensile modulus of elasticity of the cracked FRCM composite material and ϵ_{fv} the ultimate tensile strain in the FRCM composite material.
- $\epsilon_{fv} \leq 0.004$

For single-layer TRM strengthening on both sides:

$$\epsilon_{fv} = \min(\epsilon_{fu}, 0.004) = \min(0.073, 0.004) = 0.004$$

$$f_{fv} = E_{TRM} \epsilon_{fv} = 2.98 * 10^3 * 0.004 = 11.9 \text{ MPa}$$

$$V_{TRM} = 2 * 1 * 0.1 * 1098 * 11.9 * 10^{-3} = 2.5 \text{ kN}$$

$$V_{Rd} = 2.5 + 35 = 37.5 \text{ kN}$$

• ACI549.6R (ACI approach)

$$V_{Rd} = V_m + V_{TRM}$$

Contribution of FRCM composite material, V_{TRM} :

$$V_{TRM} = nA_f E_f \epsilon_{fd}$$

where,

- E_f is the tensile modulus of elasticity of the cracked FRCM composite material.
- n is the number of wall strengthened sides.
- A_f is the area of the textile reinforcement effective in shear.
- ε_{fd} is the ultimate tensile strain in the FRCM composite material

For single-layer TRM strengthening on both sides:

$$A_f = \min(H, L) \cdot t_f = \min(1098, 1110) \cdot 0.1 = 104.2 \text{ mm}^2$$

$$\varepsilon_{fd} = 7.3\%$$

$$V_{TRM} = 2 \cdot 104.2 \cdot 7.3 \cdot 0.01 \cdot 2.98 \cdot 1000 = 45.3 \text{ kN}$$

$$V_{Rd} = 35 + 45.3 = 80.3 \text{ kN}$$

- ACI549.6R (RILEM approach)

$$V_{Rd} = V_m + V_{TRM}$$

Contribution of FRCM composite material, V_{TRM} :

$$V_{TRM} = n A_f E_f \varepsilon_{fd}$$

where,

- E_f is the tensile modulus of elasticity of the dry textile.
- n is the number of wall strengthened sides.
- A_f is the area of the textile reinforcement effective in shear.
- ε_{fd} is the ultimate strain in the FRCM composite material, either at debonding or textile rupture, through the equation: $\varepsilon_{fd} = \min(a_1 \varepsilon_{fb}, \frac{\varepsilon_{tk}}{a_2})$, where a_1 and a_2 are taken as 1.5 and 1.0, respectively.

For single-layer TRM strengthening on both sides:

$$A_f = \min(H, L) \cdot t_f = \min(1098, 1110) \cdot 0.1 = 104.2 \text{ mm}^2$$

$$\varepsilon_{fd} = \min(1.5 \cdot 3.24, 3.8) = 3.8\%$$

Hence, the product $E_f \varepsilon_{fd}$ is taken as the tensile strength of the dry textile.

$$V_{TRM} = 2 \cdot 104.2 \cdot 289 = 60.2 \text{ kN}$$

$$V_{Rd} = 42.3 + 60.2 = 102.5 \text{ kN}$$

- Triantafillou

Shear resistance of TRM retrofitted specimen, V_{Rd} :

$$V_{Rd} = \min(V_m + V_{TRM}, V_{Rd, \max})$$

TRM contribution, $V_{Rd,t}$:

$$V_{TRM} = 0.9 H n t_f f_{td}$$

where,

- $n = 2$ for double-sided TRM jacketing
- f_{td} the design strength of TRM, equal to: $f_{td} = \min\left(\frac{f_{tk}}{\gamma_k}, f_{tbd}\right)$

For single-layer TRM strengthening on both sides:

$$f_{td} = \min(177.8, 208.1) = 177.8 \text{ MPa}$$

$$V_{TRM} = 0.9 \cdot 1098 \cdot 2 \cdot 0.1 \cdot 177.8 = 35.1 \text{ kN}$$

Maximum value, $V_{Rd, \max}$:

$$V_{Rd, \max} = 2 t L = 2 \cdot 102 \cdot 1098 \cdot 10^{-3} = 226.4 \text{ kN}$$

Hence,

$$V_{Rd} = \min(41.7 + 35.1, 229.5) = 76.8 \text{ kN}$$

- Thomoglou et al.

$$V_{Rd} = V_m + (V_f + V_{\text{mortar}}) \cdot k$$

where, $k = 0.55$ for Glass-TRM and clay brick masonry

$$V_f = 2 \cdot n \cdot A_f \cdot H \cdot E_{\text{TRM}} \cdot \varepsilon_{fd}$$

$$V_{\text{mortar}} = A_{\text{mortar}} \cdot E_{\text{mortar}} \cdot \varepsilon_{tm}$$

For single-layer TRM strengthening on both sides:

$$\varepsilon_{fd} = 3.24\%$$

$$A_{\text{mortar}} = (2t_{\text{mortar}})L = 2 \cdot 6 \cdot 1098 = 13176 \text{ mm}^2$$

$$V_{\text{mortar}} = 13176 \cdot 3.81 \cdot 10^3 \cdot 0.057 \cdot 0.01 \cdot 10^{-3} = 28.8 \text{ kN}$$

$$V_f = 2 \cdot 1 \cdot 0.1 \cdot 1098 \cdot 2.98 \cdot 1000 \cdot 3.24 \cdot 0.01 = 20.1 \text{ kN}$$

$$V_{Rd} = 40.9 + 0.55 \cdot (20.1 + 28.8) = 67.8 \text{ kN}$$

- CNR DT 215

$$V_{\text{TRM}} = n t_f H \alpha_t \varepsilon_{fd} E_f = 2 \cdot 0.1 \cdot 1098 \cdot 0.8 \cdot 177.8 \cdot 10^{-3} = 31.6 \text{ kN}$$

$$V_{Rd} = 42.3 + 31.6 = 73.9 \text{ kN}$$

Notation

E_{TRM}	Modulus of elasticity of cracked TRM
f_b	brick compressive strength
f_{bt}	tensile strength of brick unit
f_{tbd}	design bond strength of TRM/masonry system
f_{td}	design tensile strength of TRM composite
f_{vk}	characteristic shear strength of masonry
f_{vko}	characteristic initial shear strength of masonry under zero compressive stress
f_{wc}	compressive strength of masonry
H	height of masonry wall specimen
h_b	brick height
h_o	effective height of masonry wall specimen
L	length of masonry wall specimen
l_b	brick length
n	number of strengthening sides
N_d	vertical load applied during the in-plane shear tests
t	thickness of masonry wall specimen
t_f	design thickness of flax textile
t_m	thickness of mortar joints
V_d	shear resistance against diagonal tension
$V_{d,lim}$	shear resistance due to failure of the brick units
V_f	shear resistance against rocking
V_m	shear contribution of masonry
V_{Rd}	shear resistance of strengthened masonry element

APPENDIX C

V_s	shear resistance against sliding
V_{tc}	shear resistance against toe crushing
V_{TRM}	shear contribution of TRM
ε_{fd}	effective tensile strain in the textile reinforcement
ε_{fu}	ultimate tensile strain of TRM composite
μ_j	local friction coefficient
σ_d	compressive stress on the wall due to vertical load N_d
φ	interlocking coefficient